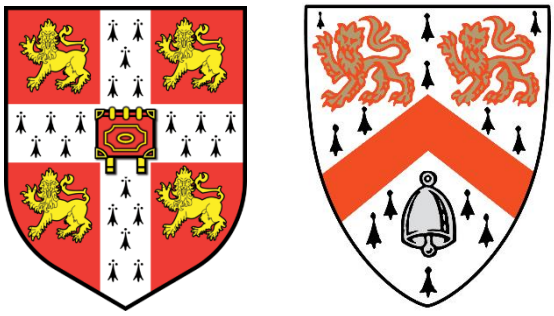

University of Cambridge

Wolfson College Cambridge

TAp73 regulates mitochondrial dynamics through an OPA1 axis

Submitted for the Degree of
Doctor of Philosophy

By

Niall Andrew Buckley BSc (Hons)

MRC Toxicology Unit

September 2022

Declaration

This thesis is the result of my own work and includes nothing which is the outcome of work done in collaboration. This thesis is not substantially the same as any work that has already been submitted before for any degree or other qualification, except as declared in the text. I further state that no substantial part of my thesis has already been submitted, or is concurrently submitted for any such degree, diploma or other qualification at the University of Cambridge or any other University of similar institution except as declared in the text. This thesis does not exceed the word limit set by the Degree Committee for the Faculty of Biology.

Niall Buckley

September 2022

Abstract

TAp73 regulates mitochondrial dynamics through an OPA1 axis

MRC Toxicology Unit, University of Cambridge, Gleeson Building, Tennis Court Road, Cambridge, CB2 1QR

Mitochondria are energy-producing organelles. They are highly adaptive and undergo the processes of fusion and fission to couple mitochondrial function with changing cellular demands. In this thesis, I have identified a new molecular mechanism involving TAp73/OPA1 that controls mitochondrial morphology (Buckley et al., 2020). OPA1 drives fusion of the inner mitochondrial membrane and controls cristae remodelling, a process facilitating the execution of apoptosis. I have shown that TAp73 regulates OPA1 expression in TAp73$^{-/-}$ cell lines which were generated using CRISPR/Cas9 targeting. Concurrently, I show that disruption of this TAp73/OPA1 axis results in a fragmented mitochondrial network owing to impaired mitochondrial fusion. Disruption of this axis also reduces the capacity for TAp73$^{-/-}$ cells to produce energy via oxidative phosphorylation. Further, the ectopic expression of OPA1 in TAp73$^{-/-}$ cells rescued defective mitochondria and restored bioenergetic function, placing OPA1 downstream of TAp73 in the regulation of mitochondrial dynamics.

Decreased expression of OPA1 also results in altered cristae structure in cellular and *in vivo* models with deletion of TAp73. Importantly, owing to the role of OPA1 in modulating cytochrome c release, TAp73$^{-/-}$ cells have an increased sensitivity to apoptotic cell death, e.g., on exposure to BH3-mimetics. Further, many cancers such as lung and colon have upregulated expression of TAp73 which is associated with poor survival outcomes. This raises the possibility that the TAp73/OPA1 axis may be hijacked in cancer to evade apoptotic cell death and increase energy production, thereby facilitating tumorigenesis and supporting a growth-promoting role of TAp73 isoforms.

This TAp73/OPA1 axis is also important in the respiratory system, owing to high levels of TAp73 expression in airway epithelial cells. Indeed, the correct ciliation of airway cells is severely perturbed in TAp73 null mice. I therefore propose that these profound defects in ciliogenesis may be driven by dysregulated mitochondrial function. This was highlighted by the fact that the airway epithelium of p73 null mice displayed downregulation of OPA1 and an altered morphology of the mitochondrial network in the ciliated cell lineage. Further, defective cilia have a reduced capacity for mucociliary clearance of inhaled toxic particles. Loss of TAp73 function and the concomitant increase in sensitivity to apoptosis may therefore further enhance vulnerability to inhaled pathogens or pollutants, highlighting a possible role for TAp73 in the incidence and progression of airway diseases such as COPD.

Acknowledgements

I would firstly like to thank my supervisors Prof. Marion MacFarlane and Dr. L. Miguel Martins for their support and mentoring. In particular, I am extremely grateful for the renewed impetus and guidance you have provided to me, as without this it would not have been possible to navigate through the COVID-19 pandemic, lab moves, and a change of supervisors. Moreover, your expertise has been extremely valuable for addressing questions that were not previously at the forefront of the project. I would also like to thank Dr. Mat Van de Pette and his lab group for kindly hosting me at the LMB for a short period after the first lockdown.

Thank you to Prof. Gerry Melino and Dr. Ivano Amelio the early conception of my project and for your supervision over the first year and three quarters of my PhD. Thanks also for your kind help and support, including with the use of existing reagents after you returned to Italy.

Moreover, I'm very grateful to have been able to benefit from input and support from such a long list of people from the different lab groups I have been a part of. I would particularly like to thank Dr. Emanuele Panatta for your guidance on experimental setup and the use of new lab equipment at the beginning of my PhD (even when the use of English was not as familiar!). I would also like to thank the wider members of the Melino group, and wish you and your young families all the best.

I would also like to extend a huge thank you to Dr. Lucia Pinon for your involvement in various experimental approaches, in particular your assistance with confocal microscopy and Incucyte experiments. To this end, I would like to thank Dr. Andy Craxton for your technical guidance, and also the time you devoted to the culture of my CRISPR cells when I was having to isolate due to COVID-19 infection! Thank you also to Dr. Xiao-Ming Sun for your help with Seahorse experiments. My project has also greatly benefitted from the input of the fantastic facilities staff in the Unit. Thank you to Cat Ficken for carrying out tissue sectioning and staining throughout almost the entire four years, and for doing do with a friendly willingness to help! Similarly, thank you do Dr. Nobu Morone and Dr. Jaime Llodre for your hard work and commitment when processing and imaging EM samples.

Finally, thank you to Emily, David, Tiago and Francesca for your friendship and support, particularly during the very busy period towards the end of the PhD. Last but not least, thank you to my parents for your support through my entire journey from undergraduate to doctoral student. I've lost track of the number of times you've had to ferry me and my possessions around!

Table of Contents

Declaration i
Abstract ii
Acknowledgements iii
Table of Contents iv
List of Figures viii
Abbreviations xi
Chapter 1: Introduction 1
1 Introduction 2
1.1 Shared structural and functional features of the p53 family 3
1.2 p73 splice isoforms 5
1.3 p53 Family regulation of apoptosis 6
1.3.1 Overview of apoptosis 6
1.3.2 Intrinsic apoptosis 7
1.3.3 BH3-Mimetics 9
1.3.4 Extrinsic apoptosis 10
1.4 DNA-damage independent roles of the p53 family 10
1.4.1 p73 is a central regulator of multiciliogenesis 12
1.4.2 p73 regulation of cell metabolism 14
1.5 Mitochondrial function 15
1.5.1 Mitochondrial structure 16
1.5.2 Mitochondrial DNA 17
1.5.3 Mitochondrial dynamics 18
1.5.4 Mitochondrial Fusion and fission 19
1.5.5 Mitochondrial biogenesis 21
1.6 Bioenergetics in eukaryotic organisms 22
1.6.1 Glycolysis 22
1.6.2 The Krebs cycle 23
1.6.3 The electron transport chain 24
1.6.4 Project aims 25
Chapter 2: Materials and Methods 27
2 Materials and Methods 28
2.1 Cell Culture 28
2.1.1 H1299 Cells 28
2.1.2 HEK-293T Cells 28
2.2 Transfection 28
2.3 Animals 29

2.3.1 *TP73*$^{-/-}$ mice 29
2.3.2 *Trp73*$^{\Delta 13/\Delta 13}$ mice 30
2.4 2.4 CRISPR/Cas9 TAp73 knockout generation 30
2.4.1 Transient Transfection 30
2.4.2 Doxycycline Inducible System 31
2.5 End-point PCR 31
2.5.1 PCR of TAp73 gene for screening of CRISPR clonal populations 31
2.5.2 TAp73 Exon 2 32
2.5.3 TAp73 Exon 3 32
2.5.4 RT-endpoint PCR on tracheal RNA 33
2.6 Mismatch Repair Assay 34
2.7 Sanger sequencing of CRISPR clones for INDEL characterisation 34
2.8 RT-qPCR 36
2.8.1 RNA isolated from mouse tracheal epithelial cells 36
2.8.2 RNA Isolated from cells 36
2.8.3 Reverse transcription and qPCR in 96-well plates 36
2.9 Chromatin Immunoprecipitation 37
2.10 Electron Microscopy 38
2.10.1 Scanning Electron Microscopy 38
2.10.2 Ultrathin Section Transmission Electron Microscopy 38
2.11 Western Blot analysis 38
2.12 Immunocytochemistry 40
2.12.1 Staining of mitochondrial network in fixed cells 40
2.12.2 Mitochondrial network measurements using intellesis trainable object segmentation 40
2.13 Immunohisochemistry on tissue sections 40
2.13.1 Immunofluorescence staining of cilia 40
2.13.2 Chromogenic detection 41
2.13.3 Multiplex Immunohistochemistry 41
2.14 Annexin V/APC measurement of cell death induction using Incucyte platform 41
2.15 Measurement of mitochondrial oxygen consumption 42
2.16 ChIP-seq Analysis 44
2.17 Gene Ontology Analysis 44
2.18 Statistical Analyses 44
Chapter 3: TAp73 regulates mitochondrial dynamics through an OPA1 axis 45
3 TAp73 regulates mitochondrial dynamics through an OPA1 axis 46
3.1 Introduction 46
3.1.1 Aims and Objectives 47
3.1.2 ChIP-seq data indicated TAp73 binding to the OPA1 promoter 48

3.2 Results 50
3.2.1 TAp73 and OPA1 expression correlate in H1299 cells 50
3.2.2 TAp73 regulates OPA1 expression and can bind to the putative OPA1 promoter 52
3.2.3 TAp73 knockout cell lines were generated using CRISPR/Cas9 targeting 55
3.2.4 Screening of clonal populations obtained by dilution plating 58
3.2.5 TAp73 Knockout cells have downregulated OPA1 protein expression 61
3.2.6 Ectopic Expression of TAp73α in TAp73 knockout cells rescues OPA1 expression 62
3.3 Discussion 64
3.3.1 TAp73 regulates OPA1 expression in H1299 cells 64
3.3.2 TAp73 regulates OPA1 expression, binds to the OPA1 promoter, and may modulate additional mediators of mitochondrial dynamics 65
Chapter 4: Disruption of a novel TAp73/OPA1 axis drives mitochondrial dysfunction 67
4 Disruption of a novel TAp73/OPA1 axis drives mitochondrial dysfunction 68
4.1 Introduction 68
4.1.1 Aims and Objectives 69
4.2 Results 69
4.2.1 Silencing of TAp73 leads to fragmentation of the mitochondrial network 69
4.2.2 TAp73 knockout cells have a fragmented mitochondrial network that is partially rescued by either TAp73 or OPA1 overexpression 72
4.2.3 TAp73 knockout decreases mitochondrial bioenergetic function in H1299 cells 77
4.2.4 The decreases mitochondrial bioenergetic function in TAp73 knockout cells was not driven by decreased mtDNA content or expression of ETC complexes 81
4.2.5 TAp73 knockout decreased basal and maximal ECAR 82
4.2.6 TAp73 knockout decreases cell proliferation and affects cell morphology 83
4.2.7 TAp73 knockout sensitises cells to apoptosis induced by BH3 mimetics 84
4.3 Discussion 87
4.3.1 TAp73 knockout drives fragmentation of the mitochondrial network 87
4.3.2 Disruption of the TAp73/OPA1 axis impairs mitochondrial bioenergetics 89
4.3.3 Expression of TAp73 determines sensitivity to the induction of apoptosis by BH3-mimetics 90
Chapter 5: The TAp73/OPA1 axis is functionally relevant in the ciliated epithelium 92
5 The TAp73/OPA1 axis is functionally relevant in the ciliated epithelium 93
5.1 Introduction 93
5.1.1 Aims and Objectives 93
5.2 Results 94
5.2.1 Multiciliated cells of the airway display defective cilia in $TP73^{-/-}$ mice 94
5.2.2 OPA1 expression is downregulated in $TP73^{-/-}$ ciliated epithelial cells 96
5.2.3 Mitochondria display a fragmented morphology in multiciliated cells of $TP73^{-/-}$ mice 99
5.2.4 $TP73^{-/-}$ ependymal cells display a reduction in size and an altered ultrastructure 99

5.2.5 The *TP73*$^{-/-}$ tracheal epithelium has an increased percentage of p63+ basal cells but they do not express TAp73 103

5.3 Discussion 105

5.3.1 Ciliated cells of the *TP73*$^{-/-}$ mouse airway display downregulated OPA1 expression and altered mitochondrial dynamics 105

5.3.2 Homozygous deletion of TP73 in mouse airway manifests as a late-stage defect in multiciliated cell differentiation 106

Chapter 6: The C-terminus of p73 is dispensable for multiciliogenesis 109

6 The C-terminus of p73 is dispensable for multiciliogenesis 110

6.1 Introduction 110

6.1.1 Aims and Objectives 111

6.1.2 *Trp73*$^{\Delta 13/\Delta 13}$ mice display an ectopic switch from p73α to p73β expression in tracheal epithelia 111

6.1.3 Airway multiciliogenesis is preserved in mice lacking p73α 112

6.1.4 Functional overlap of p73 C-terminal isoforms might underlie the preserved multiciliogenesis of Trp73$^{\Delta 13/\Delta 13}$ mice 113

6.1.5 Multiciliogenesis of brain ependymal cells is preserved in *Trp73*$^{\Delta 13/\Delta 13}$ mice 116

6.1.6 Trp73$^{\Delta 13/\Delta 13}$ mice do not show evidence of hydrocephalus 118

6.1.7 The *Trp73*$^{\Delta 13/\Delta 13}$ mouse tracheal epithelium does not display a reduction in OPA1 expression 119

6.2 Discussion 120

Chapter 7: Final Discussion 122

7 Final Discussion 123

7.1 Discussion 123

7.2 Future work 127

8 References 130

List of Figures

Figure 1.1 The conserved domain architecture of the p53 family. 4
Figure 1.2 The structure of the Trp73 gene and the identified splice isoforms 5
Figure 1.3 Apoptotic pathways. 7
Figure 1.4 Regulation of p53 family members during DNA damage-induced apoptosis 8
Figure 1.5 Mechanism of Action of BH3 mimetics, of which ABT-737 and S63845 were used in this study 9
Figure 1.6 A summary of the phenotypes of the global Trp73 and isoform-specific knockout mouse models 11
Figure 1.7 p73 induces the transcription of nearly 50 structural and functional ciliary genes 13
Figure 1.8 Schematic outlining the influence of p63 and p73 on metabolic pathways. 15
Figure 1.9 Structure of a mitochondrion 16
Figure 1.10 Structure of a mtDNA molecule 17
Figure 1.11 Mitochondria undergo fusion and fission to form highly dynamic networks. 18
Figure 1.12. OPA1 protein structure and splice isoforms 21
Figure 1.13 Schematic overview of glycolysis and mitochondrial respiration 23
Figure 1.14. Overview of the electron transport chain 24
Figure 2.1 Oxygen consumption rate (OCR) profile of a standard mitochondrial stress test 43
Figure 3.1 ChIP-seq data showed binding of TAp73α, TAp73β and p53 to regulators of mitochondrial fusion and fission. 51
Figure 3.2 Chromatin Immunoprecipitation (ChIP) of TAp73 bound regions was enriched for the OPA1 promoter 53
Figure 3.3 TAp73 expression correlates with OPA1 expression in H1299 cells **Error! Bookmark not defined.**
Figure 3.4 Gene Ontology (GO) analysis was performed on a complete set of TAp73 target genes identified through ChIP-seq. 54
Figure 3.5 Treatment of H1299 cells with 2.5 µg/µl puromycin induced cell death in non-transfected cells. 55
Figure 3.6 Mismatch repair assay performed on populations of cells transfected with Cas9 expression plasmid and gRNA. 56
Figure 3.7 Doxycycline-inducible CRISPR targeting of led to efficient knockdown of TAp73 57
Figure 3.8 The TAp73 was gene was successfully knocked out in CRISPR Clone 'G3:B4:C7' 59
Figure 3.9 TAp73 knockout was achieved using the doxycycline-inducible system in clone 'Dox3'. 60
Figure 3.10 TAp73 knockout cells have downregulated OPA1 expression. 61

Figure 3.11 The downregulation of OPA1 expression in TAp73 null cells is rescued by expression of TAp73α 63
Figure 4.1 H1299 cells treated with siRNA targeting TAp73 display fragmentation of the mitochondrial network, relative to control cells. 70
Figure 4.2 Intellesis automated segmentation module was used to quantify mitochondrial area and perimeter. 71
Figure 4.3 TAp73 KO cells display a fragmented mitochondrial phenotype which is partially rescued by expression of HA-TAp73α or OPA1. 75
Figure 4.4 Electron microscopy images TAp73 KO cells display a fragmented mitochondrial phenotype and alterations in cristae architecture. 76
Figure 4.5 Optimisation of seeding densities for mitochondrial stress test in H1299 cells. 78
Figure 4.6 TAp73 knockout decreases mitochondrial oxidative phosphorylation 79
Figure 4.7 Decreased mitochondrial bioenergetic function was not driven by depletion of mtDNA content or translation of ETC complexes 81
Figure 4.8 TAp73 KO induced a decrease in basal and maximal ECAR 82
Figure 4.9 TAp73 knockout supresses growth and alters the cell morphology of H1299 cells. 83
Figure 4.10 Inhibition of BCL-xL in combination with MCL-1 is required to induce cell death in H1299 cells. 85
Figure 4.11 TAp73 knockout sensitises H1299 cells to apoptosis induced by BH3 mimetics. 86
Figure 4.12 Stimuli of Mitochondrial Fragmentation. 88
Figure 5.1 TP73-/- mice display defective ciliogenesis in the airway epithelium 95
Figure 5.2 OPA1 expression is downregulated in the TP73-/- tracheal epithelium. 97
Figure 5.3 OPA1 expression was significantly downregulated in the ciliated cell lineage. 98
Figure 5.4 Ciliated epithelial cells of TP73-/- mice display altered mitochondrial morphology 100
Figure 5.5 3D reconstruction of the mitochondrial network in ciliated epithelial cells of Wild-type and Trp73$^{-/-}$ mice. 101
Figure 5.6 Ependymal cells of TP73-/- mice display altered mitochondrial morphology and ultrastructure. 102
Figure 5.7 Immunohistochemical staining of p63+ basal cell populations in wild-type and TP73-/- mice. 104
Figure 5.8. Reported roles of p73 in the multiciliated cell differentiation process. 107
Figure 6.1 Targeting strategy for the generation of Trp73$^{\Delta 13/\Delta 13}$ mice. 110
Figure 6.2 End-point PCR confirmed a switch in expression from p73α to p73β in tracheal epithelium. 112

Figure 6.3 Airway ciliogenesis is preserved in the absence of p73α in Trp73Δ13/Δ13 mice. 114

Figure 6.4 Trp73Δ13/Δ13 tracheal epithelia maintain expression of TAp73 and Foxj1. 115

Figure 6.5 Ciliation of Trp73Δ13/Δ13 ependymal cells is not affected despite the absence of TAp73. 117

Figure 6.6 Trp73$^{\Delta 13/\Delta 13}$ mice do not show enlargement of the lateral ventricles. 118

Figure 6.7 Trp73$^{\Delta 13/\Delta 13}$ mice maintain wild-type levels of OPA1 expression in trachea and cortex 119

Abbreviations

AA: Antimycin A

Acetyl-coA: Acetyl-coenzyme A

ADP: Adenosine diphosphate

ADOA: Autosomal dominant optic atrophy

ALI: Air-liquid interface

AMPK: AMP-activated protein kinase

APAF-1: Apoptotic protease activating factor-1

ATM: Ataxia Telangiectasia Mutated

ATP: Adenosine triphosphate

A.U: Arbitrary units

BAK: Bcl-2 homologous antagonist/killer

Bax: Bcl-2-associated X protein

Bcl-2: B-cell lymphoma 2

tBID: truncated BH3-interacting domain death agonist

BSA: Bovine serum albumin

Cas9: CRISPR associated protein 9

Caspase: Cysteine dependent aspartyl specific protease

CLL: Chronic lymphocytic leukaemia

CNS: Central nervous system

COPD: Chronic obstructive pulmonary disease

CoA: Coenzyme A

CoQ: Ubiquinone

Cox4i1: Complex 4 cytochrome C oxidase subunit 4

CR: Cajal-Retzius

CRISPR: Clustered regularly interspaced short palindromic repeats

CSF: Cerebrospinal fluid

DAPI: 4',6-diamidino-2-phenylindole

DISC: Death Inducing Signalling Complex

DMEM: Dulbecco's Modified Eagle's Medium

DMSO: Dimethyl sulfoxide

DNA: Deoxyribonucleic acid

DRP1: Dynamin-1-like protein

ECAR: Extracellular acidification rate

ER: Endoplasmic reticulum

ESC: Embryonic stem cell

ETC: Electron transport chain

EV: Empty vector

FACS: Fluorescence-activated cell sorting

FAD: Flavin adenine dinucleotide

FADD: Fas-associated protein with death domain

FBS: Foetal bovine serum

FCCP: Carbonyl cyanide-p-trifluoromethoxyphenylhydrazone

FIS1: Mitochondrial fission 1 protein

FOXJ1: Forkhead Box J1

G6P: Glucose-6 phosphate

G3P: Glycerol-3 phosphate

GAPDH: Glyceraldehyde 3-phosphate dehydrogenase

GLS2: Gutaminase type 2

GLUT: Glucose transporter

GTP: Guanosine triphosphate

H+: Protons

h: Hours

HEPES: 4-(2-hydroxyethyl)-1-piperazineethanesulfonic acid

HRP: Horseradish peroxidase

IMM: Inner mitochondrial membrane

MEF: Mouse embryonic fibroblast

MCC: Multiciliated cell

MDM2: Mouse double minute 2, human homolog

MFF: Mitochondrial fission factor

MFN-1: Mitofusin-1

MFN-2: Mitofusin-2

Min: Minutes

MOMP: Mitochondrial outer membrane permeabilization

MRC: Medical Research Council

mRNA: Messenger ribonucleic acid

MTEC: Mouse tracheal epithelial cell

mtDNA: Mitochondrial DNA

mTORC1: Mammalian target of rapamycin complex 1

NaCl: Sodium chloride

NADH: Nicotinamide adenine dinucleotide

NOXA: Phorbol-12-myristate-13-acetate-induced protein 1

O2- : Superoxide

OCR: Oxygen consumption rate

OMA1: OMA1 zinc metallopeptidase

OMM: Outer mitochondrial membrane

OXPHOS: Oxidative phosphorylation

OPA1: Optic atrophy-1

PAM: Protospacer adjacent motif

PBS: Phosphate-buffered saline

PFA: Paraformaldehyde

PPARGC1A: Peroxisome proliferator-activated receptor gamma coactivator 1-alpha

PPP: Pentose phosphate pathway

PUMA: p53 upregulated modulator of apoptosis

QH2: Ubiquinol

ROS: Reactive oxygen species

RPM: Revolutions per minute

SAM: Sterile alpha motif

SEM: Scanning electron microscopy

SDS: Sodium dodecyl sulphate

SVZ: Subventricular zone

TA: Transactivation

TBST: Tris-buffered saline with Tween-20

TEM: Transmission electron microscopy

Tris-HCl: Tris hydrochloride

Trp53: Tumour protein p53

Trp73: Tumour protein p73

ΔN: Dominant negative

Chapter 1: Introduction

1 Introduction

The transcription factor p73 is a structural and functional homolog of *TP53*, the most widely studied and frequently mutated tumor-suppressor gene (Logotheti et al., 2021). Following the discovery of the p53 gene, which has been known for over three decades, p73 and p63 were more recently identified in 1997 (Kaghad et al., 1997; Jost et al., 1997). Hence, the p53 family was formed due to their conserved function in the regulation of the DNA-damage response (Yang et al., 1998). On account of a common overall domain structure and a highly conserved DNA-binding domain, all three members of the family can induce cell-cycle arrest and cell death following DNA damage. However, they also have distinct mechanisms of regulation by upstream signaling pathways and post-translational modifications (Levine at al., 2011; Vikhreva et al., 2018).

Evolutionarily, a common ancestor of the p53 family is first detected in descendants of single cell choanoflagellates and the early metazoan sea anemone (Belyi et al., 2010). It is thought that this gene functioned to protect germ-line gametes from DNA damage, making this role over one billion years old (Belyi et al., 2010). In early vertebrates, the ancestral gene was duplicated to produce the p53 gene, which took on the function of protecting somatic stem cells and progenitor cells from DNA damage (Belyi et al., 2010; Ou et al., 2007). Thus, the p53 gene acquired a surveillance function in somatic cells that the ancestor performed in the germ line. As vertebrates developed, a second duplication event produced the p63 and p73 genes.

Although the p73 gene retained the ability to regulate the DNA-damage response, it took on its own unique roles including roles in development and tissue homeostasis (Yang et al., 2000). These have been elucidated through the study of p73 knockout mouse models and include roles in development of the nervous system (Yang et al., 2000; Dötsch et al., 2010), the control of metabolism (Nemajerova et al., 2018), spermatogenesis (Inoue et al., 2014), multiciliogenesis (Nejamerova et al., 2016) and angiogenesis (Amelio et al., 2015). The focus of my thesis has been to add to this body of work surrounding DNA-damage independent roles of p73, where I have uncovered a role in regulating mitochondrial dynamics through modulating the pro-fusion protein OPA1. This may provide a connecting mechanism for how p73 elicits control of metabolism and development, as the control of mitochondrial dynamics is inherent to these processes. This function also represents a growth-promoting role of p73 and may be relevant in tumorigenesis.

Indeed, although p53 is lost or mutated in about half of human cancers, the same is not true for p73 (Alonso et al., 2001; Ganini et al., 2021). On the contrary, certain p73 isoforms are overexpressed in a range of cancers and determine prognosis in various tumour types. These include non-small lung cancer (Mai et al., 1998), breast cancer (Dominguez et al., 2001), gliomas (Ugur et al., 2004) and several

other solid tumour types (Engelmann et al., 2015). It is therefore likely that this pattern of overexpression in human cancers represents an out of context activation of functions of p73 which are necessary for development and tissue homeostasis (Logotheti et al., 2021). However, these expression patterns contrast with studies in mice, which showed that the loss of specific p73 isoforms promote spontaneous lung adenocarcinomas and lymphomas (Tomasini et al., 2008). This demonstrates a highly ambiguous role for p73 in tumorigenesis which is likely to be dependent on isoform expression and the relevant interactome, including heteroligomerisation with other members of the p53 family (Vikhreva et al., 2018).

In this introduction, I firstly review the conserved structural elements of the p53 family. Following this, I introduce the canonical functions of the family in regulating cell death induction, which are found in both the extrinsic and intrinsic pathways of apoptosis. Next, I provide details of DNA-damage independent roles of p73, with a focus on metabolic functions and ciliogenesis, as multiciliated cells of the brain and airways were used a model to study the proposed axis between TAp73 and OPA1 *in vivo*. Finally, I outline the structure and function of the mitochondrion, including the regulation of mitochondrial dynamics and its importance for cellular function and tissue homeostasis.

1.1 Shared structural and functional features of the p53 family

The p53, p63 and p73 genes display a highly similar overall domain structure. Each member of the family is comprised of two different promoter sites, which either produce transcriptionally proficient isoforms containing a transactivation (TA) domain, or as N-terminally truncated isoforms that transcriptionally inactive (Nemajerova et al., 2018). These transcriptional isoforms are derived from promoters denoted 'P1' and 'P2' (figure 1.1). In the case of p73 and p63, the truncated proteins are referred to as ΔN isoforms (Collavin et al., 2010). Whereas for p53, the transcription deficient protein Δ40p53 is generated by a second start codon downstream of the P1 promoter, and Δ133p53 is generated by the P2 promoter. Importantly, evidence suggests that the ratio between TA domain containing, and dominant negative isoforms dictates the functional outcome of p53 family proteins (Levine et al., 2011).

In contrast with the low sequence homology of the TA domain between p53 family members, their DNA-binding domains (DBD) share high sequence homology (figure 1.1). As a result, studies have shown that each member of the family is able to recognize many of the same DNA-binding sites (Lokshin et al., 2007), such as those involved in the regulation of the DNA-damage response, cell cycle arrest and apoptosis. Moreover, a conserved oligomerization domain means that different family members and isoforms form hetereo-tetramers to compete for binding to DNA and regulate this shared transcriptional signature (Vikhreva et al., 2018).

Furthermore, the C-terminus of the p73 and p63 genes encode a functionally important sterile alpha motif (SAM) domain that is absent in p53. It is therefore likely to be responsible for the differential activities of p73 and p63 responsible for roles in mammalian development. To this end, the SAM domain facilitates protein-protein interactions regulating p73/p63 stability, localisation and transcriptional activity (Chi, et al., 1999). Indeed, deletion of the p63 SAM domain has been shown to recapitulate features of a global p63 deletion in mouse models (Lena, et al., 2021). However, the mechanistic importance of the SAM domain for the unique functions of p73 remain poorly understood. To address this problem, a mouse model was generated with a deletion of a C-terminal region of the p73 *Trp73*$^{\Delta 13/\Delta 13}$, thereby abrogating SAM domain function (Buckley et al., 2020; Amelio et al., 2020). Interestingly, the phenotype of these mice revealed that the SAM domain is in fact dispensable for some of the developmental processes regulated by p73, with these data presented in chapter 6 (Buckley et al., 2020).

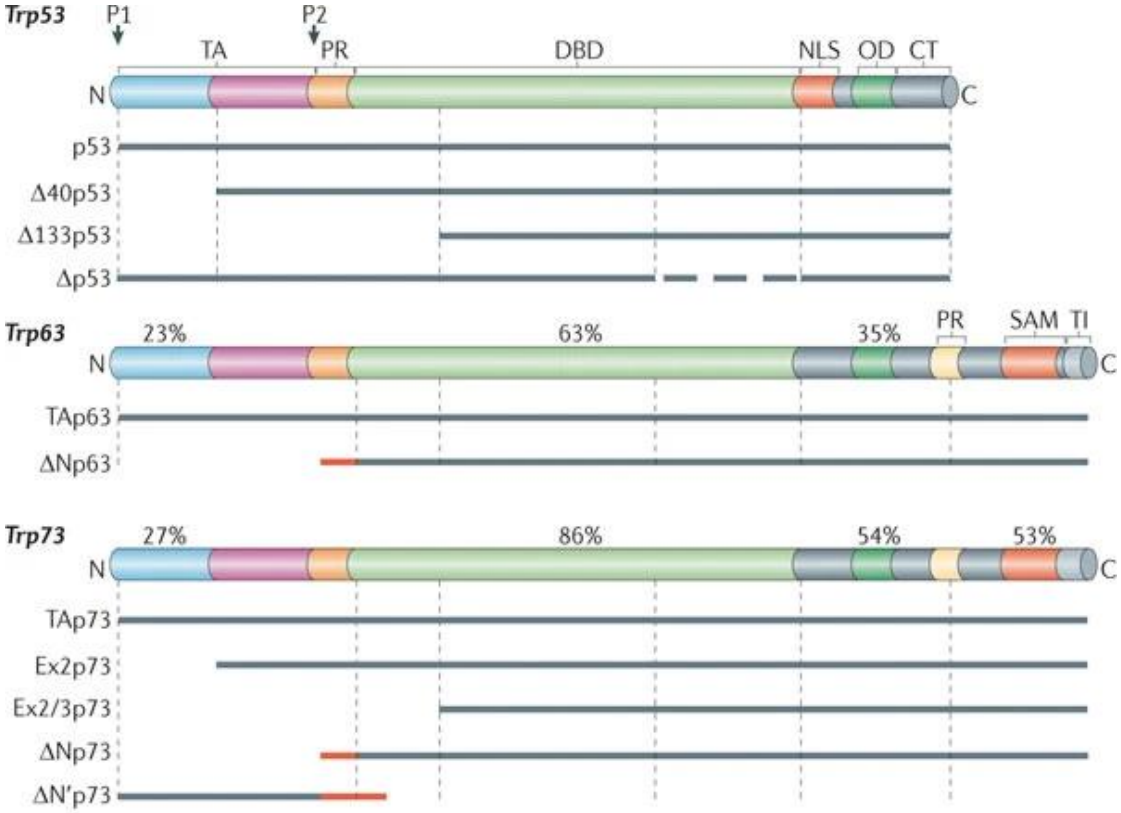

Figure 1.1 The conserved domain architecture of the p53 family.

The genes encoding p53, p63 and p73 are transcribed as distinct protein isoforms from two alternate promoters (P1 or P2). TA; transactivation domain, DBD; DNA-binding domain, NLS; nuclear localization signal, OD; oligomerization domain; PR; Pro domain, SAM; sterile alpha motif, TI; transcription inhibitory domain. The *Trp63* gene DBD has 63% sequence identity with p53 DBD. Similarly, the Trp73 DBD has 86% identity with that of *Trp63* (Levine at al., 2011).

1.2 p73 splice isoforms

In addition to isoform generation through transcription at alternative promoters, p73 transcripts have the potential for extensive alternative splicing. This has resulted in the identification of a number of different p73 transcripts (Murray-Zmijewski, et al., 2006). However, it is an open question as to whether many of these splice forms are expressed at the protein level (Vikhreva et al., 2018). The *TP73* gene is located on the short arm of chromosome 1 (1p36.33), and is comprised of 15 exons (Kaghad, et al., 1997). Alternative splicing of exons 11, 12 and 13, yields an additional 7 so far identified C-terminal isoforms each of which may or may not contain the TA domain (figure 1.2) (Vikhreva, et al., 2018). The SAM domain is encoded in exons 11-13, and TAp73α is the only transcriptionally active isoform to contain a functional SAM domain. This is because the alternative splicing generating p73β, p73γ, p73δ and p73η isoforms produces an alternative reading frame, thus leading to a premature stop codon (Vikhreva et al., 2018). Although extensive RNA-seq has revealed that TAp73α is the most abundantly expressed p73 isoform in a wide range of tissues tested in mouse and human, the reported data were indicative of a tissue specific role of specific C-terminal isoforms (Marshall et al., 2021). Taken together this highlights the need for a spatio-temporal analysis of p73 C-terminal isoform expression in development and tumorigenesis to fully elucidate the precise relevance of C-terminal splicing events (Vikhreva et al., 2018)

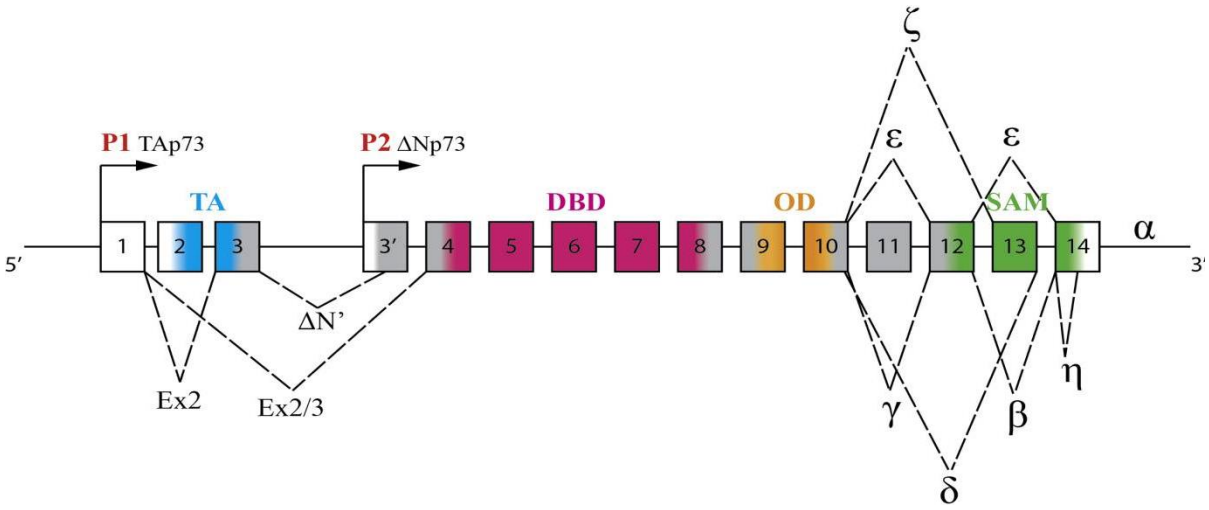

Figure 1.2 The structure of the *TP73* gene and the identified splice isoforms

(a) The *TP73* gene is comprised of 15 exons (dotted lines). TAp73α is both the most abundantly expressed and the only isoform to express a functional SAM domain. Adapted from Vikhreva et. al., (2018).

1.3 p53 Family regulation of apoptosis

p53 and p73 are activated in response to a variety of genotoxic agents that cause DNA damage, and in response oncogenes such as *E1A* and *myc* (Zaika et al., 2001). Indeed, activated p73 regulates the induction of apoptosis and cell cycle arrest in a manner highly similar to p53. This is evidenced by the ability to transcriptionally activate pro-apoptotic genes which are also p53 targets. However, the identified repertoire of apoptosis signalling molecules regulated by p53 is much more extensive (Pietsch et al., 2008). In this section I summarise the extrinsic and extrinsic pathways of apoptosis and provide details of the mechanisms of regulation by p73 and p53.

1.3.1 Overview of apoptosis

The term apoptosis was first used by Kerr, Wyllie and Currie in 1972 to describe a programmed and morphologically distinct type of cell death (Kerr et al., 1972). The initiation of apoptosis is dependent on the sequential activation of cysteine-aspartic proteases known as caspases (D'Arcy 2019). These fall into two categories, the initiator caspases and the executioner caspases (Elmore, 2007). Following the detection of cell damage, inactive initiator procaspases (procaspases 8 and 9) are cleaved by autocatalysis and activated (Lavrik et al., 2003). Once activated, initiator caspases activate the executioner caspases (caspases 3, 6 and 7) by proteolytic cleavage (figure 1.3). The activity of executioner caspases subsequently initiates a cascade of events that results in DNA fragmentation, destruction of the nuclear proteins and cytoskeleton, protein crosslinking, and the expression of ligands for phagocytic cells (Martinvalet et al., 2005; Poon et al., 2014). During apoptosis, dead or dying cells can be removed by macrophages (Elmore, 2007), and the inhibition of secretion of pro-inflammatory cytokines prevents unwanted immune cell activation (McArthur & Kile; 2020). This contrasts with necrosis, which releases pro-inflammatory mediators and leads to rapid leukocyte infiltration (McArthur & Kile; 2020). However, there are exceptions to this rule as prototypical death receptor activation has been shown to stimulate a strong inflammatory response (Faouzi et al., 2001).

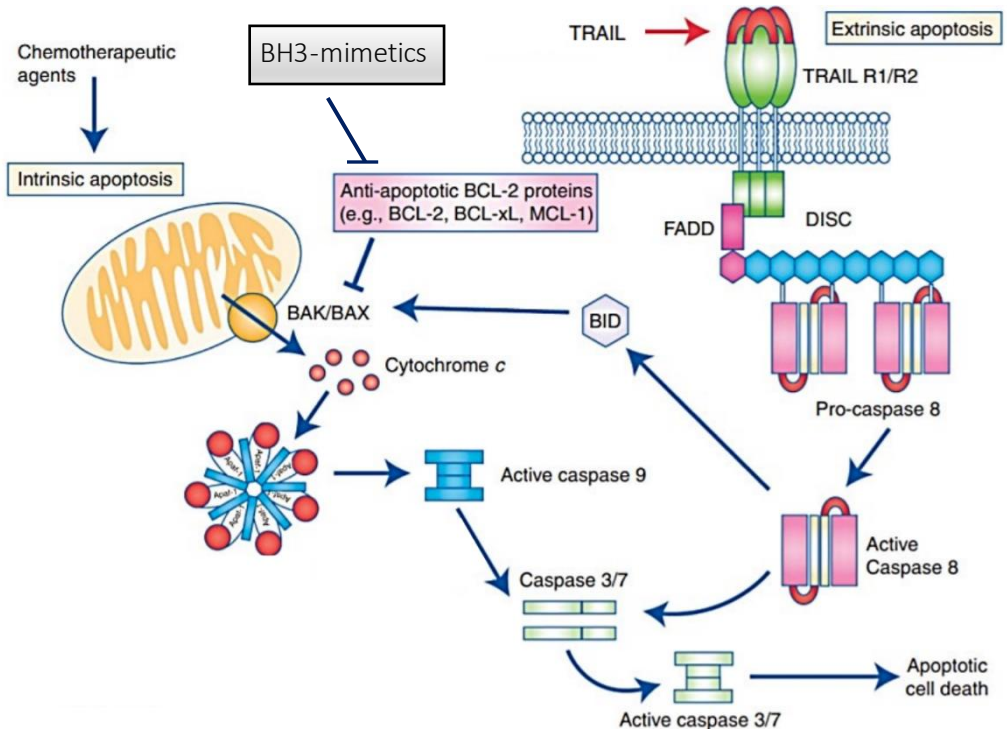

Figure 1.3 Apoptotic pathways.

Intrinsic and extrinsic pathways of apoptosis. Both converge on the activation of the executioner caspases 3 and 7 to cleave specific intracellular proteins and induce cell death (modified from Fox and MacFarlane, 2016).

1.3.2 Intrinsic apoptosis

The intrinsic apoptosis pathway is initiated by various stimuli such as DNA damage (including that induced by chemotherapeutic agents), viral infection (Nainu et al., 2017), and ROS accumulation (Aggarwal et al., 2019). These stress signals lead to the activation of p53 and p73, albeit through differing mechanisms (Melino et al., 2004; Blandino & Dobbelstein, 2004; figure 1.4).

In steady-state conditions, p53 activity is inhibited by the ubiquitin ligase MDM2, which targets p53 for proteasomal degradation (Haupt et al; 1997). Following different types of DNA damage, protein kinases such as ATM phosphorylate MDM2 and p53, thereby modifying this interaction and leading to an increase p53 levels (Saadatzadeh et al., 2017). However, steady-state levels of p73 are not controlled by complex formation with MDM2 (Dobbelstein et al., 1999). Instead, the stabilisation of p73 appears to occur predominantly through the activity of c-Abl, another tyrosine kinase that is activated in response to DNA damage and ITCH, an E3 ubiquitin ligase (Agami et al., 1999; Rossi et al., 2005) (figure 1.4).

The stabilisation of p53 and p73 is also accompanied *via* modification by a multitude of other enzymes, resulting in phosphorylation, acetylation, methylation, ubiquitination and sumolation (Apella and Anderson; 2001), some of which are indicated in figure 1.4. It therefore appears that the specific type

of DNA-damage that occurs determines the set of modifications to fine tune the activies of p53 and p73, which ultimately modulate the stress response (Colman et al., 2010).

The transcriptional activity of the p53 family elicits an upregulation of the expression of BCL-2 family proteins such as PUMA and NOXA (Shibue at al., 2006). Collectively, these proteins are referred to as 'BH3-only' proteins (Youle and Strasser, 2008). Following their upregulation, BH3-only proteins associate with diverse pro-survival proteins of the BCL-2 family, such as Bcl-2 and Mcl-1, which are located on the outer surface of mitochondria (Giam et al., 2008). The resulting sequestration of these anti-apoptotic proteins prevents their inhibition of Bax and Bak, which are then able to oligomerise and induce mitochondrial outer membrane permeabilisation (MOMP). This results in the release of cytochrome *c* and other soluble proteins such as Smac and Diablo into the cytosol (Saelens et al., 2004). There, cytochrome c interacts with apoptotic protease activating factor-1 (APAF-1), leading to the formation of the 'apoptosome' (Chinnaiyan, 1999, Fox and MacFarlane, 2016). This heptameric complex then activates the cascade of caspase activation, culminating in apoptotic cell death.

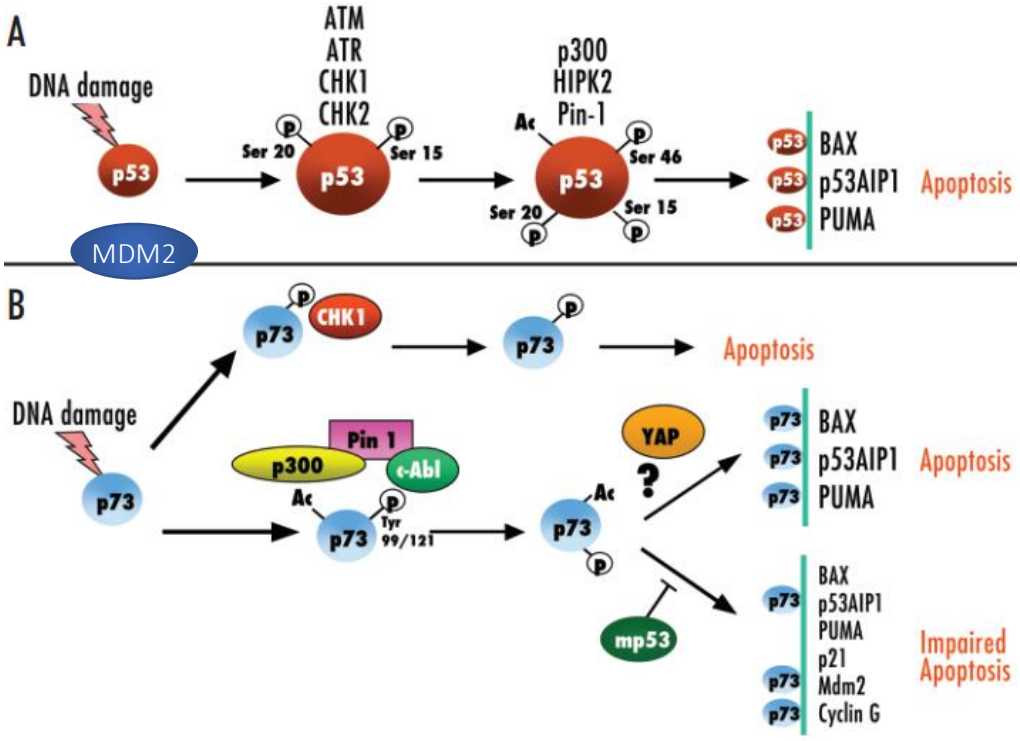

Figure 1.4 Regulation of p53 family members during DNA damage-induced apoptosis

(a,b) In response to DNA damage, p53 and p73 are stabilized, phosphorylated, and acetylated. These post-translational modifications result in the potentiation of p53 family mediated apoptosis. (b) Both c-Abl-mediated tyrosine phosphorylation of p73 and the recruitment of selective coactivators define the selectivity of p73-mediated apoptosis. Mutant p53 can act as an inhibitor of p73 through heterooligomer formation (modified from Blandino & Dobbelstein, 2004).

1.3.3 BH3-Mimetics

As a tool for inducing apoptosis in TAp73 knockout cells in this study, I have employed the use of a class of compounds known as BH3-mimetics. These compounds bind to the hydrophobic groove of the pro-survival BCL-2 family members (indicated in figure 1.5a), thereby releasing BH3-only proteins to activate downstream effectors of apoptosis (figure 1.5b). These compounds therefore allowed me to interrogate sensitivity to apoptosis downstream of DNA damage or extrinsic stimuli (figure 1.3).

Clinical trials using BH3-mimetics have shown promising findings for the treatment of blood cancers such as CLL (Merino et al., 2018). However, studies have also shown that ABT-737 and navitoclax induce on-target death of platelets, immature lymphoid cells, and several other BCL-XL-dependent cell types (Mason et al., 2007; Merino et al., 2012). Furthermore, the clinical efficacy of treatment with single agent BH3 mimetic commonly has been limited by primary and secondary mechanisms of resistance (Diepstraten et al., 2022).

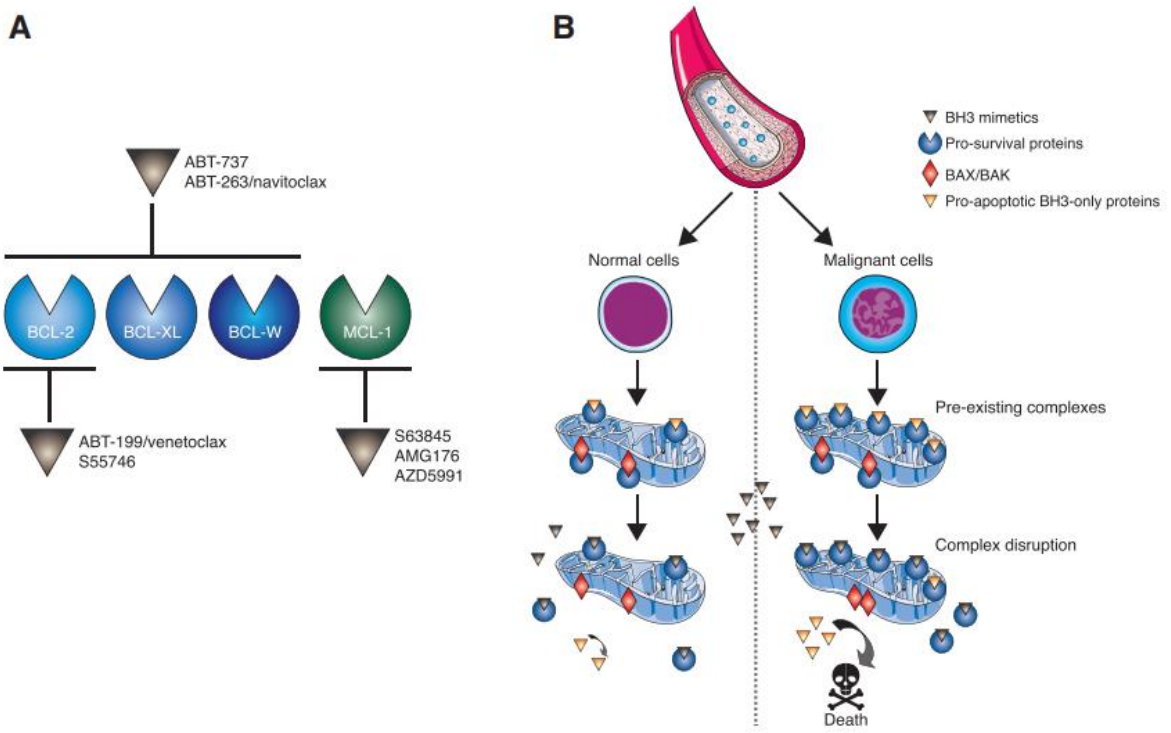

Figure 1.5 Mechanism of Action of BH3-mimetics, of which ABT-737 and S63845 were used in this study

(a) BH3-mimetics target the indicated pro-survival BCL-2 family members. (b) The increased abundance of pro-survival BCL-2 family member and BH3-only protein complexes results in an increased sensitivity of cancer cells to BH3-mimetic drugs. The release of sequestered BH3-only proteins lead to the activation of the effectors of apoptosis, BAX and BAK (Merino et al., 2018).

1.3.4 Extrinsic apoptosis

Apoptosis can also be induced by the activation of specific membrane receptors, for example through TNF-related apoptosis-inducing ligand (TRAIL) binding to TNF-related apoptosis-inducing ligand receptor 1 and 2 (TRAIL-R1/TRAIL-R2) (Fox and MacFarlane, 2016; figure 1.3). This leads to the recruitment of Fas-associated protein with death domain (FADD), which exposes its N-terminal DED domain. The activated death receptor and FADD complex provides a platform for the recruitment of multiple caspase 8 molecules via interactions of their own DED domains. The multiprotein structure produced is known as the death inducing signalling complex (DISC), which facilitates the cleavage of procaspase 8 to the active caspase molecules. Like the intrinsic apoptosis pathway, these active initiator caspases subsequently activate the executioner caspases 3 and 7, leading to cell death (Tummers and Green, 2017, Dickens et al., 2012).

The proteins p53 and p73 are also able to regulate the extrinsic apoptosis pathway. Indeed, p53 directly influences sensitivity of the extrinsic pathway by transcriptionally regulating death receptor expression (Müller et al., 1998), although this regulation is not essential for receptor-mediated cell death (Aubrey et al., 2017). Furthermore, both p53 and p73 are cleaved by caspases 3 and 8 downstream of TRAIL receptor activation (Sayan et al., 2006; Sayan et al., 2008). Cleaved fragments of p53 and p73 directly associate with the surface of the mitochondrion, where they modulate MOMP and cytochrome *c* release, thereby providing a link with the intrinsic pathway (Sayan et al., 2006).

1.4 DNA-damage independent roles of the p53 family

Unique to p73 and p63 are their defined roles in DNA-damage independent processes. Whilst p63 has been strongly implicated in epidermal development (Mills, et al., 1999), mice with a deleted p73 gene (p73 KO) are characterised by a diverse phenotype. This includes chronic infections, inflammation, infertility and a severe brain phenotype which entails defective dentate gyrus architecture, reduced cortical thickness, ventriculomegaly, and a reduced proliferative capacity of neural stem cells (Agostini, et al., 2010; Gonzalez-Cano, et al., 2016; Fujitani, et al., 2017; Yang, et al., 2000). They are also characterised by defective ciliogenesis, which is one of the focuses of my work (Marshall, et al., 2016; Nemajerova, et al., 2016). As a result of these abnormalities, 80% of p73 deficient mice do not survive to adulthood (Yang, et al., 2000).

As mice with a global deletion of the p73 gene are targeted through an insertion that abrogates function of the DNA-binding domain, they lack both the TAp73 and ΔNp73 isoforms. Therefore, using this model, it is not possible to delineate the specific functions of transcriptional isoforms of p73. To address this

question, mice have been generated that have a depletion of either the TAp73 or ΔNp73 isoforms (Tomasini et al., 2008, Wilhelm et al., 2010). It has been reported previously that mice lacking TAp73 isoforms (TAp73$^{-/-}$ mice) are infertile, show a high incidence of spontaneous tumours, and are very sensitive to chemical carcinogens (Tomasini et al. 2008). Importantly, this work demonstrated that in this setting TAp73 is a bona fide tumor suppressor, which was significant as mice lacking all isoforms did not appear to be tumour prone (Wilhelm et al., 2010; Yang et al., 2000). Taken together, this suggested that the balance between TAp73 and ΔNp73 isoforms is crucial for influencing tumour progression, and their opposing functions may explain why TAp73$^{-/-}$ mice develop spontaneous tumours but *TP73*$^{-/-}$ mice do not (Rufini et al., 2011).

It was also notable that TAp73$^{-/-}$ mice have a less severe phenotype than that displayed by mice with a global *TP73* deletion. Indeed, TAp73$^{-/-}$ mice (but not ΔNp73$^{-/-}$) exhibit the same hippocampal dysgenesis as global *TP73* KO mice (figure 1.6), but do not display alterations in ventricles of the brain or cortical thickness (Fujitani et al., 2010). Moreover, the fact neither TAp73$^{-/-}$ or ΔNp73$^{-/-}$ mice display elements of the brain phenotype observed in Trp73$^{-/-}$ mice, such as reduced cortical thickness, highlights how isoforms must function in a cooperative manner (Wilhelm et al., 2010). However, these studies also highlight how the role of p73 in regulating hippocampal development is dependent on TAp73 isoforms. Together, these studies are indicative of a highly complex and tissue specific functions of p73 isoforms in mammalian development, which I addressed in this thesis through the investigation of mice with a specific deletion of TAp73α isoforms (Buckley et al., 2020; Amelio et al., 2020).

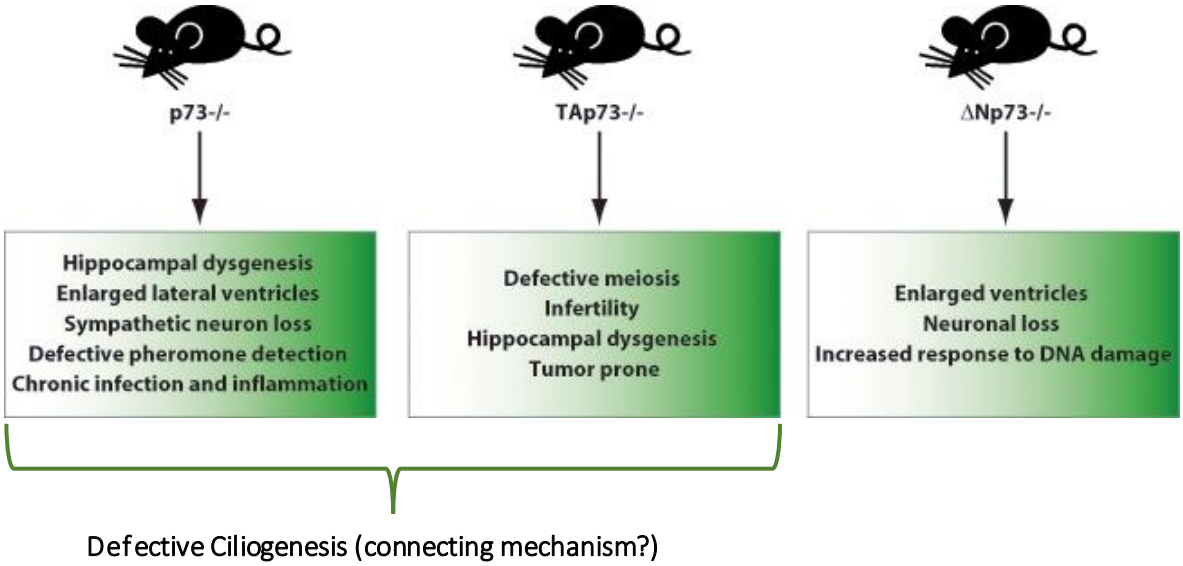

Figure 1.6 A summary of the phenotypes of the global Trp73 and isoform-specific knockout mouse models

Following the generation of mice with a global Trp73 knockout, mouse models specifically lacking TAp73 and ΔNp73 isoforms were generated, each displaying a different set of phenotypes (Adapted from Rufini et al., 2011).

1.4.1 p73 is a central regulator of multiciliogenesis

It was reported simultaneously by two independent groups that TAp73 expression is essential for motile ciliogenesis (Marshall et al., 2016; Nemajerova et al., 2016). As many of the tissues and organs affected require functional multiciliated cells (MCCs), it has been proposed that loss of ciliary function is a connecting mechanism for the diverse phenotype of p73 knockout mice, and so this work is reviewed here in detail (Marshall et al., 2016).

Cilia are microtubule-based structures positioned on the apical surface of almost every cell (Malicki & Johnson, 2017). There are two types of cilia, the non-motile or 'primary' cilium and motile cilia, which have different functions. A single primary cilium is present on most vertebrate cells and is responsible for signal transduction from the environment or other cells, such as those found on photoreceptor cells or olfactory neurons (Mitchison & Valente, 2017). Motile cilia, on the other hand, are present in large numbers on specialised, post-mitotic multiciliated cells (MCCs) responsible for the movement of extracellular fluids or the propulsion of cells (such as sperm) (Mitchison & Valente, 2017; Spassky & Meunier, 2017). The dysfunction of these extracellular structures has been implicated in a number of human diseases, collectively termed ciliopathies (Fliegauf, et al., 2007).

The process of multiciliogenesis is driven by a post-mitotic endocycle whereby modified centrioles, termed basal bodies (BBs), are amplified in large numbers through the activity of the master centriolar regulators Plk4 and Myb (Choksi, et al., 2014; Tan, et al., 2013). They then migrate to the apical surface and dock at the plasma membrane where they nucleate the formation of microtubule-based structures, a process which is dependent on p73 (Nemajerova, et al., 2016; Marshall, et al., 2016). It has been shown that p73 induces the transcription of a suite of ciliogenesis genes by binding to promoter and/or enhancer regions of essential regulators including *FOXJ1*, *Rfx2*, *Rfx3* and *miR34bc* (Figure 2) (Nemajerova, et al., 2016).

Two independent groups, led by Moll and Pietenpol (2018), simultaneously showed that genetic ablation of both global p73 and TAp73 in respiratory epithelia prevents the formation of functional cilia. The studies showed that mice deficient for these proteins can commit to the epithelial cell fate from p63+ epithelial progenitor cells and amplify their centrioles, however they are unable to dock at the apical surface. Consequently, they possess very few appendages. Those that are present are drastically reduced in length, indicative of a defect in the ability to nucleate or extend microtubules. p73 deficient epithelial cells therefore have a severely impaired ability to move extracellular fluids. It is therefore clear that p73 therefore acts downstream of ciliated cell lineage commitment and centriole amplification (Tan, et al., 2013). This information was combined with an RNA-seq approach, adopted

independently by the two groups in mouse tracheal epithelial cells (MTECs) to place p73 at the centre of the ciliogenesis gene regulatory network.

The comparison of gene expression profiles from MTECs with either wild-type or deleted p73 indicated that p73 was responsible for the differential expression (DE) of around 50 genes necessary for ciliary formation and motility. Moreover, the DE were largely associated with later-stage ciliogenesis genes, thereby confirming the observation that p73 acts downstream of Notch-mediated fate speciation of p63+ epithelial progenitors and subsequent centriole amplification to orchestrate the ciliogenesis gene network (Nemajerova, et al., 2016; Marshall, et al., 2016).

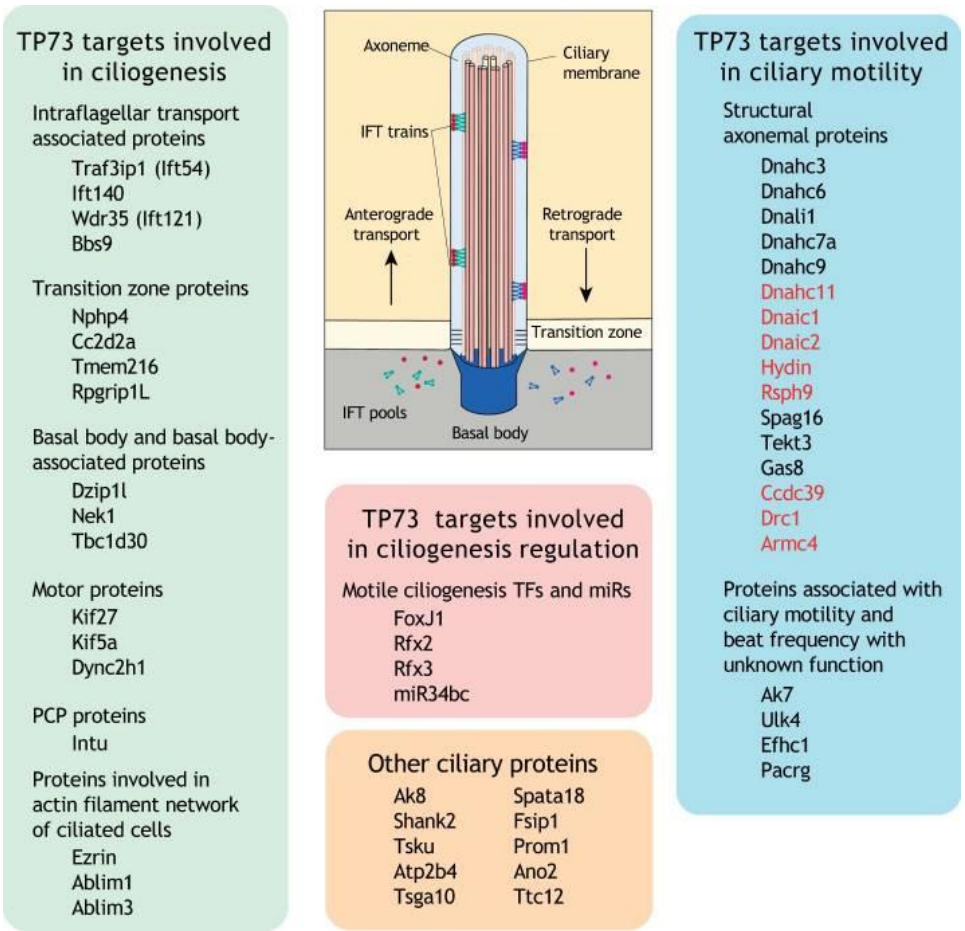

Figure 1.7 p73 induces the transcription of nearly 50 structural and functional ciliary genes

ChIP-seq data showed p73 binding in promoter and/or enhancer regions of the essential regulators ciliogenesis, including *FOXJ1, Rfx2, Rfx3* and *miR34bc*. A number of the TAp73 targets have also been associated with human ciliopathies (Nemajerova et al., 2018).

1.4.2 p73 regulation of cell metabolism

Multiple groups have identified a direct influence of p73 on cellular metabolism, which includes the regulation of key metabolic enzymes, mitochondrial oxidative phosphorylation and authophagy (Nemajerova et al., 2018; figure 1.8). As a result, *In vivo* and *in vitro* deletion of p73 reduces ATP levels, oxygen consumption and mitochondrial complex IV activity with a subsequent enhancement of the production of ROS, the latter of which accelerates aging in TAp73 $^{-/-}$ mice (Agostini et al., 2014; Rufini et al., 2012). Indeed, p73 binds and regulates the promoter of the mitochondrial complex 4 cytochrome C oxidase subunit 4, Cox4i1 (Rufini et al., 2012). Additional molecular mechanisms by which p73 regulates mitochondria and general metabolism operate through the direct transcriptional control of glutaminase type 2 (GLS2) (Velletri et al., 2013), the regeneration of glutathione (Niklison-Chirou et al., 2017), and the synthesis of serine (Amelio et al., 2014) (figure 1.8).

The significance of TAp73 mediated regulation of these metabolic pathways is an interesting topic of debate. At first glance, it seems that the upregulation of target genes such as *GLS2* are implicit of a growth promoting role of TAp73, as enhanced *GLS2* activity increases mitochondrial respiration and ATP generation (Hu et al., 2010). However, these roles in growth promotion are in opposition with the established dogma that classifies TAp73 as a tumour suppressor gene (Tomasini et al., 2008). Therefore, it was instead hypothesized that the overarching importance of TAp73 regulation of glucose catabolism, serine biosynthesis and the pentose phosphate pathway (PPP) is to facilitate the antioxidant response through increased GSH synthesis, thus in keeping with a tumour suppressive function (Nemajerova et al., 2018).

However, recent evidence has also shown that TAp73 regulates the expression of phosphofructokinase-1 (PFKL), the rate limiting enzyme in the glycolysis pathway (Li et al., 2018). Through this direct transcriptional regulation, TAp73 enhances glucose consumption and lactate excretion and promotes the Warburg effect. Crucially, the authors also showed TAp73 deficiency results in a pronounced reduction in tumorigenic potential of different cancer cell lines, which can be rescued by ectopic PFKL expression (Li et al., 2018). These findings therefore place TAp73 as a critical regulator of glycolysis and highlight a mechanism by which tumor cells facilitate the Warburg effect to enable oncogenic growth (Li et al., 2018). Such growth promoting roles of TAp73 suggest that the classification of TAp73 isoforms as tumour suppressor genes is an oversimplification. Furthermore, these findings are consistent with data presented in this thesis, which suggest that TAp73 positively regulates metabolism through the regulation of the mitochondrial fusion protein OPA1 (indicated in figure 1.8). It is also possible that the regulation of cellular metabolism by TAp73 is linked with its necessary function in the execution of ciliogenesis (Nemajerova et al., 2018).

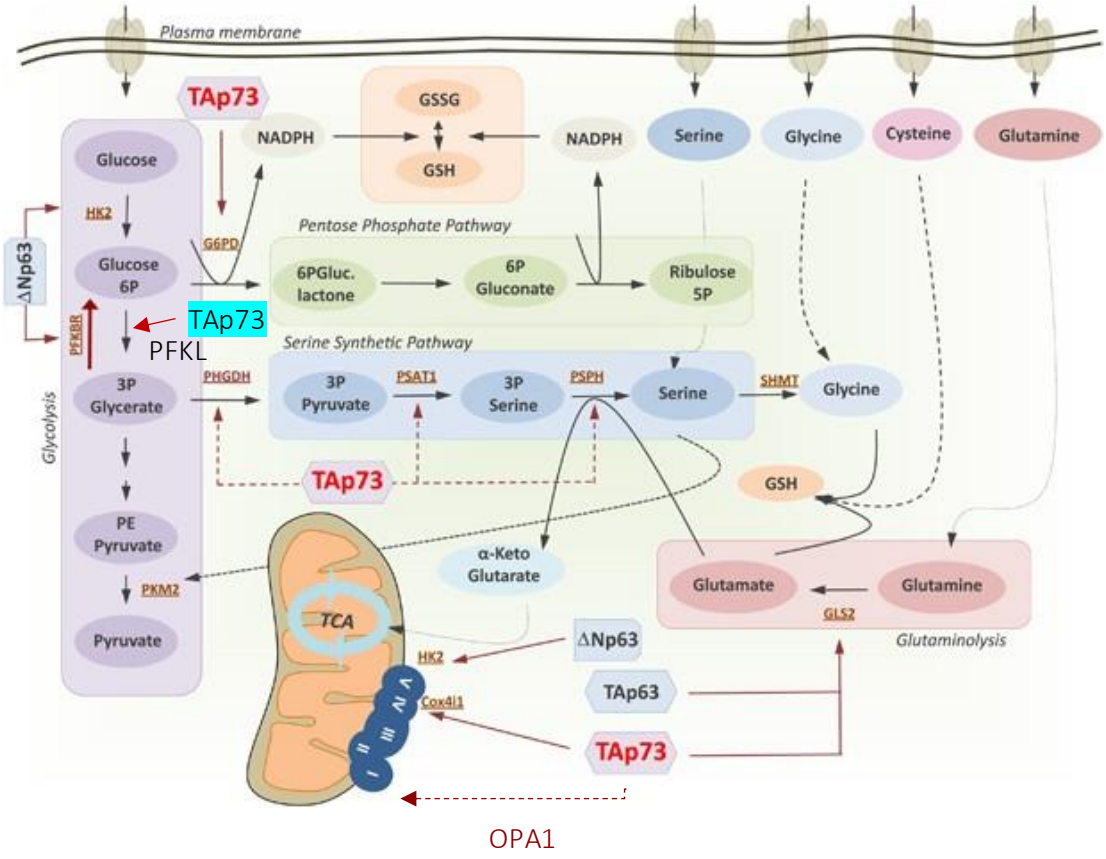

Figure 1.8 Schematic outlining the influence of p63 and p73 on metabolic pathways.

p73 promotes an increase in glucose catabolism and diverting anabolic pathways. P73 also regulates mitochondrial OXPHOS through the regulation of *Cox4i1*. Overall, the impact of p53 family members on cellular metabolism appears to be a critical process for maintaining the cellular redox balance (Adapted from Nemajerova et al., 2018).

1.5 Mitochondrial function

Phylogenetic analysis of conserved ribosomal RNA (rRNA) supports the notion that the mitochondrion originated from free living bacteria that were incorporated into an archeal cell by endocytosis, thereby supporting multicellular life (Gray et al., 2008; Margulis, 1970). The mitochondrion has a number of functions, which include ATP production through oxidative phosphorylation, the regulation of apoptosis, calcium signalling, cellular differentiation and regulation of the immune response (Brand et al., 2013; Bock and Tait, 2020 Tait & Green; 2012).

1.5.1 Mitochondrial structure

Mitochondria are dynamic structures which possess two distinct membranes: the outer and inner mitochondrial membranes (OMM and IMM; Figure 1.6). A diverse family of proteins known as porins are found inserted in the OMM, where they regulate the transport of metabolites and nucleotides between the mitochondrial matrix and the cytoplasm. For example, the voltagedependent anion channel (VDAC) is the most abundant protein on the OMM and is integral for regulating mitochondrial function (Tomasello et al., 2013). In addition, the OMM contains the Bcl-2 family proteins (Gillies and Kuwana, 2014). By contrast, the IMM is impermeable to most substrates, except for those being transported via specific carrier proteins (Kunji, 2004). This is essential for the maintenance of chemical and electrical gradients, which is necessary for oxidative phosphorylation. Indeed, this membrane contains specific respiratory proteins that comprise the electron transport chain (ETC), introduced in section 1.6.3. Large sections of the inner membrane are densely folded into cristae, which serve to increase the surface area of the IMM and enhance the activity of respiratory chain complexes (Cogliati et al., 2013).

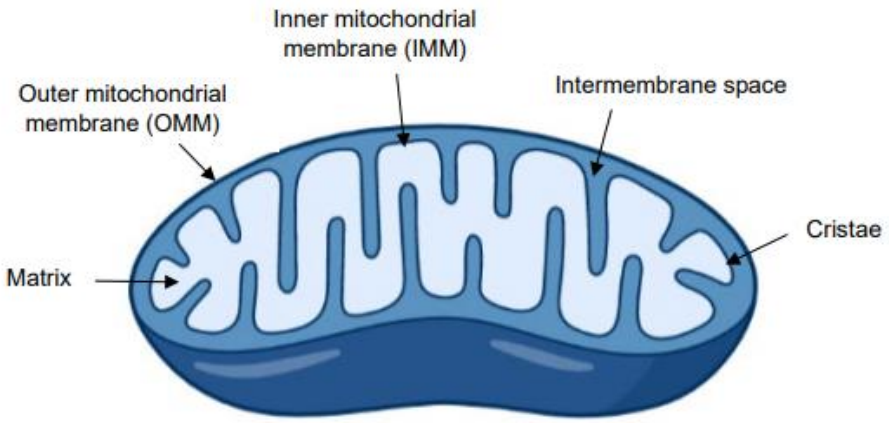

Figure 1.9 Structure of a mitochondrion

Most cells in eukaryotic organisms contain mitochondria, as they produce the vast majority of cellular ATP. Mitochondria are doublemembraned and contain two aqueous compartments: the intermembrane space and mitochondrial matrix. The IMM is densely folded into cristae, to increase the efficiency of ATP production. Created with BioRender.com.

1.5.2 Mitochondrial DNA

Mitochondria contain within the matrix a distinct, double-stranded circular genome that encodes 13 subunit proteins of the ETC, mitochondrial transfer RNAs (tRNAs) and ribosomal RNAs (rRNAs) (Figure 1.7) (Anderson et al., 1981). Each of the protein subunits encoded by mtDNA in humans are incorporated into ETC complexes I, III, IV, V, with the remainder encoded by nuclear DNA (Olgun and Akman, 2007). As a result protein synthesis of the ETC must be highly coordinated between nuclear DNA and mtDNA. This is facilitated by translocation of key metabolites, enzymes, and proteins between the nucleus and mitochondria (Wiese and Bannister, 2020). A growing body of evidence indicates that mtDNA mutations are involved in ageing, metabolic and neurodegenerative diseases, and cancer (Lawless et al., 2020). Often, mutations only affect a proportion of mtDNA molecules within the total mitochondrial pool, in a phenomenon known as heteroplasmy (Stefano et al., 2017).

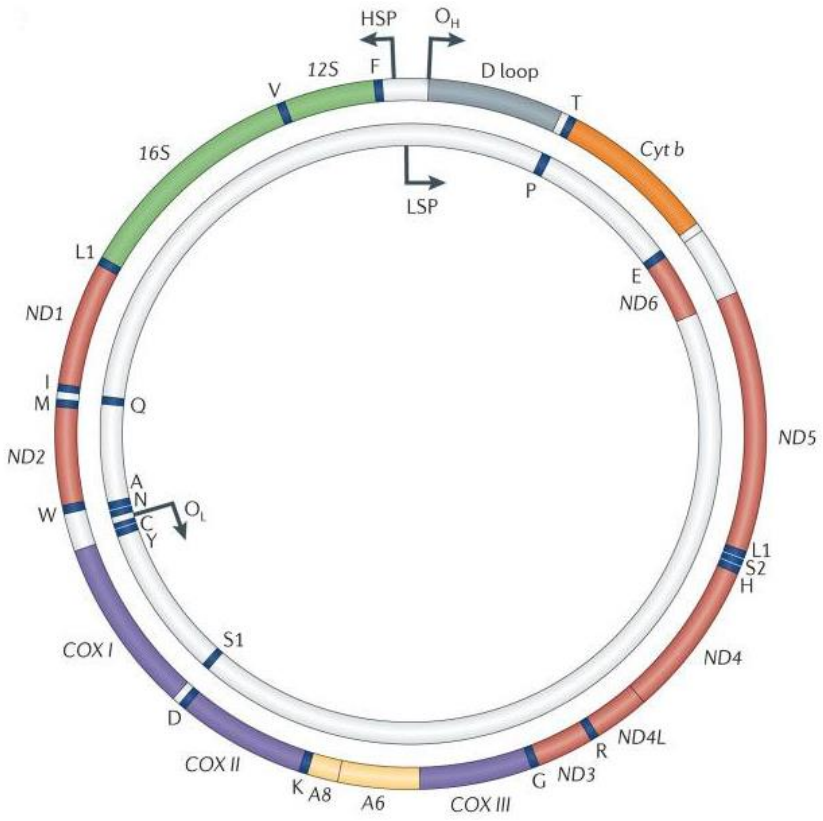

Figure 1.10 Structure of a mtDNA molecule

Individual mtDNA molecules contain ~16,000 base pairs on heavy and light strands. Transcriptionally active genes on both strands encode thirteen ETC subunits, twenty-two tRNAs and two rRNAs. No inherent repair mechanisms exist for mtDNA (in contrast to nuclear DNA), increasing the likelihood of mutation accumulation throughout an organism's lifetime (Schon et al., 2012)

1.5.3 Mitochondrial dynamics

As a result, mitochondrial activity must be tightly regulated to adapt to changing metabolic demands and physiology (Friedman & Nunnari, 2014; Patten, et al., 2014). This is evidenced by the fact that defective mitochondria have been associated with a number of human diseases (Nunnari & Suomalainen, 2012). Central to their ability to adapt to metabolic changes and maintain a quality control, is the continuous and highly dynamic processes of fusion and fission (MacVicar & Langer, 2016). For example, mitochondrial fusion enables the sharing of mtDNA, and, as hyper-fused mitochondria contain an extended cristae structure, this increases the recruitment of the oxidative phosphorylation (OXPHOS) machinery (Cogliati, et al., 2013). This has the effect of increasing respiratory efficiency. Increased mitochondrial fission, on the other hand, is necessary to obtain spatially distributed mitochondria during division (MacVicar & Langer, 2016).

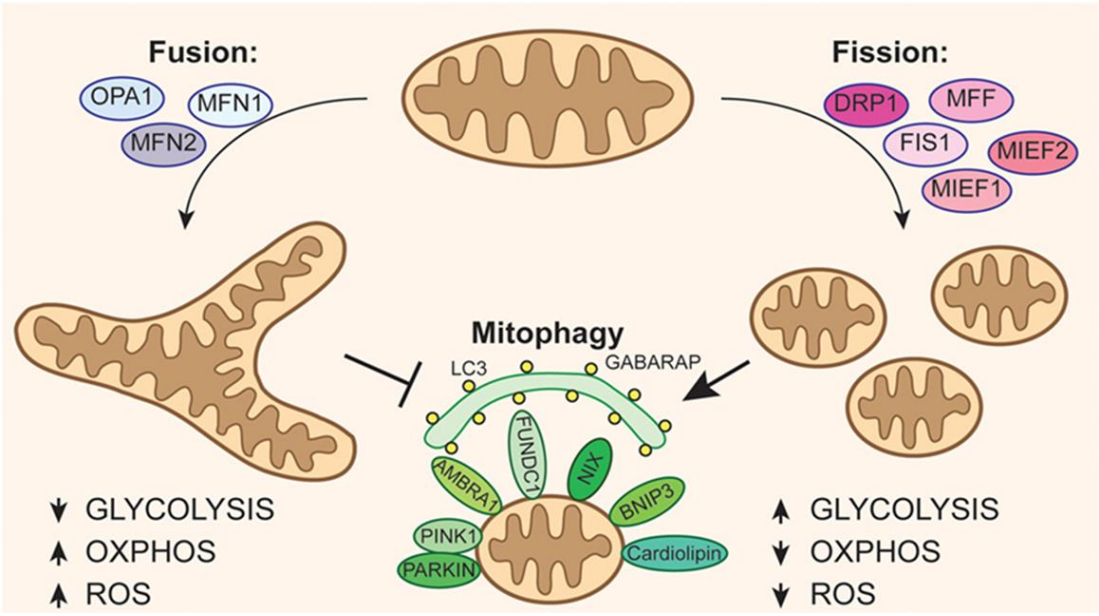

Figure 1.11 Mitochondria undergo fusion and fission to form highly dynamic networks.

Mitochondrial fusion is governed by OPA1 and the Mitofusins, which are necessary for fusion of the IMM and OMM respectively. The activity of DRP1 is sufficient and necessary to drive mitochondrial fission. A highly fused network provides an increased platform for oxidative phosphorylation, whereby a fragmented network facilitates glycolytic flux. Fragmented mitochondria may also be cleared through mitophagy and is necessary to maintain a healthy mitochondrial pool.

Mitochondrial dynamics has also been associated with cancer formation and progression, and their contribution to cellular function has a strong impact on invasiveness and metastatic profile of cancers (Vyas et al., 2016). Furthermore, a growing body of evidence suggests that many cancer cell lines and solid tumors undergo a drastic metabolic reprogramming (Bordi et al., 2017). For example, cancer cells have been shown to limit limit the tricarboxylic acid cycle (TCA) and mitochondrial OXPHOS as a consequence of mutations that affect the activity of TCA key enzymes or the activity of OXPHOS complexes (Sciacovelli et al., 2016; van Gisbergen; 2015). Therefore, cancer cells veer toward a prominent use of glycolysis as the main source for ATP production, commonly known as the "Warburg effect" (Warburg; 1956). In doing so, cancer cells have been shown to upregulate glucose uptake to sustain the dependence on glycolysis (Gaude & Frezza; 2014).

1.5.4 Mitochondrial Fusion and fission

Mitochondrial fusion describes the process that occurs when two adjacent mitochondria join, whereas fission generates two mitochondria from a single parent (Sebastián & Zorzano, 2018). These two processes are intricately balanced to control mitochondrial morphology, and the oblation of either process produces a highly fused or divided mitochondrial network (Scorrano, 2013).

Mitochondrial fusion is coordinated by the mitofusins (MFN1 and MFN2) and optic atrophy 1 (OPA1), which coordinate fusion of the OMM and IMM respectively, and in separable sequential events (Malka et al., 2005). These regulators of fusion are dynamic-like GTPases, which contain conserved catalytic GTP-binding domains at the N-terminus (figure 1.12) (Wai & Langer, 2016). Mechanistically, both OPA and the Mitofusins mediate fusion through insertion of hydrophobic heptad repeats into adjacent mitochondria (Koshiba et al., 2004). Following insertion, mitochondrial fusion proceeds through GTP hydrolysis, which brings opposing membranes into contact after a conformational change in the respective proteins (Cao et al., 2017).

The fusion regulator OPA1 is a significant focus of my report, and hence is introduced in greater detail. It is so-named due it's frequently mutated status in autosomal dominant optic atrophy (ADOA), where patients display degeneration of retinal ganglion cells and loss of optic nerve axons (Alexander, et al., 2000). It is a ubiquitously expressed protein, with the greatest expression levels in retina, brain, testis, heart and muscle (Olichon, et al., 2006). In humans, the OPA1 protein exists as 8 isoforms (figure 1.12) which are generated by alternate splicing, each of which may be proteolytically cleaved by OMA1 or YME1L to yield long and short isoforms (L-OPA1 and S-OPA1) (Olichon et al., 2007). The respective OPA1-L and OPA-s isoforms are present in the inner mitochondrial membrane (IMM) and as a soluble

form present in the intermembrane space (Baker, et al., 2014). L-OPA1 has a prominent role in regulating mitochondrial fusion, which has been well defined. Deletion of OPA1 leads to fragmented mitochondria due to the inability of mitochondria to form extended networks, a phenomenon that frequently occurs in disease, such as ADOA where cell death is rapidly induced when OPA1 is mutated (Bertholet, et al., 2016). It has also been suggested that s-OPA1 has a role in mitochondrial fission, but this has been less well defined (MacVicar & Langer, 2016). Nonetheless, the proteolytic cleavage of OPA1 is induced by different stress conditions (such as mitochondrial dysfunction or ROS accumulation), thereby shifting the balance towards s-OPA1 isoforms and a fragmentation of the mitochondrial network (Anand et al., 2014). Interestingly, l-OPA1 isoforms are able to tether, dock and partially fuse the IMM through an interaction with cardiolipin. However, homotypic *trans* interactions between OPA1 molecules on opposing membranes increase the efficiency of the process (Ban et al., 2017). Conversely, s-OPA1 isoforms only have the ability to tether mitochondrial membranes (ref). Therefore, the ratio between long and short OPA1 isoforms is critical for maintaining mitochondrial fusion (Ge et al., 2020).

Genetic oblation of OPA1 leads to a drastic reduction of mitochondrial energetic efficiency, brought about by impairment of respiratory complex assembly (Lee et al., 2017). Notably, this effect is driven by a role for OPA1 in regulating mtDNA maintenance and cristae morphogenesis (Del Dotto et al., 2017). In addition, this relationship was delineated further by conditional ablation of OPA1, which altered cristae shape, mitochondrial morphology, and complex V activity, but did not deplete mtDNA (Cogliati et al., 2013). Thus, a direct link can be established between cristae shape and RCS stability, impacting on respiratory efficiency. This was further supported by data obtained in a transgenic mouse model, which exhibits a mild overexpression of OPA1. In this context, OPA1 promoted cristae tightening, mitochondrial energetic function, and ameliorates the phenotype of mitochondrial disease models (Civiletto et al., 2015; Cogliati et al., 2013). However, the specific roles of long and short isoforms in recovering the mitochondrial respiratory capacity and cristae organization independently of each other are a topic of debate (Del dotto et al., 2018). For example, OPA1 knockout cell models expressing either L-OPA1 or S-OPA1, exhibit normal OCR and respiratory complex organization (Lee et al., 2017).

Mitochondrial fission is regulated by a number of proteins which associate with the outer mitochondrial membrane (Gao et al., 2021). However, the activity of the GTPase DRP1 is necessary and sufficient to drive mitochondrial fission. DRP1 is recruited to mitochondria at endoplasmic reticulum (ER) contact sites, where oligomers form a ring that tightens to drive separation into daughter mitochondria (Friedman et al., 2011).

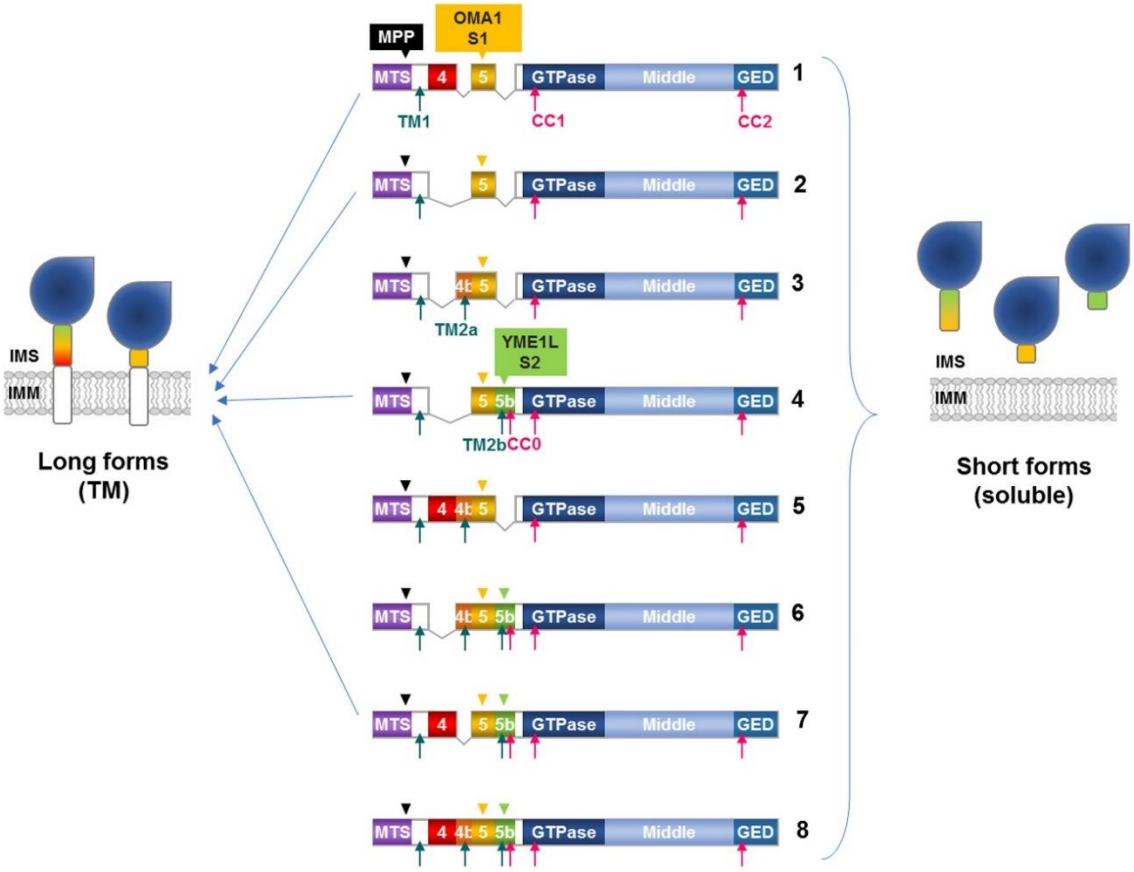

Figure 1.12. OPA1 protein structure and splice isoforms

OPA1 is alternatively spliced to produce eight isoforms. Following IMM insertion, the mitochondrial targeting sequence (MTS) is cleaved by the mitochondrial processing peptidase (MPP). The transmembrane domains (TM1, TM2a, TM2b) and coiled coil domains (CC0, CC1, CC2) are indicated with blue and red arrows, respectively. All isoforms contain the S1 cleavage site (yellow arrowhead), and half contain the S2 cleavage site (green arrowhead). Proteolytic cleavage at S1 and S2 by the OMA1 and YME1L yield OPA1-s forms (Del Dotto et al., 2017).

1.5.5 Mitochondrial biogenesis

Mitochondrial homeostasis is maintained by the balance between the generation of new mitochondria (mitochondrial biogenesis) and the removal of damaged mitochondria by mitophagy (Ploumi et al., 2017). Peroxisome proliferator-activated receptor-γ coactivator (PGC-1α) is the master regulator of mitochondrial biogenesis, which activates the transcription and translation of essential mitochondrial proteins encoded in the mitochondrial and nuclear genomes (Wenz et al., 2013). The final effector in this cascade is the mitochondrial transcription factor A (TFAM), which activates mtDNA transcription and replication (Dos Santos et al., 2018). This results in the synthesis, import and assembly of mitochondrial proteins, thereby increasing mitochondrial content. However, the fission machinery is required for the formation of new mitochondria (Popov, 2020).

1.6 Bioenergetics in eukaryotic organisms

As discussed, a major function of mitochondria is to produce cellular ATP, providing the energy for tissues to perform their physiological roles. Accordingly, mitochondrial dysfunction leads to the development of numerous diseases. The majority of mitochondrial ATP production occurs electron transport down a series of protein complexes located on the IMM which is coupled to oxidative phosphorylation (Herst et al., 2017). Complementary metabolic pathways such as the Krebs Cycle is essential for maintaining optimal ETC function as they produce essential cofactors and metabolites, namely in the form of the electron carriers NADH and $FADH_2$ (Bonora et al., 2012). Furthermore, cells are able to generate ATP in a less efficient and anaerobic manner through the glycolytic pathway, which occurs in the cytoplasm. In this section I therefore introduce glycolysis, the Krebs cycle and the electron transport chain.

1.6.1 Glycolysis

Aerobic glycolysis is a rapid yet also inefficient method of producing ATP. It occurs *via* a series of reactions that also result in the production of key metabolic intermediates which can feed into diverse anabolic pathways (Chaudhry and Varacallo; 2021). Glucose is firstly transported from the bloodstream into cells by glucose transporters (GLUT). There, the first reaction is catalysed by hexokinase, which converts glucose to glucose-6-phosphate (G6P). A series of sequential reactions then converts G6P to pyruvate, which is transported into mitochondria for flux in the Krebs cycle (figure 1.13). The first committed step of glycolysis is catalysed by phosphofructokinase (PFK), as before this step G6P may have various fates in aforementioned anabolic pathways, such as the PPP (figure 1.8). Importantly, the expression of PFK has been shown to be regulated by TAp73 (Li et al., 2018). The glycolytic pathway also produces reduced nicotinamide adenine dinucleotide (NADH), which is transported into the mitochondria, from which it serves as an electron carrier during oxidative phosphorylation (Cederbaum et al., 1973). Alternatively, under hypoxic conditions, pyruvate is converted to lactic acid, which also regenerates NAD^+ from NADH (Rogatzki et al., 2015).

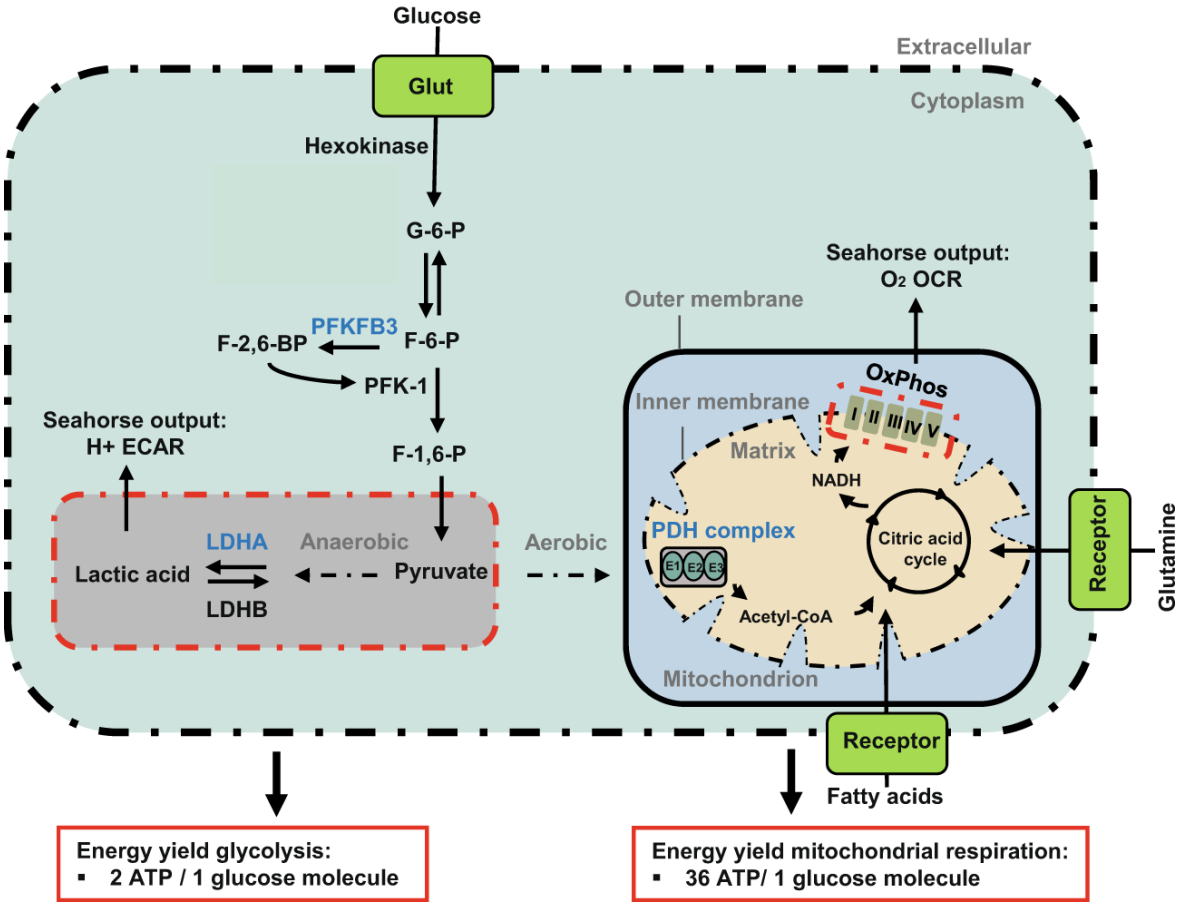

Figure 1.13 Schematic overview of glycolysis and mitochondrial respiration

The two major energy yielding pathways from the metabolism of glucose (glycolysis and mitochondrial OXPHOS). In anaerobic conditions, pyruvate is converted into lactate. PFK regulates one of the rate-limiting steps of glycolysis through the conversion of fructose-6-phosphate (F6P) to fructose-1,6-biphosphate (F1,6P2). ECAR is a measure of lactic acid levels, and is used as a proxy measurement for glycolytic rate in this study in Seahorse assays. In aerobic conditions, pyruvate enters the citric acid cycle and is catabolized by oxidative phosphorylation. OCR is a measure of oxygen utilization in cells and is an indicator of ETC function. The conversion of glucose into lactate generates 2 ATP per glucose molecule whereas OXPHOS generates 36 ATP. Glut; glucose transporters. G-6-P; glucose-6-phosphate. F-6-P; fructose-6-phosphate. PFKFB3; 6-phosphofructo-2-kinase/fructose-2,6-biphosphatase 3. F-2,6-BP; fructose-2,6-biphosphate. F-1,6-P; fructose-1,6-phosphate. LDHA; lactate dehydrogenase A. LDHB; lactate dehydrogenase B. PDH; pyruvate dehydrogenase. NADH; nicotinamide adenine dinucleotide. FADH2; flavin adenine dinucleotide. (Adapted from Yetkin-Arik et al., 2019).

1.6.2 The Krebs cycle

The Krebs cycle is a bioenergetic pathway that produces reducing equivalents utilised by the ETC (Williamson and Cooper, 1980). It also produces 1 molecule of ATP for each turn of the cycle. The first reaction of the cycle is the decarboxylation of lactate to acetyl-coenzyme A (acetyl-coA) by pyruvate

dehydrogenase. Citric acid is then synthesised from a combination of Acetyl-coA and oxaloacetate. The cycle then proceeds to produce oxaloacetate, from which the cycle continues. In addition to 1 ATP molecule, the cycle produces a single molecule of flavin adenine dinucleotide ($FADH_2$) and 3 molecules of NADH (Williamson and Cooper, 1980).

1.6.3 The electron transport chain

The electron transport chain is comprised of 5 protein complexes and 2 electron carriers embedded in the inner mitochondrial membrane (Matsuno-yagi and Hatefi, 1985). ATP production is achieved by coupling electron transfer to H^+ translocation across the IMM, resulting in an electrochemical gradient which drives ATP synthase when H^+ pass through this complex into the mitochondrial matrix (Mitchell, 1985). Electrons are donated to the ETC from NADH and $FADH_2$, where they pass through complexes I and II to ubiquinone (Hirst 2009). Next they pass through complex III, cytochrome c, and arrive at complex IV, where O_2 is reduced to H_2O (Papa et al., 2012). The assembly process of the OXPHOS complexes is intricately controlled and requires many structural, catalytic, and assembly proteins to execute this process (Bergman and Ben-Shachar, 2016). Moreover, the assembly involves proteins encoded by nuclear DNA (~70 proteins), which much translocate into the mitochondria and assemble with mitochondrially encoded proteins (Walker et al., 2007).

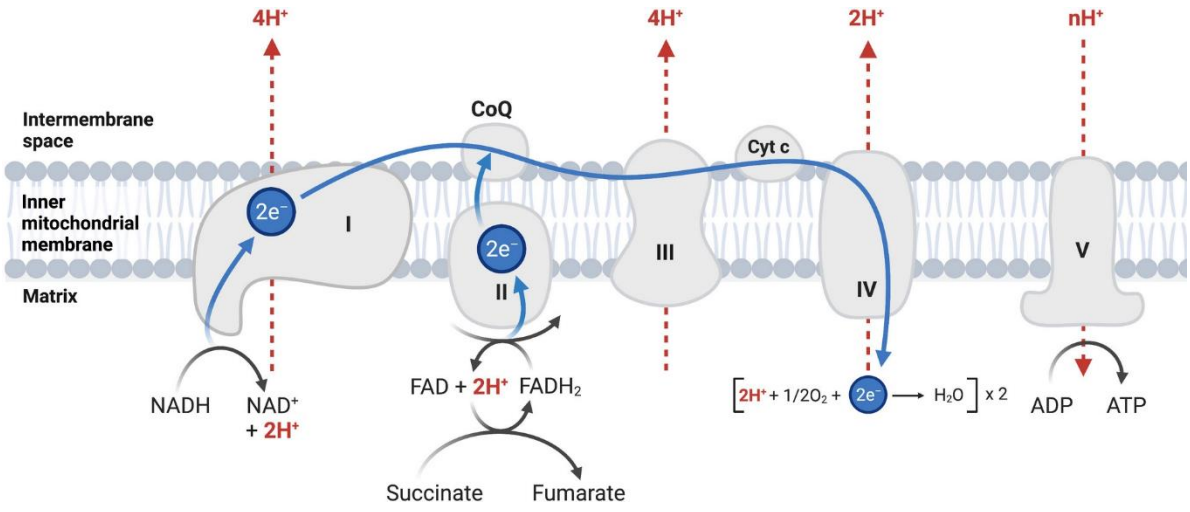

Figure 1.14. Overview of the electron transport chain

The blue pathway represents the electron transport and red pathway indicates proton translocation. Electrons enter the ETC from NADH at complex I, and from FADH2 at complex II. Electrons are then transferred to complex III by Coenzyme Q. Finally, electrons are shuttled to complex IV by Cytochrome c where they reduce O_2 to H_2O. The transfer of electrons is coupled with the translocation of H^+ across the IMM to create an electrochemical gradient that drives the synthesis of ATP at complex V (Yin and O'Neill, 2021).

1.6.4 Project aims

As outlined in section 1.4, the *TP73* gene is responsible for a wide range of DNA-damage independent functions. This is evidenced by the diverse phenotypes of global *TP73*$^{-/-}$ and isoform specific knockout mice (Yang et al., 2000; Tomasini et al., 2008). Although defective ciliogenesis has been proposed as a connecting mechanism that underlies abnormalities in the brain, respiratory, and reproductive tissues (Nemajerova et al., 2016, Marshall et al., 2016), aspects such as neuronal cell death in the developing hippocampus (Amelio et al., 2020) indicate that additional molecular mechanisms underpin the reported tissue dysfunction. To this end, a number of *in vitro* and *in vivo* studies have indicated that TAp73 regulates cellular bioenergetics, which include the modulation of mitochondrial function through transcriptional regulation of a subunit complex IV of the ETC (Rufini et al., 2012). This leads to a decrease in ATP production and a premature aging phenotype *in vivo*, functionally connecting mitochondrial regulation with the TAp73$^{-/-}$ mouse phenotype. Therefore, the overarching goal of my study was to identify novel functions of TAp73 in regulating mitochondrial biology and to demonstrate the importance of this regulation in ciliated epithelial tissues.

To address this, the aims of this project were as follows:

- To interrogate *In situ* tracheal and *in vitro* ChIP-seq data sets to identify potential mitochondrial targets of TAp73 isoforms.
- To functionally validate the transcriptional control of OPA1 by TAp73 which was identified by ChIP-seq data
- To investigate the functional impact of disruption of the TAp73/OPA1 axis on mitochondrial morphology and function, performed in both a cell model and in mouse epithelial tissues
- To the importance of the C-terminal SAM domain of p73 in executing its developmental roles, with a focus on ciliated epithelial and ependymal tissues

In greater detail, in Chapter 3, I validated the binding of TAp73 to the OPA1 promoter region using ChIP to pull down TAp73 bound chromatin and performing RT-qPCR directed against the OPA1 promoter. Following this, I characterised the transcriptional relationship between TAp73 and OPA1 by generating a cell model in which all TAp73 isoforms were ablated using CRISPR/Cas9 targeting.

Following this, in Chapter 4 and 5 I investigated the functional impact of disruption of the TAp73/OPA1 axis in CRISPR targeted cells and Trp73$^{-/-}$ epithelial tissues. Specifically, I looked for evidence of disruption of mitochondrial fusion, owing to an essential role of OPA1 in fusion of the IMM. Further, the TAp73$^{-/-}$ cell model provided the opportunity to interrogate a dysregulation of fusion independent roles of OPA1. As OPA1 has a role in modulating mitochondrial oxidative phosphorylation through the

regulation of cristae architecture and ETC complex assembly (ETC), I investigated mitochondrial bioenergetics in TAp73 KO cells. This enabled me to implicate the TAp73/OPA1 axis in the control of mitochondrial function independently of additional metabolic roles of p73.

Lastly, in Chapter 6, I investigated the importance of the p73 C-terminal SAM domain by interrogating the epithelial cell phenotype in Trp73$^{\Delta 13/\Delta 13}$ mice. This mouse models lack exon 13 in *TP73* gene, producing an ectopic switch from the C-terminal isoforms p73α to p73β. This also provided the opportunity to determine the capacity for p73β isoforms to regulate OPA1 expression *in vivo*, confirming the findings of ChIP-seq analysis which showed that isoforms alpha and beta both have the capacity to regulate *OPA1* gene transcription.

Chapter 2: Materials and Methods

2 Materials and Methods

2.1 Cell Culture

Cell culture was performed using established aseptic techniques. Cells were cultured in T175 flasks and passaged 1:6 every three days or once 80% confluent. During passage, cells were washed once with PBS and detached from culture flasks using 10% trypsin (Gibco). Trypsin was inactivated by the addition of growth medium, and cells centrifuged at 300g for 5 mins at room temperature. The supernatant was aspirated and the cell pellet resuspended growth medium and seeded in the appropriate cell culture vessel. Cells were frozen for long term storage by resuspending cell pellets in growth medium containing 10% DMSO (Sigma) and 10% FBS (Thermofisher).

2.1.1 H1299 Cells

NCI-H1299 cells (ATCC #CRL-5803) were cultured in modified RPMI 1640 (Gibco, Life Technologies #A4736401) containing L-glutamine, 4.5 g/L of D-glucose, 2,383 g/L of HEPES Buffer, 1.5 g/L of Sodium Bicarbonate, 110 mg/L of Sodium Pyruvate, 10% FBS at 37°C and 5% CO_2. H1299 cells stably expressing CRISPR targeting and Cas9 constructs were a kind gift from Prof Gerry Melino. They were cultured in RPMI 1640 (Gibco #A1049101) supplemented with 10% Tetracycline system approved FBS (Gibco). Cells were not cultured beyond passage 30.

2.1.2 HEK-293T Cells

HEK-293T cells (ATCC #CRL-3216) were cultured in Dulbecco's Modified Eagle's Medium (Gibco) supplemented with 10% FBS and 2mM L-glutamine (Gibco) at 37°C and 5% CO_2. Cells were not cultured beyond passage 30.

2.2 Transfection

Cells were seeded at a density of 400,000 cells per well in 6cm dishes and incubated overnight before transfection with Lipofectamine 2000 reagent (Invitrogen). For each well to be transfected, lipid-DNA complexes were formed in 500mL Opti-MEM medium (Gibco) by incubating 10ul lipofectamine with 4ug plasmid DNA. The mixture was incubated for 20 mins at room temperature and added to cell culture dishes after removing an equal volume of media. The media was replaced after 6h and cells incubated for a further 16-42h depending on the downstream application.

Plasmid constructs for overexpression of TAp73 were a kind gift from Dr Ivano Amelio. Full-length TAp73 isforms alpha or beta fused to a haemagglutinin (HA) tag were cloned into a pcDNA3 backbone (Amelio et al., 2018) and the empty vector used as a control. Expression plasmid for OPA1 was purchased from Origene (#SC128155). It contains *OPA1* transcript variant 1 (Accession number

NM_015560) cloned into the pCMV6-XL4 backbone. Additional plasmid DNA was obtained by transforming 100ng plasmid into DH5a (NEB), following the manufacturer's protocol. 10 µl of outgrowth culture in SOC was plated on LB plates containing 100 µg/mL ampicillin (Sigma) and the plates incubated overnight at 37°C. Colonies were picked to inoculate 4mL LB broth and incubated at 230rpm, 37°C for 6h after which 100 µl of culture was used to inoculate 100ml overnight culture. Bacterial cells were centrifuged at 3273 x g and plasmid DNA obtained using QIAGEN Plasmid Maxi Kit (#12165) spin columns. DNA was eluted in 200 µl sterile filtered TE buffer (Thermofisher).

siRNA transfection was carried out using Lipofectamine RNA iMAX (Invitrogen). 6-well plates were seeded with 200,000 cells per well, incubated for 24 hours and transfected with complexes containing 5 µg predesigned *TP73* siRNA (Invitrogen; AM51331), OPA1 siRNA (AM16708) or scrambled negative control (Invitrogen) plus 5 µl RNA iMAX reagent. After 24 hours, cells were detached using trypsin (Gibco) and transferred to 6cm dishes and cultured for a further 48 hours.

2.3 Animals

Mice used in this study were from the BALB/c or C57BL/6 mouse strains (under Dr Ivano Amelio's Home Office License at the MRC Toxicology Unit, University of Leicester). All procedures followed guidelines and legislation as regulated under the Animal's Scientific Procedures Act 1986 (ASPA) and were approved by the University of Leicester Animal Welfare and Ethical Review Body (AWERB). Euthanasia of animals was carried out by the University of Leicester animal facility. For all experiments excluding electron microscopy (EM), mice were euthanised by CO_2 asphyxiation to preserve the trachea prior to dissection. For EM experiments, anaesthetised mice were perfused via transcardiac perfusion.

2.3.1 *TP73*$^{-/-}$ mice

The generation of global *TP73*$^{-/-}$ mice was performed previously in the BALB/c background (Yang, et al., 2000). In brief, a targeting vector was generated and electroporated into the JI ES cell line10. A region of the Trp73 gene containing exon 5 and part of exon 6 was replaced by a NEOR gene for selection of cells that have undergone homologous recombination. The targeting vector contained homology arms 5.5kb upstream and 2.5kb downstream of the resistance gene. Vector expression was driven by the mouse phosphoglycerol kinase (PGK1) promoter and linked to the PKG1 poly(A) sequences. ES cell lines heterozygous for disrupted p73 were microinjected into blastocysts from BALB/c mice.

2.3.2 *Trp73*$^{\Delta 13/\Delta 13}$ mice

Trp73$^{\Delta 13/\Delta 13}$ mice were generated using the Cre-LoxP system. Firstly, floxed (*Trp73*$^{fl/fl}$) mice were obtained by the introduction of a vector containing LoxP sites flanking exon 13 of the p73 gene, which was replaced by a NeoR cassette for selection. Immediately upstream and downstream of these sites were long terminal repeats (LTRs) which facilitated incorporation of the vector into ESCs by homologous recombination. Floxed mice were subsequently crossed with mice ubiquitously expressing Cre-recombinase under the human cytomegalovirus promoter (CMV-CRE) to delete exon 13 of the *TP73* in all tissues.

2.4 2.4 CRISPR/Cas9 TAp73 knockout generation

2.4.1 Transient Transfection

H1299 cells were seeded at a density of 500,000 cells per 6cm dish in 5mL growth medium and incubated for 24 hours. Cas9 expression plasmid (Horizon Discovery) was reconstituted in TE buffer to obtain a 100ng/µl stock solution. 10uM guide RNA (gRNA) stocks for three different guide RNA (gRNA) oligonucleotides targeting exon 3 of TAp73 were obtained by adding 500 µl TE buffer to 5nmol RNA (Custom synthesis, Horizon Discovery). An aliquot of guide RNA was then diluted to 2uM before use. The following five transfection mixtures were prepared in 500mL OPTI-MEM (Gibco), and incubated for 15 mins at room temperature. 500mL culture media was removed from each well and replaced with transfection mixture.

Transfection Condition	Lipofectamine 2000	Cas9 Plasmid (100ng/uL)	gRNA (2uM)
Cas9 Control	10 ul	20 ul	0
Cas9 + sgRNA-1 (ATTATTCCCCCGGCTTGACT)	10 ul	20 ul	10 ul
Cas9 + sgRNA-2 (CATTATTCCCCCGGCTTGACT)	10 ul	20 ul	10 ul
Cas9 + sgRNA-3 (CAGGTGGAAGACGTCCATGCT)	10 ul	20 ul	10 ul
Empty Vector Control	10 ul	0 ul	0

Table 2.1. Summary of transfection mixtures added to H1299 cells to generate CRISPR knockouts. Three different gRNA oligonucleotides were co-transfected with Cas9 plasmid to induce double-strand breaks.

Cell culture media was aspirated after 6 hours and replaced with fresh RPMI, 10% FBS and cells incubated for a further 18 hours. Puromycin was added at a final concentration of 2.5 µg/µl to each transfection condition and incubated for 16 hours. Selection media was removed from the plates, cells washed twice with fresh RPMI media, and cells cultured for a further 24 hours. Cells were detached using 500 µl 1x trypsin/PBS solution, made up to 2mL in growth media, and centrifuged at 300g for 5 mins. The cell pellet was re-suspended in conditioned growth media to yield 2.5 cells/mL and 200 µl added to each well of a 96-well plate to give a final density of 0.5 cells/mL. The remaining cells were maintained in culture as a mixed population for analysis by mismatch repair assay. Clonal populations were expanded for 14 days before transferring to 12-well and then 6-well plates for analysis of TAp73 expression by western blot.

2.4.2 Doxycycline Inducible System

H1299 cells with stably integrated Cas9 and gRNA expression constructs were a kind gift from Prof. Gerry Melino. In brief, Lentiviral vector pFU-Cas9-mCherry was used for constitutive expression of Cas9 and mCherry protein under the control of the ubiquitin promoter and separated by a T2A linker (Aubrey et al., 2015). sgRNA oligonucleotides were cloned into the pFgh1tUTG vector downstream of a tetracycline response element for doxycycline-inducible sgRNA expression (sgRNA sequence: TTCCCCACGCCGGCCTCCGA). Lentivirus was produced using a lentiviral packaging cocktail containing pMDL, pRSV-REV and pVSV-G vectors expressed in 293FT cells. Virus containing supernatant was harvested and supplemented with 8ug/ml polybrene and added to H1299 cells cultured in 6-well plates. The plate was spun at 500g for 2h and 32°C, incubated for 24h at 37°C and fresh growth medium added. Cells were passaged when confluent and sorted using FACS to yield greater than 95% GFP and mCherry double positive cells. Expression of sgRNAs and subsequent Cas9 activation was induced by plating H1299 in a 6cm dish and supplementing growth medium with 1 µg /ml doxycycline hyclate (Sigma-Aldrich) for 48h. Growth medium was replaced with RPMI containing 10% Tetracycline free FBS (Gibco) and was used for subsequent culture to prevent further Cas9 activation.

2.5 End-point PCR

2.5.1 PCR of TAp73 gene for screening of CRISPR clonal populations

Genomic DNA (gDNA) was obtained from potential TAp73 knockout cells generated using the two approaches using the DNeasy Blood & tissue kit (Qiagen) according to the manufacturer's instructions. DNA was eluted in 100ul and quantified using Nanodrop spectrophotometer. Primers were designed to

amplify either exon 2 or exon 3 of the TAp73 gene and amplification performed using Q5 polymerase master mix (NEB). PCR reactions were set up using 500ng of gDNA template, 12.5 ul Q5 Hot Start High-Fidelity 2X Master Mix (NEB) and 0.5 µM final forward and reverse primer concentration in a total reaction volume of 25 µl. The PCR reaction was then performed in a thermocycler with the following settings:

2.5.2 TAp73 Exon 2

Forward primer: GCTAGCCTTAGCCACCCTCA, Reverse Primer: TTGGTTGTACAGCTTCCCCT, expected amplicon: 614 bp.

Cycle Step	Temperature (°C)	Time (seconds)	Cycles
Initial Denaturation	98	30	1
Denaturation Annealing Extension	98 67 72	5 10 30	30
Final Extension	72	120	1
Hold	4	Infinite	1

Table 2.2. PCR cycling parameters for the amplification of TAp73 Exon 2 from H1299 gDNA.

2.5.3 TAp73 Exon 3

Forward primer: GAAATGACAGTGGAGAGGGCA, Reverse Primer: CCAGTGAGGGTTGCCAAGTT, expected amplicon: 435 bp.

Cycle Step	Temperature (°C)	Time (seconds)	Cycles
Initial Denaturation	98	30	1
Denaturation Annealing Extension	98 69 72	5 10 30	35
Final Extension	72	120	1
Hold	4	Infinite	1

Table 2.3. PCR cycling parameters for the amplification of TAp73 Exon 3 from H1299 gDNA.

Primers were validated by running the PCR product from wild-type H1299 gDNA template on a 0.1% agarose gel containing 1x SYBR safe for 1h at 100V. The gel was imaged using a ChemiDoc imager (Bio-Rad) to confirm the presence of a single molecular weight amplicon of the expected size.

2.5.4 RT-endpoint PCR on tracheal RNA

Mouse trachea from wild-type and Trp73$^{\Delta 13/\Delta 13}$ mice were carefully dissected from just below the larynx to the bronchiolar junction in a biosafety cabinet using sterile forceps and scissors. The dissected tissue was added to 1mL Eppendorf tubes containing modified Dulbecco's phosphate-buffered saline (DBPS; Gibco #14287080) on ice. The DBPS was aspirated, and RNA isolated using TRIzol reagent (Invitrogen #155906026). 1mL cold TRIzol reagent was added to the tissue and samples added to 2mL Lysing Matrix D tubes containing ceramic beads (MP Biomedicals # 116913050-CF). The sample was homogenized using the FastPrep-24 lysis system (MP Biomedicals) using 3 cycles at 6m/s. The lysate was centrifuged for 5 mins at 12,000 x g at 4°C and the supernatant transferred to a new tube. The samples were incubated for 5 mins, 0.2mL chloroform (Thermofisher) added and centrifuged for 15 mins at 12,000 at 4°C and the aqueous phase transferred to a new sterile Eppendorf. 10ul of Glycoblue coprecipitant (Thermofisher #AM9516) was added as a carrier to the aqueous phase. Next, 0.5mL isopropanol (Sigma) was added and total RNA precipitated according to the manufacturer's instructions for TRIzol reagent. The RNA pellet was resuspended in 30 µl RNAase-free water (Gibco), incubated in a water bath set at 55°C for 10 mins, and stored at -80°C.

For PCR, 2 µg of RNA was reverse transcribed using SuperScript® III Reverse Transcriptase with oligo-dT (ThermoFisher) according to the manufacturer's instructions. The primer sequences for the Trp73 C-terminal isoforms are listed in Table x. Reactions were carried out using the RED Extract-N-AmpTM PCR ReadyMixTM (Sigma # R4775). The samples were prepared according to the manufacturer's instructions and using a 0.4uM final primer concentration for forward and reverse primers. The thermocycler settings are given below. The products were run on a 2% agarose gel in TAE buffer (Thermofisher) and were visualized using a Gene Genius Bio Imaging System (Syngene).

TAp73 C-terminal isoforms RT-endpoint PCR Primer Sequences	
Name	**Sequence 5' - 3'**
mp73 **alpha** Fw	GAGGCCGGGAGAACTTTGAG
mp73 **alpha** Rev	CAGTCATGGCTCTGCTTCAGG
mp73 **beta** Fw	TCCTACAGAGGCCGAGTCACCTG
mp73 **beta** Rev	AGCCCCAAGGTCCTGACGAGGCT

Table 2.4. Primer sequences used for RT-PCR performed on tracheal RNA. mp73 beta sequences spanned the exon 12-14 junction of the splice isoform.

2.6 Mismatch Repair Assay

T7 endonuclease digestion of PCR products obtained using the CRISPR protocol described previously was performed using the EnGen® Mutation Detection Kit (NEB) to screen for gRNA activity at target loci. A control PCR reaction was performed using control template and primer mix according to the manufacturer's instructions. Heteroduplexes were formed by denaturing 5ul of the PCR reactions with 2 µl 10x NEBuffer 2 and 12ul nuclease free water and thermocycling with the following program:

Cycle Step	Temperature (°C)	Ramp Rate	Time (seconds)
Initial Denaturation	95	None	1
Annealing	95-85 85-25	-2°C/second -0.1°C/second	5 600
Hold	4	None	Infinite

Table 2.3. PCR cycling parameters for generation of DNA heteroduplexes in mismatch repair assay.

1 µl of T7 endonuclease was added per reaction, mixed by pipetting, and incubated at 37°C for 15 mins in a heat block. 1 µl of Proteinase K was added and the mixture incubated for a further 5 mins at 37°C to stop the reaction. 4 µl of 6x gel loading dye (NEB) was added to the reaction with or without endonuclease, and samples run on a 2% agarose gel to visualise digestion.

2.7 Sanger sequencing of CRISPR clones for INDEL characterisation

Exon 2 (for transient transfection) or exon 3 (for doxycycline-inducible system) spanning PCR fragments obtained from gDNA of clonal CRISPR populations were cloned into the pJET1.2 blunt cloning vector using the CloneJET PCR cloning kit (Thermofisher #K1232). This approach has the advantage of enabling sequencing to be performed on PCR products obtained a single chromosome. The ligation reaction was performed following the manufacturer's instructions and using 1ul of PCR product and incubating at room temperature for 5 mins. The ligation mixture was stored at -20°C if the transformation was postponed. The blunt-ended insertion site is located within a lethal eco47IR gene, allowing for positive selection of transformed E.coli. NEB 5-alpha competent E.coli (NEB #C2987H) were thawed on ice for 5 mins and 20ul of cells transferred to an Eppendorf tube for each transformation. 1 µl ligated plasmid was added to the E.coli and the mixture placed on ice for 30 mins, and the cells heat shocked at 42°C for 30 seconds. The cells were returned to ice for 5 mins, and 950ul room temperature SOC media added. Outgrowth was achieved by incubation at 37°C for 60 mins and 300 rpm. Either 10ul or 100ul of cells was spread on pre-warmed LB Agar plates containing 100 µg/mL ampicillin (Sigma) and the

plates incubated overnight at 37°C. A minimum of 6 colonies were picked and added to to 4mL agar broth containing 100 µg/mL ampicillin and incubated overnight at 37°C with shaking at 230rpm. Plasmid DNA was obtained using the QIAprep Spin Miniprep Kit (Qiagen #27106) and eluted in 30 µl TE buffer (Thermofisher). Sanger sequencing was performed by SourceBioscience (Cambridge, United Kingdom). Plasmid DNA was supplied at 100ng/ul and the pJET1.2 forward sequencing primer at 3.2 uM, with 5ul of each supplied per reaction. Sequencing reads were aligned to the human TAp73 gene (GRCh38) using Geneious Prime software and INDELS identified.

2.8 RT-qPCR

2.8.1 RNA isolated from mouse tracheal epithelial cells

To increase the purity of isolated epithelial cells from mouse trachea, surface cells were stripped using protease digestion of tissue. Dissected mouse tracheas were transferred to a 10cm cell culture dish containing Ham's F12 (Gibco) on ice. Adhered muscle tissue was removed under a dissection microscope and tracheas added to a new dish. The trachea were cut open longitudinally to expose the inside surface. Three trachea from either wild-type or *TP73-/-* mice were pooled together in 15mL falcon tubes containing 2mL 0.15% filter sterilised Pronase (Roche) and incubated at 4°C overnight. The next morning, the tubes were gently inverted 3 x and FBS (Gibco) added at a final concentration of 10% and tubes invertfed a further 3 times. In a sterile tissue culture hood, the tracheas were then transferred to a new 15ml tube containing Ham's F12/10% FBS and inverted. The process was repeated in a third and final tube and the contents from each tube pooled. The trach eas were removed using a sterile pasteur pipette and cells centrifuged at 300g, 4°C for 10 mins. The supernatant was carefully aspirated, the pellet resuspended in 600 uL DNase solution (Sigma; 0.5 mg/mL crude pancreatic DNase I, 10 mg/ml BSA, in Ham's F12), and incubated on ice for 5 mins. The cells were centrifuged as before and RNA extracted using TRIzol reagent (Invitrogen), according to the manufacturer's instructions.

2.8.2 RNA Isolated from cells

RNA was extracted from cell pellets using the RNeasy Plus mini kit (Qiagen #74136) according to the manufacturer's instructions. RNA was eluted in 30 µl DNAse/RNAse free water and the concentration and purity measured using a nanodrop spectrophotometer (Thermofisher).

2.8.3 Reverse transcription and qPCR in 96-well plates

1 µg of RNA was used per reverse transcription reaction using RevertAid minus first strand cDNA synthesis kit (Thermofisher) according to the manufacturer's instructions. Transcribed cDNA was diluted 2x before use in qPCR. Primer sequences (Sigma) are listed in Table 1. Reactions were carried out in triplicate using Fast SYBR Green PCR Master Mix (Thermofisher #4385612). The relative quantification was obtained using the Applied Biosystems 7500 thermocycler and quantitative comparative (ΔΔCt) method normalised to *TBP*, which was used as an endogenous control. Quantification of miR449a was performed using the TaqMan miRNA Assay kit (Thermofisher; 001030) according to the manufacturer's instructions. The RT reaction was carried out using the TaqMan™ MicroRNA Reverse Transcription Kit (Thermofisher; 4366596) using the specific probe for mir449a and U16 as an endogenous control.

Gene	Forward Primer (5'-3') Sequence	Reverse Primer (5'-3') Sequence
hTAp73	CCAGACCTCTTCTTCCTC	GTCAAAGTAGGTGCTGTC
hDNp73	ATGCTTTACGTCGGTGAC	CTGCCCATCTGGTCCATG
mTAp73	GCACCTACTTTGACCTCCCC	GCACTGCTGAGCAAATTGAAC
mDNp73	ATGCTTTACGTCGGTGACCC	GCACTGCTGAGCAAATTGAAC
hp21	CCTGTCACTGTCTTGTACCT	GCGTTTGGAGTGGTAGAAATCT
hOPA1	TCAAGAAAAACTTGATGCTTTCA	GCAGAGCTGATTATGAGTACGATT
mOPA1	CAGTTTAGCTCCCGACCTGG	TGATGACACCAGGCAAGTCC
hTBP	TCAACCCAGAATTGTTCTCCTTAT	CCTGAATCCCTTTAGAATAGGGTAGA
mTBP	TTGGCTAGGTTTCTGCGGTC	TGGAAGGCTGTTGTTCTGGT
hMFN2	TCTCCCGGCCAAACATCTTC	ACCAGGAAGCTGGTACAACG
hOPA1 promoter 1	TCCATGCGCCATTGGGAG	CCTGCACTTACCAGGCCACA
hOPA1 promoter 2	ATGTAAGCCTCCCTCCCACT	TGTTACATGCCTAACCCACGAA
hMDM2 promoter	GGTTGACTCAGCTTTTCCTCTTG	GGAAAATGCATGGTTTAAATAGCC
SAT2 Promoter	CTGCAATCATCCAATGGTCG	GATTCCATTCGGGTCCATTC
Mt-Co2	GCTGTCCCCACATTAGGCTT	ACCGTAGTATACCCCCGGTC
β2-microglobulin	TGCTGTCTCCATGTTTGATGTATCT	TCTCTGCTCCCCACCTCTAAGT

Table 2.4. Primer sequences used in RT-qPCR reactions.

2.9 Chromatin Immunoprecipitation

The MAGnify™ chromatin immunoprecipitation kit (Invitrogen) was used according to the manufacturer's instructions. In brief, H1299 cells were transfected with TAp73α overexpression construct as described previously. Following trypsinization, cells were pelleted at 300 x g for 5 mins and resuspended in PBS. 3x10^6 cells were suspended in 500 µl PBS and fixed by adding PFA at a final concentration of 1% and incubating for 10 minutes at RT. The reaction was stopped by adding glycine and cells washed twice in PBS. Cells were lysed using 150 µl lysis buffer prepared according to the manufacturer's instructions and stored at -80°C. Chromatin was sheared using the Covaris S220 set at a duty factor of 2%, intensity 4, and 200 cycles/burst for 6 mins to obtain fragments approximately 500 bp in size for qPCR analysis. 2.5 ug anti-HA antibody or mouse immunoglobulins were bound to Dynabeads® by rotating end-over-end at 4°C for 1h. Chromatin was diluted to 200,000 per IP and immunoprecipitated according to the manufacturer's instructions and eluted in 150 ul elution buffer.

2.10 Electron Microscopy

2.10.1 Scanning Electron Microscopy

Mouse trachea and ependyma were carefully dissected and chemically fixed with 2.5% glutaraldehyde (GA) and 2% paraformaldehyde (PFA) in 0.1M cacodylate buffer (pH7.4) for 3 hours at room temperature. The specimens were cut to expose to the surface of cilia organization. After several washes with 0.1M cacodylate buffer, post-fixation was performed by immersion in 1% osmium tetroxide/1% potassium ferrocyanide in 0.1M cacodylate buffer for 1 hour. After several washes in distilled water, a second post-fixation was performed with 5% uranyl acetate solution for overnight at 4 °C in the dark fridge and then the dehydration with a series of ethanol (from 70% to absolute 100%) were completed. Finally, after special treatment with hexamethyldisilazane (HMDS, Sigma-Aldrich, St. Louis USA), the dried specimens were sputter coated with pure gold (EMITECH k950K, Quorum Technologies, Kent UK). Fine observation was performed using FEI Quanta FEG250 (Thermo Fischer Scientific, Oregon USA).

2.10.2 Ultrathin Section Transmission Electron Microscopy

Mouse tissue sections and cells were fixed with 2.5% glutaraldehyde (GA) and 2% paraformaldehyde (PFA) in the NaHCa buffer (100 mM NaCl, 30 mM HEPES, 2 mM CaCl2, adjusted at pH 7.4 with NaOH) for 4 hours at room temperature. Post-fixation was performed with 0.25% osmium tetroxide/0.25% potassium ferrocyanide and 1% tannic acid. After staining en bloc with 5% aqueous uranyl acetate, dehydration with a series of ethanol and infiltration were completed for the plastic embedding in TER (TAAB Epoxy Resin). After the polymerization at 65°C for a few days, the ultrathin-sections (~60 nm) obtained by Ultramicrotome (Leica Ultracut UCT, Vienna Austria) were mounted in EM grids, stained with lead citrate, and then observed by FEI Talos F200C 200kV transmission electron microscope (Thermo Fischer Scientific, Oregon USA) with Ceta-16M CMOS-based camera (4kx4k pixels under 16bit dynamic range) to visualise cilia and mitochondrial morphology.

2.11 Western Blot analysis

Cells were washed in 6cm culture dishes by adding cold PBS and gently rocking. PBS was aspirated and the cells were lysed by adding 100ul of RIPA buffer (Merck) supplemented with 0.1 % (v/v) protease and phosphatase inhibitor cocktail (Sigma-Aldrich, US). Cells were incubated for 20 min on ice, the lysate centrifuged at 13,500 x g for 10 min at 4°C, and the supernatant collected. Protein concentration was measured using the Bio-Rad protein assay, a colorimetric assay based on the Bradford dye-binding method (Bradford, 1976). Samples were mixed with 4 x Laemmli sample buffer (to give a 1 x final concentration of 10 % Glycerol, 50 mM 2-mercaptoethanol, 62.5 mM Tris-HCL pH 6.8, 1 % LDS, 0.005 % Bromophenol Blue) and then denatured at 95° C for 3 min. Proteins were resolved by SDS-PAGE using

4-20 % TRIS-glycine gradient midi gels (Bio-Rad), in electrode buffer (0.1% w/v SDS, 192 mM glycine, 25 mM Tris base, pH 8.3; Bio-Rad) in BioRad criterion tanks. Proteins were resolved firstly at 100 V to migrate through the stacking gel then at 150 V until the dye front reached the end of the gel. Proteins were then transferred onto a nitrocellulose membrane (Immobilon-P, Millipore Corporation) using wet transfer. Transfer stacks comprised of the gel, membrane, Whatman paper and sponges, were assembled in Bio-Rad cassettes and transferred for 16 h at 25V in transfer buffer (25 mM Tris base, pH 8.3, 192 mM glycine and 20 % methanol). The membranes were then blocked with 5 % non-fat dry milk (Marvel) in TBST (0.1%) for 1h at room temperature. The membrane was then probed with the appropriate primary antibody (Table 2.5) for 1h at room temperature and washed with TBST 3 times for 5 mins. Membranes were then incubated with HRP conjugated secondary antibodies against IgG of the primary antibody host species for 1h at room temperature. Following 3 x washes in TBST, Clarity Max Western ECL substrate was added to the membranes for 5 mins (Bio-Rad #1705062) and chemiluminescent signal imaged using a Chemidoc imager (Bio-Rad).

Antibody Target	Manufacturer	Catalogue Number	Host Species	Antibody Dilution
TAp73	Bethyl	A300-126A	Rabbit	1:1000
OPA1	BD Biosciences	612606	Mouse	1:1000
Mitofusin-1	Cell Signaling	14739	Rabbit	1:1000
Mitofusin-2	Cell Signaling	9482	Rabbit	1:1000
p21	Santa Cruz	Sc-6246	Mouse	1:200
ATP5B	Abcam	Ab14730	Mouse	1:1000
HA	Santa Cruz	Sc-7392	Mouse	1:500
GAPDH	Sigma-Aldrich	G8795	Mouse	1:5000
B-Actin	Santa-Cruz	Sc-47778	Mouse	1:1000
HSP-90	Santa-Cruz	Sc-13119	Mouse	1:1000
Total Human OXPHOS Cocktail	Abcam	Ab110411	Mouse	1:1000

Table 2.5. List of antibodies used for Western Blotting experiments.

2.12 Immunocytochemistry

2.12.1 Staining of mitochondrial network in fixed cells

H1299 cells were transfected as described previously, seeded onto sterile glass coverslips (Type 1.5 thickness) in 6cm dishes and cultured overnight. Cells were then fixed in 4 % paraformaldehyde (PFA, VWR) diluted in PBS at room temperature for 20 mins. The cells were washed 3 times in PBS and permeabilised at room temperature for 20 min in 0.2% Triton-X 100/PBS. Cells were washed with PBS/Tween (0.1%) 3 times, cover slips transferred to 12-well plates, and blocked in 5% Goat Serum/PBS/Tween for 1h at room temperature. Anti-ATP5B antibody (mouse monoclonal, Abcam) was diluted 1:1000 in PBS and cover slips incubated overnight at 4°C. Cells were washed 3 times with PBS/Tween (0.1 %) and incubated with Alexa Fluor 488 goat anti-mouse secondary antibody diluted 1:1000 in PBS for 1 h at room temperature whilst protected from light. Cover slips were washed 3 times with PBS/Tween (0.1 %) and where appropriate cells transfected with HA-TAp73-pcDNA3 plasmid were incubated with rabbit anti-HA antibody (Santa Cruz #805) diluted 1:200 in PBS for 1h at room temperature. Wash steps were repeated and cover slips incubated in Alexa Fluor 568 goat anti-rabbit secondary antibody diluted 1:1000 in PBS. Cover slips were washed 3 x in PBS/Tween (0.1%) and cells mounted to glass slides with Vectashield plus antifade mounting medium with DAPI (Vector Laboratories #H-2000). Once mounting medium had set, images were acquired using a Zeiss LSM880 confocal microscope and 63x oil objective.

2.12.2 Mitochondrial network measurements using intellesis trainable object segmentation

Fluorescent images acquired using the Zeiss LSM880 multiphoton confocal microscope and 'Tiff files' were used to measure mitochondrial area utilising the Zen Blue image analysis software intellesis module. An analysis protocol devised to identify the ATPB5- stained mitochondria, with Alexa 488 conjugated secondary antibody generated masks around each individual mitochondrion for quantitative measurement. A minimum of 20 cells from each different treatment were analysed In conditions where the mitochondria were fragmented, there were more mitochondria that were shorter (with a smaller area) and in treatment conditions were mitochondria were fused there were fewer mitochondria with a larger area.

2.13 Immunohisochemistry on tissue sections

2.13.1 Immunofluorescence staining of cilia

Dissected trachea or whole brains were fixed in 4% paraformaldehyde (PFA) for 48h and embedded in paraffin. Traverse sections of trachea and coronal brain sections containing the lateral ventricles were obtained for analysis of ciliated cell populations. Sections were deparaffinised by immersion in Xylene

(Sigma) followed by a gradient of 100%-70% ethanol (Sigma). Antigen presentation was performed by heating in a microwave at 292W for 15 minutes in 0.01M sodium citrate. Tissue was blocked with 5% normal goat serum for 1h at room temperature (RT) and incubated with anti-Ac-a-tubulin (Thermofisher; T7451) diluted 1:1000 in PBS overnight at 4°C in a humidified atmosphere. Samples were washed 3 times in PBS and incubated for 1 h with Alexa Fluor 488 secondary antibodies (Molecular Probes; Invitrogen) at RT. Samples were washed 3x in PBS and 500nM DAPI/PBS solution added for 10 mins at RT. Samples were washed again 3x and mounted using Prolong Gold Antifade mountant (Thermofisher; P36930). Images were acquired through confocal microscopy (LSM 510, Zeiss), fitted with an argon laser (488 nm excitation), and UV excitation at 405 nm.

2.13.2 Chromogenic detection

For single-channel detection of TAp73 and FOXJ1, tissue sections were fixed and embedded as described above. IHC was carried out using the Ventana Discovery Ultra platform (Roche). Deparaffinization was performed by immersion in Ventana Discovery Wash buffer (Roche; 950-510) for 3 x 8 minute washes at 69°C. Antigen Retrieval was performed by incubation in Ventana CC1 buffer at 95°C for 32 minutes. The slides were blocked by incubation with Discovery goat IgG block (Roche; 760-6008) for 12 mins at 37°C. Primary antibody incubations were carried out using Anti-p73 (Bethyl #A300-126A) diluted 1:200 for 3h at 37°C or anti-Foxj1 (eBioscience #14-9965-82) diluted 1:200 for 1h 37°C. Antibodies were diluted in EnVision Flex Antibody Diluent (Dako; DM830). The detection reaction was performed using UltraMap DAB anti-Rb Detection Kit (Roche; 760-151) according to the manufacturer's instructions. Single-channel chromogenic detection was also performed for OPA1 (Abcam #157457; 1:200 dilution) and Ac-a-tubulin (Thermofisher; T7451; 1:200 dilution). to optimise the staining protocol before sequential staining for multiplex IHC. Slides were imaged using the Hamamatsu slide scanner.

2.13.3 Multiplex Immunohistochemistry

Tissue sections were fixed, embedded and stained with primary antibodies as previously described in section 2.13.2. Secondary antibody incubation was perfoemd with anti-rabbit secondary (Ventana Omni-map) incubated for 16 mins. Multiplex antibody detection was performed using Opal fluorophores according to the manufacturer's instructions (OPA1; Opal 690, TAp73; Opal 570 , Ac-α-tubulin; Opal 540). Slides were imaged using the Ventana Discovery imaging system and quantification of signal intensity performed using In-form software.

2.14 Annexin V/APC measurement of cell death induction using Incucyte platform

H1299 cells (TAp73 CRISPR KO and Cas9 control) were seeded at a density of 100,000 cells/well in a 12 well plate and cultured overnight at 37°C and 5% CO_2. Cell culture media was aspirated and fresh media

added containing 1:3000 Annexin V/APC dye (made in house by Dr Xiao-Ming Sun), 1 µM $CaCl_2$, and incubated for a further 30 mins. The BH3 mimetics ABT-737 (Inhibitor of BCL-2 and BCL-xL) and S63845 (Inhibitor of MCL-1) were added to cells at a range of concentrations ranging from 0.25um-10 µm per well or vehicle control (0.1% DMSO) and the cell culture plate placed in the IncuCyte live cell imager. Assay plates were scanned using the adherent cell-by-cell module with four images acquired per well to track cell death induction. Images were acquired every 15 mins for 6 hours using the 20x objective. Label-free counts were obtained using the phase contrast channel with a segmentation adjustment of 0.2 and a minimum area of 50 μm^2. The green channel was imaged using an acquisition time of 300 ms and objects counted using the Top-Hat segmentation method with a threshold of 2.0 green calibrated units (GCU). Autofluorescence of the media was subtracted using the mean GCU of control wells which did not contain Annexin V/APC. Green objects were calculated as a percentage of total cells counted in the phase channel to obtain percentage values for cell death induction.

2.15 Measurement of mitochondrial oxygen consumption

Mitochondrial stress tests were performed using the SeaHorse XFe96 extracellular flux analyser (Agilent). Wild-type or TAp73 knockout (TAp73 KO) H1299 cells were seeded using a range of seeding densities spanning 10,000 – 40,000 cells per well in 80 ul of growth medium in 96-well Seahorse microplates. After seeding, the plates were spun at 200g for 3 mins at room temperature. Only cell culture media was added to the four corner wells for background subtraction. The plate was incubated overnight at 37°C, 5% CO_2. Sensor cartridges were hydrated by pipetting 200ul XF calibrant into the utility plate and placing in a non-CO2 incubator 37 °C overnight. The following day, growth media was removed, and cells washed three times in unbuffered DMEM Seahorse assay medium (32 mM NaCl, 2 mM GlutaMAX, 1 mM sodium pyruvate, 11 mM D-glucose, pH 7.4). The plate was then incubated in a 37 °C non-CO2 incubator for 1h. The canonical mitochondrial toxins oligomycin A (port A), FCCP (port B), antimycin A and rotenone (port C) were diluted in 5mL media as described in the table below and added to the injection ports of the sensor cartridge plate at the following respective volumes: 20 µl, 22 µl, 25 µl.

Oligomycin A	FCCP	Antimycin A/ Rotenone
2 µM	500 nM	2 µM

Table 2.6. List of concentration of canonical ETC inhibitors

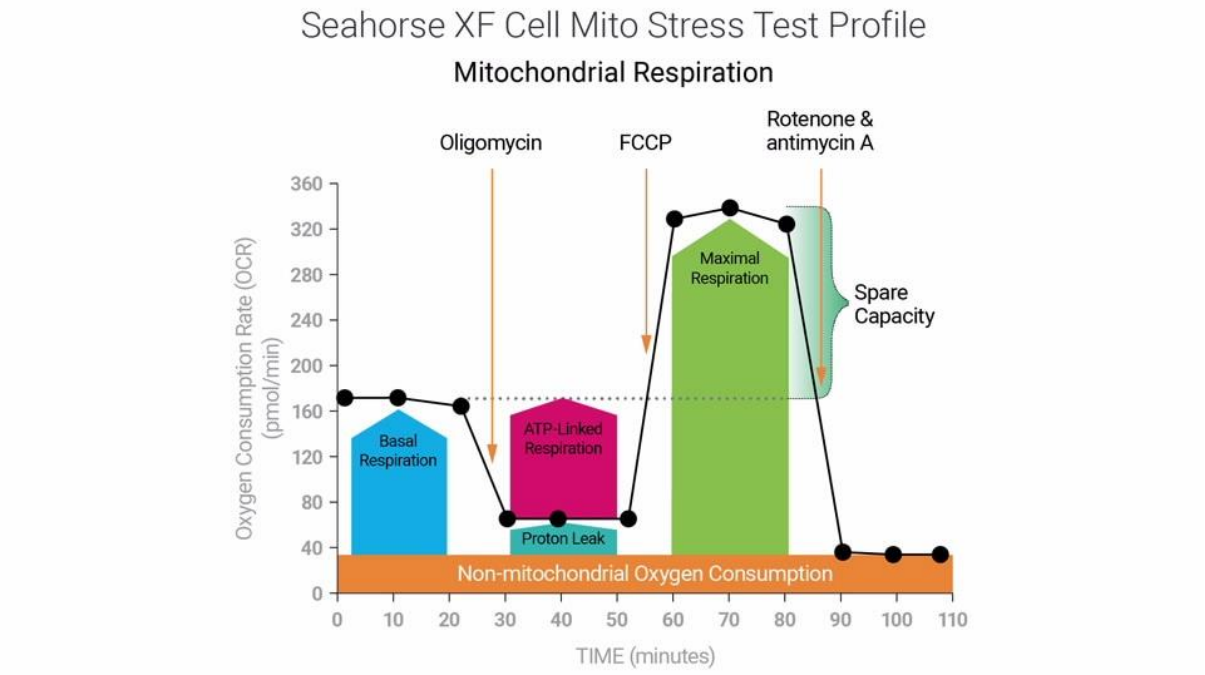

Figure 2.1 Oxygen consumption rate (OCR) profile of a standard mitochondrial stress test

(sourced from Agilent Technologies Agilent Seahorse XF Cell Mito Stress Test Kit User Guide).

A standard mitochondrial stress test was performed by measuring oxygen consumption rate (OCR) in real time following the time addition of canonical inhibitors of the electron transport chain (ETC). The readouts of OXHPHOS activity obtained are outlined in figure 2.1. Firstly, basal OCR is measured in untreated cells. The injection of the complex V inhibitor oligomycin determines the ATP-linked OCR, as hyperpolarisation of the mitochondrial membrane prevents protons passing through the complexes. Next, injection of FCCP serves as an uncoupling agent by carrying protons across the mitochondrial inner membrane. Finally, the addition of rotenone and antimycin A inhibits mitochondrial complexes I and III respectively, thereby abolishing mitochondrial respiration. The persisting OCR can be considered as non-mitochondrial respiration and was subtracted from all measurements. OCR was expressed as pmol/minute per 10,000 cells. The data was normalised to cell number using Hoechst 33342 (16 µM) which was added to the Seahorse assay plate wells at a 1 in 10,000 dilution after obtaining OCR measurements and the cells incubated at 37°C for 10 mins. Individual wells were imaged using the 5x objective on a Zeiss Observer 7 microscope fitted with a Colibri 7 LED fluorescence light source.

2.16 ChIP-seq Analysis

Publicly available ChIP-seq data sets (GEO series GSE15780) against p53 and p73 isoforms (TAp73α and TAp73β) in the human osteosarcoma cell line Saos-2 were interrogated for genes associated with the regulation of mitochondrial fusion and fission (Koeppel et. al., 2011). BED files were converted to WIG files, and UCSC Genome Browser annotated tracks generated using the ChIP-Seq tools and web server (Ambrosini et. al, 2016). ChIP-seq tracks were generated for each replicate and cross-checked against input tracks to account for non-specific signal. The maximum Y-axis scale was set to 100 for each genomic loci to a allow for relative depiction of signal strength.

2.17 Gene Ontology Analysis

GO analysis was performed on the complete set of genomic binding sites of p73 (1769 genes) identified In-Situ by Marshall et. al. (2016) using dissected murine trachea. The list of genes was analysed using the PANTHER GO tool v.17 overrepresentation test. Genes were analysed against the complete set of Mus musculus genes annotated with the GO biological process complete annotation data set. Fold-enrichment values were plotted for selected GO classes ($p = <0.01$).

2.18 Statistical Analyses

Statistical analyses were performed using GraphPad Prism (www.graphpad.com). Data are presented as mean values and error bars indicate the standard error of the mean (±SEM) or standard deviation (±S.D). The number of biological replicates for each experimental condition (n) is indicated in the corresponding figure legend.

Student's t-test (unpaired) was used to determine if there was a significant difference between the means of two experimental groups. The t-test assumes that the data was randomly sampled and that the data variables follow a normal distribution.

Chapter 3: TAp73 regulates mitochondrial dynamics through an OPA1 axis

3 TAp73 regulates mitochondrial dynamics through an OPA1 axis

3.1 Introduction

As discussed in the introduction (Chapter 1), TAp73 knockout mice are characterized by defective ciliogenesis in diverse tissues. Indeed, studies have shown that multiciliated cells of the brain, airways, and reproductive system in TAp73$^{-/-}$ mice display abnormal cilia abundance and function. This has a profound relevance for human health, as dysfunctional ciliogenesis underlies a large number of human diseases. These include hydrocephalus, hippocampal dysgenesis, Primary Ciliary Dyskinesia, Bardet-Biedl syndrome, asthma, chronic obstructive pulmonary disease (COPD), and sterility. For example, it was observed by Li and colleagues that increased expression of p73 was associated with abnormal ciliogenesis - namely increased cilia density and length – in the development of hyperplastic regions in patients with nasal polyps (Li et al., 2011). However, further work is needed to directly implicate alterations in p73 function with chronic respiratory diseases, for example through the use of genome-wide association data.

Recent evidence indicates that the correct execution of ciliogenesis is associated with the abundance of functional mitochondria (Burkhalter et al., 2019). To this end, ciliated epithelial cells contain mitochondria with highly folded cristae localized to the apical surface (Cloonan et al., 2016). This enables multiciliated cells to generate sufficient amounts of ATP for axonemal extension and ciliary beating (Cloonan et al., 2016). Moreover, studies have shown mitochondrial dysfunction to be a driver of disease pathogenesis in COPD and emphysema (Mizumura, et al., 2014). Specifically, it was shown that mitochondria from airway epithelial cells of COPD patients display a loss of cristae and fragmentation of the mitochondrial network (Hara et al., 2013; Hoffmann et al., 2013). Taken together, these studies provide evidence that the regulation of mitochondrial biology is important for ciliated cell function and the maintenance of airway homeostasis.

It is therefore plausible that the regulation of mitochondrial function by TAp73 is required for the correct execution of ciliogenesis in epithelial cells. Indeed, we and other groups have previously identified numerous roles of p53 and p73 in regulating mitochondrial function (reviewed in the thesis introduction) which may be dysregulated in the ciliated epithelium of TAp73$^{-/-}$ mice. In the case of p53, it has been implicated in regulating targets such as MFN2, DRP-1, and PGC1a, which regulate mitochondrial fusion, fission and biogenesis respectively. However a similar role for TAp73 in regulating fusion and fission has not yet been reported. I therefore started by performing bioinformatic analysis of publicly available ChIP-seq data, where experiments were performed both *in situ* on mouse trachea and *in vitro* to identify TAp73 targets. A notable TAp73 target gene identified from these data sets was the pro-fusion gene *OPA1*, which has a well-established role in regulating mitochondrial fusion,

respiratory complex assembly, cristae morphogenesis and cytochrome c release (Scorrano multiple references). I therefore sought experimentally validate a relationship between TAp73 and OPA1 and examine the consequences of its disruption for mitochondrial function.

3.1.1 Aims and Objectives

- To experimentally validate the potential transcriptional regulation of OPA1 by TAp73 identified through analysis ChIP-seq data
- To perform chromatin immunoprecipitation experiments to investigate if this regulation occurs by direct binding to the OPA1 promoter
- To generate TAp73 knockout cell lines using CRISPR as a tool to investigate this novel TAp73/OPA1 axis

To achieve this, I selected the H1299 cell line to interrogate the effect of TAp73 modulation on OPA1 expression and study the resultant impact on mitochondrial function. H1299 cells were selected due to their lung epithelial origin, a tissue with relatively high levels of TAp73 expression. Moreover, H1299 cells harbor a homozygous partial deletion of the p53 gene and lack expression of functional protein. The use of this model provided the benefit of eliminating any confounding and compensatory role of p53, which shares many transcriptional targets with TAp73. To study the importance of the TAp3/OPA1 axis, I employed CRISPR/Cas9 gene editing to generate TAp73 knockout (TAp73 KO) H1299 cells. I also performed chromatin immunoprecipitation to identify a direct association between TAp73 and the OPA1 promoter region, which validated my findings from previously published ChIP-seq data. Using these tools, I present data supporting a novel role for TAp73 in regulating mitochondrial morphology and function.

3.1.2 ChIP-seq data indicated TAp73 binding to the OPA1 promoter

Genome-wide binding sites for TAp73α, TAp73β and p53 were interrogated from previously published ChIP-seq data (Koeppel at al., 2011). TAp73 and p53 binding patterns for genes of interest were visualized using the USCS Genome browser, with the signal strength indicated being proportional to the number of reads obtained at a given genomic locus. The study employed overexpression of TAp73α, TAp73β, and p53 in Saos-2 cells followed by IP with antibodies directed against the overexpressed protein to identify gene targets. By interrogating the *OPA1* gene locus, I found that the region upstream of the OPA1 transcription start site (TSS) had a significant enrichment of reads at distinct loci that were not evident for the input sample (figure 3.1). Three peaks were evident for TAp73 binding, with the most distal to the TSS having the strongest signal. Moreover, this enrichment was evident for both TAp73α and TAp73β isoforms, suggesting that the SAM domain of TAp73α is not required for this interaction. Furthermore, signal was also evident for p53 adjacent to the OPA1 transcription start site (figure 3.1). This suggests that the ability to bind the OPA1 promoter region may be conserved throughout the p53 family, owing to the presence of a highly homologous DNA-binding domain.

The data sets also provided the opportunity to explore the possibility that TAp73 may have the ability to physically bind additional genes responsible for the regulation of mitochondrial fusion and fission. Obvious candidates to investigate were the Mitofusins, which are responsible for fusion of the outer mitochondrial membrane. Interestingly, defined peaks were evident for TAp73α, TAp73β and p53 at the *MFN-2* promoter region. However, the signal observed at the *MFN-1* locus was negligible when compared with input control, particularly for TAp73α, indicating that it was not bound to this genomic region (figure 3.1). Furthermore, TAp73 target genes may also include regulators of mitochondrial fission, as a strong signal of reads was observed at the *MFF* and *FIS1* genes, albeit the signal observed for *FIS1* was intronic and therefore may not represent a response element. This therefore raises the possibility that TAp73 regulates mitochondrial biology through the control of additional fission and fusion. It was of interest that no signal was observed at the gene locus encoding Drp-1 (*DNM1L*), a fundamental component of mitochondrial fission. The regulation of Drp-1, however, frequently occurs via activating phosphorylation.

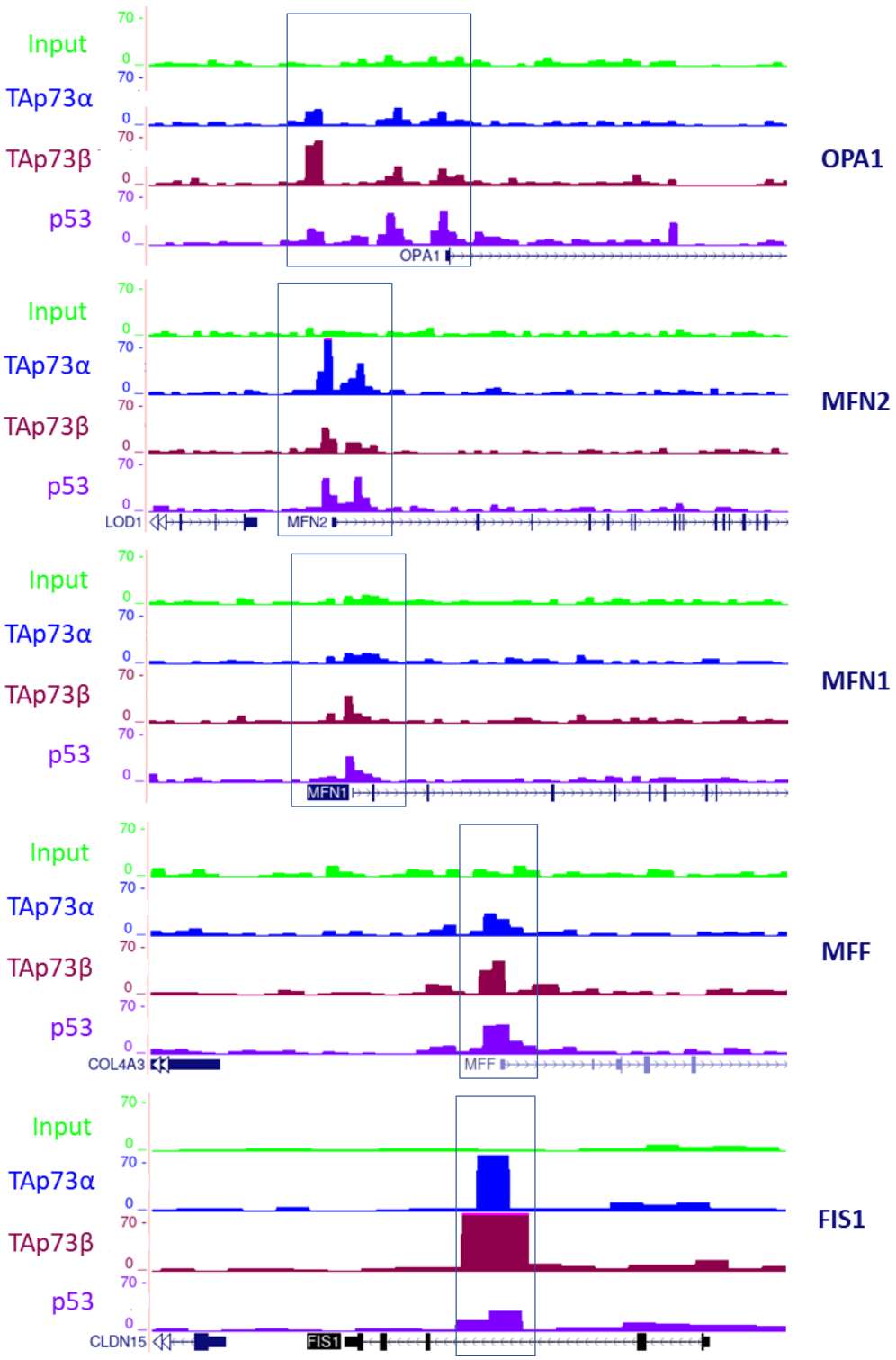

Figure 3.1 ChIP-seq data showed binding of TAp73α, TAp73β and p53 to regulators of mitochondrial fusion and fission.

The binding profiles were obtained by overexpressing the indicated transcription factors in Saos-2 cells and bound chromatin immunoprecipitated. Input control is shown in green. The peak height for each track is proportional to the number of reads at each loci (indicated right). ChIP-seq tracks were obtained for the *OPA1, MFN2, MFN1, MFF* and *Fis1* genes and upstream regions of DNA. Sequencing read files were obtained from the GEO data set GSE15780 (Koeppel et al., 2011).

3.2 Results

3.2.1 TAp73 and OPA1 expression correlate in H1299 cells

I next sought to investigate whether alterations in TAp73 expression had a downstream effect on OPA1 transcription in H1299 cells. In order to address this, ectopic expression of either HA-fused TAp73α or TAp73β isoforms was induced for 48 hours using overexpression constructs. Firstly, RT-qPCR was performed analyzing expression of TAp73 mRNA to confirm successful overexpression (Figure 3.2a)and immunoblots against hemagglutinin confirmed translation of TAp73 protein (figure 3.2d). This led to a significant increase in OPA1 transcripts following overexpression of both isoforms of TAp73 (3.2b). Notably, an approximately 30-fold increase in OPA1 mRNA was observed following the overexpression of TAp73β due to its increased stability and transcriptional activity relative to TAp73α, which increased expression of OPA1 10-fold. The expression of p21, a known transcriptional target of TAp73 was also increased, therefore serving as a positive control (figure 3.2c). I also observed an increase in OPA1 expression at the protein level following overexpression of TAp73α and TAp73β (figure 3.2d). Next, I investigated the effect on OPA1 expression following TAp73 silencing using siRNA. Depletion of TAp73 mRNA transcripts using this approach led to a concurrent reduction in OPA1 expression by more than 60%, with a similar effect observed for p21 mRNA (figure 3.2e-g). Taken together, these data indicate that TAp73 regulates OPA1 gene expression in H1299 cells.

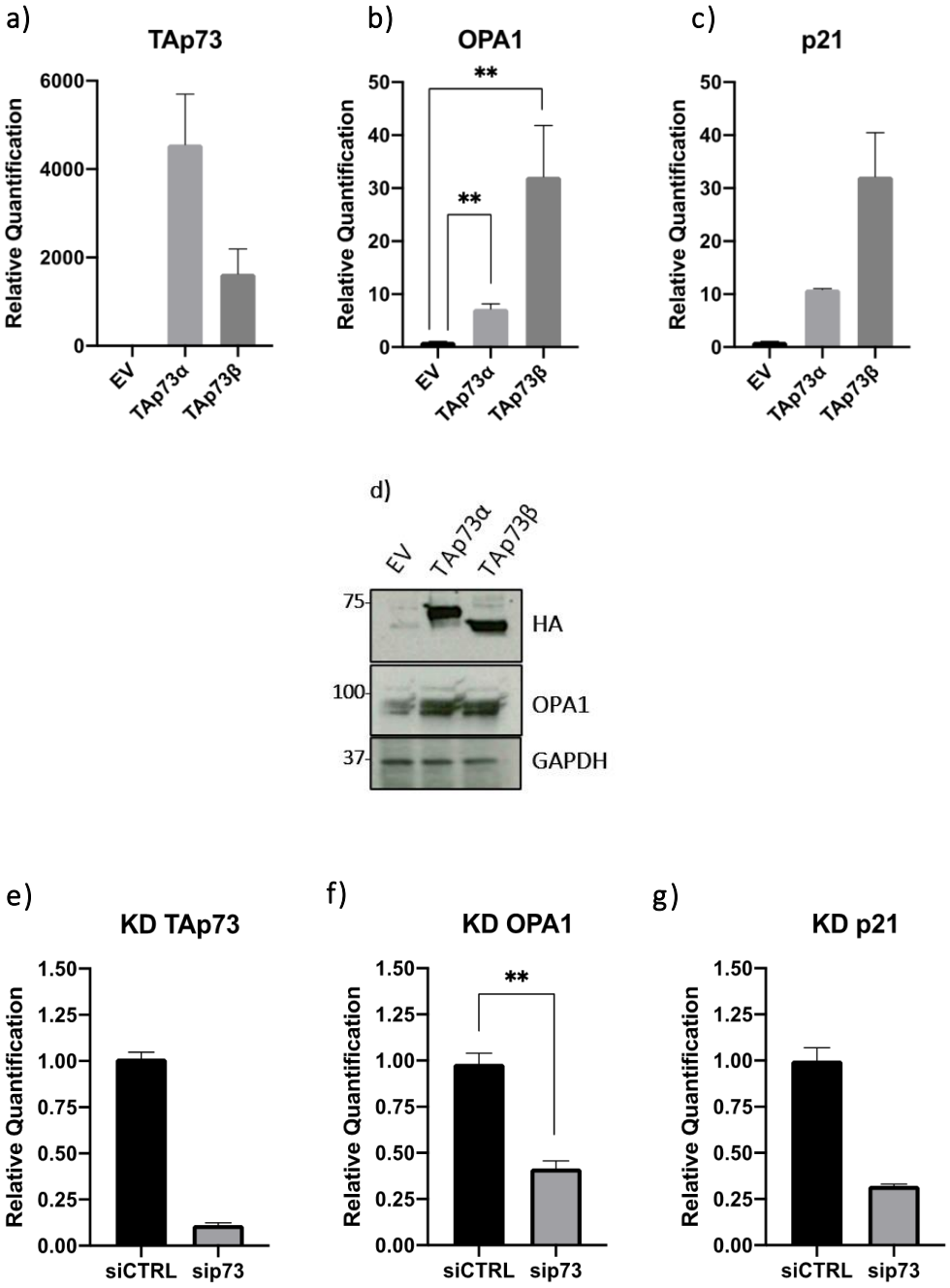

Figure 3.2 TAp73 expression correlates with OPA1 expression in H1299 cells.

(a-c) H1299 cells were transfected with HA-TAp73α or HA-TAp73β overexpression constructs and RT-qPCR performed to assay the abundance of TAp73, OPA1 and p21 (positive control) transcripts relative to empty vector (EV) control.(d) Protein lysate was collected from the experiment described in (a-c) and immunoblotted for HA and OPA1. (e-g) TAp73 was silenced in H1299 using siRNA transfection and RT-qPCR performed against the same targets. Relative expression to EV control was calculated using the ΔΔCt method and data shown as mean ± SEM (n=3). (**) $p<0.01$ (Student's t-test).

3.2.2 TAp73 regulates OPA1 expression and can bind to the putative OPA1 promoter

In order to determine whether the correlation between TAp73 and OPA1 expression was due to transcriptional regulation, I performed chromatin-immunoprecipitation (ChIP) followed by RT-qPCR. After ectopic TAp73α overexpression in H1299 cells, cross-linked gDNA was isolated and sonicated to obtain fragments approximately 700 base pairs in size (figure 3.3b), and TAp73-bound regions of chromatin immunoprecipitated using anti-HA antibody. To perform qPCR, an experimentally validated sequence for the OPA1 promoter region which spanned 800bp downstream and 100bp upstream of the transcription start site (TSS) was obtained from the Eukaryotic Promoter Database (Dres et a., 2017; Figure 3.3a).

Two different primer pairs were designed within the OPA1 promoter region to amplify these regions of interest in chromatin obtained from the anti-HA IP fraction and IgG control. The relative primer positions and size of the amplicons, denoted OPA1 'A' and OPA1 'B', are indicated in figure 3.3b. When RT-qPCR was performed using these primers, a greater than 10-fold enrichment for both pairs was observed (figure 3.3c) in the TAp73 pull-down relative to the IgG control. This indicated that TAp73 regulates OPA1 expression by direct binding to the promoter sequence. The specificity of the pull-down was confirmed by RT-qPCR of the MDM2 promoter region, which was significantly enriched relative to the IgG control (greater than 30-fold enrichment; figure 3.3c). There was also no enrichment of the SAT2 promoter locus, used as a control for unspecific enrichment of non-TAp73 target genes.

In addition, analysis of the putative OPA1 promoter region was performed using the JASPAR transcription factor binding prediction tool (Khan et al., 2018). Analysis of the OPA1 promoter showed that two regions of the genome upstream of the OPA1 transcription start site were highly enriched for the *TP73* binding motif, indicated by red boxes in figure 3.2a, further demonstrating the ability of TAp73 to regulate OPA1 transcription.

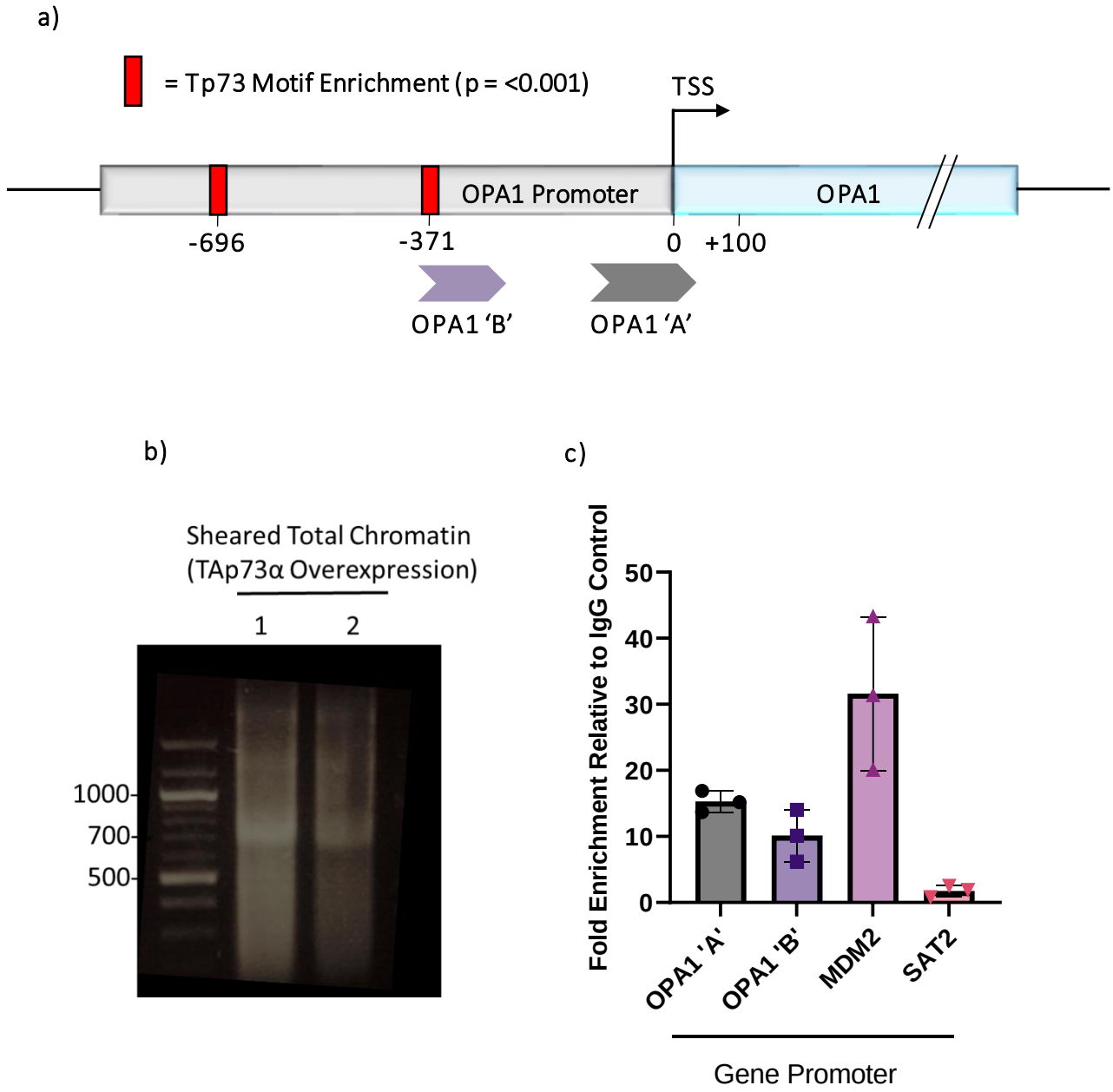

Figure 3.3 Chromatin Immunoprecipitation (ChIP) of TAp73 bound regions was enriched for the OPA1 promoter

HA-TAp73 was overexpressed in H1299, and cross-linked chromatin immunoprecipitated using anti-HA antibody. (a) RT-qPCR primers were designed in the promoter region of the OPA1 gene (indicated as OPA1 'A' and OPA1 'B'), immediately upstream of the TSS. The red squares indicate regions highly enriched for the *TP73* motif ($p<0.001$). Chromatin was sheared to yield fragments around 700bp in size (b), and RT-qPCR performed to quantify the fold enrichment of the OPA1 promoter region in IP sample relative to IgG control. Positive and negative control promoter regions were assayed by calculating the enrichment of chromatin with primers specific to the *MDM2* (positive) and *SAT2* (negative) genes. RT-qPCR was carried out on 3 independent ChIP experiments and data shown as individual data points ± SEM (n=3).

To perform an unbiased analysis of a complete list of p73-bound genes, previously published ChIP-seq data was analysed using the PANTHER GO overrepresentation test. In this analysis, the fold enrichment of the inputted list of genes is calculated based on number of genes expected to feature in each GO category. Marshall and colleagues (2016) performed ChIP sequencing *in-situ* on mouse trachea to identify a complete list of p73 bound genes (1769 genes).

The results showed that there was an overrepresentation of genes that regulate mitochondrial membrane organization (Gene Ontology ID: 0007006). These included *OPA1*, *MFN2* and *PPARGC1A*, the gene encoding a subunit of PGC-1α. Analysis of this additional data set corroborated the finding that TAp73 regulates OPA1 expression and suggests that this regulation, together with other potential candidates highlighted, represents a role for TAp73 in regulating mitochondrial dynamics. The highest significance values for overrepresentation were ascribed to the regulation of cell cycle and cellular response to stress, which, as the most commonly appreciated canonical functions of p73, validated the findings of the overrepresentation test.

The generation of these data from mouse trachea also highlighted an *in-vivo* relevance for the relationship between TAp73 and OPA1 in ciliated epithelial cells, as TAp73 expression is specific to this cell type within the trachea. As a result, the relevance of the TAp73/OPA1 axis in this tissue was explored in chapter 5.

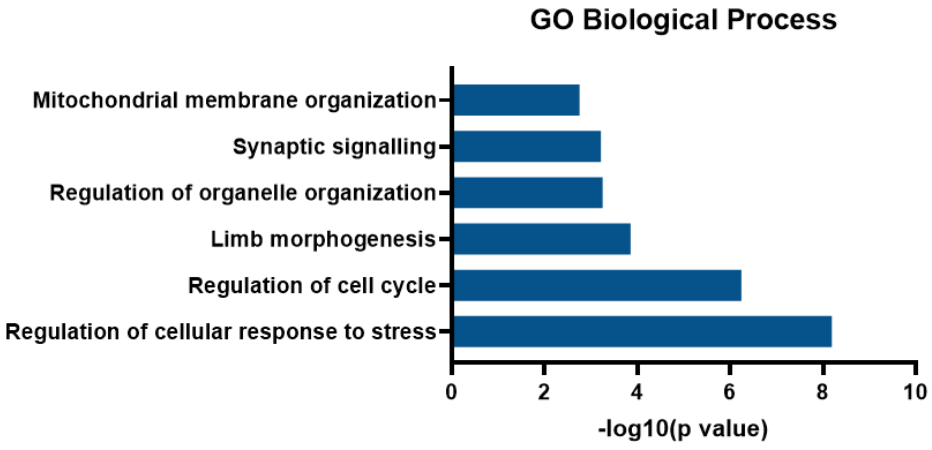

Figure 3.1 Gene Ontology (GO) analysis was performed on a complete set of TAp73 target genes identified through ChIP-seq.

An overrepresentation test was performed using 1769 TAp73 targets identified in mouse tracheal samples (Marshall et al., 2016). Enriched GO classes are listed according to their relative p values.

3.2.3 TAp73 knockout cell lines were generated using CRISPR/Cas9 targeting

To perform a deeper investigation of the proposed TAp73/OPA1 axis, I generated TAp73 knockout cell lines using CRISPR/Cas9 targeting. In addition to being used to validate the observation that TAp73 regulates OPA1 expression, it provided a valuable tool to investigate the importance of this axis in functional assays. Two different experimental approaches were used, separately targeting exon 2 and exon 3, to generate two distinct cell lines that do not express functional TAp73 protein.

Knockout Generation by Transient Transfection of H1299 Cells

The first approach taken was to transiently transfect H1299 cells with Cas9 expression plasmid and sgRNA's for 24 hours using lipofectamine. The three different guides were designed to target Exon 2 of the TAp73 gene. Selection of transfected cells was achieved by treatment with 2.5 µg/µl puromycin for a further 24 hours. This concentration was selected as it induced almost complete cell death in cells that were not transfected with Cas9 expression plasmid, clearly evident from rounded and detached cells (figure 3.5). Next, the activity of gRNA's was assayed by performing a mismatch repair assay on genomic DNA from the mixed population of transfected cells to look for evidence of gene editing. Exon 2 of TAp73 was amplified by PCR, and heteroduplexes formed by denaturing and annealing Wild-type with edited DNA strands, which should be present in the mixture of DNA products. The mismatched bases that form were digested by T7 endonuclease. The resultant PCR fragments were run on a gel and shown in figure 3.5.

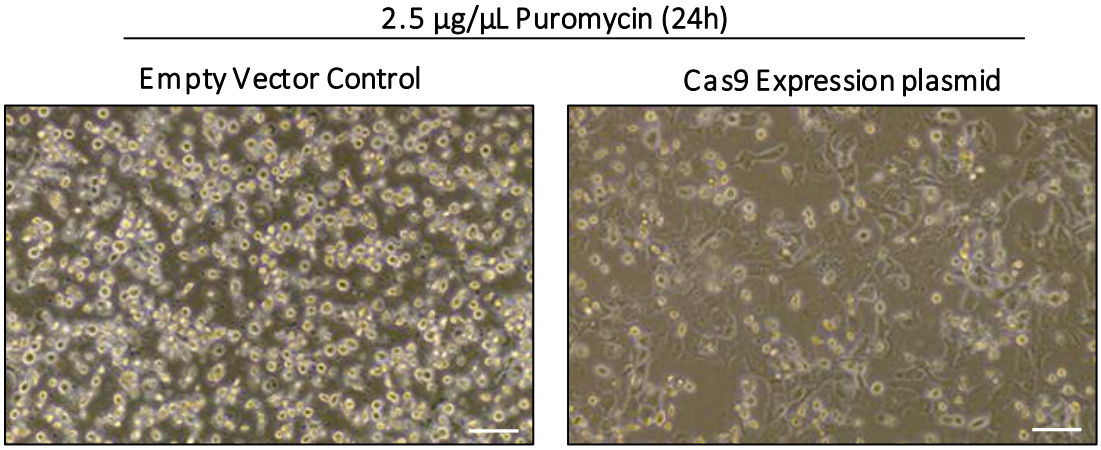

Figure 3.2 Treatment of H1299 cells with 2.5 µg/µl puromycin induced cell death in non-transfected cells.

Phase contrast images of cells (transfected with either Cas9 expression plasmid or empty vector control) were obtained following selection with 2.5 µg/µl puromycin for 24 hours. Scale bar = 100 µM.

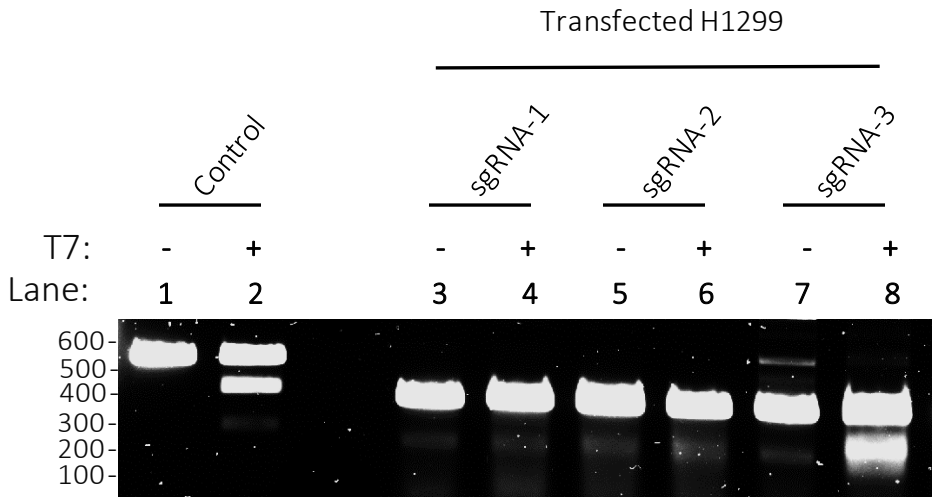

Figure 3.3 Mismatch repair assay performed on populations of cells transfected with Cas9 expression plasmid and gRNA.

gDNA was isolated from CRISPR edited pools of cells, transfected with the indicated gRNA's targeting TAp73 exon 2. Following PCR amplification of a portion of exon 2 (355bp) heteroduplexes were formed and mismatches digested by T7 endonuclease. Control PCR sample was digested to confirm activity of the enzyme. Each T7 treated sample was loaded next to the undigested control.

The activity of T7 endonuclease was confirmed by the digestion of a control PCR fragment (figure 3,6; lane 1 & 2). An amplicon of expected size in all transfected populations (355bp) confirmed the amplification of the region of DNA surrounding the target sites of CRISPR gRNA. Strong evidence of T7 endonuclease mediated cleavage was observed in heteroduplexes derived from cells targeted with sgRNA-3 (lane 8), which was not evident in the corresponding control (lane 7). The population of cells transfected with this guide was therefore prioritized for dilution plating and clonal populations screened for knockout of the TAp73 gene.

Knockout Generation By Doxycycline-Inducible gRNA expression

In parallel to transient transfection of H1299 cells, TAp73 knockout cells were generated using a doxycycline-inducible system. H1299 cells that constitutively express a lentiviral Cas9-mCherry vector and a separate gRNA-GFP expression vector under the control of a Tetracycline repressor (*TetR*) were seeded in 6cm plates (Kind gift from Prof. Melino). The expression of these constructs was confirmed by imaging green and red fluorescence (figure 3.7a). Expression of sgRNA and subsequent Cas9 activation was induced by incubating cells in culture media containing 2ug/mL doxycycline for 48 hours. The guides in the construct used a different targeting strategy to that employed with the transiently transfected cells as they were directed against Exon 3. This therefore provided a second, genetically

distinct cell line to validate my findings. Following Cas9 activation with doxycycline, TAp73 expression was analysed by western blot of the mixed population of cells (so-called due to the mixture of gene editing events the population will have)(Figure 3. 7b). Samples were loaded alongside lysate from H1299 overexpressing HA-TAp73α (performed as described in previous sections) to confirm that the higher molecular weight band of the two present was TAp73α. The strong knockdown of this band in doxycycline treated cells indicated successful CRISPR targeting of TAp73 compared with the WT control which expressed Cas9 protein only. Notably, the protein knockdown was stronger than obtained with siRNA mediated knockdown and suggested a large number of cells were edited and indicating that the induction of double-strand breaks using this system was highly efficient.

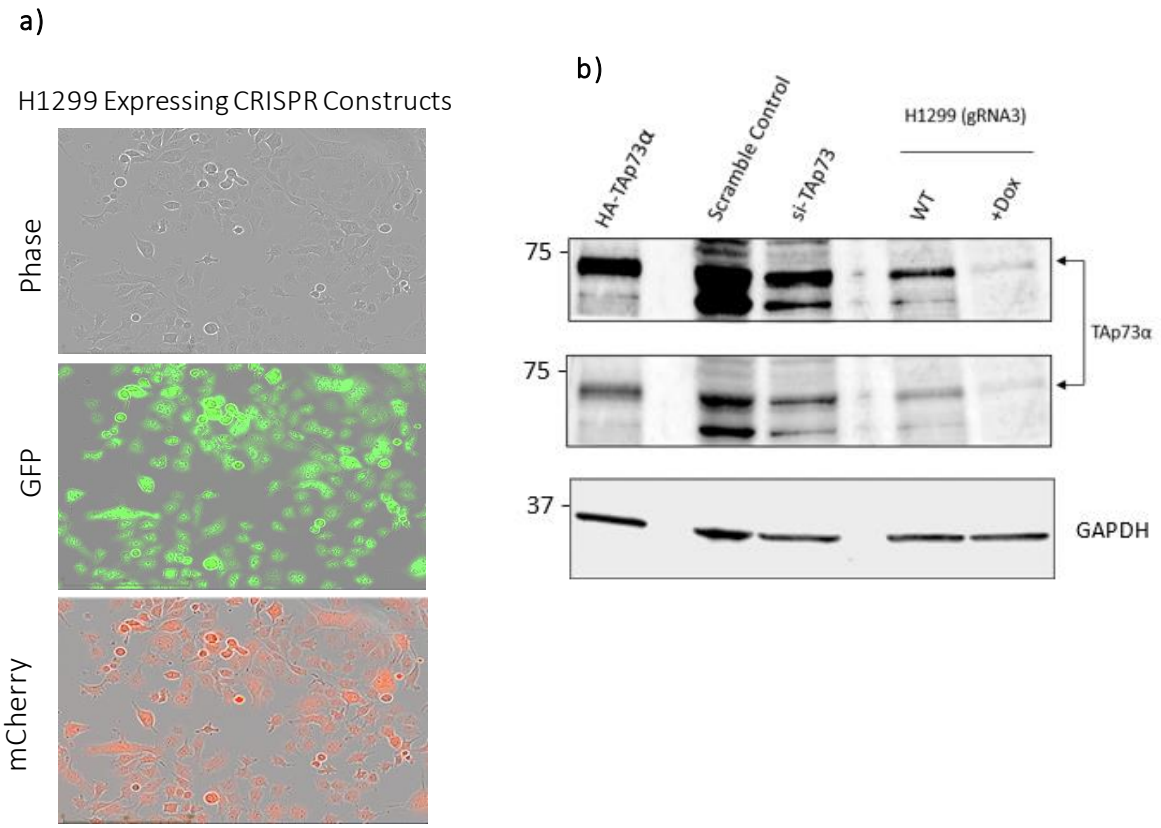

Figure 3.4 Doxycycline-inducible CRISPR targeting of led to efficient knockdown of TAp73

a) H1299 cells stably expressing gRNA-eGFP and Cas9-mCherry expression constructs were imaged using red and green fluorescent channels. Scale bar = 100 µM. b) Western blot against TAp73 following induction of Cas9 activity with doxycycline treatment for 48 hours. Lysate from the mixed population of Doxycycline induced cells (+Dox) was loaded next to WT control which expressed only Cas9 protein. Samples from cells overexpressing TAp73a and with TAp73 silenced were loaded as a control. Two different exposure times for the TAp73 blot are shown.

3.2.4 Screening of clonal populations obtained by dilution plating

After induction of Cas9 activity using both of the previously described methods, clonal populations derived from individual cells were generated by dilution cloning in 96-well plates. Cells were seeded at a density of 0.5 cells/mL and cultured for 14 days in pre-conditioned growth medium. Typically, 10-15% of wells yielded single colonies and these were expanded for culture in 6-well plates. Populations of cells were screened by western blot to identify potential knockout colonies to later be submitted for sanger sequencing of INDELS.

A representative western blot carried out to screen colonies is shown in figure 3.8a, with the colonies assayed displaying a range of TAp73 expression levels. Overexpressed TAp73 α was loaded as a positive control. TAp73 expression appeared to be knocked out in Clone 7 (indicated with a purple box on the gel), and was therefore selected as a clone of interest for further characterization by sanger sequencing. Interestingly, there was also a strong downregulation of the lower molecular weight band present, suggesting it may be an alternative TAp73 isoform. However, it is not possible to determine if it is an N terminal (ΔEx2/3p73) or C-terminal splice variant of TAp73 since the antibody used is direct against N-terminus and does not discriminate between C-terminal TAp73 isoforms. Importantly, we observed an ablation of TAp73α, the most abundant C-terminal isoform.

Genomic DNA was isolated from Clone 7 (herein denoted as G3:B4:C7), and the region surrounding the guide sequence within exon 2 was amplified by PCR. The product was cloned into pJet1.2 blunt-ended vector and expanded in *E.coli.* That way, when isolating plasmid DNA from single colonies, sequencing reads obtained were derived from a single PCR oligonucleotide product, and therefore a single chromosome. A minimum of 5 colonies were picked for each clone to achieve a highly probable coverage of both chromosomes from the resultant reads. In the case of G3:B4:C7, 14 colonies were picked for and the sequencing in total and reads aligned to the wild-type sequence (figure 3.8b). TAp73 knockout was confirmed by the presence of the same two editing events across all reads, namely a one or two base pair deletion (Indicated by the green INDEL panel). No wild-type reads were observed, indicating that the cell line was clonally pure. Notably, the INDEL identified was 4bp upstream of the PAM sequence, as described in the literature for *S. pyogenes* Cas9 protein, demonstrating that a DSB break induced precisely at the target sequence. Moreover, the editing events lead to a premature stop codon in exon 3, preventing the translation of functional protein. These data therefore demonstrate the successful generation of a TAp73 knockout cell line using this approach. The cells generated were used for downstream experiments to investigate the proposed TAp73/OPA1 axis.

a)

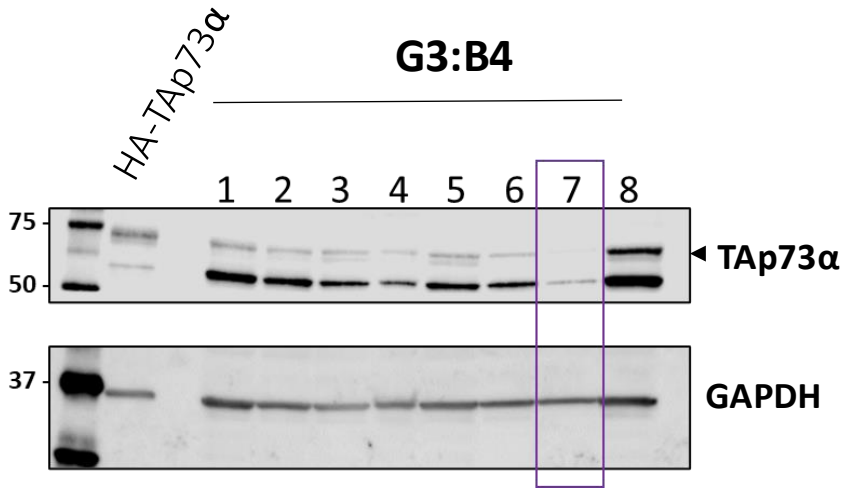

b)

```
Consensus                                 CCCCCACTCACCATGACAGATGTAGTCATGCCCTCCAGGTGGAAGACGTCC-TGCTGGAA
WT 614 (reversed)                         CCCCCACTCACCATGACAGATGTAGTCATGCCCTCCAGGTGGAAGACGTCCATGCTGGAA
465800101_C7-1_pJetFw_G06.abl             CCCCCACTCACCATGACAGATGTAGTCATGCCCTCCAGGTGGAAGACGTCC-TGCTGGAA
465800101_C7-3_pJetFw_A07.abl             CCCCCACTCACCATGACAGATGTAGTCATGCCCTCCAGGTGGAAGACGTCC-TGCTGGAA
465800101_C7-4_pJetFw_B07.abl             CCCCCACTCACCATGACAGATGTAGTCATGCCCTCCAGGTGGAAGACGTCC-TGCTGGAA
465800101_C7-5_pJetFw_C07.abl (reversed)  CCCCCACTCACCATGACAGATGTAGTCATGCCCTCCAGGTGGAAGACGTCC-TGCTGGAA
465800101_C7-6_pJetFw_D07.abl (reversed)  CCCCCACTCACCATGACAGATGTAGTCATGCCCTCCAGGTGGAAGACGTCC-TGCTGGAA
465884801_7-1_pJetFw_A01.abl              CCCCCACTCACCATGACAGATGTAGTCATGCCCTCCAGGTGGAAGACGTCC-TGCTGGAA
465884801_7-3_pJetFw_C01.abl              CCCCCACTCACCATGACAGATGTAGTCATGCCCTCCAGGTGGAAGACGTC--TGCTGGAA
465884801_7-4_pJetFw_D01.abl (reversed)   CCCCCACTCACCATGACAGATGTAGTCATGCCCTCCAGGTGGAAGACGTCC-TGCTGGAA
465884801_7-5_pJetFw_E01.abl              CCCCCACTCACCATGACAGATGTAGTCATGCCCTCCAGGTGGAAGACGTC--TGCTGGAA
465884801_7-6_pJetFw_F01.abl (reversed)   CCCCCACTCACCATGACAGATGTAGTCATGCCCTCCAGGTGGAAGACGTCC-TGCTGGAA
465884801_7-7_pJetFw_G01.abl              CCCCCACTCACCATGACAGATGTAGTCATGCCCTCCAGGTGGAAGACGTC--TGCTGGAA
465884801_7-8_pJetFw_H01.abl              CCCCCACTCACCATGACAGATGTAGTCATGCCCTCCAGGTGGAAGACGTCC-TGCTGGAA
465884801_7-9_pJetFw_A02.abl              CCCCCACTCACCATGACAGATGTAGTCATGCCCTCCAGGTGGAAGACGTCC-TGCTGGAA
```

Figure 3.5 The TAp73 was gene was successfully knocked out in CRISPR Clone 'G3:B4:C7'

a) Representative western blot to screen for knockdown of TAp73 protein. Lysate from CRISPR clones was loaded alongside lysate from cells overexpressing TAp73α as a control. Clone G3:B4:C7 has lost expression of TAp73α, as the indicated band was not present. b) Alignment of sanger sequencing reads obtained by amplifying gDNA surrounding the PAM sequence (blue box). The site of gene editing (INDEL) is shown in the green box at the DNA bases where CRISPR cells had a single or double base pair deletion immediately upstream of the PAM sequence. The wild-type H1299 (second row) was homologous with the listed CRISPR cell reads except for the indicated DNA bases.

Clonal populations obtained using the doxycycline-inducible CRISPR system were also characterized for the presence of TAp73 knockout. TAp73 expression was assayed using western blot, as previously performed, on a panel of candidate clones. A representative blot is shown in figure 3.8a. Clone 'Dox-3' appeared to be a knockout clone as it did not express detectable TAp73 protein. Unlike western blots performed on transiently transfected cells, only a single band was present. The region surrounding the

target site was amplified by PCR and sequenced, and the results are shown in figure 3.9b. The reads indicated the presence of two different gene editing events: deletions of 13bp and 30bp. No reads were obtained of the wild-type sequence, indicated the generation of a knockout cell line. This CRISPR knockout was therefore used as a second experimental model to compliment the cell line characterized in the previous section.

a)

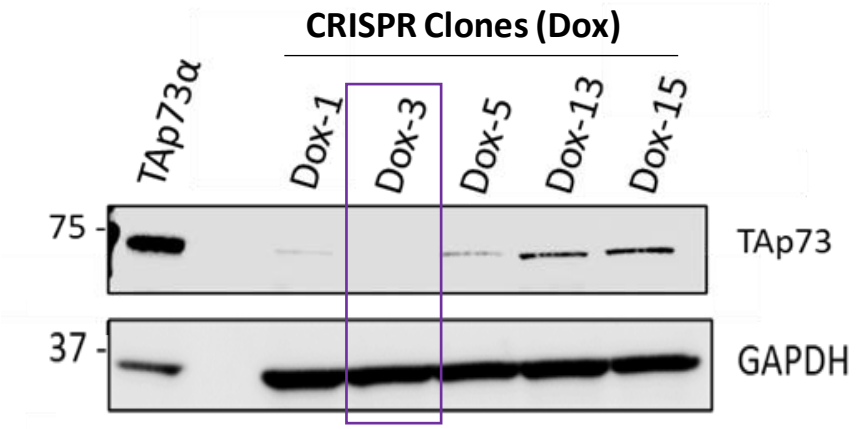

b)

```
Consensus                                GC-------------AGGCCGGCGTGGGGAAGATGGCCCAGTCCACCGCCACCTCCCCTG
WT Exon 2                                GCGAGCTGCCCTCGGAGGCCGGCGTGGGGAAGATGGCCCAGTCCACCGCCACCTCCCCTG
466271301_3-1_pJetFw_D09.abl (reversed) -------------------------------GATGGCCCAGTCCACCGCCACCTCCCCTG
466271301_3-2_pJetFw_E09.abl (reversed) -------------------------------GATGGCCCAGTCCACCGCCACCTCCCCTG
466271301_3-3_pJetFw_F09.abl             GC-------------AGGCCGGCGTGGGGAAGATGGCCCAGTCCACCGCCACCTCCCCTG
466271301_3-4_pJetFw_G09.abl (reversed) GC-------------AGGCCGGCGTGGGGAAGATGGCCCAGTCCACCGCCACCTCCCCTG
466271301_3-5_pJetFw_H09.abl             GC-------------AGGCCGGCGTGGGGAAGATGGCCCAGTCCACCGCCACCTCCCCTG
```

Figure 3.6 TAp73 knockout was achieved using the doxycycline-inducible system in clone 'Dox3'.

a) Representative western blot to screens for knockdown of TAp73 protein. Lysate from CRISPR clones was loaded alongside lysate from cells overexpressing TAp73α as a control. Clone 'Dox 3' has lost expression of TAp73α. b) Sanger sequencing reads obtained by amplifying gDNA surrounding the PAM sequence. The site of gene editing (INDEL) is shown by dashed lines where bases have been deleted from CRISPR cells. The short-deleted sequences produced a premature stop codon and hence TAp73 knockout.

3.2.5 TAp73 Knockout cells have downregulated OPA1 protein expression

I firstly analysed the expression of OPA1 protein in TAp73 knockout cell lines to corroborate the findings in section 3.2.1 where TAp73 expression (after silencing or overexpression) correlated with OPA1 expression. Western blot for OPA1 protein indicated there was a downregulation of OPA1 in TAp73 knockout cells compared with wild-type control, in both transiently transfected and doxycycline inducible CRISPR cell lines (figure 3.10a-c).

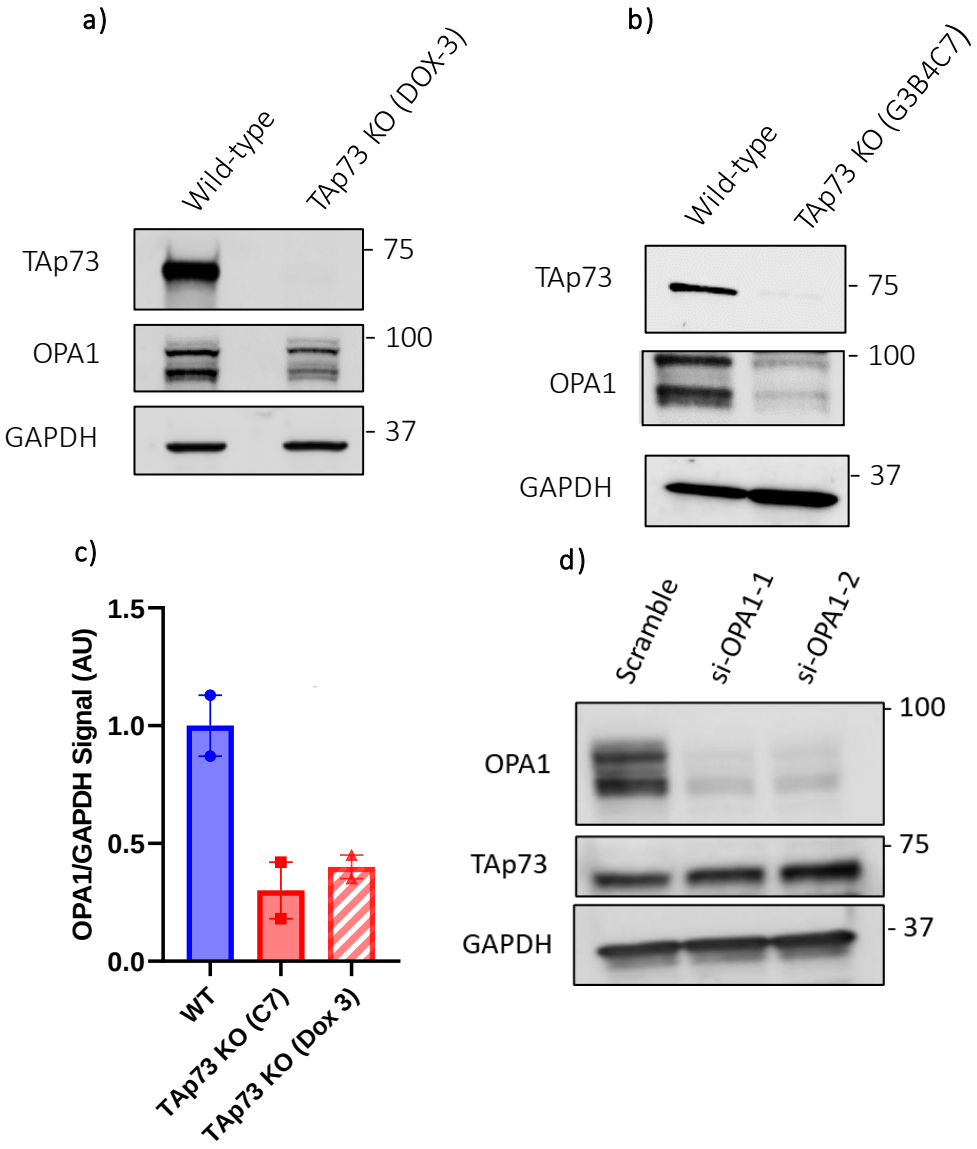

Figure 3.7 TAp73 knockout cells have downregulated OPA1 expression.

(a,b) Western blot of OPA1 expression in CRISPR knockout cell lines generated using the two approaches. (c) Quantification of OPA1 expression obtained using densitometry measurements in ImageJ. Data points indicate two independent experiments per cell line (n=2) and shown as mean ± SEM. (d) Western blot of OPA1 and TAp73 expression following OPA1 silencing in WT H1299 cells with two different siRNA's.

Interestingly, in the knockout cell line generated using the inducible system, the downregulation of OPA1 was more profound for OPA1-s compared with OPA-l isoforms (figure 3.9a). This may suggest that OPA1-l was upregulated by a compensatory mechanism, for example a downregulation of OPA1 cleavage by YME1L or OMA1 proteases. It was also prudent to address the possibility that there may be an inverse relationship between OPA1 and TAp73, where modulation of OPA1 expression impacts expression of TAp73. To address this, I induced efficient knockdown of OPA1 using two different siRNA's that target OPA1 mRNA, and found that there was no detectable change in TAp73 expression at the protein level (figure 3.10c).

3.2.6 Ectopic Expression of TAp73α in TAp73 knockout cells rescues OPA1 expression

Next, I utilized the TAp73α overexpression construct to attempt to rescue OPA1 expression in CRISPR knockout cells. Ectopic expression of TAp73α for 48 hours in the TAp73 null background largely rescued OPA1 expression in line with wild-type cells at the protein level. Interestingly, the experiment also recapitulated the previously observed effect on OPA1 isoforms. Namely, TAp73 knockout induced a stronger downregulation of OPA-s than OPA1-L. Moreover, rescue of OPA1 by TAp73α overexpression was more profound for the OPA1-L isoform, which was strongly upregulated compared with knockout cells transfected with empty vector. The nature of the balance of isoforms rescued may therefore be suggestive of a feedback mechanism to rescue the pro-fusion function of OPA1, owing to the respective pro-fusion and pro-fission roles of OPA1-L and OPA1-S. To confirm the activity of ectopic HA-tagged TAp73, I also assayed p21, a known transcriptional target of TAp73 in overexpression models. There was an induction of p21 in WT and TAp73 KO cells transfected with TAp73α plasmid, confirming the expression of functional TAp73 protein in transfected cell populations (figure 3.11).

As results from ChIP-seq analysis were suggestive of a broader role of TAp73 in the regulation of mitochondrial fusion and fission (section 3.2.3). I also performed immunoblots against the Mitofusins (MFN1 & MFN2). This showed that Mitofusin-2 followed the same pattern of regulation as OPA1; it was downregulated in TAp73 knockout cells, and subsequently rescued by ectopic TAp73α expression. There was however no change in MFN1 expression between each condition. Strikingly, this recapitulates the ChIP-seq data, which showed a binding of TAp73 to the enhancer regions of MFN2, but not MFN1. These data, together with Gene Ontology analysis, are suggestive of a novel role for TAp73 in regulating mitochondrial dynamics that is not limited to OPA1 and may represent a broad feature of the p53 family.

I also collected mRNA from the same experiment and performed RT-qPCR to investigate changes in gene transcription. *OPA1* transcripts were downregulated by more than 75% in TAp73 null cells and expression was partially rescued in cells transfected with TAp73 α. The expression of MFN2 mRNA also followed the same pattern, which placed MFN2 downstream of TAp73 and was consistent with western blot data. RT-qPCR data also confirmed a transcriptional basis for the upregulation of p21 (CDKN1A gene) following TAp73 overexpression in WT and TAp73 KO cells. Taken together, these data place OPA1 downstream of TAp73 and positions TAp73 as a regulator of mitochondrial dynamics. This therefore warranted a morphological and functional analysis of the mitochondrial network in TAp73 null cells, which is shown in the subsequent chapter.

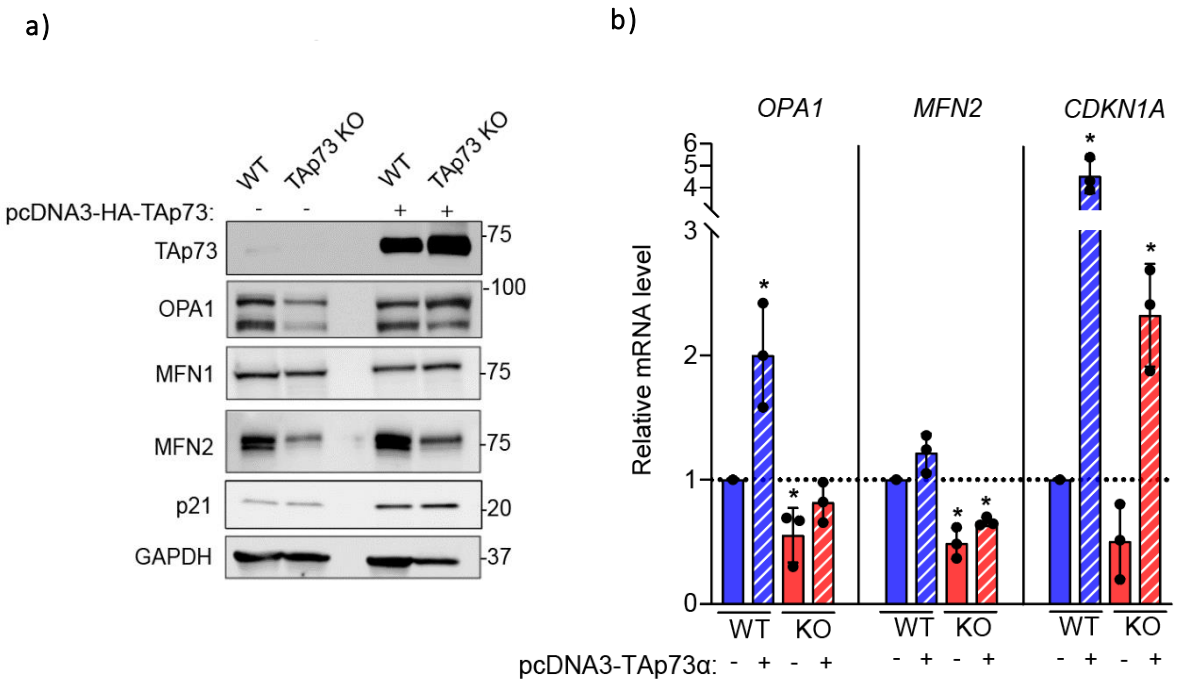

Figure 3.8 The downregulation of OPA1 expression in TAp73 null cells is rescued by expression of TAp73α

(a) Western blot of mitochondrial fusion proteins in TAp73 KO and WT control were transfected with either EV or TAp73α expression construct. (b) RT-qPCR was performed against *OPA1*, *MFN2* and *p21* on mRNA from the same experimental conditions. Data shown as mean ± SD (n=3).

3.3 Discussion

3.3.1 TAp73 regulates OPA1 expression in H1299 cells

The expanding set of TAp73 functions in embryonic development, tissue homeostasis and cancer demonstrate its vast functional pleiotropy (Logotheti et al., 2021). These unique functions extend beyond induction of the DNA-damage response and apoptosis, which was the initial focus of p73 research. One such function of TAp73 is the control of metabolism and mitochondrial function (Nemajerova et al., 2018). For example, TAp73 deletion from mouse embryonic fibroblasts (MEFs) leads to a downregulation of the complex IV subunit gene *Cox4i1*. This results in reduced complex IV activity, and a concomitant decrease in cellular ATP and oxygen consumption (Rufini et al., 2012). Additional molecular mechanisms by which TAp73 regulates mitochondrial function and general metabolism are through the direct transcriptional control of *GLS2*, the gene encoding glutaminase type 2 (Velletri et al., 2013), glutamine metabolism (Niklison-Chirou et al., 2017), and the synthesis of serine (Amelio et al., 2014).

Using overexpression and CRISPR knockout models, I have identified a novel transcriptional role for TAp73 in regulating OPA1 expression, through direct association with the OPA1 promoter. This role was evident in two different CRISPR cell lines with INDELS and a resultant premature stop codon in exons 2 and 3 of the TAp73 gene. The use of a 'Tet-on' inducible system was advantageous as it led to high editing efficiency. However, the constitutive expression of Cas9 protein increases the possibility of off-target gene editing; a potential cause of phenotypic variation between knockout clones. It was therefore reassuring to observe a downregulation of OPA1 using both CRISPR approaches. In addition, expression of TAp73 in TAp73 knockout CRISPR cells partially rescues basal OPA1 expression levels observed in wild-type controls. This finding adds to the repertoire of mitochondrial and metabolic targets of TAp73, and indeed the p53 family (Berkers et al., 2013). A role for TAp73 in regulating OPA1 expression is in keeping with a decreased capacity for oxidative phosphorylation previously reported in TAp73 null cells (Rufini et al., 2012). The control of OPA1 may represent an additional layer of regulation by which loss of TAp73 contributes to this observed phenotype. For example, OPA1-dependent mitochondrial fusion supports increased rates of mitochondrial oxidative phosphorylation in non-transformed proliferative cells (Yao 2019). Moreover, OPA1 has been shown to regulate respiratory complex assembly and OXPHOS efficiency independently of its role in mitochondrial fusion, owing to its function in maintaining cristae morphogenesis (Frezza et al., 2006; Cogliati et al., 2013). This is therefore highlights the possibility that, through the control of OPA1, TAp73 may regulate the assembly and efficiency of respiratory complexes as well as regulating core components such as Cox4i1.

The importance of OPA1 in the maintenance of mitochondrial structure, genome, and function is evident from the various consequences of its dysfunction. Indeed, in mouse and patient models, loss of OPA1 gives rise to several pathophysiological outcomes including wasting of skeletal muscle, neutrophil dysfunction and ADOA. (Romanello et al., 2019; Amini et al., Pesch et al., 2001). As such, the regulation of OPA1 by TAp73 reinvigorates the previously posed suggestion that TAp73-dependent metabolic regulation may participate in the multiciliogenesis process (Nemajerova et al., 2018), or indeed the broader phenotype of p73 knockout mouse models. Therefore, the effect of TAp73 knockdown on OPA1-dependent maintenance of mitochondrial morphology and bioenergetics was explored in the following two chapters, with a focus on the ciliated epithelium.

3.3.2 TAp73 regulates OPA1 expression, binds to the OPA1 promoter, and may modulate additional mediators of mitochondrial dynamics

I have shown through independent approaches that TAp73 regulates the expression of OPA1 , and has the ability to associate with the promoter region. First, using chromatin immunoprecipitation I showed that TAp73α-bound chromatin was highly enriched for the OPA1 promoter, showing that it is a target gene of TAp73α. Next, this was corroborated by previously published ChIP-seq data, which when analysed showed enrichment of TAp73α at the *OPA1* locus (Koeppel at al., 2011). Overexpression of TAp73 isoforms alpha and beta in H1299 also showed that there was not TAp73 isoform specific selectivity of OPA1 regulation, confirmed by overlapping binding loci of TAp73 α/β in ChIP-seq data. This is notable because the expression of a functional SAM domain, present in TAp73α, has been reported to facilitate the recognition of differential gene promoter architectures by different TAp73 isoforms (Logotheti et al., 2021). For example, gene promoters occupied by TAp73α are frequently enriched in the AP1 motif (Koeppel et al., 2011). This regulation occurs Through C-terminal association between TAp73α and Jun/Fos family hetereodimers which regulate gene transactivation in a p73-responsive element (RE)- independent manner (Buhlmann et al., 2008). However, the overlapping regulation of *OPA1* gene transcription by TAp73α and TAp73β suggest that it is not dependent on one of many protein-protein interactions at the C-terminus and is likely brought about the direct association with a p73-RE. This view is strengthened by a significant enrichment of the p73-RE in the promoter region of OPA1. Nonetheless, additional experiments such as using a luciferase reporter assay and subsequent mutation of the p73-RE would conclusively that the regulation of OPA1 expression occurs *via* direct binding, as currently these data are correlative. Furthermore, a co-immunoprecipitation of TAp73 with any other bound proteins at the OPA1 locus would shed further light on the mechanism of regulation.

ChIP-seq data also indicated binding of p53 to the OPA1 promoter region, suggesting that the binding and regulatory function is conserved throughout the p53 family. Recent evidence has implicated p53 in

the control of mitochondrial dynamics, however the study did not report that this occurs through direct transcriptional regulation of fusion and fission proteins (Phan et al., 2022). Instead, the authors showed how mitochondrial fragmentation occurs as a result of p53 inactivation, which relieves the inhibition of mTORC signalling. Indeed, the mTORC/MTFP1/DRP1 axis is a well-established mechanism linking environmental and intracellular stimuli to mitochondrial dynamics (Morita et al., 2017). Nevertheless, it has also been reported that Mitofusin-2 is a transcriptional target of p53 (Wang et al., 2010), reinforcing the possibility that the p53 family directly regulates genes responsible for mitochondrial fusion and fission. However, this was studied in the context of the induction of apoptotic pathways, which may be promoted by MFN2 (Wang et al., 2012), and not the context of mitochondrial dynamics. Therefore, the finding that TAp73 and p53 bind various genes responsible for mitochondrial fusion and fission is an exciting area for future investigation. This should be independently verified by targeted ChIP, as was performed for OPA1. In addition to underpinning the phenotype of TAp73 null mice, this may have important implications for tumorigenesis, where TAp73 is frequently upregulated. Indeed, the role of TAp73 in tumorigenesis is ambivalent as a number of growth promoting roles have been identified, to which the regulation of OPA1 may now be added. My investigations were carried out in a p53 null background, and so this may have enhanced the effect observed on OPA1 expression following TAp73 deletion as it eliminated the possibility of any compensatory mechanism of p53. Future work investigating the TAp73/OPA1 axis in H1299 cells modified to express functional p53 would therefore shed light on overlapping functions of the p53 family.

The molecular pathways involving p73 stabilization and activation that occur downstream of DNA damage have been well defined. However, the upstream signals influencing the activity of p73 in regulating cellular metabolism are poorly understood. Indeed, there are a plethora signaling pathways regulating p73 transcription, translation, and stability (Rozenberg et al., 2021). Therefore in a cancer setting, such as the H1299 cells utilized in this study, a basal activation of p73 may be induced by the enhanced activity of a number of upstream activators such as PKC, c-Abl, or YAP1 (Raj and Bam, 2019; Nyman et al., 2009). An altered p73 basal activity or transcriptional program in cancer cells may consequently represent present a specific vulnerability, and further work is required to elucidate the mechanisms that fine tune p73 activities in normal and cancer cells (Rozenberg et al., 2021).

Chapter 4: Disruption of a novel TAp73/OPA1 axis drives mitochondrial dysfunction

4 Disruption of a novel TAp73/OPA1 axis drives mitochondrial dysfunction

4.1 Introduction

Given that OPA1 is downregulated in TAp73 knockout cells, I sought to investigate the effect of disruption of this axis on mitochondrial morphology and function. Indeed, the balance between fusion and fission of the mitochondrial network is tightly regulated to couple mitochondrial function with the demands of the cell. As a result, the control of fusion and fission of mitochondria influences numerous physiological processes in which they are involved. These include energy production via oxidative phosphorylation (OXPHOS), programmed cell death, innate immunity, autophagy, calcium homeostasis and stem cell programming (Kamer & Mootha, 2015; Rambold & Pearce, 2018). Mitochondrial fusion is therefore an evolutionarily conserved process in mammals, the details of which are discussed in the thesis introduction. In brief, mitochondrial fusion is a two-step process mediated by three large GTPases of the dynamin superfamily: with the Mitofusins (MFN1 & MFN2) being integral for outer membrane fusion and OPA1 necessary for inner membrane fusion (Mishra & Chan, 2016).

Genetic ablation of OPA1 in cellular models therefore blocks mitochondrial fusion and causes mitochondria to fragment, due to its essential role in fusion of the inner mitochondrial membrane (Anand et al., 2014). A fragmented mitochondrial network is often linked with mitochondrial dysfunction, and this morphological state is evident during cellular stress and cell death (Zemirli et al., 2018). As a result, mutations in OPA1 cause autosomal dominant optic atrophy (ADOA), the most common form of inherited neuropathy in humans (Burte at al., 2015). However, mitochondrial fragmentation may also predominate in non-stress conditions, for example in the G2/M phase of the cell cycle, which facilitates mitochondrial segregation into daughter cells and mtDNA inheritance (Pickes at al., 2018).

The importance of OPA1 is also evident from homozygous and heterozygous deletion of the gene from mice. Although complete oblation of OPA1 in mice is incompatible with life, heterozygous knockout mice develop tissue-specific pathologies such as retinal degeneration and cardiac dysfunction (Chen et al., 2012). Strikingly, this shows how a reduction in steady-state expression of OPA1 by 50% is sufficient to drive mitochondrial dysfunction and disease pathogenesis. It therefore seemed logical to speculate that the decrease OPA1 expression observed in the TAp73 knockout cells I generated may possess a phenotype of dysfunctional mitochondria, owing to a downregulation of mitochondrial fusion.

To understand the functional impact of disruption of the TAp73/OPA1 axis it is also important to consider functions of OPA1 that are independent of mitochondrial fusion. These include the regulation of cristae morphology; including in the context of apoptotic remodelling, respiratory complex assembly, and mtDNA maintenance (Cogliati et al., 2013; Frezza et al., 2006; Burte et al., 2015). I therefore

conducted a raft of experiments to functionally connect this axis to mitochondrial dysfunction in cellular models.

4.1.1 Aims and Objectives

- To investigate the effect of TAp73 ablation on the morphology and ultrastructure of the mitochondrial network and to directly implicate downregulation of OPA1 as the underlying mechanism
- To investigate the concomitant impact of disruption of this axis on mitochondrial bioenergetics, with a focus on oxidative phosphorylation
- To induce apoptosis in TAp73 KO cells using BH3-mimetics and to study the impact of TAp73 KO on the kinetics of cell death induction, owing to a role for OPA1 in modulating cristae morphogenesis and cytochrome *c* release

To investigate alterations to the mitochondrial network, immunohistochemical staining of mitochondria in TAp73 KO or TAp73 silenced cells was performed, and imaged using confocal microscopy. This approach was also complimented by electron microscopic analysis of the mitochondrial network.

4.2 Results

4.2.1 Silencing of TAp73 leads to fragmentation of the mitochondrial network

Following the finding presented in chapter 3 that TAp73 regulates OPA1 expression, I investigated the morphology of the mitochondrial network firstly in cells treated with TAp73 siRNA. This was achieved using immunohistochemical staining of the mitochondrial network with an antibody directed against ATP5β, a subunit of the ATP synthase.

There was a striking phenotypic difference between TAp73 silenced cells and those treated with the scrambled transfection control (figure 4.1a). Control cells treated with scrambled siRNA sequences display a predominantly elongated mitochondrial network, whereas mitochondria were largely fragmented in TAp73 knockout cells. Interestingly, siRNA mediated knockdown of OPA1 elicited an effect highly similar to TAp73 knockdown and served as a positive control in the experiment. Knockdown of the respective proteins was confirmed by western blot (figure 4.1b,c).

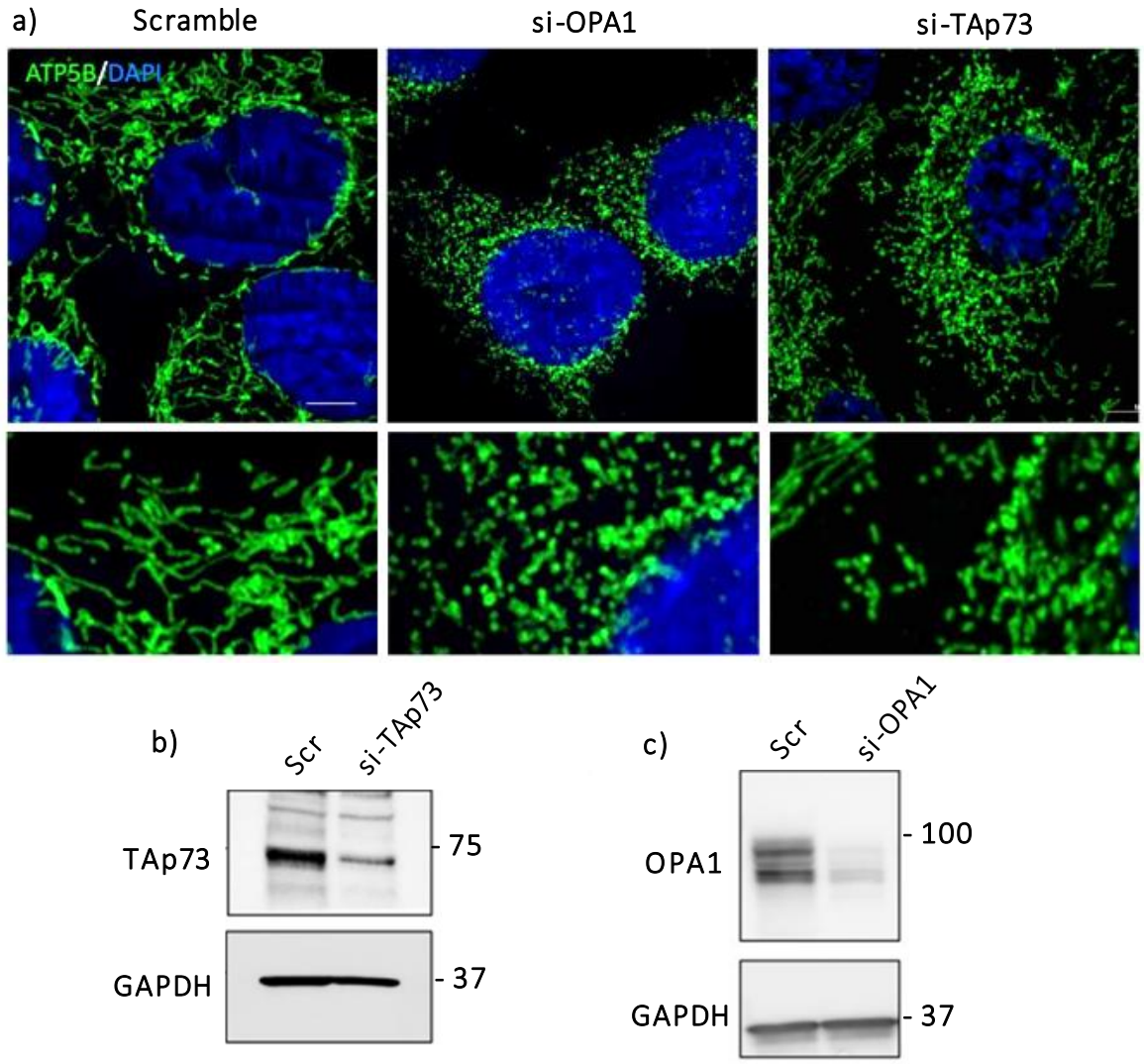

Figure 4.1 H1299 cells treated with siRNA targeting TAp73 display fragmentation of the mitochondrial network, relative to control cells.

(a) Knockdown was induced by transfection for 72 h. Cells were subsequently fixed and probed for ATP5B to visualise the mitochondrial network by immunofluorescence. The observed phenotype in TAp73 knockout cells is consistent with a depletion of OPA1 (middle panel). (b) siRNA mediated knockdown of TAp73 and OPA1 was confirmed by western blot. Images representative of two independent experiments (n=2).

To perform a robust and unbiased quantification of the morphological state of the mitochondrial network from cells of different treatment conditions, I performed an automated analysis using the Intellesis trainable segmentation module in ZenBlue software (Zeiss). The software was trained to draw a mask around each mitochondrion, using representative images from each condition. Following training, the software effectively segmented the mitochondrial network, with representative masks shown in red (figure 4.2a). From each image the mean mitochondrial area (nm2) and perimeter (nm)

was calculated, which was then repeated using a minimum of 20 images per condition. The results of the analysis are shown in figure 4.2b and 4.2c. Consistent with a fragmented mitochondrial network, si-TAp73 treated cells exhibit a significant decrease in mitochondrial area and perimeter. The fragmentation observed was less severe than the OPA1 knockdown, which was expected given the approximately 60% reduction in OPA1 mRNA observed following TAp73 silencing (figure 3.1).

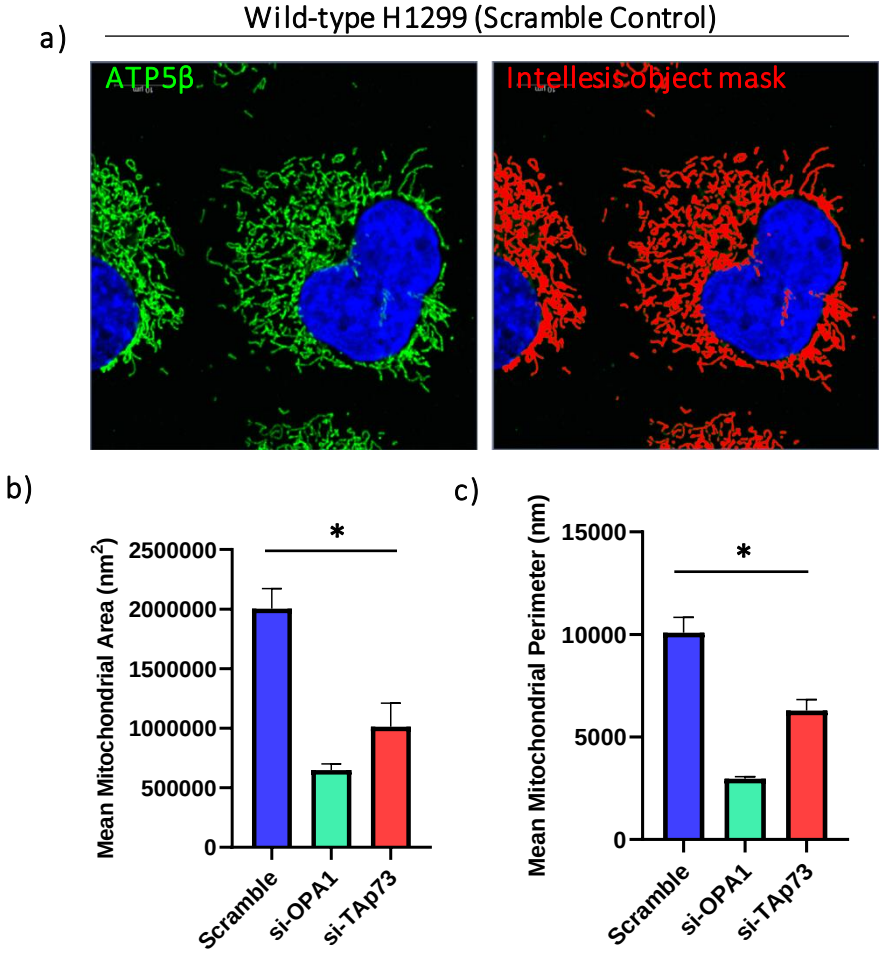

Figure 4.2 Intellesis automated segmentation module was used to quantify mitochondrial area and perimeter.

(a) The machine learning module was trained to recognise mitochondria labelled with ATP5β antibody (FITC channel) by inputting 6 representative images including fragmented and elongated mitochondria. The object masks obtained (red) showed a good agreement with ATP5β staining (green). (b) Mean mitochondrial area and perimeter was calculated following gene silencing with the indicated siRNA's or scramble control for 72 h. A minimum of 20 cells were counted per condition from two biological replicates (n=2).

4.2.2 TAp73 knockout cells have a fragmented mitochondrial network that is partially rescued by either TAp73 or OPA1 overexpression

After finding that silencing of TAp73 induces a fragmentation of the mitochondrial network in a manner similar to OPA1 silencing, I investigated the morphology of the mitochondrial network in TAp73 KO cells. Importantly, stable knockout of TAp73 allowed for an analysis of the mitochondrial network in TAp73 KO cells following overexpression of either TAp73α or OPA1, to decipher whether expression of the respective proteins was sufficient to rescue an elongated mitochondrial morphology. To address this possibility, one of the following constructs: empty vector control, pcDNA3 -TAp73α or pCMV6-OPA1 were expressed Wild-type and TAp73 KO H1299 and incubated for 48 hours before fixation of cells. Immunofluorescence staining showed a striking fragmentation of the mitochondrial network in TAp73 KO cells compared with WT control (figure 4.3a), consistent with siRNA knockdown of TAp73. Severe mitochondrial fragmentation was also evident when using the Intellesis segmentation module (Zeiss) to quantify mitochondrial area in images acquired from biological replicates (figure 4.3c).

To attempt to rescue mitochondrial morphology in TAp73 KO cells, transfection was performed with TAp73α overexpression construct, which was selected for number of reasons. Firstly, as confirmed in section 3.2.7, it is both a weaker activator of p73 target genes than TAp73β and the most abundant isoform *in vivo* (Marshall et al., 2021). Second, TAp73α overexpression was sufficient to rescue OPA1 expression in TAp73 KO cells, suggesting that this upregulation in OPA1 may be sufficient to rescue mitochondrial morphology (figure 3.10). Third, although its overexpression led to a modest increase of p21 expression (figure 3.10), the mitochondrial morphology of TAp73α overexpressing cells did not suggest that apoptosis had been induced (figure 4.3a). It is notable that in order to activate inducers of apoptosis such as PUMA, BAX and BAK, previous studies were performed using the overexpression highly potent isoforms of p73 (such as TAp73β), often in the context of cells that do not express TAp73 or p53. A critical view of these data therefore suggest that apoptosis might only be induced due to the fictitious nature of the system. Indeed, conflicting evidence has shown that overexpression of TAp73α alone does not induce apoptosis but rather antagonises cell death induction (Nyman et al., 2005). This was further demonstrated by Annexin V staining of H1299 cells following overexpression of TAp73α and tracking the induction of apoptosis for 48 hr. Quantification of apoptotic cells did not indicate significant apoptosis induction in cells transfected with TAp73α, relative to empty vector control (figure 4.3d). Taken together, these data show that experiments to attempt to rescue mitochondrial morphology with TAp73α overexpression plasmid are not fundamentally convoluted by the parallel induction of apoptosis pathways.

Following overexpression of TAp73α in TAp73 KO cells and immunofluorescence staining of the mitochondria, images showed that fragmentation of the network was partially rescued and was corroborated by automated quantification (figure 4.3a; middle column, figure 4.3c). Importantly, TAp73α was expressed as an HA-tagged protein therefore analysis was performed on HA expressing cells after co-staining, thereby eliminating non-expressing cells from the analysis. Indeed, quantification indicated that following TAp73α overexpression, mean mitochondrial area increased from 34% to 69% of wild-type cells. It may be possible that the rescue was not more comprehensive because TAp73 KO has induced stress pathways or cellular senescence. For example, metabolic stress caused by dysfunctional mitochondria activates AMPK signalling, owing to high levels of ADP (adenosine diphosphate). Nonetheless, this data therefore directly implicates TAp73 expression level in the control of mitochondrial dynamics.

Similar to TAp73α, rescue experiments using overexpression of OPA1 in TAp73KO cells also led to an increase in the number of elongated mitochondria (figure 4.3a). Overexpression of OPA1 was performed using an untagged protein and was therefore confirmed by western blot (figure 4.3b). There was a robust increase in OPA1 expression following transfection of overexpression construct in wild-type and TAp73 KO cells. Western blot for OPA1 also indicated that the overexpression in TAp73 KO cells increased OPA1 expression to a level highly comparable to that observed in wild-type cells (4.3b). Crucially, such expression of OPA1 was sufficient to partially rescue mitochondrial morphology. However, it did not elicit a rescue to the same degree as expression of TAp73α, with the mean mitochondrial area being 50% of wild-type cells (Compared with 69% observed for TAp73 overexpression). As expected, analysis of wild-type cells overexpressing OPA1 displayed an increase in mitochondrial area, thereby confirming the specific pro-fusion activity of the overexpressed protein follow transfection for 48 hr.

This finding places OPA1 downstream of TAp73 in the control of mitochondrial dynamics. It also shows that a superabundant expression was not required to induce the partial rescue of mitochondrial morphology (figure 4.3b). Nonetheless, the weaker effect observed with OPA1 overexpression compared with TAp73 raises the possibility that the overexpression of OPA1 alone did not resolve an imbalance in the expression or activity of additional mitochondrial fusion or fission regulators. However, overexpression of a tagged OPA1 protein to select for transfected cells may increase the extent to which mitochondrial morphology is rescued in automated analysis and should be incorporated into future experiments. Taken together, these data place TAp73 upstream of OPA1 in the regulation of mitochondrial fusion and fission.

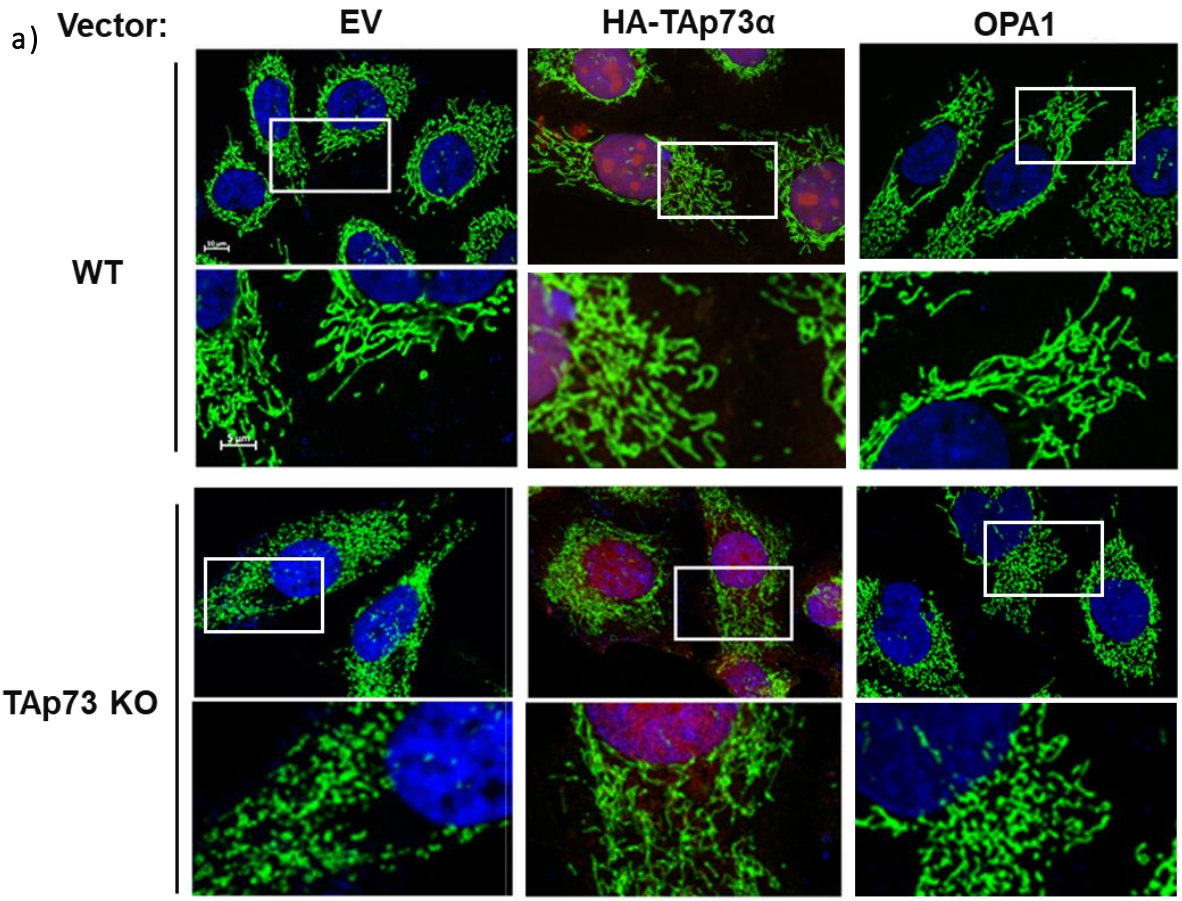
a)
Vector:
EV
HA-TAp73α
OPA1
WT
TAp73 KO

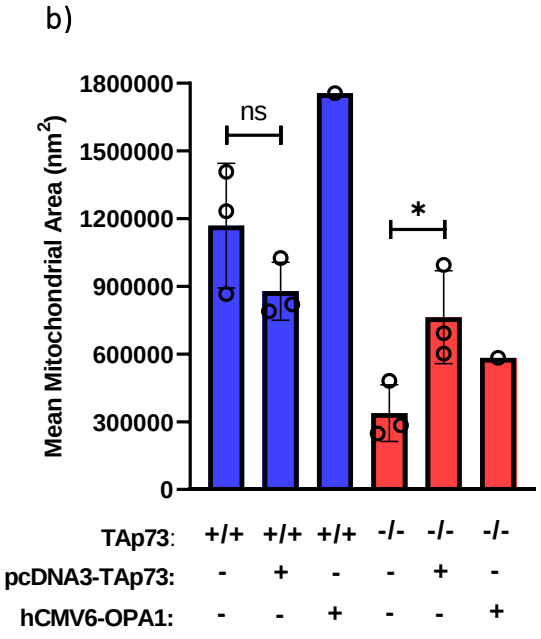
b)
Mean Mitochondrial Area (nm²)
1800000
1500000
1200000
900000
600000
300000
0
ns
*
TAp73: +/+ +/+ +/+ -/- -/- -/-
pcDNA3-TAp73: - + - - + -
hCMV6-OPA1: - - + - - +

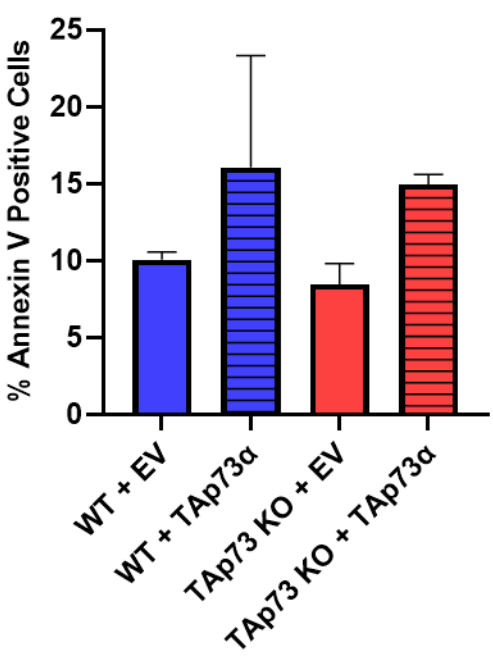
c)
% Annexin V Positive Cells
25
20
15
10
5
0
WT + EV
WT + TAp73α
TAp73 KO + EV
TAp73 KO + TAp73α

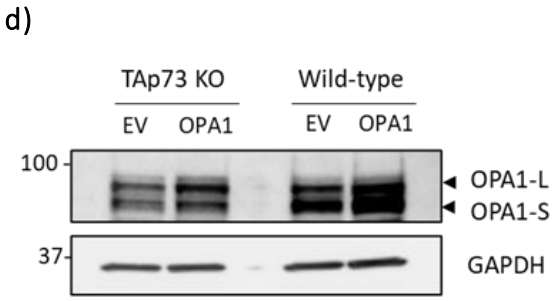

Figure 4.3 TAp73 KO cells display a fragmented mitochondrial phenotype which is partially rescued by expression of HA-TAp73α or OPA1.

(a) Wild-type or TAp73 KO H1299 cells were transfected with the indicated plasmids for 48 h and IF carried out against ATP5B (green) with DAPI nuclear counterstain (blue). Cells transfected with HA-TAp73α expression plasmid were stained for HA as a transfection control (red). (b) A minimum of 20 images were counted per transfection condition for each genotype, with the following number of biological replicates: EV, HA-TAp73α transfection n=3, OPA1 transfection n=1. Statistical significance for rescue with HA-TAp73α plasmid was calculated using Student's T-test; (*) $p < 0.1$, (ns) not significant. (c) Quantification of Annexin V positive cells following 48 hr transfection with EV or TAp73α overexpression construct, obtained using Incucyte live-cell imager (n=2). (d) Transfection of untagged OPA1 plasmid was confirmed by western blot.

Further to investigating the mitochondrial morphology of TAp73 knockout cells using confocal immunofluorescence, cells were imaged using electron microscopy. To preserve the morphology of mitochondria, cells were seeded on carbon-coated sapphire discs and immobilized using freeze substitution instead of conventional chemical fixation using glutaraldehyde. This approach maintains the hydration shell of macromolecular structures, resulting in improved structural preservation and retention of diffusible cellular components (Hippe-Sanwald; 1993). Following the immobilisation of cells, they were processed and imaged using two complementary electron microscopy streams. Firstly, sections were cut and mounted onto EM grids for imaging by conventional 2D TEM (figure 4.4) to obtain cross-sectional images of mitochondria in individual sections. These images showed that the mitochondria in TAp73 knockout cells displayed a striking fragmentation of the mitochondrial network when compared with the wild-type control, which contained highly connected and tubular mitochondria. This was therefore in agreement with immunofluorescence images and confirmed a role for TAp73 in maintaining mitochondrial dynamics.

Furthermore, the high-resolution TEM images obtained provided information about the organisation of mitochondrial cristae (figure 4.4; bottom row). In wild-type cells the mitochondrial inner membrane was tightly folded to form condensed cristae, whereas numerous empty spaces were evident inside the

mitochondria of TAp73 knockout cells. This finding is congruous with the role of OPA1 in maintaining cristae junctions (Varanita et al., 2015) and showed that the impact of OPA1 downregulation on mitochondrial function in TAp73 KO cells was not limited to fusion and fission and also influenced mitochondrial ultrastructure.

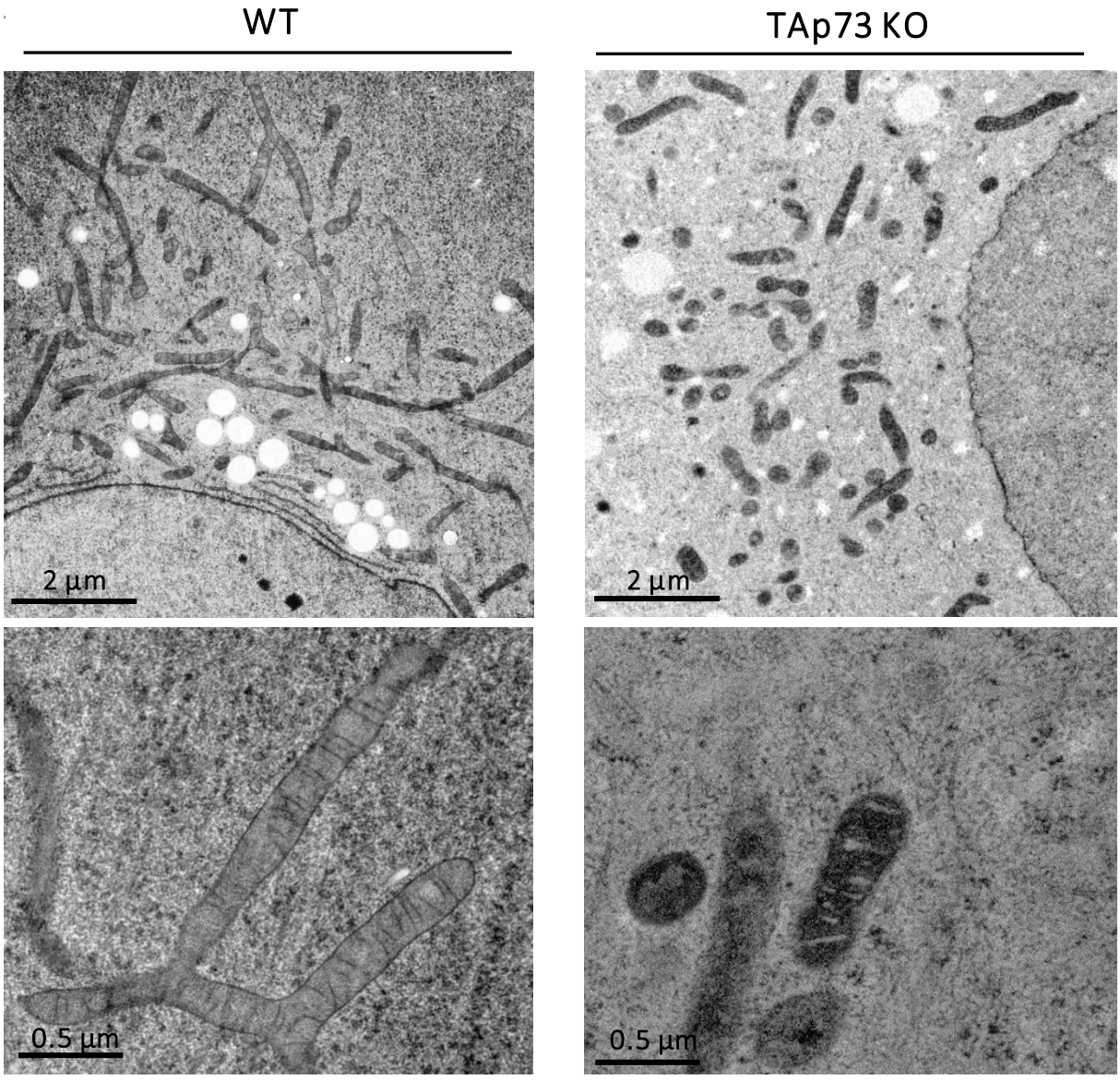

Figure 4.4 Electron microscopy images TAp73 KO cells display a fragmented mitochondrial phenotype and alterations in cristae architecture.

Wild-type or TAp73 KO H1299 were seeded on carbon-coated sapphire discs and immobilized using a freeze-substitution prior to sectioning. Representative images of the mitochondrial network for the indicated genotype are shown.

4.2.3 TAp73 knockout decreases mitochondrial bioenergetic function in H1299 cells

Next, I sought to investigate the impact of OPA1 downregulation and resultant alterations in mitochondrial morphology on mitochondrial bioenergetic function in TAp73 KO cells. To do so, oxygen consumption rate was measured using the Seahorse Extracellular Flux analyser, where a mitochondrial stress test was performed to obtain key parameters: basal OCR, maximal OCR, and spare respiratory capacity. Importantly, the use of canonical mitochondrial inhibitors to calculate these parameters also allows for a subtraction of non-mitochondrial oxygen consumption. I was therefore able to specifically interrogate the effect of mitochondrial fragmentation and alterations in cristae morphology on the efficiency of mitochondrial oxidative phosphorylation, whilst eliminating non-mitochondrial respiration, a process in which TAp73 also plays a role (Li et al., 2018).

Before investigating the effect of TAp73 knockout, it was necessary to establish suitable mitochondrial inhibitor concentrations and seeding densities to elicit a standard mitochondrial stress test profile in H1299 cells. A cell density analysis was therefore performed by seeding three different cell densities of Wild-type cells (1×10^4, 2×10^4, and 3×10^4 per well), shown in figure 4.5. At all three cell densities, the addition of 2µM Oligomycin A (ATP synthase inhibitor) induced a rapid and stable decrease in ATP-linked respiration. The subsequent addition of 500 nM FCCP (H^+ carrier and uncoupler of IMM electrochemical gradient) robustly increased the OCR and demonstrated a high spare respiratory capacity of H1299 cells. Finally, 2µM Rotenone and Antimycin A rapidly induced a decrease in OCR to below values obtained following Oligomycin addition, enabling the calculation of proton leak and non-mitochondrial respiration. Inhibitor concentrations used in this experiment were therefore suitable for subsequent analysis of TAp73 function. Of the cell densities tested, 3×10^4 cells were discounted as they were over-confluent after 24 hours. To account for the potential growth differences between wild-type and TAp73 KO H1299, densities of both 1×10^4, 2×10^4 cells per well were used in subsequent experiments to obtain comparable cell densities between cell lines on the day of the assay. Any further differences were normalised by Hoechst counts of assay plate wells after the experiment.

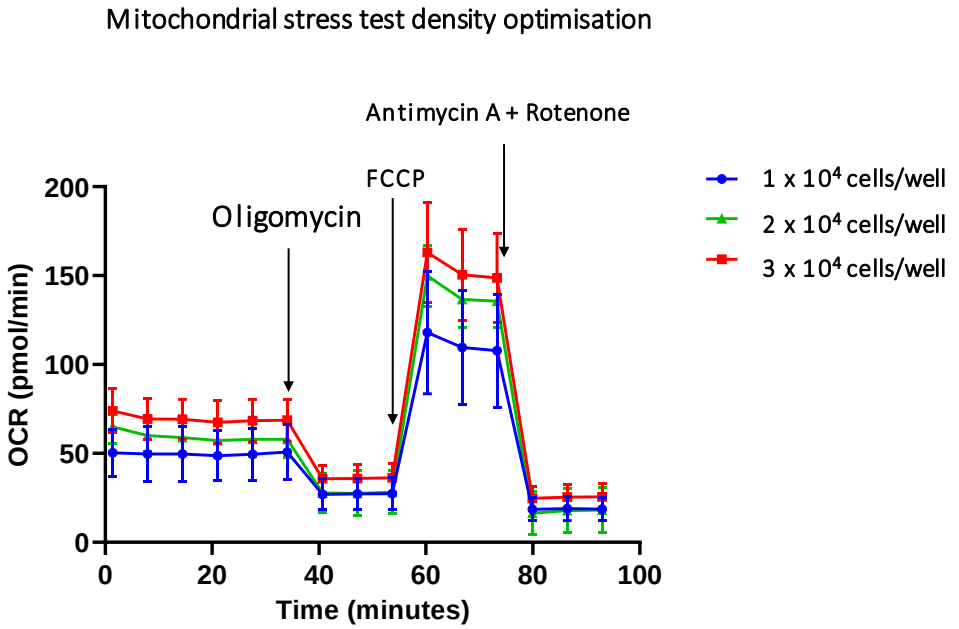

Figure 4.5 Optimisation of seeding densities for mitochondrial stress test in H1299 cells.

Cells were seeded at the indicated densities in growth medium (RPMI) for 16h . Culture media was replaced with glucose rich DMEM medium and cells cultured in a non-CO2 incubator for 1h prior to assay. OCR rate was measured using Seahorse XFe96 analyser and canonical mitochondrial inhibitors injected sequentially as labelled (Oligomycin = 2µM, FCCP = 500nM, Antimycin A/ Rotenone = 2µM).

Once optimal conditions for the mitochondrial stress test were established, I studied the effect of TAp73 knockout on OCR as a redout of mitochondrial bioenergetic function (figure 4.6). To account for the differences in growth rate between wild-type and TAp73 KO cells (shown in figure 4.5), OCR measurements were compared between wild-type cells seeded at 10,000 cells/well with TAp73 KO at 20,000 cell/well. At the end of the assay, cell nuclei were immediately stained with Hoechst and whole wells for each condition imaged using a brightfield microscope fitted with a UV laser. Nuclei were then counted using ImageJ software, which revealed that after seeding twice as many knockout cells as wild-type, there were 0.87 times fewer wild-type cells. OCR values obtained for the knockout were therefore multiplied by this correction factor to obtain values normalised to 10,000 cells.

After correction for cell number and non-mitochondrial respiration, the results showed TAp73 knockout induced an approximately 50% reduction in basal OCR, demonstrating reduced energy production by mitochondrial OXPHOS (figure 4.6b). Similarly, uncoupling of the proton gradient across the IMM by the addition of FCCP revealed a 64% decrease in maximal OCR in KO cells (figure 4.6c). When deducting basal from maximal OCR values, the decrease in spare capacity of TAp73 KO cells indicated an impaired ability of these cells to upregulate ETC function (figure 4.6d). These data therefore show that in addition

to morphological changes, TAp73 KO drives mitochondrial dysfunction through a reduced capacity for OXPHOS.

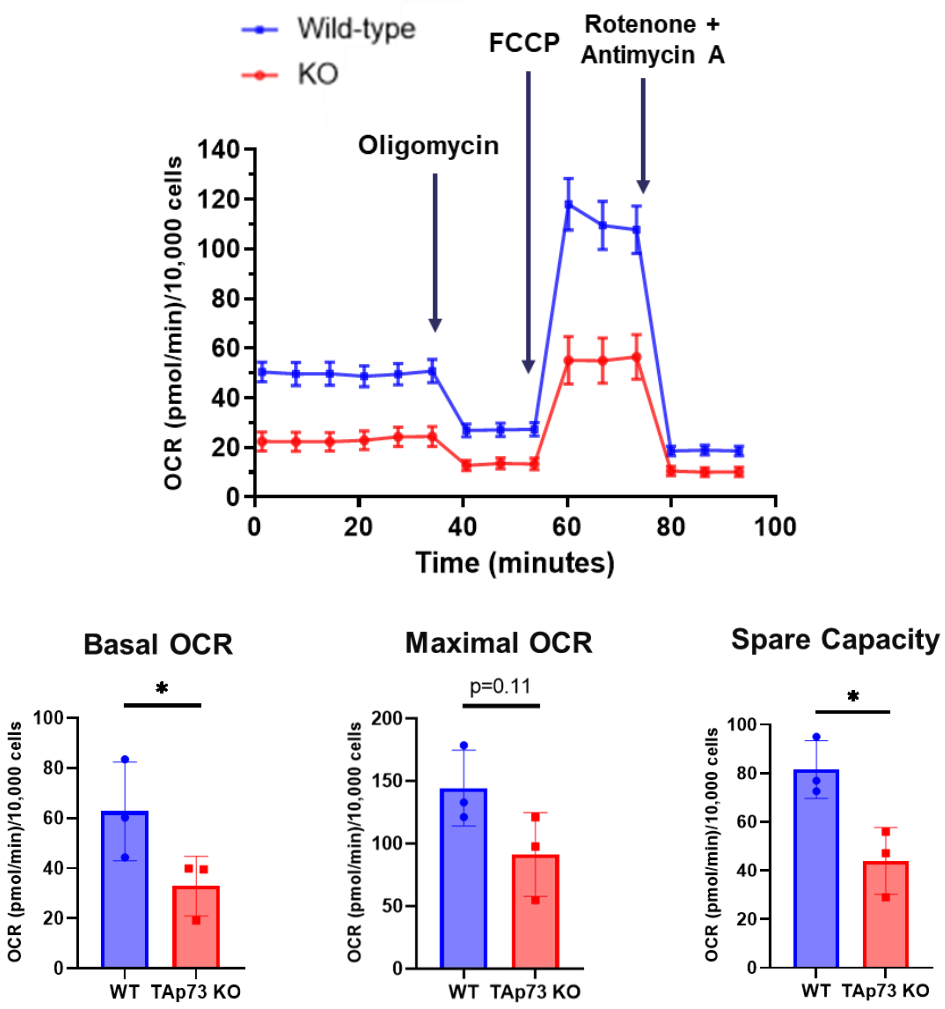

Figure 4.6 TAp73 knockout decreases mitochondrial oxidative phosphorylation

(a) Cells were seeded in standard growth medium (RPMI) for 16 h at either 1 x 10^4 or 2 x 10^4 cells per well for wild-type and TAp73 KO H1299 cells respectively. Culture media was replaced with glucose rich DMEM medium and cells cultured in a non-CO2 incubator for 1h prior to assay. OCR rate was measured using Seahorse XFe96 analyser and canonical mitochondrial inhibitors injected sequentially as labelled (Oligomycin = 2µM, FCCP = 500nM, Antimycin A/ Rotenone = 2µM). (b-d) The indicated mitochondrial stress test parameters were calculated from OCR data, which were corrected for non-mitochondrial OCR, normalised to cell number and are shown as mean ± SEM (n=3). (*) P ≤ 0.05 (Student's T-test).

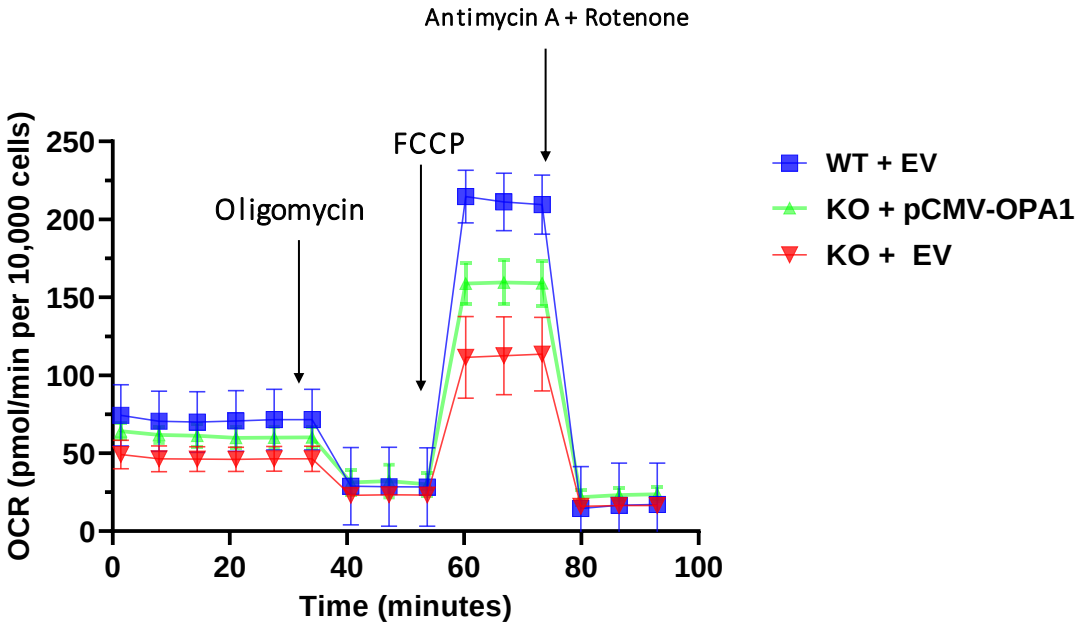

Figure 4.7 Ectopic expression of OPA1 partially rescues OCR

Cells were seeded in standard growth medium (RPMI) for 16 h at either 1 x 10^4 or 2 x 10^4 cells per well for wild-type and TAp73 KO H1299 cells respectively. Cells were transfected with the indicated plasmid or EV for 24 hours prior Seahorse assay. Culture media was replaced with glucose rich DMEM medium and cells cultured in a non-CO2 incubator for 1h prior to assay. OCR rate was measured using Seahorse XFe96 analyser and canonical mitochondrial inhibitors injected sequentially as labelled (Oligomycin = 2µM, FCCP = 500nM, Antimycin A/ Rotenone = 2µM). Data are representative of a single experiment and error bars indicate SEM of technical replicates (6 per data point).

Next, I sought to functionally implicate downregulated OPA1 expression as the mechanism driving decreased OCR. For this purpose, cells were transfected with OPA1 expression plasmid to identify a possible rescue of the mitochondrial phenotype (figure 4.7). Wild-type or TAp73 KO cells were also transfected with empty vector as a control. The results indicated that overexpression of OPA1 partially rescued OCR, and hence mitochondrial ETC function. This therefore places OPA1 downstream of TAp73 in the regulation of mitochondrial OXPHOS. However, similar to immunofluorescence staining of the mitochondrial network, the rescue following OPA1 overexpression was only partial, therefore indicating a deficiency of additional regulators of fusion or fission. In addition, it should be noted that the extent to which mitochondrial function is rescued is dependent on the transfection efficiency. Indeed, it is likely that a number of cells in the transfected experimental group may not be expressing OPA1 plasmid.

4.2.4 The decreases mitochondrial bioenergetic function in TAp73 knockout cells was not driven by decreased mtDNA content or expression of ETC complexes

It was possible that the decrease in mitochondrial OXPHOS observed in TAp73 KO cells was caused by a decreased expression of components of the ETC, of which 12 of the subunits are encoded in the mitochondrial genome. Mutation or loss of OPA1 leads to a depletion of mitochondrial DNA (mtDNA), secondary to inhibition of mtDNA replication (Elachouri et al., 2011). I therefore investigated the levels of mt-DNA relative to nuclear encoded DNA in wild-type and TAp73 knockout cells. Quantitative PCR was carried out against *mt-CO2* and *β2-microglobulin* genes as a proxy of mitochondrial and nuclear DNA content respectively (figure 4.8a). The ratio of Ct values between the two PCR reactions was calculated and the value expressed as a percentage of wild-type cells. Values indicated that significant depletion of the mitochondrial genome had not occurred, as there was only a modest 18% reduction of mtDNA content in TAp73 KO cells, and hence mtDNA depletion is unlikely to drive the decrease in OXPHOS. Furthermore, I performed western blot against specific subunits of the ETC using an antibody cocktail (figure 4.8b). The results indicated that there was no detectable decrease in the protein level of ETC subunits, either in mitochondrially encoded *COXII* or the remaining nuclear encoded genes. These data therefore show that the decrease in OXPHOS observed in TAp73 KO cells is unlikely to be driven by mtDNA depletion or decreased expression of ETC complexes.

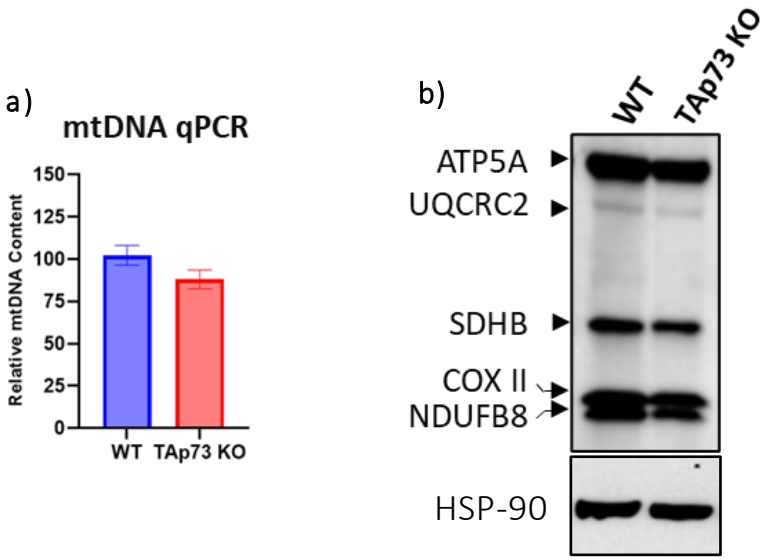

Figure 4.8 Decreased mitochondrial bioenergetic function was not driven by depletion of mtDNA content or translation of ETC complexes

(a) Quantitative PCR was carried out against mitochondrially encoded *mt-CO2* as an indicator of mtDNA content. Relative expression values were normalised to expression of nuclear encoded *β2-microglobulin* using the ΔΔCt method and expressed as a percentage of wild-type control (n=2) (b) Western blot of protein expression of the indicated ETC subunits in wild-type and TAp73 KO cells. Expression of HSP-90 was used as a loading control.

4.2.5 TAp73 knockout decreased basal and maximal ECAR

The Seahorse extracellular flux assay also allowed for an analysis of ECAR data obtained during the mitochondrial stress test. Due to the decrease in energy production *via* oxidative phosphorylation in TAp73 KO cells, I explored the possibility that glycolysis may be upregulated to sustain ATP generation and cellular growth. However, ECAR data showed that there was instead a decrease in basal glycolysis (figure 4.9a,b). The addition of oligomycin and culture in a high concentration of glucose caused a shift to maximal ECAR (figure 4.8a), as it inhibits ATP synthase. This showed that TAp73 KO cells had a ~50% reduction in maximal ECAR (figure 4.9c). These data therefore confirm previous reports that TAp73 regulates glycolytic flux (Li et al., 2018), and together with OCR data, show impaired energy production in TAp73 KO by distinct mechanisms.

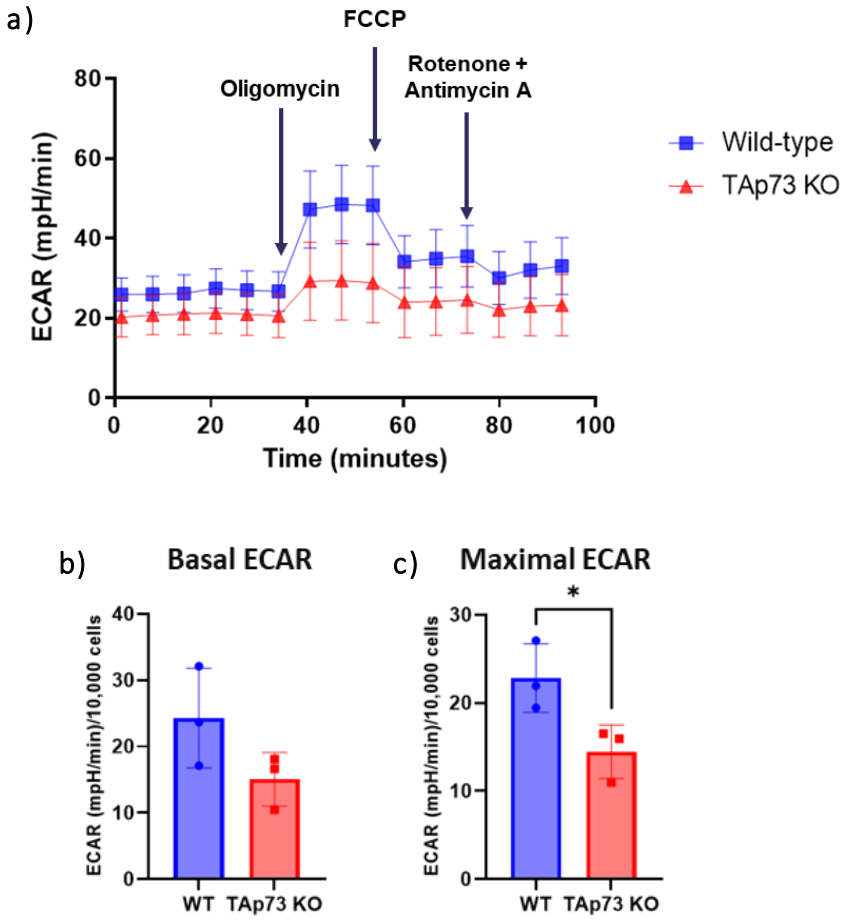

Figure 4.9 TAp73 KO induced a decrease in basal and maximal ECAR

(a) The Seahorse extracellular flux analyser was used to obtain ECAR data from the mitochondrial stress test described previously on wild-type (blue) and TAp73 KO (red) cells (figure 4.6). Time points for the injection of canonical mitochondrial inhibitors are indicated. (b,c) Basal and maximal ECAR values were obtained and normalised to cell number. Data are shown as mean ± SEM (n=3). (*) $P \leq 0.05$ (Student's T-test).

4.2.6 TAp73 knockout decreases cell proliferation and affects cell morphology

Previous studies have connected a role for TAp73 in regulating cellular metabolism with oncogenic cell growth. Although in apparent opposition with the established tumour-suppressor roles of TAp73, it may explain why TAp73 is rarely mutated but rather is frequently overexpressed in human tumours (Du et al., 2013). Given that TAp73 supports the proliferation of human and mouse tumour cells through regulation of glycolysis and the pentose phosphate pathway (Du et al., 2013; Li et al., 2018), it seemed prudent to investigate the effect of TAp73 KO in H1299 on cellular proliferation. Consistent with previous reports, there was a 50% or greater decrease in proliferation rate in both TAp73 KO cell lines generated (figure 4.10a). The novel data presented in this chapter are therefore in support of a multi-faceted role for TAp73 in regulating cell growth, whereby defective mitochondrial dynamics might also play a role.

Alterations in cell morphology were also observed in knockout cells. Indeed, TAp73 KO cells displayed both a rounded morphology and a tendency to form distinct cell clusters, which contrasted with a more elongated morphology of the wild-type control (figure 4.10b). This is consistent with a reported role for TAp73 in regulating cytoskeletal dynamics and cell migration (Fuertes-Alvarez et al., 2018).

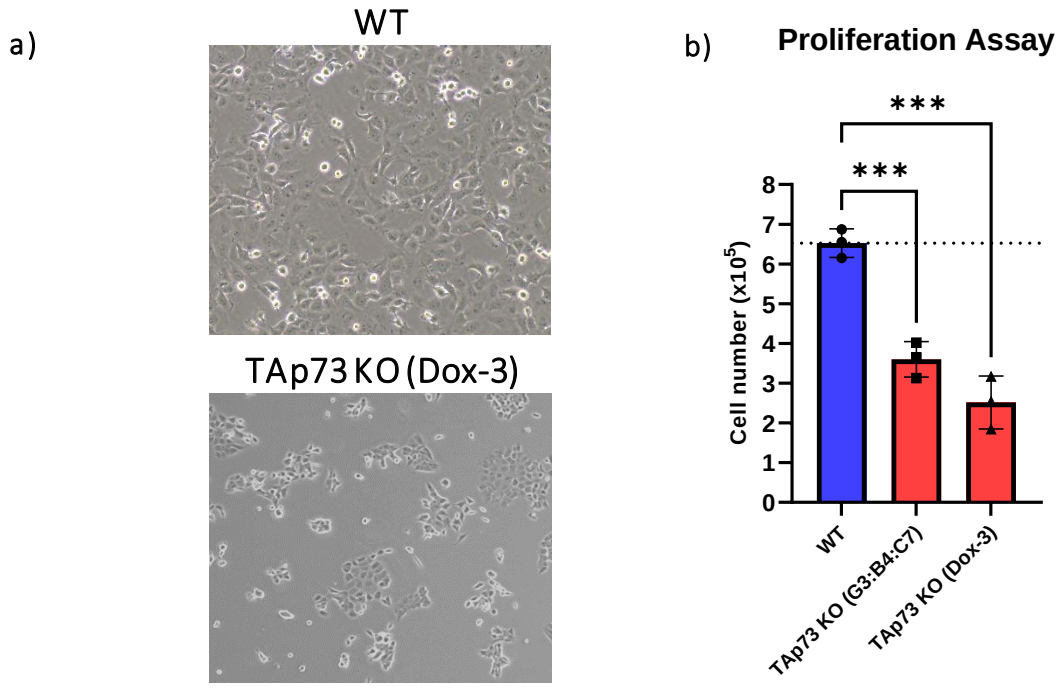

Figure 4.10 TAp73 knockout supresses growth and alters the cell morphology of H1299 cells.

(a) Phase contrast images of WT and TAp73 KO (Colony Dox-3) cells. Images were acquired after 4 days of culture at the same seeding density. (b) Cells from the indicated colonies were seeded at 20,000 cells/well in a 6 well plate and counted after 5 days to obtain relative rates of proliferation. Data are shown as mean ± SEM (n=3). (***) $P \leq 0.001$ (Student's T-test).

4.2.7 TAp73 knockout sensitises cells to apoptosis induced by BH3 mimetics

The functions of OPA1 in regulating mitochondrial fusion and cristae remodelling are inextricably linked with the execution of apoptosis. Upstream of caspase-9 activation, mitochondria fragment to facilitate the release of cytochrome *c* from cristae into the cytosol where if binds with APAF1 and activates the assembly of the apoptosome (Bao and Shi, 2007). Indeed, blocking of mitochondrial fission inhibits cytochrome *c* release and cell death, functionally linking mitochondrial morphology with cell death induction. Concurrently, overexpression of OPA1 inhibits mitochondrial fission and protects from cell death occurring through the intrinsic pathway of apoptosis (Frezza et al., 2006).

However, ectopic overexpression of OPA1 also inhibited apoptosis induction in $MFN1^{-/-}/MFN2^{-/-}$ double KO cells without rescuing mitochondrial fragmentation (Cipolat et al., 2004). This led to the discovery that cristae junctions are controlled by OPA1 and remodelled following disruption of OPA1 oligomers, for example by tBid activation, thereby increasing the cytochrome c released and enhancing apoptosis (Arnoult et al., 2005; Frezza et al., 2006). Due to the downregulation of OPA1 expression in TAp73 KO cells, I therefore decided to investigate the sensitivity of TAp73 KO cells to the induction of apoptosis.

To interrogate the impact of altered mitochondrial morphogenesis on apoptosis, MOMP was induced using treatment of TAp73 KO cells with BH3 mimetics. The mechanism of action of these compounds is detailed in the thesis introduction. They provided a valuable tool because they trigger BAX/BAK pore formation downstream of activating signalling from the intrinsic and extrinsic apoptosis pathways, which converge on the mitochondrion and trigger cytochrome *c* release. I was therefore able to probe sensitivity to apoptosis independently of functions of p53 and p73 that influence the pro-survival or pro-death signalling downstream of FADD receptor activation from the extrinsic pathway or the DNA damage response of the intrinsic pathway.

It was first necessary to determine optimal conditions for apoptosis induction in H1299 cells, which have been reported to be dependent on both BCL-xL and MCL-1 for survival (Milani et al., 2019). I therefore treated cells with the single agents ABT-737 or S63845 at 10 µM concentration, which inhibit the pro-survival proteins BCL-xL and MCL-1 respectively (reference needed?). The kinetics of cell death induction were then tracked using the Incucyte live-cell imaging system to quantify the percentage of Annexin V positive cells (figure 4.10a). Treatment with single agent of BH3 mimetic did not induce notable cell death relative to vehicle (DMSO) control (figure 4.11a). Conversely, combination treatment with 5 µM or 1 µM of both compounds in combination rapidly induced cell death above 75% after 120 mins, confirming the dependency on both BCL-2 family members.

In order to determine a suitable assay window to investigate changes in sensitivity to BH3 mimetic, cell-by-cell analysis was performed using Incucyte software to quantify dynamic changes in cell populations

using label free cell counts. For 1 µM combination treatment, there was a clear separation between Annexin V positive and negative cells after 90 mins (~50% cell death induction), evident from well scans and the histogram generated from classification of cell populations figure 4.11b,c.

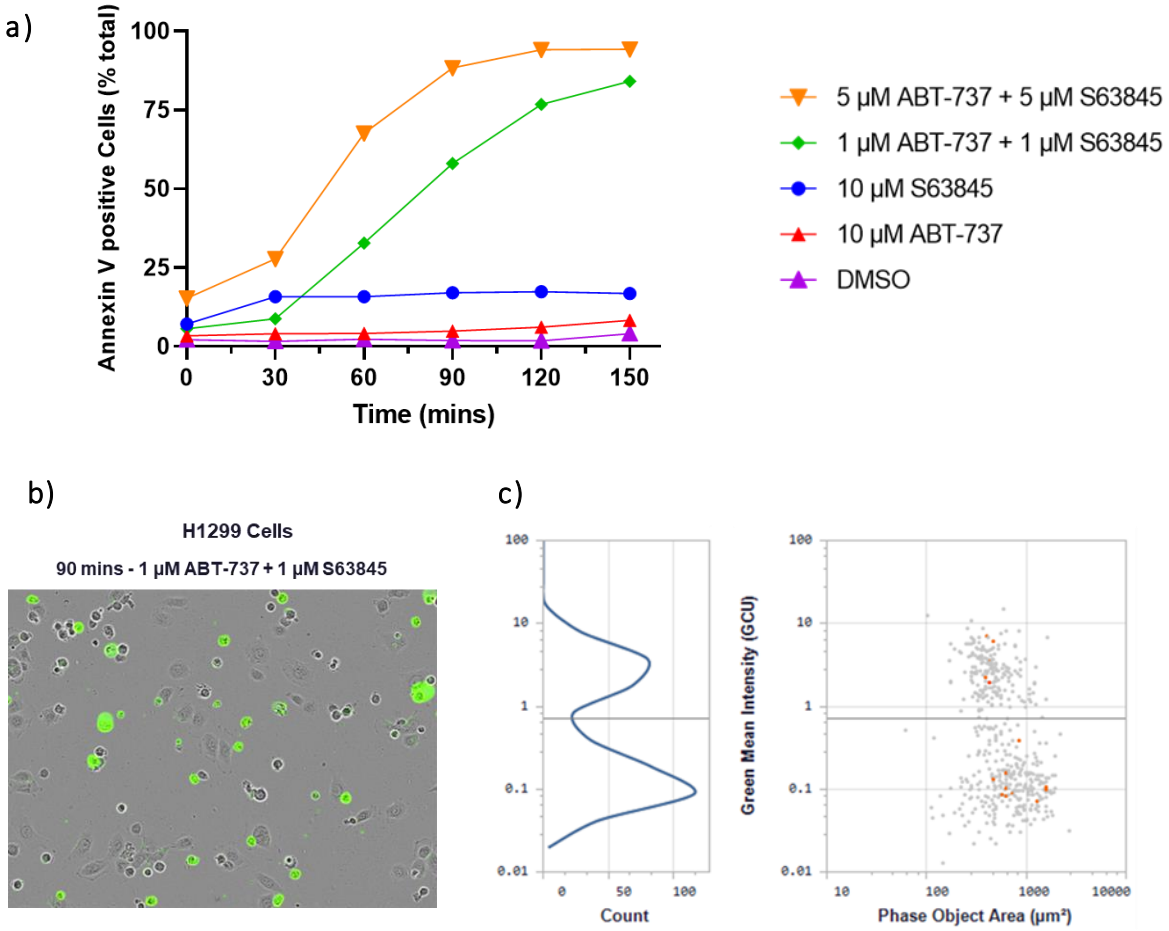

Figure 4.11 Inhibition of BCL-xL in combination with MCL-1 is required to induce cell death in H1299 cells.

(a) H1299 cells were treated with the indicated concentrations of BH3-mimetic (ABT-737 or S63845 as a single treatment or in combination). Cells were pre-incubated with Annexin V-FITC which binds to externalised PS present on apoptotic cells, in a Ca^{2+}-dependent manner. Apoptosis induction was then tracked using the adherent cell-by-cell classification module on the Incucyte platform which scanned each every 15 mins. (b) Representative image from wild-type cells treated with 1 µM combination treatment of ABT-737 & S63845 for 90 mins. (c) Segmentation of the phase contrast channel was used to obtain label-free cell counts and track dynamic changes in cell populations at each time point. The gate for identification of Annexin V^+ cells was set at 0.71 green calibrated units (GCU).

I therefore selected 1 µM or 2 µM combination treatment of BH3 mimetic as a suitable inhibitor concentration to track cell death induction in TAp73 KO cells (figure 4.12a). Quantification of apoptosis induction over time indicated that TAp73 KO cells were more sensitive to combination treatment with BH3 mimetics. At both 1h and 2h time points after 1 µM treatment with each inhibitor, there was a significant increase in the number of apoptotic cells in the TAp73 KO relative to WT control (figure 4.12b).

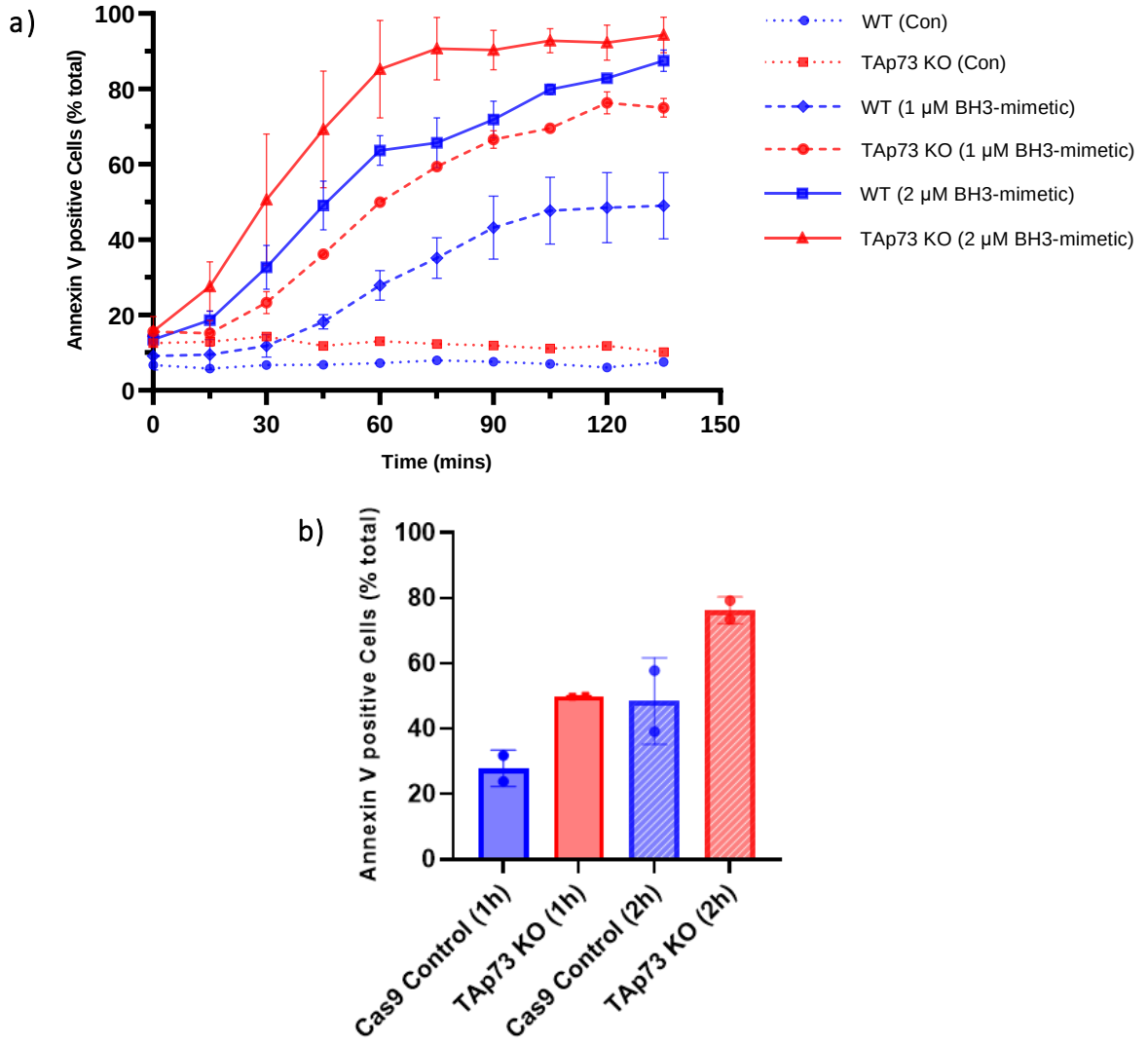

Figure 4.12 TAp73 knockout sensitises H1299 cells to apoptosis induced by BH3 mimetics.

(a) Wild-type or TAp73 KO H1299 cells were treated with combination treatment of BH3 mimetics or vehicle control (where 1 µM BH3 mimetic = 0.5 µM ABT-737 plus 0.5 µM S63845 and 2 µM mimetic = 1 µM of each compound) and apoptosis induction tracked using Annexin V/APC signal. Cell-by-cell analysis was optimised in figure 4.10 and used to quantify the percentage of annexin V positive cells. Data presented as mean value from each well scanned 4 times ± SD. (b) Percentage of Annexin V positive cells between wild-type and TAp73 KO cells treated with 1 µM BH3 mimetic and quantified at the indicated time points from two independent experiments. Data shown as mean ± SEM.

These data therefore indicate that TAp73 knockout from H1299 cells increased sensitivity to the induction of apoptosis following inhibition of BCL-xL and MCL-1. Given that the induction of apoptosis is regulated on OPA1-dependent cristae remodelling for efficient cytochrome *c* release, this finding suggests that increase sensitivity to the induction of apoptosis may be driven by downregulation of the TAp73/OPA1 axis. This hypothesis is supported by the distinct morphological changes induced by OPA1 loss in TAp73 KO cells which include fragmentation and widening of cristae.

4.3 Discussion

4.3.1 TAp73 knockout drives fragmentation of the mitochondrial network

In this chapter, I have demonstrated that the balance between mitochondrial fusion and fission is altered in TAp73 KO cells. Investigation of the mitochondrial morphology in these cells showed that TAp73 expression is necessary to maintain an elongated mitochondrial network and represents a novel function of TAp73 isoforms (figures 4.2 – 4.4). Further, the findings presented in chapter 3 indicate that the defect in mitochondrial fusion is brought about by downregulation of OPA1 expression, which is under the transcriptional control of TAp73 in H1299 cells. Importantly, through the ectopic expression of OPA1 in TAp73 KO cells, the defect in mitochondrial fusion was abrogated and the mitochondrial phenotype observed in wild-type cells mostly rescued. This places OPA1 function downstream of TAp73 and directly connects downregulated OPA1 expression with the striking dysregulation of mitochondrial dynamics observed in the TAp73 KO model. Moreover, it was evident from electron microscopy images of TAp73 KO cells that OPA1 downregulation also led to alterations in cristae architecture, and further implicates disruption of the TAp73/OPA1 axis with mitochondrial dysfunction resulting from loss of OPA1 function.

The rescue of mitochondrial morphology with ectopic expression of OPA1 was not as comprehensive as rescue using TAp73α overexpression construct (figure 4.3). This may indicate that the intricate control of additional targets of TAp73 is required for the complete maintenance of an elongated mitochondrial network. As identified in ChIP-seq data analysis, this may be brought about by, but not limited to, altered expression of additional regulators of mitochondrial dynamics such as the Mitofusins, *MFF*, and *FIS1*, which I have also identified as genes for which TAp73 can bind their response elements (Chapter 2; figure 3.3). It would therefore be of interest to validate regulation of these genes by TAp73 in future work and assess the functional impact on mitochondrial morphology and function. Another outstanding question from this work is whether expression of p53 can rescue mitochondrial morphology in this setting, in a manner similar to ectopic TAp73 expression, as H1299 cells do not express functional p53. This is particularly prudent given the recent finding that p53 can regulate

mitochondrial dynamics through mTORC signalling and through the regulation of Drp1 translocation to the mitochondria (Phan et al., 2022; Kim et al., 2020). However, a direct transcriptional control of mitochondrial fusion and fission regulators has not been reported.

Furthermore, mitochondrial morphology is adapted in response to a plethora of cellular cues or upstream signalling events (Sprenger & Langer 2019; figure 4.12). Changes in mitochondrial dynamics in a TAp73 knockout model may therefore also be driven in part by ROS accumulation, metabolic stress, or alterations in the regulation of cell cycle progression, and may explain why ectopic OPA1 expression did not completely rescue wild-type mitochondrial morphology. It would therefore be relevant to investigate the activation of cell stress pathways, such as AMPK or autophagic signalling, which may also be a driver of mitochondrial fragmentation in TAp73 KO cells. Although it has been reported that TAp73 depletion from mouse embryonic fibroblasts (MEFs) drives ROS accumulation, mitochondrial impairment, and a premature aging phenotype *in vivo*, the authors did not report any alterations in mitochondrial morphology (Rufini et al., 2012). Therefore, additional to the transcriptional control of Cox4i1, I have provided a novel mechanism by which loss of TAp73 drives mitochondrial dysfunction, through influencing mitochondrial dynamics.

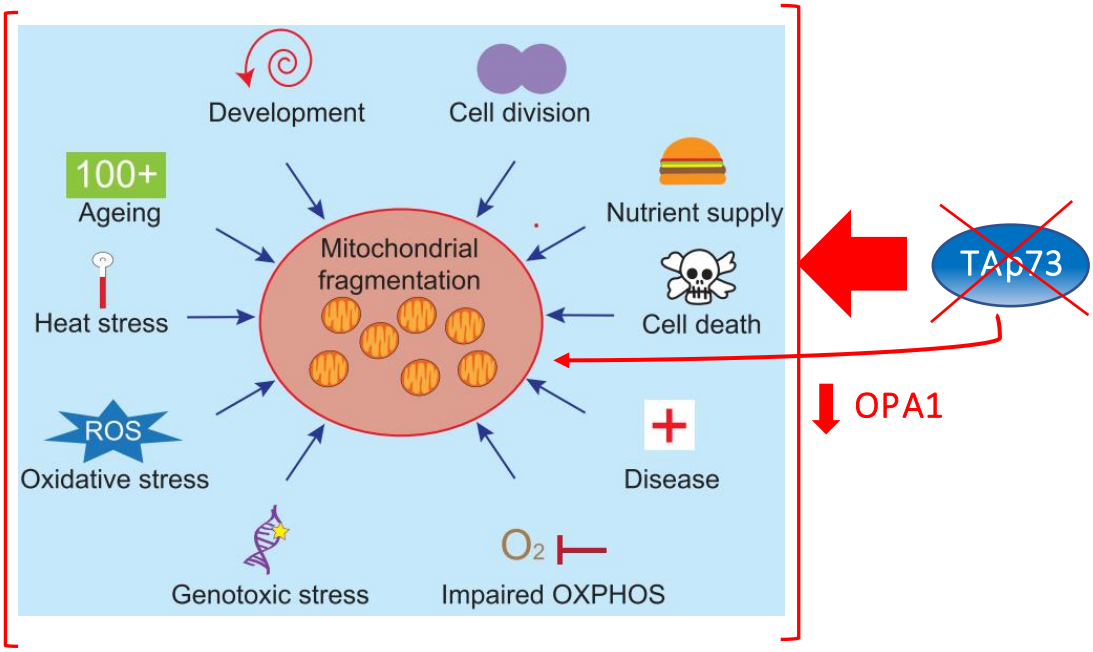

Figure 4.13 Triggers of Mitochondrial Fragmentation.

Fragmentation of the mitochondrial network has been observed under various physiological and stress conditions, during development and cell death, and in disease and ageing. Evidence suggests that some of the indicated pathways may be regulated by TAp73 function, such as the regulation of Cox4i1 and redox balance. (Springer & Langer 2019).

Moreover, mitochondrial fragmentation can be beneficial or detrimental to the cell and must be considered in a defined physiological context to understand its contribution to disease pathogenesis, development, or in ageing (Giacomello et al., 2020). Given the diverse phenotype of Trp73 and TAp73 knockout mice outlined in the introduction, it was therefore logical to speculate that mitochondrial dysfunction driven by alterations in the TAp73/OPA1 axis may underpin elements of the broad developmental, aging and tumorigenic phenotypes of p73 knockout mice. Given the striking multiciliated cell loss in the airway epithelium and of Trp73 and TAp73 knockout mice, I decided to focus on the relevance of this axis in this tissue, as presented in the following chapter.

4.3.2 Disruption of the TAp73/OPA1 axis impairs mitochondrial bioenergetics

TAp73 has been implicated in positively regulating distinct metabolic pathways, including amino acid metabolism, glycolysis, PPP, the response to oxidative stress, Krebs cycle, and fatty acid metabolism (He et al., 2015; Li et al., 2018). I have herein presented data which further implicates TAp73 in the control of cellular metabolism, achieved through the control of mitochondrial dynamics. (figure 4.6). Interrogation of OCR in TAp73 KO cells indicated that a fragmented mitochondrial network impaired ETC function, which was partially rescued when fusion of the mitochondrial network was restored by ectopic expression of OPA1. This rescue places the TAp73/OPA1 axis as a molecularly distinct mechanism from the previously reported role in regulating the ETC through control of the complex IV subunit, Cox4i1 (Rufini et al., 2012).

The efficiency of mitochondrial respiration is also governed by cristae morphogenesis, a function of OPA1 protein that is independent from inner-membrane fusion (Cogliati et al., 2013). Genetic and apoptotic manipulations of cristae structure, such as through the oblation of OPA1 or disassembly of functional OPA1 oligomers by tBid affect assembly and activity of respiratory complexes in vitro and in vivo (Cogliati et al., 2013; Patten et al., 2015). It is therefore possible that defective oxidative phosphorylation observed in the context of TAp73 KO may be driven by cristae remodelling as well as an altered balance between mitochondrial fusion and fission. This was also suggested by alterations in cristae structure observed by TEM analysis *in vitro* and *in vivo*. To specifically address this, rescue experiments should be conducted with plasmid expression of OPA1 mutant that can still oligomerize and maintain cristae structure but has no fusion activity (Patten et al., 2015). Indeed, expression of OPA1 fusion mutant partially rescued basal OCR in OPA1 KO MEFs, owing to increased ATP synthase assembly (Patten et al., 2015). Moreover, analysis of mitochondrial subunit assembly into functional oligomers could be investigated using blue native PAGE in TAp73 KO cells.

Notably, these pre-eminent studies showing the role of OPA1 in regulating cristae morphology and mitochondrial bioenergetics were carried out following complete oblation of OPA1, which may produce

a more prominent phenotype than observed following the downregulation of OPA1 described herein. A more relevant comparison can be found in $OPA1^{+/-}$ cells, where a partial reduction in OPA1 activity elicited a bioenergetic defect highly similar to that observed in TAp73 KO cells (Sun et al., 2020). This therefore confirms that an approximately 50% reduction in OPA1 expression is sufficient to induce significant bioenergetic impairment, and adds weight to my hypothesis.

Moreover, Cogliati and colleagues showed that the connection between respiratory function and OPA1 mediated regulation of cristae morphogenesis was independent of changes to mitochondrial protein synthesis or apoptotic outer mitochondrial membrane permeabilization (Cogliati et al., 2013). However, this study was performed using conditional oblation of OPA1 from $Opa1^{flx/flx}$ mouse fibroblasts using adenoviral driven Cre-recombinase expression. This eliminated a contribution of mtDNA depletion to RCS assembly or activity. Interestingly, the reduction in OPA1 expression in TAp73 KO cells was not sufficient to deplete mtDNA or inhibit translation of ETC subunits (figure 4.7). This therefore ruled out the possibility that impaired mitochondrial bioenergetics in my model was driven by mtDNA depletion. It would, however, be interesting to see if a depletion of mtDNA is observed at a higher cell passage of TAp73 KO cells, consistent with a role for OPA1 in mtDNA maintenance.

4.3.3 Expression of TAp73 determines sensitivity to the induction of apoptosis by BH3-mimetics

I have also investigated the effect of TAp73 knockout in H1299 cells on the sensitivity of cell death induction by BH3 mimetics. Combination treatment with ABT-737 and S63845 rapidly induced cell death in wild-type H1299 cells after addition of 0.5 µM of both compounds (figure 4.11). Notably, apoptosis was more rapidly induced in TAp73 knockout cells; thereby linking TAp73 expression with an anti-apoptotic function of this isoform. This is an interesting finding, given that the opposite effect has been observed for p53, where knockout of the *TP53* gene has been shown to confer resistance of cancer cells to treatment of BH3 mimetic (Nechipork et al., 2019). Such resistance following loss of TP53 is driven by downregulation of pro-apoptotic targets including *PMAIP1*, *BAK1*, and *PUMA*, albeit without notable changes to *BAX* expression (Nechipork et al., 2019). Mechanistically, it is also possible that loss of TAp73 sensitises cells to treatment with BH3-mimetics due to a downregulation of pro-survival proteins, although this has not been reported. However, the opposite effect has been observed for MCL-1 in that it has been shown to negatively regulate the transcriptional activity of p73 (Widden et al., 2020).

Given that many pro-apoptotic targets of p53 are shared with TAp73, including *PUMA* and *NOXA*, it is surprising that TAp73 expression correlates with resistance to activation of the intrinsic pathway of apoptosis by BH3-mimetics. The finding that TAp73 KO cells exhibit OPA1 downregulation and fragmentation of the mitochondrial network may go some way to explaining this phenomenon. Indeed, the regulation of mitochondrial fusion by regulators such as OPA1 is explicitly connected with cell death induction as fragmentation is observed prior to cytochrome *c* release in H1299 cells (Germain et al., 2005; Breckenridge et al., 2003). Further, OPA1 oligomers inserted in the inner mitochondrial membrane influence cristae morphogenesis protect against cytochrome *c* release (Frezza et al., 2006). I therefore propose that the positive regulation of mitochondrial fusion by TAp73 confers resistance to apoptosis induction following treatment of H1299 cells with BH3 mimetics.

Furthermore, the axis I have identified between TAp73 and OPA1 might therefore explain why TAp73 expression is highly abundant in many cancers such as lung adenocarcinoma and acute myeloid leukemias (AML) (Puig et al., 2003; Tschan et al., 2000). Notably, in the case of AML, no difference in expression was observed for ΔNp73 isoforms relative to normal CD34+ hematopoietic cells, meaning that aberrant expression of TAp73 is not inhibited by dominant-negative isoforms (Nishida et al., 2019). The TAp73/OPA1 axis may therefore explain why venetoclax (BCL-2 inhibitor of the BH3 mimetic family) resistant cells massively overexpress *TP73* in AML and *TP73* knockdown restored sensitivity to venetoclax.

Chapter 5: The TAp73/OPA1 axis is functionally relevant in the ciliated epithelium

5 The TAp73/OPA1 axis is functionally relevant in the ciliated epithelium

5.1 Introduction

After finding that an axis exists between TAp73 and OPA1 that regulates mitochondrial dynamics, I next addressed the biological significance of this relationship *in vivo*. This was performed by analysing tissues from Trp73 null mice and Wild-type littermate controls in which TAp73 isoforms have a clearly defined developmental role. These mice were generated in the Balb/c background using the homologous recombination of a targeting vector in embryonic stem cells to produce a germline mutation and oblate p73 expression in all tissues (Yang et al., 2000). Owing to the transcriptional control of OPA1 by TAp73, I sought to test the hypothesis that cell populations which physiologically exhibit high levels of TAp73 expression display a contaminant decrease in OPA1 expression *in vivo*. This raises the possibility that TAp73 expressing populations may present aberrant mitochondrial dynamics and function, as observed in the H1299 TAp73 knockout cell model. Moreover, a dysregulated TAp73/OPA1 axis may provide a connecting mechanism for the diverse developmental, premature aging and tumour prone phenotypes of p73 knockout mouse models.

To investigate the presence of an TAp73/OPA1 axis in mouse tissue, I firstly focussed on epithelial cells of the upper airway. This is a tissue with high expression of TAp73 isoforms in mouse and human, together with brain and reproductive tissues (Grespi et al., 2012; Marshall et al., 2021). Specifically, TAp73 plays an important role in multiciliated cells of the airway and brain ependyma. There, it has been shown to regulate the expression of key genes responsible for differentiation into the multiciliated cell lineage, basal body docking and axonemal extension (Nemajerova et al., 2018). To perform this role, it has also been proposed that p73 is also expressed in basal stem cells of epithelial cell populations (Marshall et al., 2016), and so my analysis included this cell type.

Furthermore, multiple pieces of evidence suggest that the p73 knockout cilia phenotype is driven by further mechanisms in addition to abrogated multiciliated fate commitment and ciliary gene regulation. For example, functional mitochondria are necessary for the correct execution of ciliogenesis in different tissues (Burkhalter et al., 2019; Chambers et al., 2020). Taken together, I therefore investigated a contribution of the TAp73/OPA1 axis to abrogated ciliary function in p73 null mice.

5.1.1 Aims and Objectives

- To confirm that multiciliated cells of the airways in *TP73* null mice are characterised by defective ciliogenesis, consistent with published reports
- To investigate whether *TP73* oblation leads to a decrease in OPA1 expression in multiciliated cells

- To identify evidence of mitochondrial dysfunction in *TP73* knockout mice, in cell populations would otherwise express functional p73

To achieve these objectives, whole trachea or brains were dissected from 8 week old *TP73*$^{-/-}$ mice and matched wild-type littermates. Tissues were then fixed in formalin and embedded in paraffin before performing immunohistochemistry to investigate ciliated cell populations. This was also complemented by analysis of dissected ciliated tissues of airway and brain ependyma using electron microscopy. For this approach, tissues were fixed by transcardiac perfusion to maintain cellular structures.

5.2 Results

5.2.1 Multiciliated cells of the airway display defective cilia in *TP73*$^{-/-}$ mice

Prior to investigating whether an axis between TAp73 and OPA1 might drive defective ciliogenesis in *TP73*$^{-/-}$ mice, it was first necessary to corroborate published data showing the abrogation of ciliogenesis in multiciliated cells of the upper airway. Moreover, this allowed for an investigation of the penetrance and severity of the cilia phenotype in respect to published observations, which have indicate a total loss of functional cilia in mice harbouring a total deletion of p73 or TAp73 isoforms (Marshall et al., 2016; Nemajerova et al., 2016).

Scanning electron microscopy (SEM) images of the luminal surface of the tracheal epithelium indicated a severe abrogation of functional cilia in *TP73*$^{-/-}$ mice. Although a number of cells showed evidence of nucleating many motile cilia, the appendages were shorter in length compared with wild-type controls (figure 5.1a). Furthermore, immunofluorescence staining for the axonemal marker Acetylated-α-tubulin in tracheal cross-sections from *TP73*$^{-/-}$ mice confirmed the defect in cilia length and abundance in knockout animals. Immunofluorescence imaging also indicated an altered morphology or integrity of epithelial cells, as the signal for Ac-a-tubulin on the apical surface of cells was not in a consistent plane across the epithelial lumen (figure 5.1b). This may be due to airway damage arising from chronic inflammation, which is often observed in *TP73*$^{-/-}$ mice, or alternatively because of alterations in cell adhesion, which is also regulated by p73.

Notably, the decreased abundance of ciliated cells in *TP73*$^{-/-}$ mice was not as profound as previously reported by Marshall and colleagues. Quantification of the number of ciliated cells indicated that 18% of total cells of the respiratory epithelium displayed motile cilia, compared with 4% previously reported (figure 4.1c). Together, these data therefore suggest that loss of ciliary function in *TP73*$^{-/-}$ mice is largely driven by the generation of abnormal cilia and not a defect of commitment to the multiciliated cell lineage, or indeed execution of the early stages of multiciliogenesis transcriptional program.

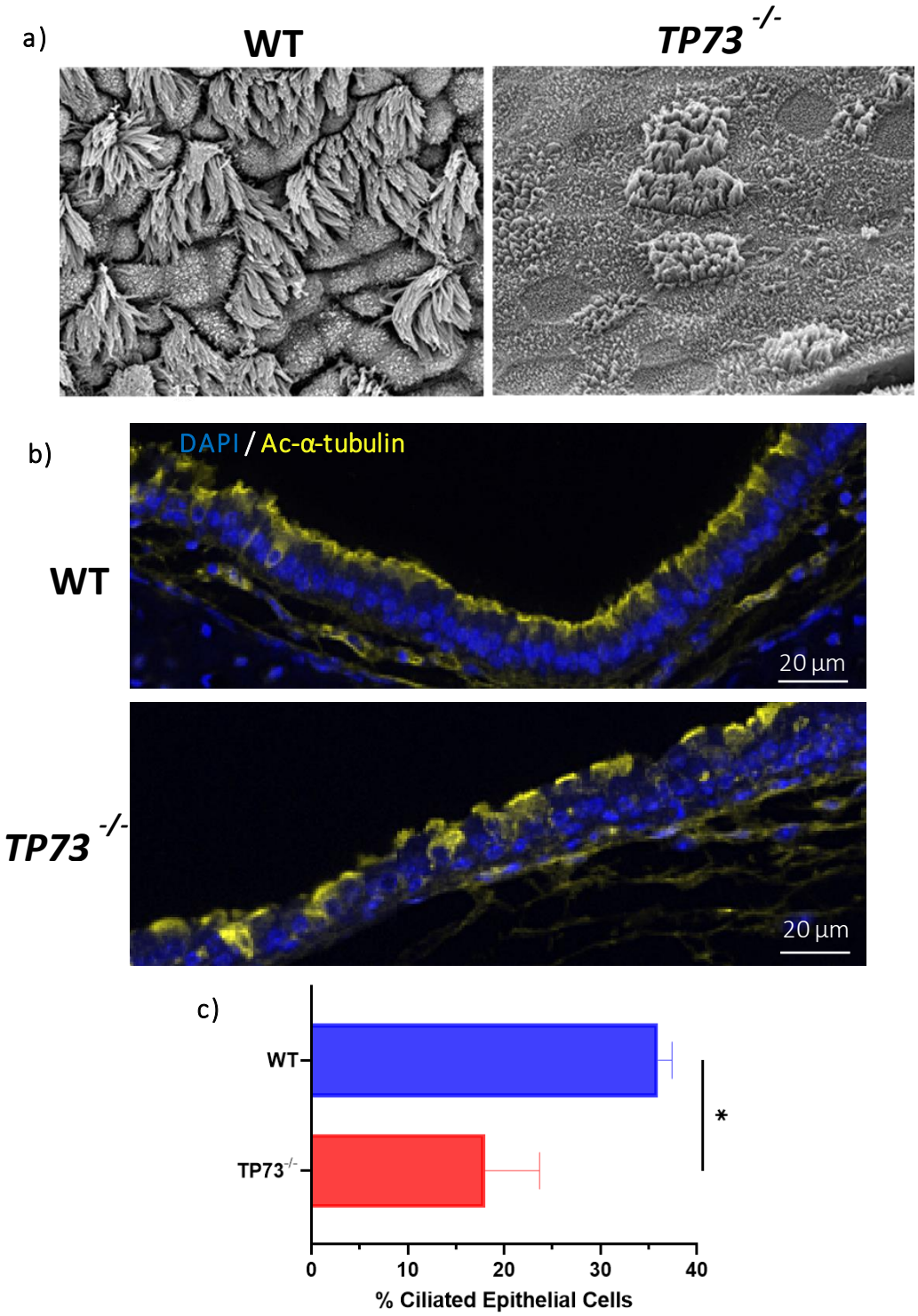

Figure 5.1 *TP73*$^{-/-}$ mice display defective ciliogenesis in the airway epithelium

(a) Representative scanning electron microscopy (SEM) micrographs of the luminal surface of the mouse tracheal epithelium from wild-type or *TP73*$^{-/-}$ mice. (b) Immunohistochemical staining performed against the cilia marker Ac-a-tubulin (yellow) with DAPI nuclear stain (blue). Tracheal cross-sections were imaged using fluorescent detection on the Vectra imaging system (Akoya biosciences). (c) Quantification of the number of cells positive for Ac-a-tub), as a percentage of total cells. A minimum of 5 images were obtained from two mice of each genotype (n=2). (*) $P \leq 0.05$ (Student's T-test)

5.2.2 OPA1 expression is downregulated in *TP73*$^{-/-}$ ciliated epithelial cells

I next sought to investigate the possibility that OPA1 is downregulated in the airway epithelium of *TP73* knockout mice. As shown in chapter 2, TAp73 transcriptionally regulates OPA1 expression by binding to the OPA1 promoter region in an H1299 cell model. A relevance for this axis in vivo was also highlighted by interrogation of p73 targets in tracheal ChIP-seq, which indicated TAp73 regulates OPA1 expression *via* direct binding. To investigate an axis between TAp73 and OPA1 *in vivo*, formalin fixed tracheal sections from wild-type and *TP73*$^{-/-}$ mice were stained for OPA1 expression using multiplex immunohistochemistry (figure 5.2a). Imaging of stained sections indicated a ubiquitous OPA1 expression across all cell types of the ciliated epithelium in Wild-type animals. However, there was a striking downregulation of OPA1 expression in *TP73* knockout mice. This downregulation was more profound in a percentage of epithelial cells and might represent cell populations that would normally express TAp73, which make up around 30% of epithelial cells in wild-type animals, as evident by co-staining for TAp73. Anti-TAp73 immunohistochemical staining also confirmed the complete oblation of TAp73 protein in *TP73* null animals (figure 5.2a).

I next sought to interrogate expression of OPA1 at the mRNA level in the ciliated epithelium of *TP73* knockout mice. Whole tracheae were dissected from Wild-type or *TP73*$^{-/-}$ mice and epithelial cell populations isolated using pronase digestion to disrupt adhesion of epithelial cells to the basement membrane. RT-qPCR was then performed against the mouse *OPA1* gene following RNA isolation from epithelial cells (figure 5.2b). Quantification of *OPA1* mRNA expression indicated a profound reduction in *OPA1* transcripts in *TP73*$^{-/-}$ mice and is consistent with a role for TAp73 in regulating *OPA1* expression.

The multiplexed staining of tracheal sections was then further developed to incorporate staining for the ciliated cell marker Acetylated-alpha-tubulin. This allowed for an analysis of OPA1 protein expression specifically in the ciliated cell lineage. Co-staining of tracheal sections for Acetylated-alpha-tubulin and OPA1 indicated that the downregulation of OPA1 expression was more pronounced in cells which physiologically express TAp73 to maintain their functionality, as loss of OPA1 signal correlated with amplification of cilia on the cell surface (cyan arrows; figure 5.3a). To this end, OPA1 fluorescence signal on stained sections was quantified using In-form software. Values for OPA1 signal intensity were obtained on a cell-by cell basis which were then sub-classified as ciliated or non-ciliated depending on the presence or absence of Ac-a-tubulin signal (figure 5.3b). The results indicated that in *TP73* knockout sections the ciliated cell lineage displayed a significant decrease in OPA1 signal in compared with non-ciliated cells, which served as a powerful internal control for comparison in the same tissue section. Moreover, fluorescence intensity values obtained indicated that the increased OPA1 signal observed in non-ciliated cells from knockout mice was more comparable to both ciliated and non-ciliated cell

populations from wild-type animals. These data therefore indicated that the downregulation of OPA1 protein expression in the tracheal epithelium was driven by deletion of p73 expression in the ciliated cell lineage, whilst non-ciliated cells maintained OPA1 expression in the knockout ciliated epithelium.

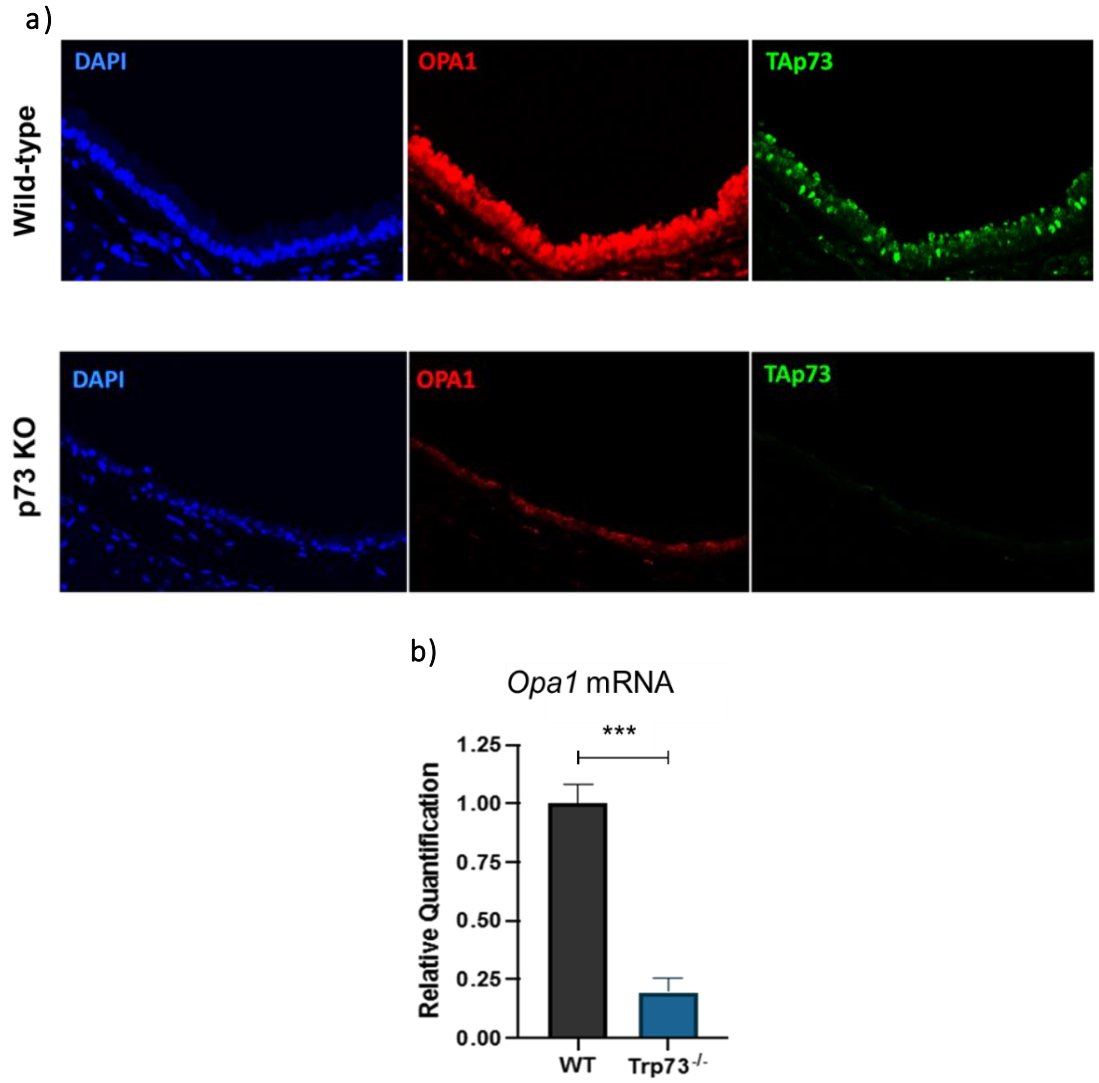

Figure 5.2 OPA1 expression is downregulated in the *TP73*$^{-/-}$ tracheal epithelium.

(a) Multiplex immunohistochemical staining performed against OPA1 (red) and TAp73 (green) with DAPI nuclear stain (blue) from mice of the indicated genotypes. Tracheal cross-sections were imaged using fluorescent detection on the Vectra imaging system (Akoya biosciences). (b) RT-qPCR was performed against *OPA1* mRNA following isolation of RNA from epithelial cells dissociated from whole mouse trachea. Three trachea from each genotype were pooled together to obtain a sufficient number of cells (n=3). (***) $P \leq 0.001$ (Student's T-test).

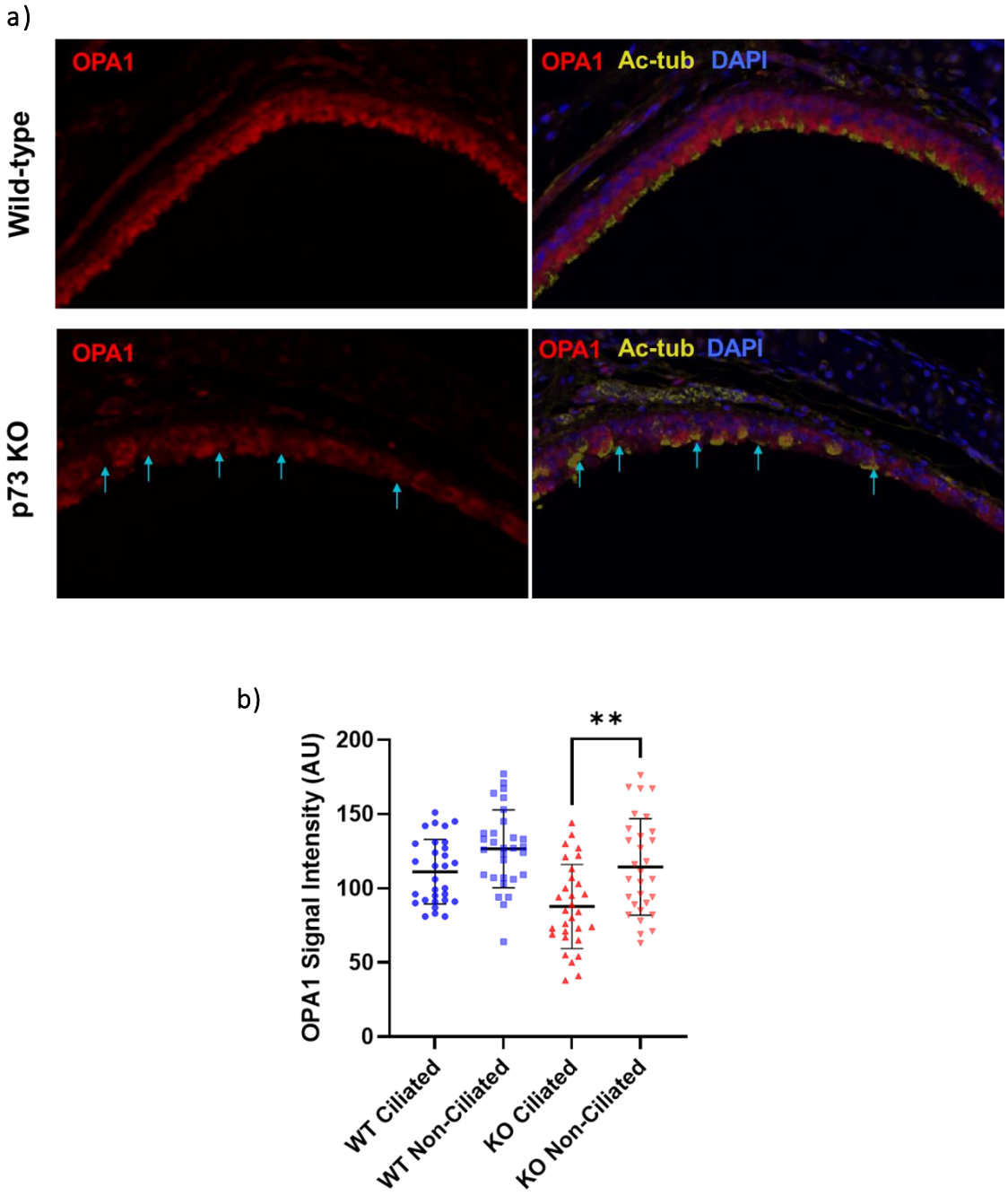

Figure 5.3 OPA1 expression was significantly downregulated in the ciliated cell lineage.

(a) Multiplex immunohistochemical staining performed against OPA1 (red) and Ac-a-tubulin (yellow) with DAPI nuclear stain (blue). Tracheal cross-sections were imaged using fluorescent detection on the Vectra imaging system (Akoya biosciences). Ciliated cells exhibiting downregulated OPA1 expression are indicated by cyan arrows. (b) Quantification of OPA1 expression in ciliated and non-ciliated cell populations in wild-type and *TP73*$^{-/-}$ animals. Images were obtained from two mice of each genotype (n=2). (**) $P \leq 0.01$ (Student's T-test).

5.2.3 Mitochondria display a fragmented morphology in multiciliated cells of *TP73*$^{-/-}$ mice

Given that multiciliated cells in *TP73*$^{-/-}$ mice displayed a decrease in OPA1 expression, I next looked for evidence of defective mitochondrial fusion, arising from the essential role of OPA1 in fusion of the IMM. Consistent with the observed downregulation of *OPA1* mRNA and protein, ciliated cells in *TP73* null mice displayed a fragmentation of the mitochondrial network (figure 5.4a). Furthermore, quantification of the mean mitochondrial length in electron microscopy micrographs indicated a remarkable similarity of mitochondrial length measurements across cells of the wild-type epithelium (ciliated and non-ciliated) and non-ciliated cells of *TP73*$^{-/-}$ epithelia (figure 5.4b). However, consistent with a role for TAp73 in regulating mitochondrial dynamics through an OPA1 axis, ciliated cells in *TP73*$^{-/-}$ cells had a striking reduction in mean mitochondrial length. This further highlighted the importance of this axis in ciliated epithelial cells. It was also evident from electron microscopy images that wild-type ciliated epithelial cells displayed a uniform localisation of mitochondria at the apical surface, whereas *TP73*$^{-/-}$ ciliated cells possessed many mitochondria located at the basal surface (indicated in callout box, figure 5.4a). This suggests that trafficking of mitochondria to the ciliary base is important for ciliary function and that the regulation of mitochondrial localisation may be abrogated in the *TP73* null epithelium. Furthermore, 3D images of the mitochondrial network were obtained using serial block-face SEM (SBF-SEM) which automatically cuts and images the sample alternatively using a diamond knife inside the SEM chamber (Kremer et al., 2015). Reconstruction of the mitochondrial network in 3D (figure 5.5a). Furthermore, quantification of the volume of each mitochondria indicated there was an increased abundance of mitochondria with a decreased volume (figure 5.5b)

5.2.4 *TP73*$^{-/-}$ ependymal cells display a reduction in size and an altered ultrastructure

TAp73 is also necessary for the ciliation of ependymal cells in the mouse brain (Gonzalez-Cano et al., 2018; Fuertes-Alvarez et al., 2018). These ependymal cell populations play key roles in central nervous system (CNS) development and physiology (Jiménez et al., 2014). A pseudostratified neuroepithelium at the interface between the developing brain and cerebrospinal fluid (CSF) is necessary for the generation of radial glial cells which determine neuronal fate and positioning (Jiménez et al., 2014). Beating of ependymal cilia is also important for propelling CSF, which is abrogated in *TP73*$^{-/-}$ mice and manifests as hydrocephalus (data shown in chapter 6). Multiciliated cell dysfunction is therefore a mechanism that drives the severe brain phenotype observed in *TP73*$^{-/-}$ mice (Gonzalez-Cano et al., 2018). It was therefore prudent to investigate the mitochondrial phenotype in *TP73*$^{-/-}$ ependymal cells. To this end, TEM micrographs of ependymal cell populations of the lateral ventricles from knockout and wild-type animals were obtained and the mitochondrial phenotype analysed (figure 5.6). Micrographs

indicated a distinct difference in mitochondrial morphology and architecture between wild-type and *TP73*$^{-/-}$ ependymal cells. Consistent with EM micrographs of airway multiciliated cells, mitochondria of ciliated cell populations appeared fragmented in knockout animals.

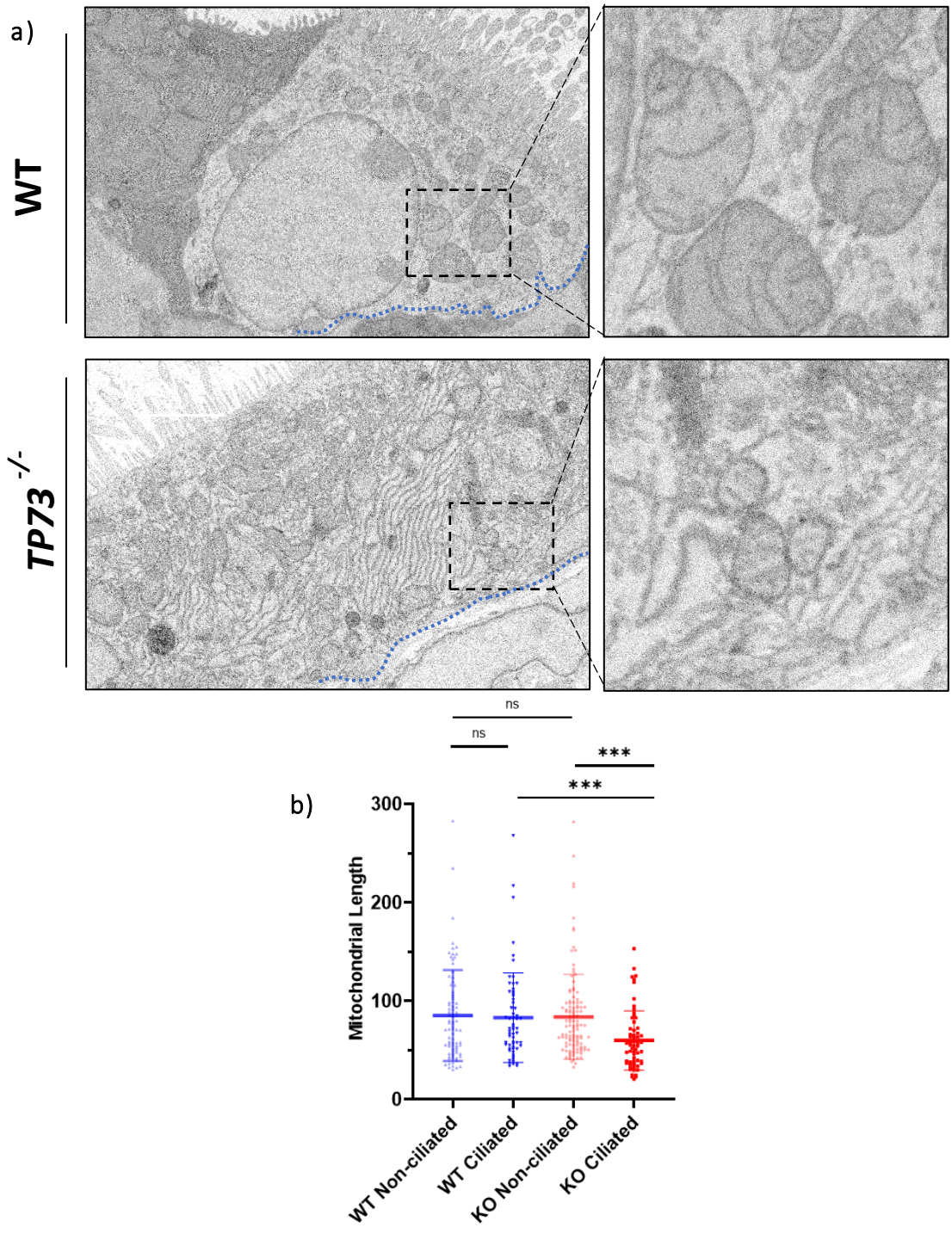

Figure 5.4 Ciliated epithelial cells of *TP73*$^{-/-}$ mice display altered mitochondrial morphology

(a) Individual cross-sections of the ciliated epithelium from wild-type or *TP73*$^{-/-}$ mice were imaged using serial-block-face SEM and representative micrographs from ciliated epithelial cells are shown. (b) Mitochondrial length was quantified using ImageJ software from ciliated and non-ciliated cell populations in wild-type and *TP73*$^{-/-}$ animals. Images were obtained from two mice of each genotype (n=2). (***) $P \leq 0.001$ (Student's T-test).

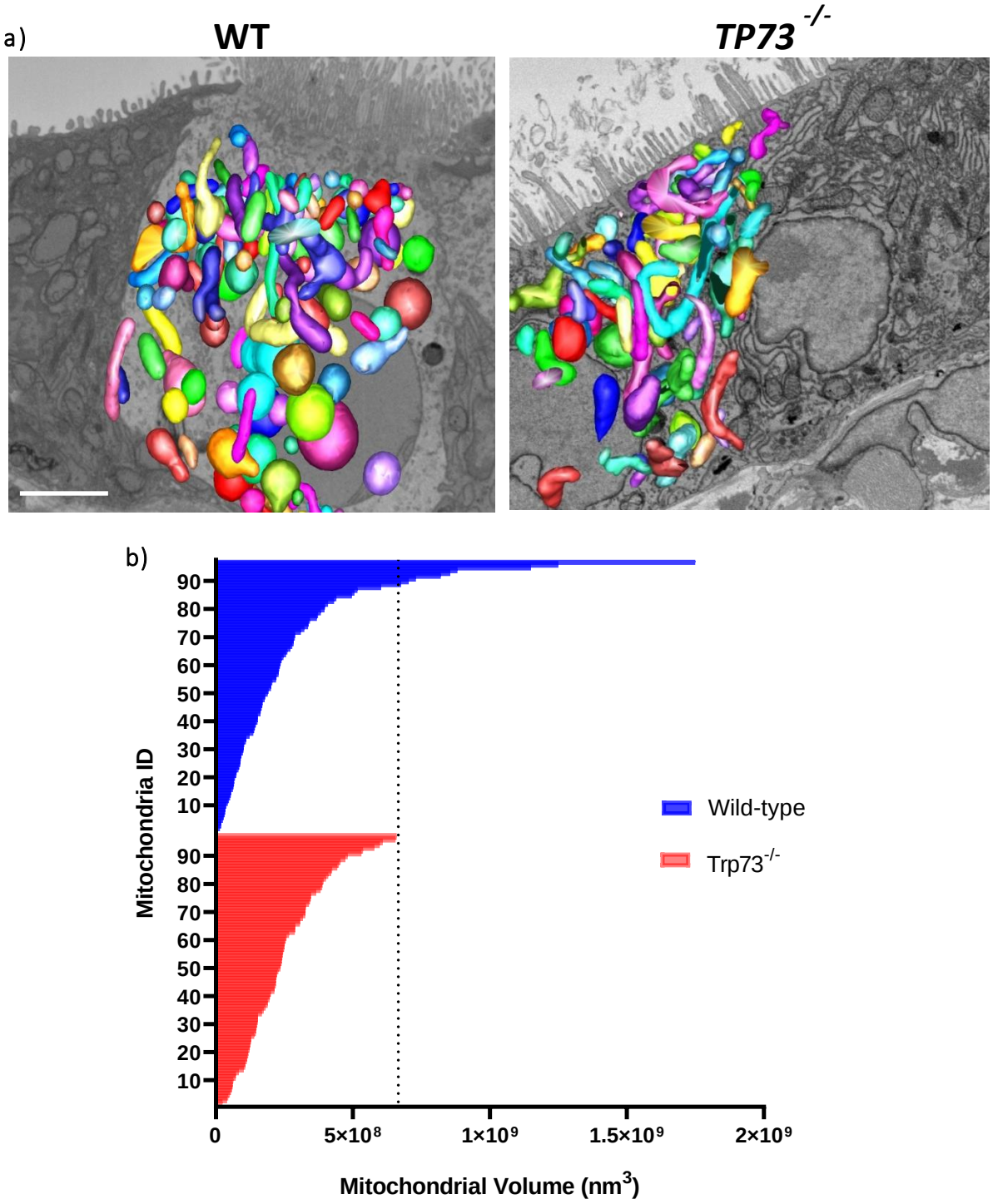

Figure 5.5 3D reconstruction of the mitochondrial network in ciliated epithelial cells of Wild-type and *TP73*$^{-/-}$ mice.

(a) Individual cross-sections obtained using serial-block-face SEM (imaged using Gatan 3View system) were used to segment and reconstruct the mitochondrial network in individual ciliated cells. Scale bar = 2 µm. (b) Mitochondrial volume was obtained and plotted for 100 individual mitochondria from a ciliated cell of each genotype (nm^3). The dotted line indicates the maximum mitochondria size from the *TP73*$^{-/-}$ ciliated cell.

Furthermore, fixation of brain tissues by transcardiac perfusion allowed for visualisation of cristae ultrastructure. Wild-type ependymal cells contained mitochondria containing densely packed cristae with no spaces in the mitochondrial matrix, consistent with the mitochondrial network of cells with high energy demand. However, the fragmented mitochondria of *TP73*$^{-/-}$ ependymal cells displayed dysfunctional mitochondrial with widened cristae, possibly arising from loss of OPA1 function. Mitochondrial ultrastructure in TP73 knockout ependymal cells was also reminiscent of mitochondrial membrane remodelling that occurs during the induction of apoptosis. However, this was not confirmed by markers of apoptosis or an investigation of cytochrome *c* release. These data therefore demonstrated that loss of p73 expression also drives mitochondrial dysfunction in ependymal tissues of the mouse brain.

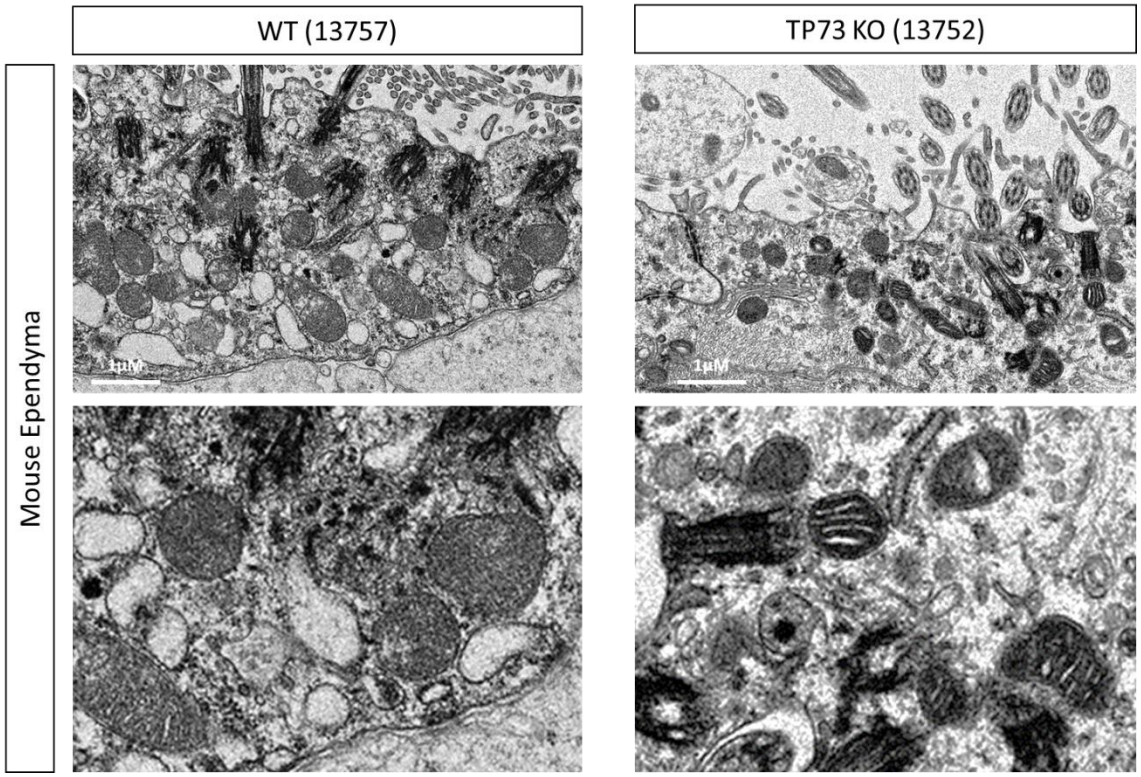

Figure 5.6 Ependymal cells of *TP73*$^{-/-}$ mice display altered mitochondrial morphology and ultrastructure.

Representative TEM micrographs of ciliated ependymal cells from wild-type or TP73$^{-/-}$ mice. Tissue was fixed using transcardic perfusion.

5.2.5 The *TP73*$^{-/-}$ tracheal epithelium has an increased percentage of p63+ basal cells but they do not express TAp73

Finally, I sought to address the possibility that the activity of TAp73 influences the differentiation of p63^{+} basal cell populations of the airway. These cell populations exhibit a progenitor capacity and can form all cell types of the airway, including ciliated and mucus-producing cells during cellular differentiation (Rock et al., 2009) and in response to injury (Musah et al., 2012). As such, mice homozygous for a disrupted p63 gene have major defects in their limb, craniofacial and epithelial development, resulting from the failure to maintain stem cell populations (Yang et al., 1999).

Interestingly, previously published data implicating p73 as a master regulator of ciliogenesis reported that 50% of basal cells were dual positive for p63 and p73 expression, suggesting a role for p73 in the basal cell compartment (Marshall et al., 2016). The authors therefore proposed a model whereby p73 is both an early marker for the MCC lineage in basal stem cells (in part through regulating cell cycle exit), but also a key regulator of the MCC differentiation process (Marshall et al., figure 5.8).

In contrast to this observation, dual immunohistochemical staining for p63 and TAp73 in the wild-type tracheal epithelium indicated that TAp73 is not expressed in basal stem cells of the airway (figure 5.8a). This therefore rules out a role for TAp73 mediated gene transactivation in airway progenitor cells. However, it remains possible that ΔNp73 isoforms may repress gene targets to regulate the process of multiciliated cell differentiation, as the p73 antibody used in this study is directed against an epitope located in amino acids 1-62 of TAp73 isoforms. However, in apparent contradiction with this possibility, the defect in multiciliogenesis in TAp73 null mice phenocopies the global disruption of all TP73 encoded protein (Nemajerova et al., 2016). These findings, together with the absence of TAp73 isoforms in p63^{+} basal cells, call into question the importance of p73 expression in airway progenitor cells.

I also investigated the impact of homozygous deletion of *TP73* on the number of p63+ basal cells present in the tracheal epithelium. Immunohistochemical staining was used to quantify p63+ cells as a percentage of total cell nuclei in tracheal cross-sections. The results showed that there was a significant increase in the number of basal cells in *TP73*$^{-/-}$ airway, which was also in contrast with previously published observations, which reported a in basal cells (Marshall et al., 2016). This finding was also recapitulated by immunofluorescence staining for the basal cell marker Krt14, which showed an increase in basal cells in knockout animals (data not shown). Mechanistically, it is possible that this observed increase in basal cells may be caused by airway inflammation, a feature of *TP73-/-* mice. Therefore, to address the significance of this finding, it would be necessary to engineer mouse models to enable p73- and p63-specific lineage tracing in the developing airway to fully elucidate the interplay between these proteins.

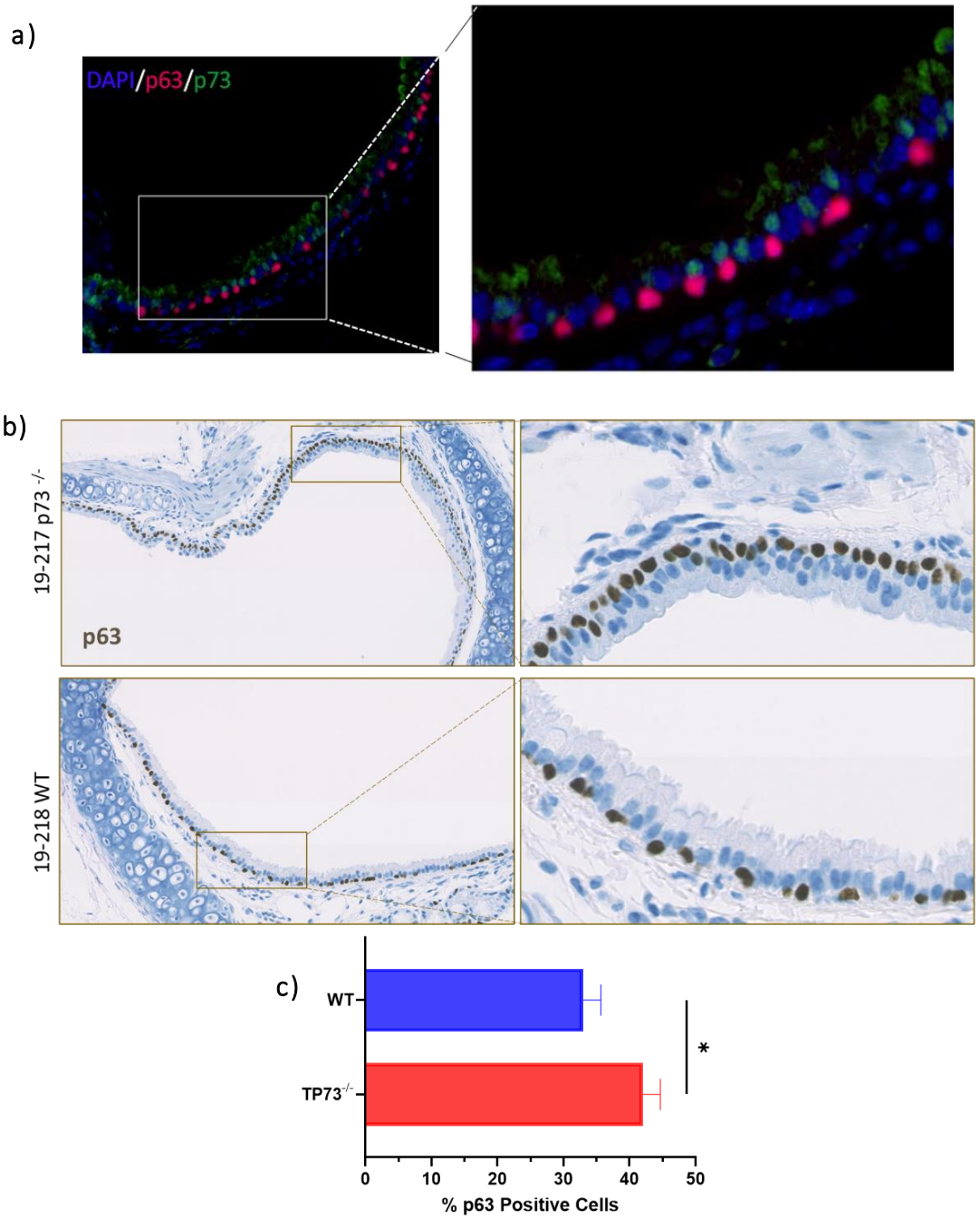

Figure 5.7 Immunohistochemical staining of p63+ basal cell populations in wild-type and *TP73*$^{-/-}$ mice.

(a) Multiplex immunohistochemical staining performed against TAp73 (green) and p63 (red) with DAPI nuclear stain (blue) from wild-type trachea. (b) Immunohistochemical staining of p63 positive basal cells in wild-type (bottom) and *TP73*$^{-/-}$ (top) mouse trachea. (c) Quantification of p63+ cells, expressed as a percentage of total cell nuclei. Images were obtained from two mice of each genotype (n=2). (*) $P \leq 0.05$ (Student's T-test).

5.3 Discussion

5.3.1 Ciliated cells of the *TP73*$^{-/-}$ mouse airway display downregulated OPA1 expression and altered mitochondrial dynamics

Following the identification of an axis between TAp73 and OPA1 in H1299 cells, I have demonstrated that TAp73 regulates OPA1 expression *in vivo*. Ciliated epithelial cells of the mouse trachea display a significant downregulation in *OPA1* expression at the protein and mRNA level in *TP73*$^{-/-}$ animals (figure 5.2-5.3). This finding is consistent with the direct transcriptional regulation of OPA1 by TAp73 demonstrated in chapter 2 and corroborates tracheal ChIP-seq data, which identified binding of p73 to the *OPA1* gene locus in mouse trachea *in-situ* (Marshall et al., 2016).

Furthermore, the downregulation of OPA1 expression in ciliated epithelial correlates with mitochondrial dysfunction in these cell populations, which are dependent on TAp73 expression for correct MCC differentiation. This places the regulation of mitochondrial dynamics downstream of TAp73 in the ciliated cell lineage, whilst non-ciliated cell populations appeared to be unaffected (figure 5.4). I therefore propose that impaired OPA1-dependent mitochondrial fusion may represent a mechanism underpinning defective ciliogenesis in *TP73*$^{-/-}$ and TAp73$^{-/-}$ mouse models. Indeed, the generation of motile cilia is a highly energy dependent process and is linked to mitochondrial function (Burkhalter et al., 2019). Microtubules form the core of motile cilia, and are regulated by post-translational modifications, associated proteins, and microtubule dynamics (Mirvis et al., 2018). Integral to microtubule polymerisation is the interaction of ATP at the exchangeable GTP site of tubulin (Duanmu et al., 1986). Accordingly, Insufficient ATP generation leads to decreased microtubule stability (Oropesa et al., 2011). Given the downregulation of OPA1 expression and ATP synthesis from oxidative phosphorylation observed in cells with a homozygous deletion of TAp73 (outlined in chapter 3), I propose that the resultant decrease in cellular ATP may be insufficient for axonemal extension in motile cilia. In keeping with this hypothesis, electron micrographs of epithelial cells also indicated that TP73 knockout increased the number of mitochondria distal to the apical surface and ATP-dependent cilia (figure 5.4) This highlights the possibility that defective mitochondrial dynamics and bioenergetics provide a mechanistic underpinning of the *TP73*$^{-/-}$ cilia phenotype. Indeed, a striking consequence of OPA1 depletion for a microtubule-dependent cellular process was demonstrated through the inability of OPA1-deficient neutrophils to form microtubule based extracellular traps (Amini et al., 2018). It would therefore be of interest to perform functional assays to attempt to rescue mitochondrial and, hence, multiciliated cell function. For example, functional rescue experiments could be attempted using *ex-vivo* air liquid interface culture and differentiation of basal epithelial cells, following the addition of exogenous ATP or ectopic expression of OPA1.

Overall, these findings could have important implications for understanding the underlying mechanisms leading to disease in patients presented with ciliopathy-associated chronic respiratory illness. Loss of functional ciliogenesis is linked with a number of human diseases including hydrocephalus, hippocampal dysgenesis, primary ciliary dyskinesia, Bardet-Biedl syndrome, asthma and COPD (Kulaga et al., 2004, Tilley et al., 2015). Deletion or mutation of *TP73* may therefore drive disease pathogenesis through dysregulated mitochondrial dynamics. Indeed, evidence suggests that p73 expression is downregulated in airway epithelial cells COPD patients (Richmond et al., 2022), together with observed defects in mitochondrial structure (Hoffman et al., 2013). The identified axis between TAp73 and OPA1 expression in ciliated epithelial cells in vivo therefore provides a possible mechanism for this observation, which may be further explored.

5.3.2 Homozygous deletion of TP73 in mouse airway manifests as a late-stage defect in multiciliated cell differentiation

I have presented data showing that ciliated cells of the *TP73*$^{-/-}$ mouse tracheal epithelium are characterised by defective cilia, however the phenotype is less profound than published observations (Marshall et al., 2016; Nemajerova et al., 2016). Immunohistochemical staining for the cilia marker acetylated-α-tubulin indicated that cell cycle exit and commitment to the ciliated cell lineage does not appear to be the main factor driving loss of functional cilia (figure 5.1). The nucleation of many motile cilia would instead suggest that the cilia phenotype of *TP73*$^{-/-}$ mice is largely driven by abrogated axonemal extension, and a loss of ciliary beating. I therefore propose a greatly diminished role of TAp73 mediated gene transcription for the early stages of multiciliated cell differentiation and centriole amplification and propose a model whereby TAp73 is of greater importance during the later stages of MCC differentiation (figure 5.8). In agreement with this, ectopic expression of FOXJ1 largely rescues the formation of full-length cilia (Marshall et al., 2016). However, the authors did not show evidence that this rescue is sufficient for normal ciliary beating and clearance, which may be perturbed by mitochondrial dysfunction.

This model was also corroborated by co-staining of tracheal epithelial sections for TAp73 and p63. The resultant images indicated that the respective transcription factors are not co-expressed in p63+ basal cells, or indeed in any cell populations of the epithelium (figure 5.8). It was therefore surprising that an expansion in the basal cell compartment in *TP73*$^{-/-}$ mouse trachea was observed, relative to wild-type controls. However, p73$^{-/-}$ mice exhibit hyperplasia of epithelial cells followed by loss of the airway epithelium in older animals (Marshall et al., 2016), implying that chronic inflammation may drive

proliferation of p63+ cells secondary to defective ciliogenesis. Furthermore, these data do not exclude a possible role of ΔNp73 isoforms in basal cells of the airway.

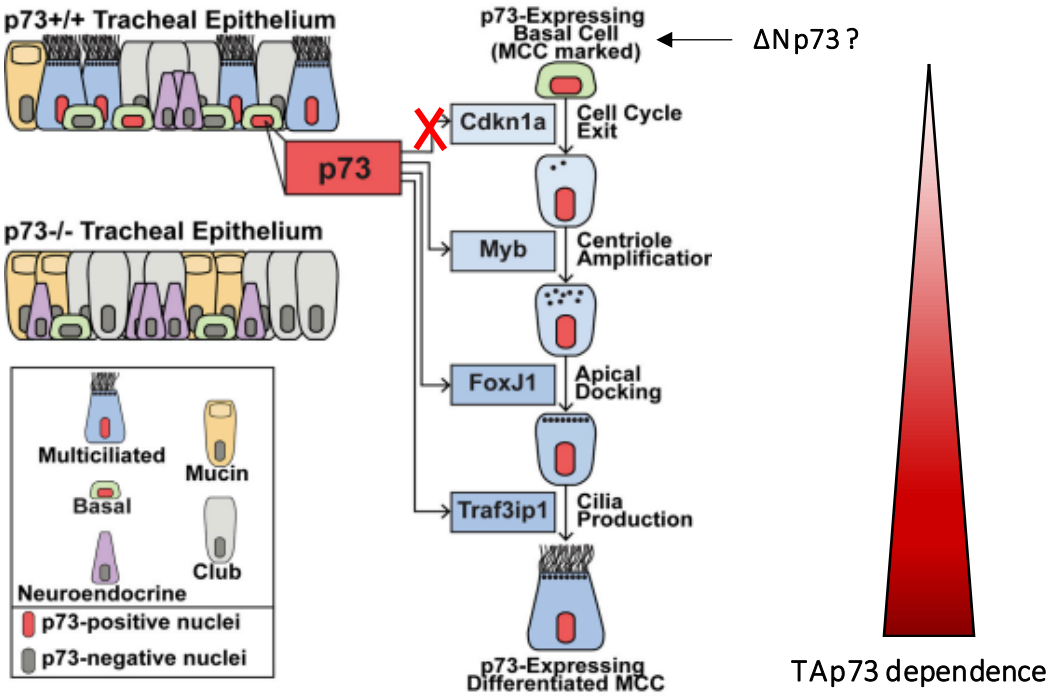

Figure 5.8. Reported roles of p73 in the multiciliated cell differentiation process.

Marshall and colleagues showed that p73 and p63 are co-expressed in a subset of basal cells, suggesting that p73 marks these cells for MCC differentiation (Marshall et al., 2016). However, TAp73 expression was not observed in basal cells in this study. p73 is essential for MCC differentiation, however loss of TAp73 isoforms result in defects in late stages of the multiciliogenesis process, suggesting an increased dependence on TAp73 expression (Adapted from Marshall et al., 2016).

It should also be considered that mitochondrial dynamics directly influences cellular differentiation pathways (Chen et al., 2018; Noguchi & Kasahara, 2018). Specifically, it has been shown that MFN2 or OPA1 down-regulation inhibits cardiomyocyte differentiation from ESCs through the inhibition of genes downstream of Notch signalling, directly implicating mitochondrial fusion in this process (Kasahara et al., 2013). Moreover, mitochondrial shape also regulates Notch signalling in neural stem cells (Hitoshi et al., 2002). Indeed, Notch signalling is required for neural stem cell (NSC) self-renewal (Hitoshi et al., 2002), a process which is impaired by loss of p73 (Agostini et al., 2010; Talos et al., 2010). As a result, Notch-dependent lineage specification and cellular differentiation of MCC cells of the airway in *TP73* and TAp73 knockout mice may be directly influenced by mitochondrial dynamics (Rock et al., 2011). Interestingly, this mechanism may also explain the severe impairment of adult neurogenic zones, the hippocampus and olfactory bulbs in TAp73$^{-/-}$ and *TP73*$^{-/-}$ mice (Meyer et al., 2004; Yang et al., 2000).

Such defects in neurogenesis manifest as a reduction in hippocampal size, and severe hippocampal dysgenesis (Meyer et al., 2004), which is largely due to the absence of TAp73 isoforms, as was revealed by TAp73 isoform-specific KO mice (Talos et al., 2010). Further, recent evidence showed that specifically it is specifically loss of TAp73α which drives these brain phenotypes (Amelio et al., 2020). Together, this suggests that a disrupted axis between TAp73 and OPA1 may therefore drive abnormal brain development. Moreover, some of the observed brain phenotypes cannot be driven by defective ciliogeneisis, which has been proposed as a unifying mechanism of the features of p73 knockout models (Gonzalez-Cano et al., 2016). These data therefore warrant a further investigation of OPA1 expression and mitochondrial dynamics in non-ciliated tissues of p73 knockout mice.

Chapter 6: The C-terminus of p73 is dispensable for multiciliogenesis

6 The C-terminus of p73 is dispensable for multiciliogenesis

6.1 Introduction

As discussed in the thesis introduction, the C-terminal region of p73 is subject to complex alternative splicing that can give rise to seven different splice isoforms of TAp73 and ΔNp73 (Vikhreva et al., 2018). Importantly, only TAp73α expresses a functional sterile alpha motif (SAM) domain at the C-terminus and can transactivate target genes. Given that TAp73α is the most abundantly expressed isoform in mouse and human tissue (Grespi et al., 2012; Marshall et al., 2021), it has been speculated that this isoform is responsible for many of the developmental roles of TAp73. Indeed, the SAM domain facilitates protein-protein interactions potentially affecting p73 stability, localisation and transcriptional activity (Chi et al., 1999). Nonetheless, the mechanistic importance of the SAM domain for the unique functions of p73 remain poorly understood.

Through the use of a newly generated mouse model, herein defined as *Trp73*$^{\Delta 13/\Delta 13}$ mice, I have explored the functional consequence of an *in vivo* ectopic switch from the physiologically expressed p73α to the shorter p73β isoform. While the developmental relevance of p73 transcriptional isoforms has been studied through a TAp73 (Tomasini et al., 2006) and ΔNp73 (Wilhelm et al., 2010) knockout mouse models, the contribution of C-terminal isoforms has not been interrogated (prior to the generation of *Trp73*$^{\Delta 13/\Delta 13}$ mice).

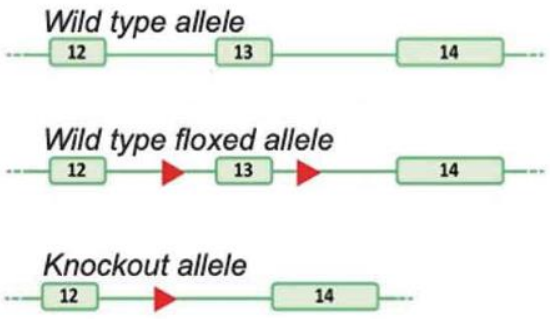

Figure 6.1 Targeting strategy for the generation of *Trp73*$^{\Delta 13/\Delta 13}$ mice.

Flox sites were incorporated into the wild-type p73 allele upstream and downstream of exon 13 in C57BL/6 mice. 'Floxed' mice were then crossed with mice ubiquitously expressing Cre-recombinase under the CMV promoter to oblate exon 13 from all tissues. This induced an ectopic switch from TAp73α to TAp73β expression, allowing for an investigation into the importance of the C-terminal SAM domain in developmental processes such as ciliogenesis.

Trp73$^{\Delta 13/\Delta 13}$ mice display severe neurodevelopmental defects ascribed to deficiency of Cajal-Retzius (CR) cells, the pool of neurons necessary for correct hippocampal architecture (Amelio et al., 2020). Here, by employing the *Trp73*$^{\Delta 13/\Delta 13}$ mice I assess the importance of p73α in the multiciliogenesis process.

6.1.1 Aims and Objectives

- To confirm an ectopic switch in TAp73 expression from alpha to beta isoforms in the tracheal epithelium
- To investigate the impact of an ectopic switch in TAp73 isoform expression on the regulation and execution of the multiciliogenesis process

To achieve these objectives, I employed immunohistochemical staining and RT-PCR to assess the expression of TAp73β and FOXJ1 in the ciliated epithelium and ependymal tissues of *Trp73*$^{\Delta 13/\Delta 13}$ mice. Electron microscopy (TEM & SEM) was then employed to investigate the correct docking of basal bodies and axonemal extension. Through this approach we sought to delineate the roles of TAp73 splice variants in the ciliogenesis process.

6.1.2 *Trp73*$^{\Delta 13/\Delta 13}$ mice display an ectopic switch from p73α to p73β expression in tracheal epithelia

Deletion of exon 13 of the p73 gene was achieved by crossing by CMV-driven Cre mice with those containing flox sites flanking exon 13. The resultant mouse strain (*Trp73*$^{\Delta 13/\Delta 13}$) lacked p73α isoforms in all tissues (Amelio et al., 2020). Before investigating the phenotype of airway epithelial cells, I first verified that in the absence of exon 13, the predicted switch from p73α to p73β was induced in tracheal epithelium of *Trp73*$^{\Delta 13/\Delta 13}$ mice. This was achieved by performing RT-PCR which amplified the 3' regions of p73 mRNA using forward and reverse primers directed against exons 10 and 14 respectively (figure 6.2b). The PCR product was run on an agarose gel and indicated that deletion of exon13 produced a shift in the size of the PCR amplicon, corresponding with transcription of p73β, 94 nucleotides shorter than p73α (figure 6.2a). Furthermore, RT-PCR was performed to amplify a fragment of p73 mRNA spanning the exon 12-14 junction of p73β, which only produced a PCR product in *Trp73*$^{\Delta 13/\Delta 13}$, confirming the deletion of exon 13 in the tracheal epithelium.

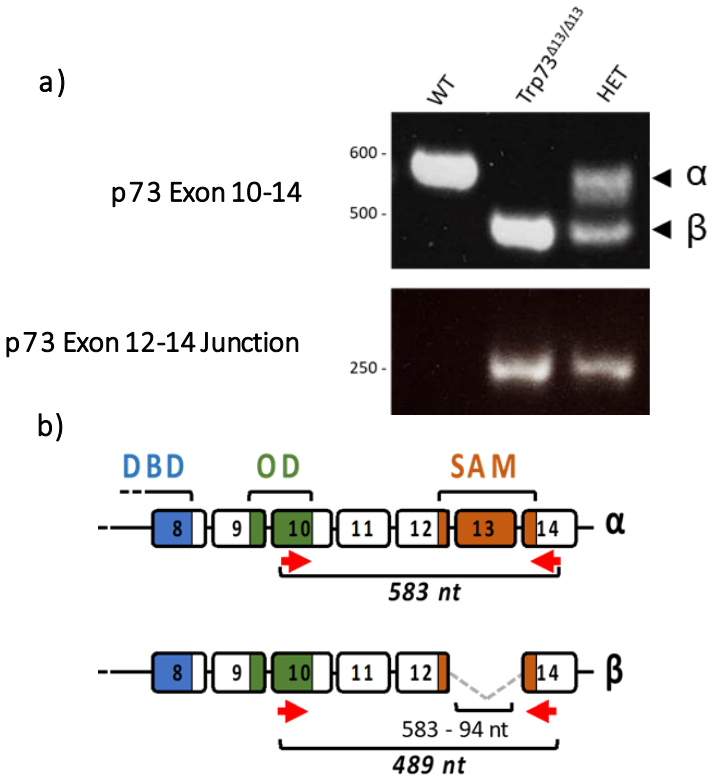

Figure 6.2 End-point PCR confirmed a switch in expression from p73α to p73β in tracheal epithelium.

(a) Primers amplifying exons 10-14 of the C terminal region (top gel) indicated a decrease in transcript length corresponding to exon 13 deletion. PCR amplifying the exon 12-14 junction of p73β indicated a switch in isoform expression (bottom gel). (b) Gene structure of the C-terminal region of p73, indicating primer sites used to identify an ectopic switch between p73α and p73β expression.

6.1.3 Airway multiciliogenesis is preserved in mice lacking p73α

I subsequently analysed the cilia phenotype in the *Trp73*$^{\Delta 13/\Delta 13}$ mouse model to assess the importance of p73α and the capacity for alternative isoforms to participate in the p73 mediated control of multiciliogenesis. Immunofluorescence staining for the cilia marker acetylated alpha-tubulin (Ac-α-tub) in the tracheal epithelium indicated that development of structurally normal cilia was maintained in the *Trp73*$^{\Delta 13/\Delta 13}$ mouse tracheal epithelium (Figure 6.3a). Furthermore, the area of Ac-α-tub staining along the epithelium as a proportion of the total epithelium length was not reduced in *Trp73*$^{\Delta 13/\Delta 13}$ mice relative to the wild-type animals (figure 6.3b). This observation contrasts with the striking cilia phenotype of mice with a global deletion of TP73 isoforms (figure 6.3a,b), which showed a total abrogation of functional cilia.

Furthermore, ciliated epithelial cells from both *Trp73*$^{\Delta 13/\Delta 13}$ and *TP73*$^{-/-}$ mice were analysed using TEM, together with wild-type littermate controls (figure 6.3c). The micrographs obtained confirmed a highly organised arrangement of motile cilia at the apical surface of epithelial cells in *Trp73*$^{\Delta 13/\Delta 13}$ mice, with basal bodies mostly displaying the expected localisation. This contrasts with defective docking of basal bodies at the apical surface in mice with a homozygous deletion of the TP73 gene.

I also corroborated data obtained using confocal immunofluorescence and TEM using scanning electron microscopy (SEM) analysis. This yielded 3D images of the surface of ciliated cells also showed the presence of full-length extensions in *Trp73*$^{\Delta 13/\Delta 13}$ cilia and severe defects in TP73$^{-/-}$ tracheal epithelium (6.3d). These data, therefore, show that the deletion of exon 13 of the p73 gene maintains functional ciliogenesis in the upper airways, indicating a functional redundancy of C-terminal isoforms of p73.

6.1.4 Functional overlap of p73 C-terminal isoforms might underlie the preserved multiciliogenesis of Trp73$^{\Delta 13/\Delta 13}$ mice

I next sought to investigate the p73 expression level in *Trp73*$^{\Delta 13/\Delta 13}$ mouse tracheal epithelial cells. Despite a reduction in total TAp73 and ΔNp73 mRNA level (Figure 6.4a), detected using RT-qPCR on total RNA isolated from the tracheal epithelium, there was no detectable alterations in the distribution of TAp73 protein in trachea epithelium (Figure 6.4b,c). This might suggest that the lack of phenotype in the *Trp73*$^{\Delta 13/\Delta 13}$ mice might be ascribed to the functional overlap of C-terminal isoforms p73α and p73β. Consistent with this hypothesis, *Trp73*$^{\Delta 13/\Delta 13}$ tracheal epithelia had no alterations in the pattern of protein expression of Foxj1 (Figure 6.4d,e), a p73 downstream target, which plays essential roles in multiciliogenesis (Nemajerova et al., 2016). Taken together, these data are suggestive of a potential tissue specific functional overlap in p73 C-terminal isoforms, that are capable of orchestrating ciliogenesis in *Trp73*$^{\Delta 13/\Delta 13}$ mice.

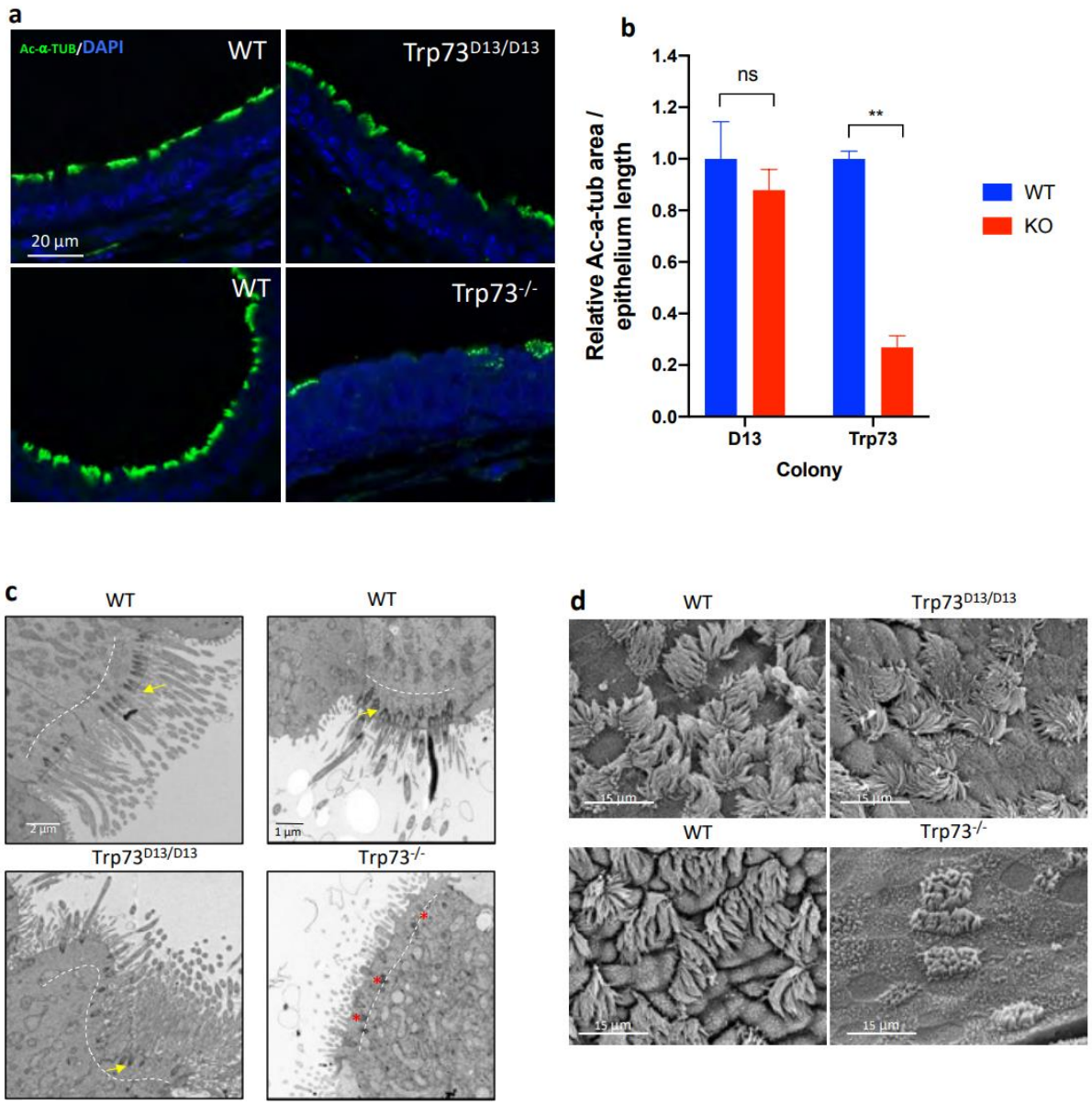

Figure 6.3 Airway ciliogenesis is preserved in the absence of p73α in *Trp73$^{\Delta13/\Delta13}$* mice.

(a) Representative immunofluorescence images of Ac-α-tub expression (green) in tracheal epithelial cells of *Trp73$^{\Delta13/\Delta13}$* (top), p73 KO (bottom) mice and the corresponding wild-type shown adjacent. Nuclei were labelled with DAPI (blue). (b) Quantification of Ac-α-tub IF signal area normalised to the length of epithelia (Δ13 colony; WT & KO (*Trp73$^{\Delta13/\Delta13}$*) n = 3 images from 3 mice. Trp73 colony; WT n = 3 images from 2 mice, p73 KO n = 3 images from 2 mice). (c) Representative TEM photomicrographs of tracheal epithelial cells in *Trp73$^{\Delta13/\Delta13}$* (left) and p73 KO (right) mice and the corresponding wild-type shown above. Dotted lines indicate the apical surface. Basal bodies were correctly docked at the surface of WT and most *Trp73$^{\Delta13/\Delta13}$* cells (yellow arrows) and aberrantly located in *Trp73$^{\Delta13/\Delta13}$*, as in the p73 KO (red asterisks). (d) Representative SEM images of *Trp73$^{\Delta13/\Delta13}$* and p73 KO mice. Adjacent is the corresponding wild-type. All data are presented as mean values relative to WT ± SEM and ** = $P < 0.01$, ns = not significant.

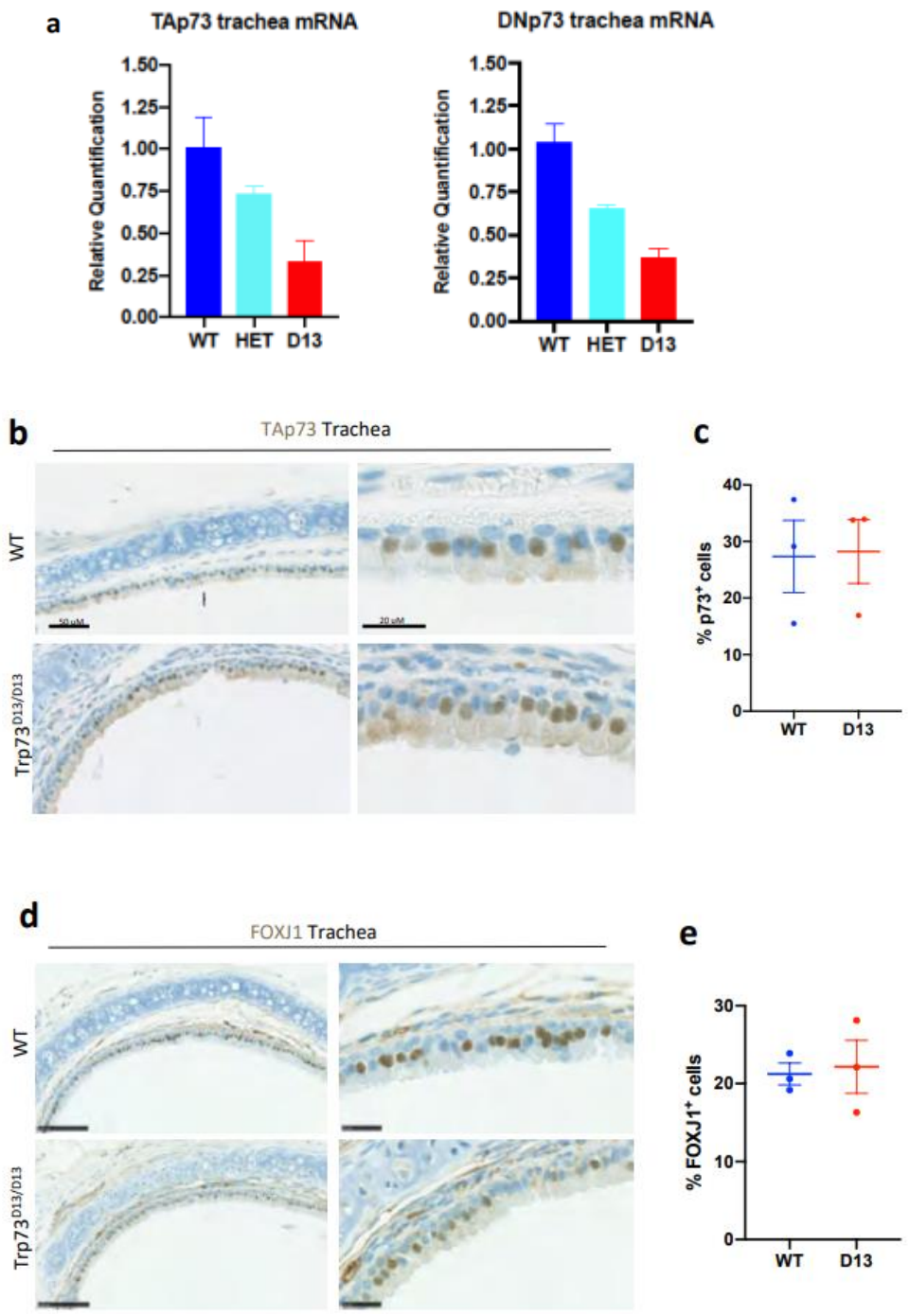

Figure 6.4 *Trp73*$^{\Delta 13/\Delta 13}$ tracheal epithelia maintain expression of TAp73 and Foxj1.

(a) RT-qPCR analysis of relative TAp73 and ΔNp73 transcript expression in WT, *Trp73*$^{+/\Delta 13}$ and *Trp73*$^{\Delta 13/\Delta 13}$ mice (n=3). (b) Representative IHC images showing TAp73 expression in tracheal epithelia of WT and *Trp73*$^{\Delta 13/\Delta 13}$ mice. (c) Quantification of the percentage of p73 positive cells from staining shown in (a) (WT & *Trp73*$^{\Delta 13/\Delta 13}$ n = 3 images from 2 mice). Data plotted as individual points with means ± SEM. (d) Representative IHC images showing Foxj1 expression in tracheal epithelia of WT and *Trp73*$^{\Delta 13/\Delta 13}$ mice. (e) Quantification of the percentage of Foxj1 positive cells from staining shown in (d) (WT & *Trp73*$^{\Delta 13/\Delta 13}$ n = 3 images from 2 mice). Data plotted as individual points with means ± SEM.

6.1.5 Multiciliogenesis of brain ependymal cells is preserved in *Trp73$^{\Delta 13/\Delta 13}$* mice

Ependymal cells are multiciliated cells forming the neuroepithelium of the ventricular system of the brain. These cells functionally contribute to production and regulation of cerebrospinal fluid (Ohata et al., 2016). Consistent with the phenotype of multiciliated cells of the airways, p73 knock-out ependymal cells display defective maturation and ciliogenesis (Gonzalez-Cano et al., 2016). Consequently, *TP73$^{-/-}$* mice have defective functionality of cerebrospinal fluid which manifests as hydrocephalus (Yang et al., 2000). I therefore investigated the ependymal neuroepithelium lining in *Trp73$^{\Delta 13/\Delta 13}$* mice. Consistent with the tracheal epithelium, ependymal ciliogenesis appears to be largely unperturbed in the absence of p73α. Ependymal cells displayed a similar coverage and length of cilia in *Trp73$^{\Delta 13/\Delta 13}$* mice and the corresponding wild-type, as shown by Ac-α-tub staining (Figure 6.6a) and scanning electron microscopy of the surface of ependymal cells (Figure 6.6b). This contrasted with the phenotype of ependymal cells in *TP73$^{-/-}$* mice, which displayed a complete abrogation of functional cilia. Unexpectedly, the ciliogenesis of *Trp73$^{\Delta 13/\Delta 13}$* ependymal cells was preserved, despite the immunohistochemical staining for TAp73 indicating an apparent absence of any TAp73 isoforms (Figure 6.6c,e).

To better understand the basis of *Trp73$^{\Delta 13/\Delta 13}$* ependymal cells phenotype, I analysed the levels of FOXJ1 expression using immunohistochemical staining. Consistent with a lack of any evident abrogation of ciliogenesis, no alteration was observed in the pattern of expression of this master regulator of the ciliogenesis programme (Figure 6.5d,e). It is therefore plausible that TAp73 may be bypassed in the ependyma to maintain the ciliogenesis pathway and activate downstream effectors such as FOXJ1. This therefore demonstrates that TAp73 isoforms are necessary for airway ciliogenesis but dispensable in brain ependyma (Marhsall et al., 2016). To this end, recently published data has suggested that the upregulation of miRNAs such as *miR449* may compensate for TAp73 loss to maintain ependymal ciliogenesis (Wildung et al., 2019). I therefore investigated the possibility that *miR449* expression was upregulated in the *Trp73$^{\Delta 13/\Delta 13}$* mouse brain due to loss of TAp73 expression using RT-qPCR. The results indicated an upregulation of *miRNA-449a* in *Trp73$^{\Delta 13/\Delta 13}$* brain cortex (Figure 6.5f), supporting the hypothesis of a compensatory mechanism leading to execution of multiciliogenesis.

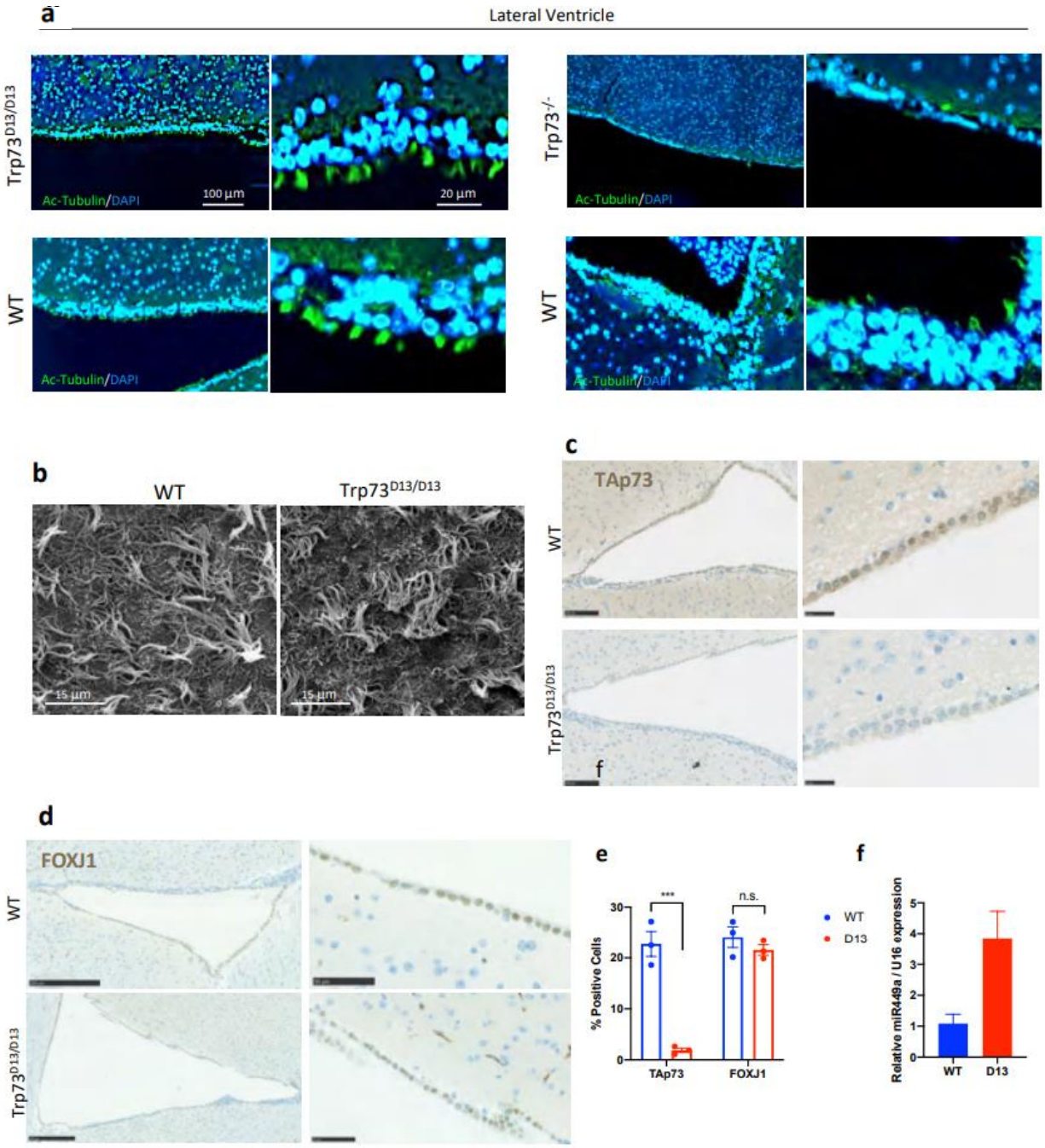

Figure 6.5 Ciliation of Trp73$^{\Delta 13/\Delta 13}$ ependymal cells is not affected despite the absence of TAp73.

(a) Representative immunofluorescence images of Ac-a-tub expression (green) in ependymal cells of the lateral ventricle from *Trp73*$^{\Delta 13/\Delta 13}$ (left) and p73 KO (right) mice shown above the corresponding WT. Nuclei were labelled with DAPI (blue). (b) Representative SEM micrographs showing the apical surface of ependymal cells of the lateral ventricles of *Trp73*$^{\Delta 13/\Delta 13}$ and WT animals. (c, d) Representative IHC images showing TAp73 (c) and Foxj1 (d) expression in cells lining the lateral ventricle of WT and *Trp73*$^{\Delta 13/\Delta 13}$ mice. (e) Quantification of the percentage of p73^{+} and Foxj1^{+} ependymal cells from IHC images as shown in (c, d) (WT & *Trp73*$^{\Delta 13/\Delta 13}$ n = 6 images from 2 mice). (f) RT-qPCR analysis of *miR449a* expression in *Trp73*$^{\Delta 13/\Delta 13}$ mouse cortex relative to WT. Data was normalised to expression of U16. n= 2, data plotted as individual points and means relative to WT ± SEM and *** = P < 0.001, n.s. = not significant.

6.1.6 Trp73$^{\Delta 13/\Delta 13}$ mice do not show evidence of hydrocephalus

To further assess the functionality of the ependymal neuroepithelium in the *Trp73*$^{\Delta 13/\Delta 13}$ mouse model, I analysed coronal sections of the brain to evaluate a potential expansion of the lateral ventricles. No evidence of the development of hydrocephalus was observed in *Trp73*$^{\Delta 13/\Delta 13}$ mice, indicating that the abundant cilia observed in the previous figure are capable of orchestrating cerebrospinal fluid flow to maintain the integrity of ependymal cell populations (Figure 6.8). This contrasted with the *TP73*$^{-\backslash -}$ mice which showed a striking expansion of the lateral ventricles (Figure 6.8). Taken together, these data indicated that functional ciliogenesis in maintained in *Trp73*$^{\Delta 13/\Delta 13}$ mice in both airway and brain.

It should also be noted however, that the deletion of TAp73α did produce a malformation of the dentate gyrus (Amelio et al., 2020), as is present in the TAp73 and global p73 knockouts, indicating highly tissue and cell-specific functions of p73 isoforms.

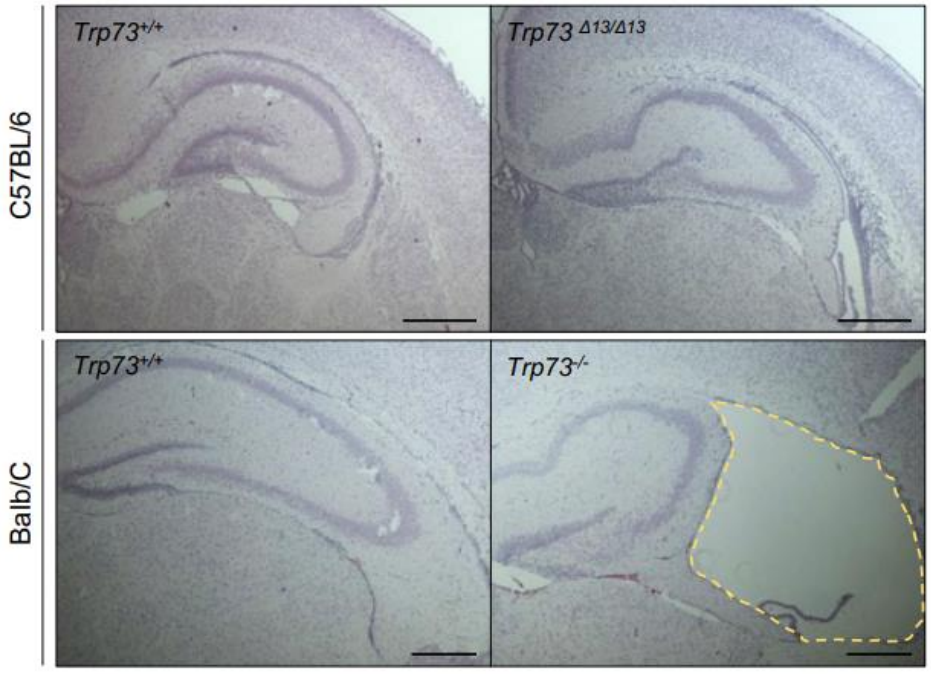

Figure 6.6 *Trp73*$^{\Delta 13/\Delta 13}$ mice do not show enlargement of the lateral ventricles.

Haematoxylin and Eosin (H&E) staining on brain coronal section from *Trp73+/+* (C57BL/6 and Balb/C), *Trp73* $^{\Delta 13/\Delta 13}$ and *TP73*$^{-/-}$ five days old mice (bars=500 µm). The yellow dotted line shows the boundary between the neuroepithelium and lateral ventricle (LV), which is enlarged in TP73$^{-/-}$ mice.

6.1.7 The *Trp73*$^{\Delta 13/\Delta 13}$ mouse tracheal epithelium does not display a reduction in OPA1 expression

Lastly, I sought to investigate OPA1 expression status in *Trp73*$^{\Delta 13/\Delta 13}$ mice to determine whether the ectopic switch from TAp73α to TAp73β could maintain wild-type levels of OPA1 expression. Firstly, total protein lysate from wild-type, *Trp73*$^{\Delta 13/\Delta 13}$, and *Trp73*$^{+/\Delta 13}$ (heterozygous) trachea was immunoblotted for OPA1 expression (figure 6.7a). The expression of OPA1 was also investigated in E18.5 cortex as an alternative tissue, as p73 is highly expressed in Cajal-Retzius cells in the developing cortex (Amelio et al., 2020). The results indicated that *Trp73*$^{\Delta 13/\Delta 13}$ mice did not show a reduction in OPA1 expression in either of the tissues tested, with the OPA1 signal quantified after normalisation to GAPDH expression (figure 6.7a,b). There was also no significant reduction in expression of *OPA1* mRNA, assayed by RT-qPCR (figure 6.7c). This therefore indicates that TAp73β expression can maintain expression of *OPA1*, contrary to the effect observed in mice lacking all TAp73 isoforms, where OPA1 is strongly downregulated.

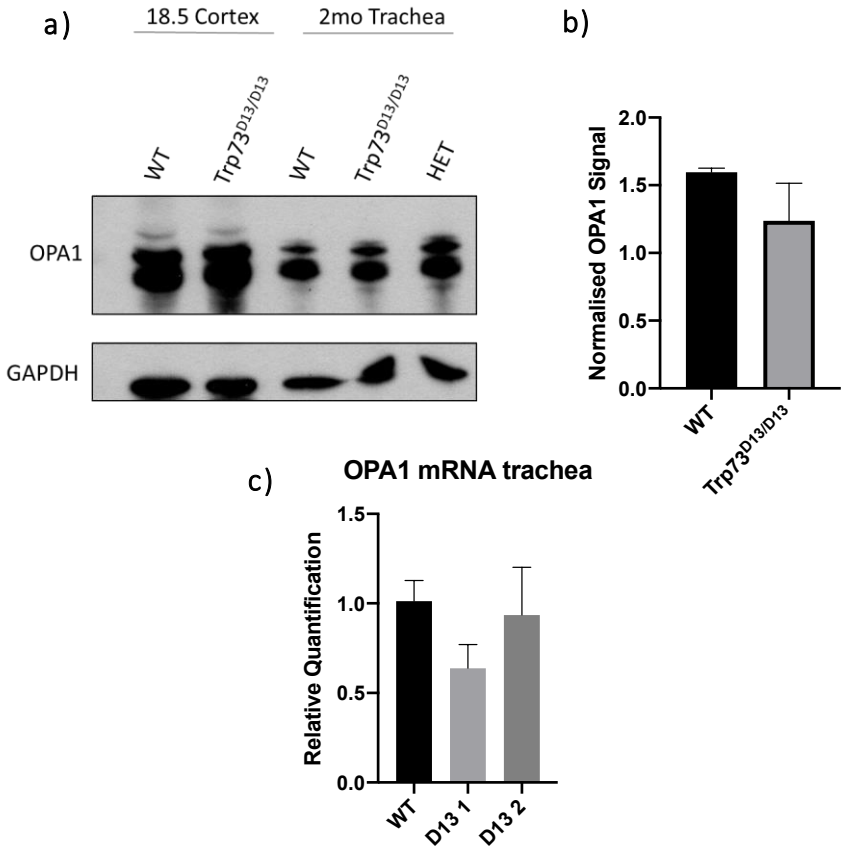

Figure 6.7 Trp73$^{\Delta 13/\Delta 13}$ mice maintain wild-type levels of OPA1 expression in trachea and cortex

(a) Western blot for OPA1 expression in E18.5 cortex and 2-month-old tracheal samples in *Trp73*$^{\Delta 13/\Delta 13}$ mice. (b) Quantification of OPA1 signal shown in (a), normalised to GAPDH signal. Densitometry values were obtained in ImageJ software. (c) RT-qPCR data showing *OPA1* mRNA expression in trachea from two different *Trp73*$^{\Delta 13/\Delta 13}$ mice (n=3). Data presented as mean ± SEM.

6.2 Discussion

Through the induction of a global switch from predominantly p73α to p73β expression, I have found that C-terminal isoforms of p73 functionally overlap to regulate ciliogenesis. Indeed, it has been hypothesised that post-translational modifications of C-terminal regions of p73 that are unique to p73α modulate the stability, transcriptional activity and localisation of this isoform facilitate the regulation of developmental networks (Vikhreva, et al., 2018). However, I have shown in this model, through deletion of the C-terminal SAM domain, that p73α is dispensable for respiratory ciliogenesis. Indeed, in the absence of p73α in tracheal epithelia, essential gene targets of p73 in the ciliogenesis network remain activated to coordinate the assembly of functional cilia, such as foxj1. This is despite the fact that p73α is the predominantly expressed isoform in mouse and human (Grespi, et al., 2012; Marshall et al., 2021). The functional significance of the SAM domain therefore remains to be determined *in vivo*.

I have also shown the redundancy of p73α for ependymal ciliogenesis. However, the lack of detectable TAp73 of all isoforms in brain tissues suggests that the reason for this is different to that identified in tracheal epithelia. Taking into consideration the profound cilia defect of $p73^{-/-}$ mice, the absence of TAp73 in ependymal cells of the $Trp73^{\Delta 13/\Delta 13}$ model is suggestive of a compensatory role of ΔNp73. This reaffirms recently published data showing the lack of a major cilia phenotype in the brain of $TAp73^{-/-}$ mice, thereby demonstrating the redundancy of this isoform in ependyma (Wildung et al., 2019). And further, the absence of TAp73 indicates that the recently proposed compensatory role of ΔNp73 is not dependent of ΔNp73α (Wildung, et al., 2019). However, this is a compensatory mechanism that cannot be present in tracheal epithelium as the study of $TAp73^{-/-}$ knockout mice indicated that ciliogenesis is severely impaired in this context (Nemajerova, et al., 2016). Taken together, this therefore indicates highly complex and tissue specific roles of both C-terminal and TAp73/ΔNp73 isoforms.

Furthermore, the characterisation I have shown of the hippocampal phenotype of $Trp73^{\Delta 13/\Delta 13}$ mice sheds further light on the complexity of tissue-specific and cell type specific roles of p73 C-terminal isoforms (figure 6.6). Even though $Trp73^{\Delta 13/\Delta 13}$ mice show none of the striking consequences of perturbed ependymal biology such as severe hydrocephalus and reduced cortical thickness, which are present in the TAp73 knockout (Medina-Bolívar, et al., 2014), they still display defective dentate gyrus architecture also present in the $p73^{-/-}$ and $TAp73^{-/-}$ knockouts. This therefore demonstrates the necessity of p73α for directing hippocampal development, as when p73α is replaced with p73β in the mouse brain, the lower blade of the dentate gyrus is truncated and malformed (Amelio et al., 2020). Moreover, as I have shown that $Trp73^{\Delta 13/\Delta 13}$ mice maintain functional ependyma, this enables a distinction to be made between the defects in neurogenesis brought about by defective ependymal biology and those that are brought about independently of their function, which may also be evident in the $Trp73^{\Delta 13/\Delta 13}$ model (Nemajerova, et al., 2018). For example, as cerebral spinal fluid (CSF) flow and

the vitality of ependymal cells is critical for the maintenance of the subventricular zone (SVZ) neurogenetic niche, it would be interesting to understand the exact extent to which neurogenesis is impaired in different neurogenic regions of *Trp73*$^{\Delta 13/\Delta 13}$ mice, when ependymal cells show no apparent defect (Gonzalez-Cano, et al., 2016; Gonzalez-Cano, et al., 2010; Talos, et al., 2010). It would also be of interest to interrogate the potential disruption of the TAp73/OPA1 axis in specific tissues or districts, such as the hippocampus, where defects are observed resulting from loss of p73. This would address the possibility that the regulation of mitochondrial dynamics by TAp73α in these tissues regulates neuronal functional independently of alterations in ependymal cell biology or cerebrospinal fluid flow, which function as normal in Trp73$^{\Delta 13/\Delta 13}$ mice. Functional ciliogenesis in Trp73$^{\Delta 13/\Delta 13}$ knockout mice was also accompanied by OPA1 expression levels comparable with wild-type animals. This therefore demonstrates the capacity for TAp73β to maintain OPA1 abundance, a finding which was corroborated by ChIP-seq data, which indicated that both isoforms TAp73α and TAp73β bind the promoter region of the *OPA1 gene* (chapter 3; figure 3.3).

Chapter 7: Final Discussion

7 Final Discussion

7.1 Discussion

The aim of my research was to investigate the molecular mechanisms underpinning the roles of p73 in tissue development and homeostasis. In particular, I focussed on the role of the transcriptionally active isoform TAp73 in ciliated tissues, as it has been shown to be functionally critical for the execution of multiciliogenesis (Marshall et al., 2016; Nemajerova et al., 2016). Although these studies have shown that TAp73 is a central regulator of key ciliogenesis genes, multiple pieces of evidence point to additional functions of p73 that contribute to the dysfunctional phenotype of ciliated cells. For example, I have shown through confocal immunofluorescence imaging of the cilia axoneme that the penetrance of the ciliated cell phenotype is not as profound as first reported. Indeed, 18% of tracheal epithelial cells of $Trp73^{-/-}$ mice displayed cilia on the apical surface (figure 5.7), compared with just 4% previously reported (Marshall et al., 2016). This shows that the importance of TAp73 is diminished in the earlier stages of multiciliated cell differentiation, as basal precursors are able to successfully commit to the ciliated cell lineage, amplify basal bodies, and dock them at the apical surface (figure 5.8). Furthermore, dual immunohistochemical staining for TAp73 and p63 showed that TAp73 is not expressed in basal stem cells, meaning that genetic oblation of $TAp73^{-/-}$ from these cell populations does not impair ciliated cell fate specification. However, this finding does not rule out a role for ΔNp73 isoforms in cell cycle exit and lineage commitment of $p63^{+}$ basal cells to the ciliated cell type. Furthermore, although ectopic expression of Foxj1 largely rescued the abundance of cilia in *ex-vivo* culture of airway epithelial cells using air-liquid interface (ALI) differentiation, the authors did not report on whether there was a concomitant rescue of ciliary beating in functional assays, which is profoundly inhibited following TAp73 knockout (Marshall et al., 2016). Taken together, these findings suggest that additional mechanisms might contribute to the ciliated cell phenotype of $TAp73^{-/-}$ mice, such as p73 mediated control of cellular metabolism and mitochondrial bioenergetics (Agostini et al., 2016; Nemajerova et al., 2019).

In support of this hypothesis, I have interrogated data sets comprised of a complete list of p73 targets identified through *in-situ* tracheal ChIP-seq (Marshall et al., 2016; NCBI BioProject accession PRJNA310161). This approach indicated that p73 binds to genes that regulate mitochondrial membrane organisation (GO term: 0007006), which showed a significant fold enrichment against expected values. This resulted from binding to genomic loci that included the *OPA1*, *MFN2*, and *PPARGC1A* genes. Moreover, this finding was corroborated by *In-vitro* ChIP-seq data (Koeppel et al., 2011), which indicated that TAp73 isoforms alpha and beta bind to overlapping genomic loci within the promoter region of numerous genes responsible for mitochondrial dynamics (figure 3.1). Moreover, highly similar binding patterns were observed for p53, which strongly suggest a conserved ability of the p53 family to regulate mitochondrial dynamics by direct transcriptional regulation. This finding has a number of

implications, as the regulation of mitochondrial dynamics represents a mechanism by which the p53 family executes a variety of functions including regulation of cell metabolism (including metabolic shifts observed in cancer) (Liu et al., 2019), tumour cell growth and dissemination (Phan et al., 2022), and differentiation (Moulder et al., 2013). Indeed, some evidence has previously shown that p53 regulates the balance between mitochondrial fusion and fission through the transcriptional regulation of *MFN2* (Wang et al., 2010). As a result of this regulation, a reduction in mitochondrial respiratory capacity has been reported upon loss of p53 (Saleem et al., 2015). Nonetheless, a broader role of p53 and p73 in regulating additional modulators of mitochondrial fusion and fission regulators has not been reported.

As a result, I selected OPA1 for further investigation as it represented a novel target of p73. To this end, I have successfully validated ChIP-seq data to show a direct transcriptional regulation of *OPA1* by TAp73, which is presented in chapter 3. This was achieved by targeted ChIP experiments, which showed a significant enrichment of the *OPA1* promoter region following IP of TAp73α bound chromatin (figure 3.3). The transcriptional regulation of *OPA1* by p73 was also interrogated in TAp73$^{-/-}$ H1299 cells, generated by CRISPR/Cas9 targeting. In this model, the downregulated expression of OPA1 manifested as a profound alteration in mitochondrial morphology. Namely, TAp73 KO cells displayed a fragmented mitochondrial network, and crucially, this was rescued by ectopic expression of OPA1. This therefore demonstrates a clear molecular dependence of the TAp73/OPA1 axis for the maintenance of mitochondrial dynamics (figure 7.1).

The alterations in OPA1 expression also represent a poignant example of the inextricable connection between mitochondrial dynamics and bioenergetics. As discussed in the preceding chapters, OPA1 oligomers perform a myriad of functions that include, but are not limited to, fusion of mitochondria, the modulation of cristae morphogenesis and cytochrome c release, and respiratory complex efficiency (Cogliati et al., 2013; Scorrano et al., 2015). The status of OPA1 as an effector of these mitochondrial functions therefore adds an additional layer by which TAp73 regulates mitochondrial bioenergetics and this may indeed extent more broadly to cellular physiology and proliferation. This was highlighted by the fact that Following the oblation of TAp73, the growth rates of TAp73 KO cells were significantly impaired (figure 4.10). This thereby presents an important area for further study that is beyond the scope of this thesis. Indeed, the regulation of OPA1 is broadly indicative of a growth promoting role of TAp73 isoforms due to both its role in energy production *via* oxidative phosphorylation, and the anti-apoptotic impact of the tightening of cristae junctions by OPA1 oligomers. This is consistent with a number of other roles of TAp73, such as the recently reported observation that it is required for cell cycle progression in H1299 cells (Klein et al., 2021) and the regulation of glycolytic flux (Li et al., 2018). Importantly, the overexpression of TAp73α in the context of TAp73 knockout induced the upregulation of p21 expression at the mRNA or protein level (figure 3.11), despite a reported cross-talk between

TAp73 MDM2 and other cell cycle regulators coordinates their function to restrain cell cycle inhibition (Klein et al., 2021).

The apparent paradox between growth promoting and tumour suppressive roles of TAp73 isoforms is highlighted in figure 7.1. Work carried out surrounding the DNA-damage independent functions of TAp73 indicates that in the tumour cell milieu, a complex interplay must exist between the multitude of TAp73 functions to balance the regulation of cellular growth, as they are comprised of both growth promoting and inhibiting functions (Amelio et al., 2015; Logotheti et al., 2021; Zhao and Sanyal; 2022). Therefore, the functional output of TAp73, such as the positive regulation of OPA1 function described herein, is likely regulated by the specific expression and interaction of p73 isoforms (Logotheti et al., 2021). Indeed, the complex p73 interactome, that is largely mediated *via* the C-terminal SAM domain, is one mechanism by which TAp73 function is coordinated (Nemajerova et al., 2019).

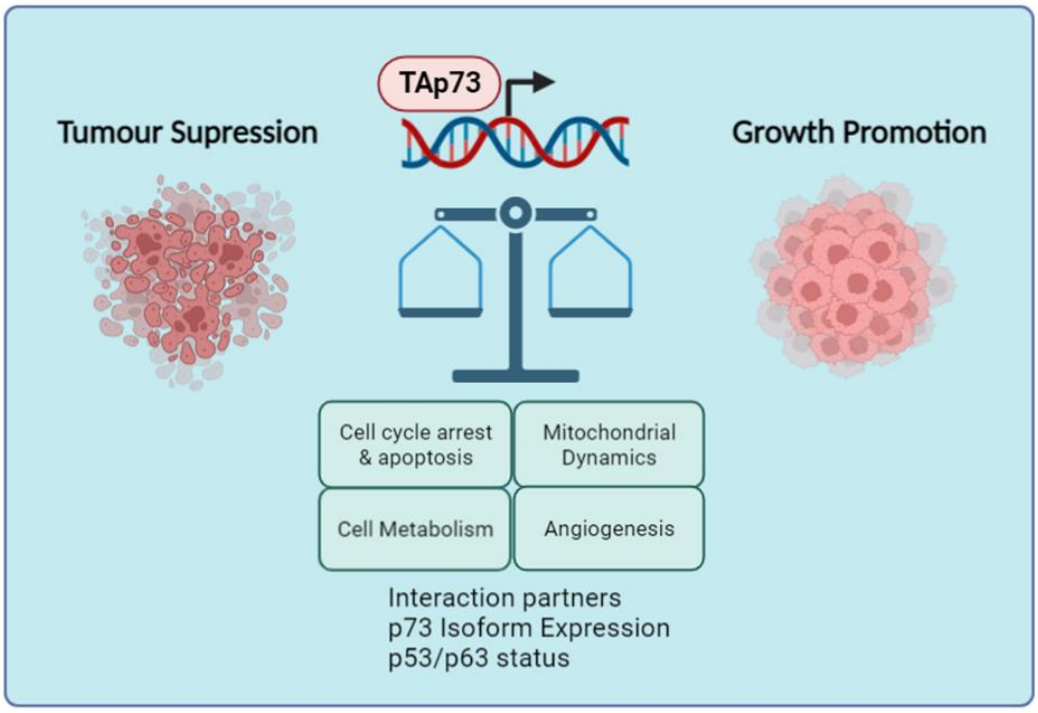

Figure 7.1. The functions of TAp73 isoforms are supportive of both tumour suppression and cell growth.

Canonical tumour suppressive functions of TAp73 contrast with the growing body of evidence in support of roles that support growth promotion. The regulation of mitochondrial dynamics through transcriptional control of OPA1 presents a novel function of OPA1 that supports mitochondrial OXPHOS and confers resistance to apoptosis.

Overall, the contribution of the TAp73/OPA1 axis to cell growth and tumorigenesis should be more extensively investigated. This is highlighted by the fact that TAp73 is overexpressed in many human cancers (Rufini et al., 2011). The results presented in my thesis therefore also suggest a molecular mechanism for this overexpression, not least because TAp73 expression confers resistance to

treatment to BH3-mimetics (figure 4.12), an observation that has also been made in the treatment of CLL (Merino et al., 2018).

The interrogation of this axis in H1299 cells meant experiments were performed in the absence of expression of p53 protein. This allowed for an interrogation of OPA1 expression and mitochondrial function independently of a possible conserved function of the p53 family to regulators of mitochondrial fusion and fission. Indeed, this was evidenced by conserved binding profiles of the p53 family to a number of genes that modulate mitochondrial dynamics (figures 3.3 and 3.4). On the other hand, following the characterisation of an axis between TAp73 and OPA1, it would now be of interest to express functional p53 in TAp73 knockout cells. This would allow for an investigation of the possibility that p53 is capable of rescuing mitochondrial fusion in a manner similar to rescue with TAp73. Similarly, the finding that p73 has the ability to bind to additional regulators of fusion and fission aside from OPA1 (figure 3.3) has not been explored further. In addition, rescue experiments with ectopic expression of OPA1 plasmid did partially rescue mitochondrial morphology and bioenergetics (figure 4.5 and 4.5), however the respective functions were not rescued in line with wild-type levels. This suggests that altered expression of additional mitochondrial regulators may prevent complete rescue.

In addition, I have demonstrated that OPA1 expression is downregulated in the ciliated tracheal epithelium of $Tp73^{-/-}$ mice, demonstrating a relevance for the TAp73/OPA1 axis *in vivo* (chapter 5). In line with this observation, I observed alterations in mitochondrial morphology and ultrastructure. Moreover, the downregulation of OPA1 observed was specific to the ciliated cell lineage, specifically implicating TAp73 in modulating its expression. I hypothesise that the disruption of mitochondrial function in ciliated epithelial cells may underpin the phenotype of dysfunctional cilia, which is a highly energy dependent process (figure 7.2). However, functional assays to attempt to rescue MCC differentiation and function with OPA1 expression are necessary to show that the TAp73/OPA1 axis is critical for multiciliated cell function (detailed further in chapter 7.2). Taken together with the role of TAp73 in regulating important ciliogenesis genes (Marshall et al., 2016), my findings also suggest that p73 may represent a mechanistic link between chronic inflammation and MCC loss, which is a driver of airway diseases such as COPD. Interestingly, a relationship has been defined between cigarette smoke, decreased p73 expression and epithelial differentiation *in vivo* (Richmond et al., 2022). Given the importance of p73 for airway homeostasis and it's defined contribution to chronic inflammation, it

would be of interest to investigate the relationship between p73 expression and airway disease in patient cohorts.

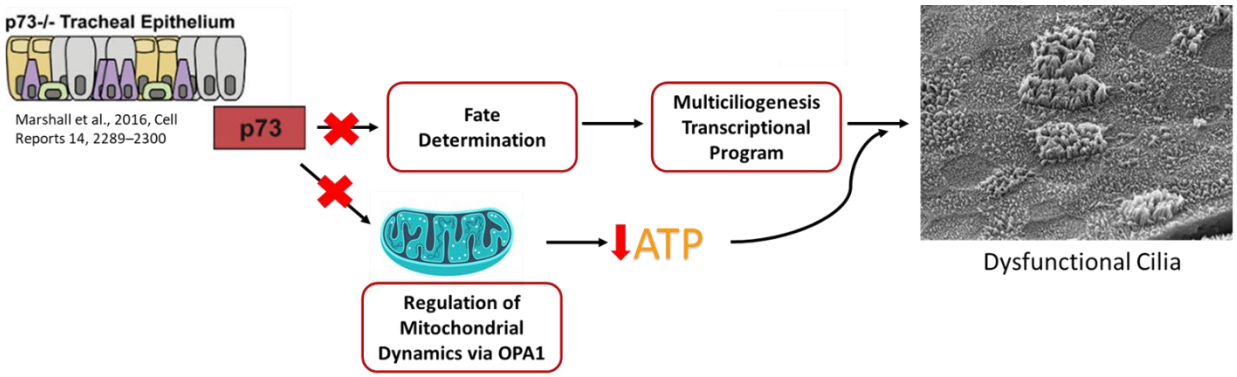

Figure 7.2 The proposed mechanisms underpinning the contribution of p73 to the ciliated cell phenotype in Trp73$^{-/-}$ mice

Deletion of p73 alters multiciliated cell fate determination and the multiciliogenesis transcriptional program. I have presented a possible adjacent mechanism by which p73 regulates the abundance of functional cilia. Disruption of an axis between TAp73 and OPA1 drives mitochondrial dysfunction in ciliated epithelial cells. I therefore propose that the bioenergetic impact of OPA1 depletion (namely reduced ATP production *via* OXPHOS), drives the phenotype of defective ciliogenesis and ciliary beating.

7.2 Future work

The p53 family member p73 plays a critical role in brain development (Yang et al., 2000). p73 knockout mice exhibit a number of defects in the nervous system, such as neuronal death, hydrocephalus, hippocampal dysgenesis, and pheromonal defects (Gonzalez-Cano et al., 2016). Presented with the opportunity to conduct further experiments, I would interrogate the possibility that the axis between TAp73 and OPA1 is present in additional tissues. Firstly, this could be achieved by multiplex IHC staining of ependymal cells to assess the OPA1 status in these cells in Trp73 knockout sections, which I have already utilised for other purposes in this study. Furthermore, although defective ciliogenesis has been proposed as a connecting mechanism for the diverse phenotype of Trp73$^{-/-}$ mice, additional non-ciliated tissues are also defective. For example disruption of p73 causes abnormal hippocampal development, as loss of p73 expression leads to the generation of a truncated and malformed lower blade of the dentate gyrus (Amelio et al., 2020). Therefore the interrogation of OPA1 expression at key developmental stages may reveal altered expression drives neuronal cell loss. Indeed, Reduction of OPA1 activity has also been associated with neurodegenerative diseases, such as Alzheimer's, Huntington, and Parkinson diseases (Archer et al., 2013).

Although I have uncovered a transcriptional relationship between TAp73 and OPA1, and its importance for mitochondrial morphology and function, functional assays are required to show a direct relevance of this axis for multiciliated cell function. If given the opportunity to conduct further experiments, I would employ the *ex-vivo* and differentiation of airway epithelial cells (Lacroix et al., 2018) obtained from Tp73 null mice to investigate the potential for OPA1 expression to rescue multiciliogenesis. Following the isolation of epithelial cell populations for mice trachea (as previously performed and described for RT-qPCR analysis; figure 5.2b), basal stem cells can be readily selected and expanded in cell culture dishes. Lentiviral transfection of these cell populations could then be employed to increase the abundance of OPA1.

In addition, targeted chromatin IP for TAp73 bound chromatin could be further interrogated to investigate an enrichment of gene promoters of additional fusion and fission regulators. Indeed, the analysis of ChIP-seq data (Koeppel et al., 2011) showed TAp73 binds to the *MFN2*, *MFF*, and *Fis1* genes. The H1299 TAp73 KO cell model may then be employed to assay the transcription of these genes compared with wild-type controls. These experimental approaches would therefore shed light on a broader role for TAp73 in regulating mitochondrial dynamics.

References

Agami, R., Blandino, G., Oren, M., Shaul, Y., 1999. Interaction of c-Abl and p73alpha and their collaboration to induce apoptosis. Nature 399, 809–812. https://doi.org/10.1038/21697

Aggarwal, V., Tuli, H.S., Varol, A., Thakral, F., Yerer, M.B., Sak, K., Varol, M., Jain, A., Khan, M.A., Sethi, G., 2019. Role of Reactive Oxygen Species in Cancer Progression: Molecular Mechanisms and Recent Advancements. Biomolecules 9. https://doi.org/10.3390/BIOM9110735

Agostini, M., Tucci, P., Chen, H., Knight, R.A., Bano, D., Nicotera, P., McKeon, F., Melino, G., 2010. p73 regulates maintenance of neural stem cell. Biochem Biophys Res Commun 403, 13–17. https://doi.org/10.1016/J.BBRC.2010.10.087

Alavi, M. v., Bette, S., Schimpf, S., Schuettauf, F., Schraermeyer, U., Wehrl, H.F., Ruttiger, L., Beck, S.C., Tonagel, F., Pichler, B.J., Knipper, M., Peters, T., Laufs, J., Wissinger, B., 2007. A splice site mutation in the murine Opa1 gene features pathology of autosomal dominant optic atrophy. Brain 130, 1029–1042. https://doi.org/10.1093/BRAIN/AWM005

Alexander, C., Votruba, M., Pesch, U.E.A., Thiselton, D.L., Mayer, S., Moore, A., Rodriguez, M., Kellner, U., Leo-Kottler, B., Auburger, G., Bhattacharya, S.S., Wissinger, B., 2000. OPA1, encoding a dynamin-related GTPase, is mutated in autosomal dominant optic atrophy linked to chromosome 3q28. Nat Genet 26, 211–215. https://doi.org/10.1038/79944

Alonso, M.E., Bello, M.J., Lomas, J., Gonzalez-Gomez, P., Arjona, D., de Campos, J.M., Gutierrez, M., Isla, A., Vaquero, J., Rey, J.A., 2001. Absence of mutation of the p73 gene in astrocytic neoplasms. Int J Oncol 19, 609–612. https://doi.org/10.3892/IJO.19.3.609

Ambrosini, G., Dreos, R., Kumar, S., Bucher, P., 2016. The ChIP-Seq tools and web server: a resource for analyzing ChIP-seq and other types of genomic data. BMC Genomics 2016 17:1 17, 1–15. https://doi.org/10.1186/S12864-016-3288-8

Amelio, I., Inoue, S., Markert, E.K., Levine, A.J., Knight, R.A., Mak, T.W., Melino, G., 2015. TAp73 opposes tumor angiogenesis by promoting hypoxia-inducible factor 1α degradation. Proc Natl Acad Sci U S A 112, 226–231. https://doi.org/10.1073/pnas.1410609111

Amelio, I., Markert, E.K., Rufini, A., Antonov, A. v., Sayan, B.S., Tucci, P., Agostini, M., Mineo, T.C., Levine, A.J., Melino, G., 2014a. p73 regulates serine biosynthesis in cancer. Oncogene 33, 5039–5046. https://doi.org/10.1038/ONC.2013.456

Amelio, I., Markert, E.K., Rufini, A., Antonov, A. v., Sayan, B.S., Tucci, P., Agostini, M., Mineo, T.C., Levine, A.J., Melino, G., 2014b. P73 regulates serine biosynthesis in cancer. Oncogene 33, 5039–5046. https://doi.org/10.1038/onc.2013.456

Amelio, I., Panatta, E., Niklison-Chirou, M.V., Steinert, J.R., Agostini, M., Morone, N., Knight, R.A., Melino, G., 2020. The c terminus of p73 is essential for hippocampal development. Proc Natl Acad Sci U S A 117, 15694–15701. https://doi.org/10.1073/PNAS.2000917117/-/DCSUPPLEMENTAL

Amini, P., Stojkov, D., Felser, A., Jackson, C.B., Courage, C., Schaller, A., Gelman, L., Soriano, M.E., Nuoffer, J.M., Scorrano, L., Benarafa, C., Yousefi, S., Simon, H.U., 2018. Neutrophil extracellular trap formation requires OPA1-dependent glycolytic ATP production. Nat Commun 9. https://doi.org/10.1038/s41467-018-05387-y

Anand R, Wai T, Baker MJ, Kladt N, Schauss AC, Rugarli E, Langer T. The i-AAA protease YME1L and OMA1 cleave OPA1 to balance mitochondrial fusion and fission. J Cell Biol. 2014 Mar 17;204(6):919-29. doi: 10.1083/jcb.201308006.

Anderson, S., Bankier, A.T., Barrell, B.G., de Bruijn, M.H.L., Coulson, A.R., Drouin, J., Eperon, I.C., Nierlich, D.P., Roe, B.A., Sanger, F., Schreier, P.H., Smith, A.J.H., Staden, R., Young, I.G., 1981. Sequence and organization of the human mitochondrial genome. Nature 290, 457–465. https://doi.org/10.1038/290457A0

Appella, E., Anderson, C.W., 2001. Post-translational modifications and activation of p53 by genotoxic stresses. Eur J Biochem 268, 2764–2772. https://doi.org/10.1046/J.1432-1327.2001.02225.X

B, T., DR, G., 2017. RIPped for neuroinflammation. Cell Res 27, 1074. https://doi.org/10.1038/CR.2017.97

Baker, M.J., Lampe, P.A., Stojanovski, D., Korwitz, A., Anand, R., Tatsuta, T., Langer, T., 2014. Stress-induced OMA1 activation and autocatalytic turnover regulate OPA1-dependent mitochondrial dynamics. EMBO J 33, 578–593. https://doi.org/10.1002/EMBJ.201386474

Bao, Q., Shi, Y., 2006. Apoptosome: a platform for the activation of initiator caspases. Cell Death & Differentiation 2007 14:1 14, 56–65. https://doi.org/10.1038/sj.cdd.4402028

Belyi VA, Levine AJ. One billion years of p53/p63/p73 evolution. Proc Natl Acad Sci U S A. 2009 Oct 20;106(42):17609-10. doi: 10.1073/pnas.0910634106.

Bertholet, A.M., Delerue, T., Millet, A.M., Moulis, M.F., David, C., Daloyau, M., Arnauné-Pelloquin, L., Davezac, N., Mils, V., Miquel, M.C., Rojo, M., Belenguer, P., 2016. Mitochondrial fusion/fission dynamics in neurodegeneration and neuronal plasticity. Neurobiol Dis. https://doi.org/10.1016/j.nbd.2015.10.011

Blandino, G., Dobbelstein, M., 2006. p73 and p63: Why Do We Still Need Them? https://doi.org/10.4161/cc.3.7.996 3, 884–892. https://doi.org/10.4161/CC.3.7.996

Bock, F.J., Tait, S.W.G., 2020. Mitochondria as multifaceted regulators of cell death. Nat Rev Mol Cell Biol 21, 85–100. https://doi.org/10.1038/S41580-019-0173-8

Bononi, A., Missiroli, S., Poletti, F., Suski, J.M., Agnoletto, C., Bonora, M., de Marchi, E., Giorgi, C., Marchi, S., Patergnani, S., Rimessi, A., Wieckowski, M.R., Pinton, P., 2012. Mitochondria-associated membranes (MAMs) as hotspot Ca(2+) signaling units. Adv Exp Med Biol 740, 411–437. https://doi.org/10.1007/978-94-007-2888-2_17

Bordi, M., Nazio, F., Campello, S., 2017. The Close Interconnection between Mitochondrial Dynamics and Mitophagy in Cancer. Front Oncol 7. https://doi.org/10.3389/FONC.2017.00081

Brand, M.D., Orr, A.L., Perevoshchikova, I. v., Quinlan, C.L., 2013. The role of mitochondrial function and cellular bioenergetics in ageing and disease. Br J Dermatol 169 Suppl 2, 1–8. https://doi.org/10.1111/BJD.12208

Buckley, N., Panatta, E., Morone, N., Noguchi, M., Scorrano, L., Knight, R.A., Amelio, I., Melino, G., 2020. P73 C-terminus is dispensable for multiciliogenesis. Cell Cycle 19, 1833–1845. https://doi.org/10.1080/15384101.2020.1783055

Buhlmann, S., Racek, T., Schwarz, A., Schaefer, S., Pützer, B.M., 2008. Molecular mechanism of p73-mediated regulation of hepatitis B virus core promoter/enhancer II: implications for hepatocarcinogenesis. J Mol Biol 378, 20–30. https://doi.org/10.1016/J.JMB.2008.02.021

Burkhalter, M.D., Sridhar, A., Sampaio, P., Jacinto, R., Burczyk, M.S., Donow, C., Angenendt, M., Hempel, M., Walther, P., Pennekamp, P., Omran, H., Lopes, S.S., Ware, S.M., Philipp, M., 2019. Imbalanced mitochondrial function provokes heterotaxy via aberrant ciliogenesis. Journal of Clinical Investigation 129, 2841–2855. https://doi.org/10.1172/JCI98890

Burté, F., Carelli, V., Chinnery, P.F., Yu-Wai-Man, P., 2015. Disturbed mitochondrial dynamics and neurodegenerative disorders. Nat Rev Neurol 11, 11–24. https://doi.org/10.1038/NRNEUROL.2014.228

Caglayan, S., Hashim, A., Cieslar-Pobuda, A., Jensen, V., Behringer, S., Talug, B., Chu, D.T., Pecquet, C., Rogne, M., Brech, A., Brorson, S.H., Nagelhus, E.A., Hannibal, L., Boschi, A., Taskén, K., Staerk, J., 2020. Optic Atrophy 1 Controls Human Neuronal Development by Preventing Aberrant Nuclear DNA Methylation. iScience 23. https://doi.org/10.1016/J.ISCI.2020.101154

Cao, X., Wang, H., Wang, Z., Wang, Q., Zhang, S., Deng, Y., Fang, Y., 2017. In vivo imaging reveals mitophagy independence in the maintenance of axonal mitochondria during normal aging. Aging Cell 16, 1180–1190. https://doi.org/10.1111/ACEL.12654

Cederbaum, A.I., Rubin, E., 1973. Role of citrate in stimulation of the fatty acid shuttle for the transport of reducing equivalents into mitochondria. Biochem Biophys Res Commun 52, 980–986. https://doi.org/10.1016/0006-291X(73)91033-4

Chen, H., Chan, D.C., 2017. Mitochondrial Dynamics in Regulating the Unique Phenotypes of Cancer and Stem Cells. Cell Metab. https://doi.org/10.1016/j.cmet.2017.05.016

Chen, X., Glytsou, C., Zhou, H., Narang, S., Reyna, D.E., Lopez, A., Sakellaropoulos, T., Gong, Y., Kloetgen, A., Yap, Y.S., Wang, E., Gavathiotis, E., Tsirigos, A., Tibes, R., Aifantis, I., 2019. Targeting Mitochondrial Structure Sensitizes Acute Myeloid Leukemia to Venetoclax Treatment. Cancer Discov 9, 890–909. https://doi.org/10.1158/2159-8290.CD-19-0117

Chi, S.W., Ayed, A., Arrowsmith, C.H., 1999. Solution structure of a conserved C-terminal domain of p73 with structural homology to the SAM domain. EMBO J 18, 4438–4445. https://doi.org/10.1093/EMBOJ/18.16.4438

Chillemi, G., Kehrloesser, S., Bernassola, F., Desideri, A., Dötsch, V., Levine, A.J., Melino, G., 2017. Structural Evolution and Dynamics of the p53 Proteins. Cold Spring Harb Perspect Med 7, a028308. https://doi.org/10.1101/cshperspect.a028308

Chinnaiyan, A.M., 1999. The apoptosome: heart and soul of the cell death machine. Neoplasia 1, 5–15. https://doi.org/10.1038/SJ.NEO.7900003

Choksi, S.P., Lauter, G., Swoboda, P., Roy, S., 2014. Switching on cilia: transcriptional networks regulating ciliogenesis. Development 141, 1427–1441. https://doi.org/10.1242/DEV.074666

Cipolat, S., de Brito, O.M., Dal Zilio, B., Scorrano, L., 2004. OPA1 requires mitofusin 1 to promote mitochondrial fusion. Proc Natl Acad Sci U S A 101, 15927–15932. https://doi.org/10.1073/PNAS.0407043101

Cipolat, S., Rudka, T., Hartmann, D., Costa, V., Serneels, L., Craessaerts, K., Metzger, K., Frezza, C., Annaert, W., D'Adamio, L., Derks, C., Dejaegere, T., Pellegrini, L., D'Hooge, R., Scorrano, L., de Strooper, B., 2006. Mitochondrial rhomboid PARL regulates cytochrome c release during apoptosis via OPA1-dependent cristae remodeling. Cell 126, 163–175. https://doi.org/10.1016/J.CELL.2006.06.021

Cloonan, S.M., Choi, A.M.K., 2016. Mitochondria in lung disease. J Clin Invest 126, 809–820. https://doi.org/10.1172/JCI81113

Cogliati, S., Frezza, C., Soriano, M.E., Varanita, T., Quintana-Cabrera, R., Corrado, M., Cipolat, S., Costa, V., Casarin, A., Gomes, L.C., Perales-Clemente, E., Salviati, L., Fernandez-Silva, P., Enriquez, J.A., Scorrano, L., 2013. Mitochondrial cristae shape determines respiratory chain supercomplexes assembly and respiratory efficiency. Cell 155, 160–171. https://doi.org/10.1016/J.CELL.2013.08.032

Collavin, L., Lunardi, A., del Sal, G., 2010. p53-family proteins and their regulators: hubs and spokes in tumor suppression. Cell Death Differ 17, 901–911. https://doi.org/10.1038/CDD.2010.35

Davies, V.J., Hollins, A.J., Piechota, M.J., Yip, W., Davies, J.R., White, K.E., Nicols, P.P., Boulton, M.E., Votruba, M., 2007. Opa1 deficiency in a mouse model of autosomal dominant optic atrophy impairs mitochondrial morphology, optic nerve structure and visual function. Hum Mol Genet 16, 1307–1318. https://doi.org/10.1093/HMG/DDM079

de Laurenzi, V., Melino, G., 2000. Evolution of functions within the p53/p63/p73 family. Ann N Y Acad Sci 926, 90–100. https://doi.org/10.1111/j.1749-6632.2000.tb05602.x

del Dotto, V., Fogazza, M., Carelli, V., Rugolo, M., Zanna, C., 2018. Eight human OPA1 isoforms, long and short: What are they for? Biochim Biophys Acta Bioenerg 1859, 263–269. https://doi.org/10.1016/J.BBABIO.2018.01.005

del Dotto, V., Mishra, P., Vidoni, S., Fogazza, M., Maresca, A., Caporali, L., McCaffery, J.M., Cappelletti, M., Baruffini, E., Lenaers, G., Chan, D., Rugolo, M., Carelli, V., Zanna, C., 2017. OPA1 Isoforms in the Hierarchical Organization of Mitochondrial Functions. Cell Rep 19, 2557–2571. https://doi.org/10.1016/J.CELREP.2017.05.073

Di, C., Yang, L., Zhang, H., Ma, X., Zhang, X., Sun, C., Li, H., Xu, S., An, L., Li, X., Bai, Z., 2013. Mechanisms, function and clinical applications of DNp73. Cell Cycle 12, 1861–7. https://doi.org/10.4161/cc.24967

Dickens, L.S., Boyd, R.S., Jukes-Jones, R., Hughes, M.A., Robinson, G.L., Fairall, L., Schwabe, J.W.R., Cain, K., MacFarlane, M., 2012. A death effector domain chain DISC model reveals a crucial role for caspase-8 chain assembly in mediating apoptotic cell death. Mol Cell 47, 291–305. https://doi.org/10.1016/J.MOLCEL.2012.05.004

Dobbelstein, M., Wienzek, S., König, C., Roth, J., 1999. Inactivation of the p53-homologue p73 by the mdm2-oncoprotein. Oncogene 18, 2101–2106. https://doi.org/10.1038/SJ.ONC.1202512

Dominguez, G., Silva, J.M., Silva, J., Garcia, J.M., Sanchez, A., Navarro, A., Gallego, I., Provencio, M., España, P., Bonilla, F., 2001. Wild type p73 overexpression and high-grade malignancy in breast cancer. Breast Cancer Res Treat 66, 183–190. https://doi.org/10.1023/A:1010624717311

dos Santos, J.M., de Oliveira, D.S., Moreli, M.L., Benite-Ribeiro, S.A., 2018. The role of mitochondrial DNA damage at skeletal muscle oxidative stress on the development of type 2 diabetes. Mol Cell Biochem 449, 251–255. https://doi.org/10.1007/S11010-018-3361-5

Dötsch, V., Bernassola, F., Coutandin, D., Candi, E., Melino, G., 2010. p63 and p73, the Ancestors of p53. Cold Spring Harb Perspect Biol 2. https://doi.org/10.1101/CSHPERSPECT.A004887

Duanmu, C., Lin, C.M., Hamel, E., 1986. Tubulin polymerization with ATP is mediated through the exchangeable GTP site. BBA - General Subjects 881. https://doi.org/10.1016/0304-4165(86)90104-2

Elmore, S., 2007. Apoptosis: a review of programmed cell death. Toxicol Pathol 35, 495–516. https://doi.org/10.1080/01926230701320337

Engelmann, D., Meier, C., Alla, V., Pützer, B.M., 2015. A balancing act: orchestrating amino-truncated and full-length p73 variants as decisive factors in cancer progression. Oncogene 34, 4287–4299. https://doi.org/10.1038/ONC.2014.365

Faouzi, S., Burckhardt, B.E., Hanson, J.C., Campe, C.B., Schrum, L.W., Rippe, R.A., Maher, J.J., 2001. Anti-Fas induces hepatic chemokines and promotes inflammation by an NF-kappa B-independent, caspase-3-dependent pathway. J Biol Chem 276, 49077–49082. https://doi.org/10.1074/JBC.M109791200

Fliegauf, M., Benzing, T., Omran, H., 2007. When cilia go bad: cilia defects and ciliopathies. Nat Rev Mol Cell Biol 8, 880–893. https://doi.org/10.1038/NRM2278

Fox, J.L., MacFarlane, M., 2016. Targeting cell death signalling in cancer: minimising "Collateral damage." Br J Cancer 115, 5–11. https://doi.org/10.1038/BJC.2016.111

Frezza, C., Cipolat, S., Martins de Brito, O., Micaroni, M., Beznoussenko, G. v., Rudka, T., Bartoli, D., Polishuck, R.S., Danial, N.N., de Strooper, B., Scorrano, L., 2006. OPA1 controls apoptotic cristae remodeling independently from mitochondrial fusion. Cell 126, 177–189. https://doi.org/10.1016/J.CELL.2006.06.025

Friedman, J.R., Lackner, L.L., West, M., DiBenedetto, J.R., Nunnari, J., Voeltz, G.K., 2011. ER tubules mark sites of mitochondrial division. Science 334, 358–362. https://doi.org/10.1126/SCIENCE.1207385

Friedman, J.R., Nunnari, J., 2014. Mitochondrial form and function. Nature 505, 335–343. https://doi.org/10.1038/NATURE12985

Fuertes-Alvarez, S., Maeso-Alonso, L., Villoch-Fernandez, J., Wildung, M., Martin-Lopez, M., Marshall, C., Villena-Cortes, A.J., Diez-Prieto, I., Pietenpol, J.A., Tissir, F., Lizé, M., Marques, M.M., Marin, M.C., 2018. p73 regulates ependymal planar cell polarity by modulating actin and microtubule cytoskeleton. Cell Death Dis 9. https://doi.org/10.1038/s41419-018-1205-6

Fujitani, M., Cancino, G.I., Dugani, C.B., Weaver, I.C.G., Gauthier-Fisher, A., Paquin, A., Mak, T.W., Wojtowicz, M.J., Miller, F.D., Kaplan, D.R., 2010. TAp73 acts via the bHLH Hey2 to promote long-term maintenance of neural precursors. Curr Biol 20, 2058–2065. https://doi.org/10.1016/J.CUB.2010.10.029

Fujitani, M., Sato, R., Yamashita, T., 2017. Loss of p73 in ependymal cells during the perinatal period leads to aqueductal stenosis. Sci Rep 7. https://doi.org/10.1038/S41598-017-12105-Z

Ganini, C., Amelio, I., Bertolo, R., Bove, P., Buonomo, O.C., Candi, E., Cipriani, C., di Daniele, N., Juhl, H., Mauriello, A., Marani, C., Marshall, J., Melino, S., Marchetti, P., Montanaro, M., Natale, M.E., Novelli, F., Palmieri, G., Piacentini, M., Rendina, E.A., Roselli, M., Sica, G., Tesauro, M., Rovella, V., Tisone, G., Shi, Y., Wang, Y., Melino, G., 2021. Global mapping of cancers: The Cancer Genome Atlas and beyond. Mol Oncol 15, 2823–2840. https://doi.org/10.1002/1878-0261.13056

Gao, K., Cheng, M., Zuo, X., Lin, J., Hoogewijs, K., Murphy, M.P., Fu, X.D., Zhang, X., 2021. Active RNA interference in mitochondria. Cell Res 31, 219–228. https://doi.org/10.1038/S41422-020-00394-5

Gaude, E., Frezza, C., 2014. Defects in mitochondrial metabolism and cancer. Cancer Metab 2. https://doi.org/10.1186/2049-3002-2-10

Giam, M., Huang, D.C.S., Bouillet, P., 2008. BH3-only proteins and their roles in programmed cell death. Oncogene 27 Suppl 1, S128–S136. https://doi.org/10.1038/ONC.2009.50

Gillies, L.A., Kuwana, T., 2014. Apoptosis regulation at the mitochondrial outer membrane. J Cell Biochem 115, 632–640. https://doi.org/10.1002/JCB.24709

Gohy, S., Carlier, F.M., Fregimilicka, C., Detry, B., Lecocq, M., Ladjemi, M.Z., Verleden, S., Hoton, D., Weynand, B., Bouzin, C., Pilette, C., 2019. Altered generation of ciliated cells in chronic obstructive pulmonary disease. Scientific Reports 2019 9:1 9, 1–12. https://doi.org/10.1038/s41598-019-54292-x

Gonzalez-Cano, L., Fuertes-Alvarez, S., Robledinos-Anton, N., Bizy, A., Villena-Cortes, A., Fariñas, I., Marques, M.M., Marin, M.C., 2016. p73 is required for ependymal cell maturation and neurogenic SVZ cytoarchitecture. Dev Neurobiol 76, 730–747. https://doi.org/10.1002/dneu.22356

Gonzalez-Cano, L., Herreros-Villanueva, M., Fernandez-Alonso, R., Ayuso-Sacido, A., Meyer, G., Garcia-Verdugo, J.M., Silva, A., Marques, M.M., Marin, M.C., 2010. P73 deficiency results in impaired self renewal and premature neuronal differentiation of mouse neural progenitors independently of p53. Cell Death Dis 1. https://doi.org/10.1038/cddis.2010.87

Gray, C.W., Ward, R. v., Karran, E., Turconi, S., Rowles, A., Viglienghi, D., Southan, C., Barton, A., Fantom, K.G., West, A., Savopoulos, J., Hassan, N.J., Clinkenbeard, H., Hanning, C., Amegadzie, B., Davis, J.B., Dingwall, C., Livi, G.P., Creasy, C.L., 2000. Characterization of human HtrA2, a novel serine protease involved in the mammalian cellular stress response. Eur J Biochem 267, 5699–5710. https://doi.org/10.1046/J.1432-1327.2000.01589.X

Grespi, F., Amelio, I., Tucci, P., Annicchiarico-Petruzzelli, M., Melino, G., 2012. Tissue-specific expression of p73 C-terminal isoforms in mice. Cell Cycle 11, 4474–83. https://doi.org/10.4161/cc.22787

Hafner, A., Bulyk, M.L., Jambhekar, A., Lahav, G., 2019. The multiple mechanisms that regulate p53 activity and cell fate. Nat Rev Mol Cell Biol. https://doi.org/10.1038/s41580-019-0110-x

Haupt, Y., Maya, R., Kazaz, A., Oren, M., 1997. Mdm2 promotes the rapid degradation of p53. Nature 387, 296–299. https://doi.org/10.1038/387296A0

Herst, P.M., Rowe, M.R., Carson, G.M., Berridge, M. v., 2017. Functional Mitochondria in Health and Disease. Front Endocrinol (Lausanne) 8. https://doi.org/10.3389/FENDO.2017.00296

Hirst, J., 2009. Towards the molecular mechanism of respiratory complex I. Biochem J 425, 327–339. https://doi.org/10.1042/BJ20091382

Hoffmann, R.F., Zarrintan, S., Brandenburg, S.M., Kol, A., de Bruin, H.G., Jafari, S., Dijk, F., Kalicharan, D., Kelders, M., Gosker, H.R., ten Hacken, N.H.T., van der Want, J.J., van Oosterhout, A.J.M., Heijink, I.H., 2013. Prolonged cigarette smoke exposure alters mitochondrial structure and function in airway epithelial cells. Respir Res 14. https://doi.org/10.1186/1465-9921-14-97

Hu, W., Zhang, C., Wu, R., Sun, Y., Levine, A., Feng, Z., 2010. Glutaminase 2, a novel p53 target gene regulating energy metabolism and antioxidant function. Proc Natl Acad Sci U S A 107, 7455–7460. https://doi.org/10.1073/PNAS.1001006107

Inoue, S., Tomasini, R., Rufini, A., Elia, A.J., Agostini, M., Amelio, I., Cescon, D., Dinsdale, D., Zhou, L., Harris, I.S., Lac, S., Silvester, J., Li, W.Y., Sasaki, M., Haight, J., Brüstle, A., Wakeham, A., McKerlie, C., Jurisicova, A., Melino, G., Mak, T.W., 2014. TAp73 is required for spermatogenesis and the maintenance of male fertility. Proc Natl Acad Sci U S A 111, 1843–1848. https://doi.org/10.1073/PNAS.1323416111

Jiménez, A.J., Domínguez-Pinos, M.D., Guerra, M.M., Fernández-Llebrez, P., Pérez-Fígares, J.M., 2014. Structure and function of the ependymal barrier and diseases associated with ependyma disruption. Tissue Barriers. https://doi.org/10.4161/tisb.28426

Jost, C.A., Marin, M.C., Kaelin, W.G., 1997. p73 is a human p53-related protein that can induce apoptosis. Nature 389, 191–194. https://doi.org/10.1038/38298

Kaghad, M., Bonnet, H., Yang, A., Creancier, L., Biscan, J.C., Valent, A., Minty, A., Chalon, P., Lelias, J.M., Dumont, X., Ferrara, P., McKeon, F., Caput, D., 1997. Monoallelically expressed gene related to p53 at 1p36, a region frequently deleted in neuroblastoma and other human cancers. Cell 90, 809–819. https://doi.org/10.1016/S0092-8674(00)80540-1

Kerr, J.F.R., Wyllie, A.H., Currie, A.R., 1972. Apoptosis: a basic biological phenomenon with wide-ranging implications in tissue kinetics. Br J Cancer 26, 239–257. https://doi.org/10.1038/BJC.1972.33

Klein, A.M., Biderman, L., Tong, D., Alaghebandan, B., Plumber, S.A., Mueller, H.S., van Vlimmeren, A., Katz, C., Prives, C., 2021. MDM2, MDMX, and p73 regulate cell-cycle progression in the absence of wild-type p53. Proc Natl Acad Sci U S A 118, 2102420118. https://doi.org/10.1073/PNAS.2102420118/-/DCSUPPLEMENTAL

Koeppel, M., van Heeringen, S.J., Kramer, D., Smeenk, L., Janssen-Megens, E., Hartmann, M., Stunnenberg, H.G., Lohrum, M., 2011. Crosstalk between c-Jun and TAp73alpha/beta contributes to the apoptosis-survival balance. Nucleic Acids Res 39, 6069–85. https://doi.org/10.1093/nar/gkr028

Koshiba, T., Detmer, S.A., Kaiser, J.T., Chen, H., McCaffery, J.M., Chan, D.C., 2004. Structural basis of mitochondrial tethering by mitofusin complexes. Science 305, 858–862. https://doi.org/10.1126/SCIENCE.1099793

Kremer, A., Lippens, S., Bartunkova, S., Asselbergh, B., Blanpain, C., Fendrych, M., Goossens, A., Holt, M., Janssens, S., Krols, M., Larsimont, J.C., Mc Guire, C., Nowack, M.K., Saelens, X., Schertel, A.,

Schepens, B., Slezak, M., Timmerman, V., Theunis, C., van Brempt, R., Visser, Y., Guérin, C.J., 2015. Developing 3D SEM in a broad biological context. J Microsc 259. https://doi.org/10.1111/jmi.12211

Kulaga, H.M., Leitch, C.C., Eichers, E.R., Badano, J.L., Lesemann, A., Hoskins, B.E., Lupski, J.R., Beales, P.L., Reed, R.R., Katsanis, N., 2004. Loss of BBS proteins causes anosmia in humans and defects in olfactory cilia structure and function in the mouse. Nat Genet 36. https://doi.org/10.1038/ng1418

Kunji, E.R.S., 2004. The role and structure of mitochondrial carriers. FEBS Lett 564, 239–244. https://doi.org/10.1016/S0014-5793(04)00242-X

Lavrik, I., Krueger, A., Schmitz, I., Baumann, S., Weyd, H., Krammer, P.H., Kirchhoff, S., 2003. The active caspase-8 heterotetramer is formed at the CD95 DISC. Cell Death Differ 10, 144–145. https://doi.org/10.1038/SJ.CDD.4401156

Lawless, C., Greaves, L., Reeve, A.K., Turnbull, D.M., Vincent, A.E., 2020. The rise and rise of mitochondrial DNA mutations. Open Biol 10. https://doi.org/10.1098/RSOB.200061

Lee, H., Tak, H., Park, S.J., Jo, Y.K., Cho, D.H., Lee, E.K., 2017. microRNA-200a-3p enhances mitochondrial elongation by targeting mitochondrial fission factor. BMB Rep 50, 214–219. https://doi.org/10.5483/BMBREP.2017.50.4.006

Lena, A.M., Rossi, V., Osterburg, S., Smirnov, A., Osterburg, C., Tuppi, M., Cappello, A., Amelio, I., Dötsch, V., de Felici, M., Klinger, F.G., Annicchiarico-Petruzzelli, M., Valensise, H., Melino, G., Candi, E., 2021. The p63 C-terminus is essential for murine oocyte integrity. Nat Commun 12. https://doi.org/10.1038/S41467-020-20669-0

Levine, A.J., Tomasini, R., McKeon, F.D., Mak, T.W., Melino, G., 2011. The p53 family: Guardians of maternal reproduction. Nat Rev Mol Cell Biol. https://doi.org/10.1038/nrm3086

Li, Le, Li, Lijia, Li, W., Chen, T., bin Zou, Zhao, L., Wang, H., Wang, X., Xu, L., Liu, X., Wang, D., Li, B., Mak, T.W., Du, W., Yang, X., Jiang, P., 2018. TAp73-induced phosphofructokinase-1 transcription promotes the Warburg effect and enhances cell proliferation. Nat Commun 9. https://doi.org/10.1038/S41467-018-07127-8

Liu, J., Zhang, C., Hu, W., Feng, Z., 2019. Tumor suppressor p53 and metabolism. J Mol Cell Biol. https://doi.org/10.1093/jmcb/mjy070

Logotheti, S., Pavlopoulou, A., Marquardt, S., Takan, I., Georgakilas, A.G., Stiewe, T., 2022. p73 isoforms meet evolution of metastasis. Cancer and Metastasis Reviews. https://doi.org/10.1007/s10555-022-10057-z

Logotheti, S., Richter, C., Murr, N., Spitschak, A., Marquardt, S., Pützer, B.M., 2021. Mechanisms of Functional Pleiotropy of p73 in Cancer and Beyond. Front Cell Dev Biol 9. https://doi.org/10.3389/FCELL.2021.737735

Lokshin, M., Li, Y., Gaiddon, C., Prives, C., 2007. p53 and p73 display common and distinct requirements for sequence specific binding to DNA. Nucleic Acids Res 35, 340–352. https://doi.org/10.1093/NAR/GKL1047

Longo, D.L., Archer, S.L., 2013. Mitochondrial Dynamics-Mitochondrial Fission and Fusion in Human Diseases. N Engl J Med 369, 2236–51. https://doi.org/10.1056/NEJMra1215233

MacNee, W., 2005. Pathogenesis of Chronic Obstructive Pulmonary Disease. Proc Am Thorac Soc 2, 258. https://doi.org/10.1513/PATS.200504-045SR

MacVicar, T., Langer, T., 2016. OPA1 processing in cell death and disease - the long and short of it. J Cell Sci 129, 2297–2306. https://doi.org/10.1242/JCS.159186

Mai, M., Huang, H., Reed, C., Qian, C., Smith, J.S., Alderete, B., Jenkins, R., Smith, D.I., Liu, W., 1998. Genomic organization and mutation analysis of p73 in oligodendrogliomas with chromosome 1 p-arm deletions. Genomics 51, 359–363. https://doi.org/10.1006/GENO.1998.5387

Malicki, J.J., Johnson, C.A., 2017. The Cilium: Cellular Antenna and Central Processing Unit. Trends Cell Biol 27, 126–140. https://doi.org/10.1016/J.TCB.2016.08.002

Malka, F., Guillery, O., Cifuentes-Diaz, C., Guillou, E., Belenguer, P., Lombés, A., Rojo, M., 2005. Separate fusion of outer and inner mitochondrial membranes. EMBO Rep 6, 853–859. https://doi.org/10.1038/SJ.EMBOR.7400488

Margulis, L., 1970. Recombination of non-chromosomal genes in Chlamydomonas: assortment of mitochondria and chloroplasts? J Theor Biol 26, 337–342. https://doi.org/10.1016/S0022-5193(70)80023-6

Marini, A., Rotblat, B., Sbarrato, T., Niklison-Chirou, M.V., Knight, J.R.P., Dudek, K., Jones, C., Bushell, M., Knight, R.A., Amelio, I., Willis, A.E., Melino, G., 2018. TAp73 contributes to the oxidative stress response by regulating protein synthesis. Proc Natl Acad Sci U S A 115, 6219–6224. https://doi.org/10.1073/pnas.1718531115

Marshall, C.B., Beeler, J.S., Lehmann, B.D., Gonzalez-Ericsson, P., Sanchez, V., Sanders, M.E., Boyd, K.L., Pietenpol, J.A., 2021. Tissue-specific expression of p73 and p63 isoforms in human tissues. Cell Death Dis 12. https://doi.org/10.1038/S41419-021-04017-8

Martinvalet, D., Zhu, P., Lieberman, J., 2005. Granzyme A induces caspase-independent mitochondrial damage, a required first step for apoptosis. Immunity 22, 355–370. https://doi.org/10.1016/J.IMMUNI.2005.02.004

Mason, K.D., Carpinelli, M.R., Fletcher, J.I., Collinge, J.E., Hilton, A.A., Ellis, S., Kelly, P.N., Ekert, P.G., Metcalf, D., Roberts, A.W., Huang, D.C.S., Kile, B.T., 2007. Programmed anuclear cell death delimits platelet life span. Cell 128, 1173–1186. https://doi.org/10.1016/J.CELL.2007.01.037

Matsuno-Yagi, A., Yagi, T., Hatefi, Y., 1985. Studies on the mechanism of oxidative phosphorylation: effects of specific F0 modifiers on ligand-induced conformation changes of F1. Proc Natl Acad Sci U S A 82, 7550–7554. https://doi.org/10.1073/PNAS.82.22.7550

McArthur, K., Kile, B.T., 2020. Apoptotic mitochondria prime anti-tumour immunity. Cell Death Discov 6. https://doi.org/10.1038/S41420-020-00335-6

Medina-Bolívar, C., González-Arnay, E., Talos, F., González-Gómez, M., Moll, U.M., Meyer, G., 2014. Cortical hypoplasia and ventriculomegaly of p73-deficient mice: Developmental and adult analysis. Journal of Comparative Neurology 522, 2663–2679. https://doi.org/10.1002/cne.23556

Melino, G., Bernassola, F., Ranalli, M., Yee, K., Zong, W.X., Corazzari, M., Knight, R.A., Green, D.R., Thompson, C., Vousden, K.H., 2004. p73 Induces apoptosis via PUMA transactivation and Bax mitochondrial translocation. J Biol Chem 279, 8076–8083. https://doi.org/10.1074/JBC.M307469200

Merino, D., Kelly, G.L., Lessene, G., Wei, A.H., Roberts, A.W., Strasser, A., 2018. BH3-Mimetic Drugs: Blazing the Trail for New Cancer Medicines. Cancer Cell 34, 879–891. https://doi.org/10.1016/J.CCELL.2018.11.004

Mérino, D., Khaw, S.L., Glaser, S.P., Anderson, D.J., Belmont, L.D., Wong, C., Yue, P., Robati, M., Phipson, B., Fairlie, W.D., Lee, E.F., Campbell, K.J., Vandenberg, C.J., Cory, S., Roberts, A.W., Ludlam, M.J.C., Huang, D.C.S., Bouillet, P., 2012. Bcl-2, Bcl-x(L), and Bcl-w are not equivalent targets of ABT-737 and navitoclax (ABT-263) in lymphoid and leukemic cells. Blood 119, 5807–5816. https://doi.org/10.1182/BLOOD-2011-12-400929

Meyer, G., Socorro, A.C., Garcia, C.G.P., Millan, L.M., Walker, N., Caput, D., 2004. Developmental roles of p73 in cajal-retzius cells and cortical patterning. Journal of Neuroscience 24, 9878–9887. https://doi.org/10.1523/JNEUROSCI.3060-04.2004

Mi, H., Muruganujan, A., Huang, X., Ebert, D., Mills, C., Guo, X., Thomas, P.D., 2019. Protocol Update for large-scale genome and gene function analysis with the PANTHER classification system (v.14.0). Nature Protocols 2019 14:3 14, 703–721. https://doi.org/10.1038/s41596-019-0128-8

Milani, M., Beckett, A.J., Al-Zebeeby, A., Luo, X., Prior, I.A., Cohen, G.M., Varadarajan, S., 2019. DRP-1 functions independently of mitochondrial structural perturbations to facilitate BH3 mimetic-mediated apoptosis. Cell Death Discovery 2019 5:1 5, 1–11. https://doi.org/10.1038/s41420-019-0199-x

Mills, A.A., Zheng, B., Wang, X.J., Vogel, H., Roop, D.R., Bradley, A., 1999. p63 is a p53 homologue required for limb and epidermal morphogenesis. Nature 398, 708–13. https://doi.org/10.1038/19531

Mirvis, M., Stearns, T., Nelson, W.J., 2018. Cilium structure, assembly, and disassembly regulated by the cytoskeleton. Biochemical Journal. https://doi.org/10.1042/BCJ20170453

Mitchell, P., 1985. The correlation of chemical and osmotic forces in biochemistry. J Biochem 97, 1–18. https://doi.org/10.1093/OXFORDJOURNALS.JBCHEM.A135033

Mitchison, H.M., Valente, E.M., 2017. Motile and non-motile cilia in human pathology: from function to phenotypes. J Pathol 241, 294–309. https://doi.org/10.1002/PATH.4843

Moll, U.M., Slade, N., 2004. p63 and p73: Roles in development and tumor formation. Molecular Cancer Research 2, 371–386. https://doi.org/10.1158/1541-7786.371.2.7

Morita, M., Prudent, J., Basu, K., Goyon, V., Katsumura, S., Hulea, L., Pearl, D., Siddiqui, N., Strack, S., McGuirk, S., St-Pierre, J., Larsson, O., Topisirovic, I., Vali, H., McBride, H.M., Bergeron, J.J., Sonenberg, N., 2017. mTOR Controls Mitochondrial Dynamics and Cell Survival via MTFP1. Mol Cell 67, 922-935.e5. https://doi.org/10.1016/J.MOLCEL.2017.08.013

Moulder, D.E., Hatoum, D., Tay, E., Lin, Y., McGowan, E.M., 2018. The roles of p53 in mitochondrial dynamics and cancer metabolism: The pendulum between survival and death in breast cancer? Cancers (Basel). https://doi.org/10.3390/cancers10060189

Müller, M., Wilder, S., Bannasch, D., Israeli, D., Lehlbach, K., Li-Weber, M., Friedman, S.L., Galle, P.R., Stremmel, W., Oren, M., Krammer, P.H., 1998. p53 activates the CD95 (APO-1/Fas) gene in response to DNA damage by anticancer drugs. J Exp Med 188, 2033–2045. https://doi.org/10.1084/JEM.188.11.2033

Murray-Zmijewski, F., Lane, D.P., Bourdon, J.C., 2006. p53/p63/p73 isoforms: an orchestra of isoforms to harmonise cell differentiation and response to stress. Cell Death Differ 13, 962–972. https://doi.org/10.1038/SJ.CDD.4401914

Musah, S., Chen, J., Hoyle, G.W., 2012. Repair of tracheal epithelium by basal cells after chlorine-induced injury. Respir Res 13. https://doi.org/10.1186/1465-9921-13-107

Nainu, F., Shiratsuchi, A., Nakanishi, Y., 2017. Induction of Apoptosis and Subsequent Phagocytosis of Virus-Infected Cells As an Antiviral Mechanism. Front Immunol 8. https://doi.org/10.3389/FIMMU.2017.01220

Nemajerova, A., Amelio, I., Gebel, J., Dötsch, V., Melino, G., Moll, U.M., 2018. Non-oncogenic roles of TAp73: from multiciliogenesis to metabolism. Cell Death Differ 25, 144–153. https://doi.org/10.1038/CDD.2017.178

Nemajerova, A., Kramer, D., Siller, S.S., Herr, C., Shomroni, O., Pena, T., Suazo, C.G., Glaser, K., Wildung, M., Steffen, H., Sriraman, A., Oberle, F., Wienken, M., Hennion, M., Vidal, R., Royen, B., Alevra, M., Schild, D., Bals, R., Dönitz, J., Riedel, D., Bonn, S., Takemaru, K.I., Moll, U.M., Lizé, M., 2016. TAp73 is a central transcriptional regulator of airway multiciliogenesis. Genes Dev 30, 1300–1312. https://doi.org/10.1101/gad.279836.116

Nemajerova, A., Moll, U.M., 2019. Tissue-specific roles of p73 in development and homeostasis. J Cell Sci 132, jcs233338. https://doi.org/10.1242/jcs.233338

Niklison-Chirou, M.V., Erngren, I., Engskog, M., Haglöf, J., Picard, D., Remke, M., McPolin, P.H.R., Selby, M., Williamson, D., Clifford, S.C., Michod, D., Hadjiandreou, M., Arvidsson, T., Pettersson, C., Melino, G., Marino, S., 2017. TAp73 is a marker of glutamine addiction in medulloblastoma. Genes Dev 31, 1738–1753. https://doi.org/10.1101/gad.302349.117

Noguchi, M., Kasahara, A., 2018. Mitochondrial dynamics coordinate cell differentiation. Biochem Biophys Res Commun 500, 59–64. https://doi.org/10.1016/J.BBRC.2017.06.094

Nunnari, J., Suomalainen, A., 2012. Mitochondria: in sickness and in health. Cell 148, 1145–1159. https://doi.org/10.1016/J.CELL.2012.02.035

Nyman, U., Sobczak-Pluta, A., Vlachos, P., Perlmann, T., Zhivotovsky, B., Joseph, B., 2005. Full-length p73α represses drug-induced apoptosis in small cell lung carcinoma cells. Journal of Biological Chemistry 280. https://doi.org/10.1074/jbc.M500394200

Nyman U, Vlachos P, Cascante A, Hermanson O, Zhivotovsky B, Joseph B. Protein kinase C-dependent phosphorylation regulates the cell cycle-inhibitory function of the p73 carboxy terminus transactivation domain. Mol Cell Biol. 2009 Apr;29(7):1814-25. doi: 10.1128/MCB.00585-08.

Ohata, S., Alvarez-Buylla, A., 2016. Planar Organization of Multiciliated Ependymal (E1) Cells in the Brain Ventricular Epithelium. Trends Neurosci. https://doi.org/10.1016/j.tins.2016.05.004

Olgun, A., Akman, S., 2007. Mitochondrial DNA-deficient models and aging. Ann N Y Acad Sci 1100, 241–245. https://doi.org/10.1196/ANNALS.1395.025

Olichon, A., ElAchouri, G., Baricault, L., Delettre, C., Belenguer, P., Lenaers, G., 2007. OPA1 alternate splicing uncouples an evolutionary conserved function in mitochondrial fusion from a vertebrate restricted function in apoptosis. Cell Death Differ 14, 682–692. https://doi.org/10.1038/SJ.CDD.4402048

Olichon, A., Guillou, E., Delettre, C., Landes, T., Arnauné-Pelloquin, L., Emorine, L.J., Mils, V., Daloyau, M., Hamel, C., Amati-Bonneau, P., Bonneau, D., Reynier, P., Lenaers, G., Belenguer, P., 2006. Mitochondrial dynamics and disease, OPA1. Biochim Biophys Acta Mol Cell Res. https://doi.org/10.1016/j.bbamcr.2006.04.003

Oropesa, M., de La Mata, M., Maraver, J.G., Cordero, M.D., Cotán, D., Rodríguez-Hernández, Á., Domínguez-Moñino, I., de Miguel, M., Navas, P., Sánchez-Alcázar, J.A., 2011. Apoptotic microtubule network organization and maintenance depend on high cellular ATP levels and energized mitochondria. Apoptosis 16. https://doi.org/10.1007/s10495-011-0577-1

Ou HD, Löhr F, Vogel V, Mäntele W, Dötsch V. Structural evolution of C-terminal domains in the p53 family. EMBO J. 2007 Jul 25;26(14):3463-73. doi: 10.1038/sj.emboj.7601764.

Papa, S., Rasmo, D. de, Technikova-Dobrova, Z., Panelli, D., Signorile, A., Scacco, S., Petruzzella, V., Papa, F., Palmisano, G., Gnoni, A., Micelli, L., Sardanelli, A.M., 2012. Respiratory chain complex I, a main regulatory target of the cAMP/PKA pathway is defective in different human diseases. FEBS Lett 586, 568–577. https://doi.org/10.1016/J.FEBSLET.2011.09.019

Patten, D.A., Wong, J., Khacho, M., Soubannier, V., Mailloux, R.J., Pilon-Larose, K., MacLaurin, J.G., Park, D.S., McBride, H.M., Trinkle-Mulcahy, L., Harper, M., Germain, M., Slack, R.S., 2014. OPA1-dependent cristae modulation is essential for cellular adaptation to metabolic demand. EMBO J 33, 2676–2691. https://doi.org/10.15252/EMBJ.201488349

Phan, T.T.T., Lin, Y.C., Chou, Y.T., Wu, C.W., Lin, L.Y., 2022. Tumor suppressor p53 restrains cancer cell dissemination by modulating mitochondrial dynamics. Oncogenesis 11. https://doi.org/10.1038/S41389-022-00401-X

Pietsch, E. Christine, Perchiniak, E., Canutescu, A.A., Wang, G., Dunbrack, R.L., Murphy, M.E., 2008. Oligomerization of BAK by p53 utilizes conserved residues of the p53 DNA binding domain. J Biol Chem 283, 21294–21304. https://doi.org/10.1074/JBC.M710539200

Pietsch, E. C., Sykes, S.M., McMahon, S.B., Murphy, M.E., 2008. The p53 family and programmed cell death. Oncogene 27, 6507–6521. https://doi.org/10.1038/ONC.2008.315

Ploumi, C., Daskalaki, I., Tavernarakis, N., 2017. Mitochondrial biogenesis and clearance: a balancing act. FEBS J 284, 183–195. https://doi.org/10.1111/FEBS.13820

Poon, I.K.H., Lucas, C.D., Rossi, A.G., Ravichandran, K.S., 2014. Apoptotic cell clearance: basic biology and therapeutic potential. Nat Rev Immunol 14, 166–180. https://doi.org/10.1038/NRI3607

Raj N, Bam R. Reciprocal Crosstalk Between YAP1/Hippo Pathway and the p53 Family Proteins: Mechanisms and Outcomes in Cancer. Front Cell Dev Biol. 2019 Aug 9;7:159. doi: 10.3389/fcell.2019.00159.

Reza Saadatzadeh, M., Elmi, A.N., Pandya, P.H., Bijangi-Vishehsaraei, K., Ding, J., Stamatkin, C.W., Cohen-Gadol, A.A., Pollok, K.E., 2017. The Role of MDM2 in Promoting Genome Stability versus Instability. Int J Mol Sci 18. https://doi.org/10.3390/IJMS18102216

Richmond, B.W., Marshall, C.B., Lehmann, B.D., Polosukhin, V.V., Blackwell, T.S., Pietenpol, J.A., 2022. p73 Is Suppressed by Cigarette Smoke and Reduced in the Lungs of Patients with Chronic Obstructive Pulmonary Disease A4620–A4620. https://doi.org/10.1164/AJRCCM-CONFERENCE.2022.205.1_MEETINGABSTRACTS.A4620

Rock, J.R., Gao, X., Xue, Y., Randell, S.H., Kong, Y.Y., Hogan, B.L.M., 2011. Notch-dependent differentiation of adult airway basal stem cells. Cell Stem Cell 8. https://doi.org/10.1016/j.stem.2011.04.003

Rock, J.R., Onaitis, M.W., Rawlins, E.L., Lu, Y., Clark, C.P., Xue, Y., Randell, S.H., Hogan, B.L.M., 2009. Basal cells as stem cells of the mouse trachea and human airway epithelium. Proc Natl Acad Sci U S A 106, 12771–12775. https://doi.org/10.1073/PNAS.0906850106

Rogatzki, M.J., Ferguson, B.S., Goodwin, M.L., Gladden, L.B., 2015. Lactate is always the end product of glycolysis. Front Neurosci 9. https://doi.org/10.3389/FNINS.2015.00022

Rossi, M., de Laurenzi, V., Munarriz, E., Green, D.R., Liu, Y.C., Vousden, K.H., Cesareni, G., Melino, G., 2005. The ubiquitin-protein ligase Itch regulates p73 stability. EMBO J 24, 836–848. https://doi.org/10.1038/SJ.EMBOJ.7600444

Rozenberg, J.M., Zvereva, S., Dalina, A., Blatov, I., Zubarev, I., Luppov, D., Bessmertnyi, A., Romanishin, A., Alsoulaiman, L., Kumeiko, V., Kagansky, A., Melino, G., Ganini, C., Barlev, N.A., 2021. The p53 family member p73 in the regulation of cell stress response. Biol Direct 16. https://doi.org/10.1186/S13062-021-00307-5

Rufini, A., Agostini, M., Grespi, F., Tomasini, R., Sayan, B.S., Niklison-Chirou, M.V., Conforti, F., Velletri, T., Mastino, A., Mak, T.W., Melino, G., Knight, R.A., 2011. p73 in Cancer. Genes Cancer 2, 491–502. https://doi.org/10.1177/1947601911408890

Rufini, A., Niklison-Chirou, M.V., Inoue, S., Tomasini, R., Harris, I.S., Marino, A., Federici, M., Dinsdale, D., Knight, R.A., Melino, G., Mak, T.W., 2012. TAp73 depletion accelerates aging through metabolic dysregulation. Genes Dev 26, 2009–14. https://doi.org/10.1101/gad.197640.112

Rufini, S., Lena, A.M., Cadot, B., Mele, S., Amelio, I., Terrinoni, A., Desideri, A., Melino, G., Candi, E., 2011. The sterile alpha-motif (SAM) domain of p63 binds in vitro monoasialoganglioside (GM1) micelles. Biochem Pharmacol 82, 1262–1268. https://doi.org/10.1016/J.BCP.2011.07.087

Saelens, X., Festjens, N., vande Walle, L., van Gurp, M., van Loo, G., Vandenabeele, P., 2004. Toxic proteins released from mitochondria in cell death. Oncogene 23, 2861–2874. https://doi.org/10.1038/SJ.ONC.1207523

Sayan, A.E., Rossi, M., Melino, G., Knight, R.A., 2004. P73: In silico evidence for a putative third promoter region. Biochem Biophys Res Commun 313, 765–770. https://doi.org/10.1016/j.bbrc.2003.12.014

Sciacovelli, M., Gonçalves, E., Johnson, T.I., Zecchini, V.R., da Costa, A.S.H., Gaude, E., Drubbel, A.V., Theobald, S.J., Abbo, S.R., Tran, M.G.B., Rajeeve, V., Cardaci, S., Foster, S., Yun, H., Cutillas, P., Warren, A., Gnanapragasam, V., Gottlieb, E., Franze, K., Huntly, B., Maher, E.R., Maxwell, P.H., Saez-Rodriguez, J., Frezza, C., 2016. Fumarate is an epigenetic modifier that elicits epithelial-to-mesenchymal transition. Nature 537, 544–547. https://doi.org/10.1038/NATURE19353

Scorrano, L., 2013. Keeping mitochondria in shape: a matter of life and death. Eur J Clin Invest 43, 886–893. https://doi.org/10.1111/ECI.12135

Sebastián, D., Palacín, M., Zorzano, A., 2017. Mitochondrial Dynamics: Coupling Mitochondrial Fitness with Healthy Aging. Trends Mol Med 23, 201–215. https://doi.org/10.1016/J.MOLMED.2017.01.003

Shibue, T., Suzuki, S., Okamoto, H., Yoshida, H., Ohba, Y., Takaoka, A., Taniguchi, T., 2006. Differential contribution of Puma and Noxa in dual regulation of p53-mediated apoptotic pathways. EMBO J 25, 4952–4962. https://doi.org/10.1038/SJ.EMBOJ.7601359

Spassky, N., Meunier, A., 2017. The development and functions of multiciliated epithelia. Nat Rev Mol Cell Biol 18, 423–436. https://doi.org/10.1038/NRM.2017.21

Stefano, G.B., Bjenning, C., Wang, F., Wang, N., Kream, R.M., 2017. Mitochondrial Heteroplasmy. Adv Exp Med Biol 982, 577–594. https://doi.org/10.1007/978-3-319-55330-6_30

Sullivan, K.D., Galbraith, M.D., Andrysik, Z., Espinosa, J.M., 2018. Mechanisms of transcriptional regulation by p53. Cell Death Differ. https://doi.org/10.1038/cdd.2017.174

Sun S, Erchova I, Sengpiel F, Votruba M. Opa1 Deficiency Leads to Diminished Mitochondrial Bioenergetics With Compensatory Increased Mitochondrial Motility. Invest Ophthalmol Vis Sci. 2020 Jun 3;61(6):42. doi: 10.1167/iovs.61.6.42.

Tait, S.W.G., Green, D.R., 2012. Mitochondria and cell signalling. J Cell Sci 125, 807–815. https://doi.org/10.1242/JCS.099234

Talos, F., Abraham, A., Vaseva, A. v., Holembowski, L., Tsirka, S.E., Scheel, A., Bode, D., Dobbelstein, M., Brück, W., Moll, U.M., 2010. p73 is an essential regulator of neural stem cell maintenance in embryonal and adult CNS neurogenesis. Cell Death Differ 17, 1816–1829. https://doi.org/10.1038/CDD.2010.131

Tan, F.E., Vladar, E.K., Ma, L., Fuentealba, L.C., Hoh, R., Hernán Espinoza, F., Axelrod, J.D., Alvarez-Buylla, A., Stearns, T., Kintner, C., Krasnow, M.A., 2013. Myb promotes centriole amplification and later steps of the multiciliogenesis program. Development (Cambridge) 140, 4277–4286. https://doi.org/10.1242/DEV.094102/-/DC1

Thomas, P.D., Ebert, D., Muruganujan, A., Mushayahama, T., Albou, L., Mi, H., 2022. <scp>PANTHER</scp> : Making genome-scale phylogenetics accessible to all. Protein Science 31, 8–22. https://doi.org/10.1002/PRO.4218

Tilley, A.E., Walters, M.S., Shaykhiev, R., Crystal, R.G., 2015. Cilia dysfunction in lung disease. Annu Rev Physiol 77. https://doi.org/10.1146/annurev-physiol-021014-071931

Tomasello, M.F., Guarino, F., Reina, S., Messina, A., de Pinto, V., 2013. The voltage-dependent anion selective channel 1 (VDAC1) topography in the mitochondrial outer membrane as detected in intact cell. PLoS One 8. https://doi.org/10.1371/JOURNAL.PONE.0081522

Tomasini, R., Tsuchihara, K., Wilhelm, M., Fujitani, M., Rufini, A., Cheung, C.C., Khan, F., Itie-Youten, A., Wakeham, A., Tsao, M.S., Iovanna, J.L., Squire, J., Jurisica, I., Kaplan, D., Melino, G., Jurisicova, A., Mak, T.W., 2008. TAp73 knockout shows genomic instability with infertility and tumor suppressor functions. Genes Dev 22, 2677–2691. https://doi.org/10.1101/GAD.1695308

Ugur, H., Sayan, A.E., Ozdamar, S.O., Kanpolat, Y., Ozturk, M., 2004. Expression of TAP73 and ΔNP73 in malignant gliomas. Oncol Rep 11, 1337–1341. https://doi.org/10.3892/OR.11.6.1337/HTML

van Gisbergen, M.W., Voets, A.M., Starmans, M.H.W., de Coo, I.F.M., Yadak, R., Hoffmann, R.F., Boutros, P.C., Smeets, H.J.M., Dubois, L., Lambin, P., 2015. How do changes in the mtDNA and mitochondrial dysfunction influence cancer and cancer therapy? Challenges, opportunities and models. Mutat Res Rev Mutat Res 764, 16–30. https://doi.org/10.1016/J.MRREV.2015.01.001

Varanita, T., Soriano, M.E., Romanello, V., Zaglia, T., Quintana-Cabrera, R., Semenzato, M., Menabò, R., Costa, V., Civiletto, G., Pesce, P., Viscomi, C., Zeviani, M., di Lisa, F., Mongillo, M., Sandri, M., Scorrano, L., 2015. The OPA1-dependent mitochondrial cristae remodeling pathway controls atrophic, apoptotic, and ischemic tissue damage. Cell Metab 21, 834–844. https://doi.org/10.1016/J.CMET.2015.05.007

Velletri, T., Romeo, F., Tucci, P., Peschiaroli, A., Annicchiarico-Petruzzelli, M., Niklison-Chirou, M.V., Amelio, I., Knight, R.A., Mak, T.W., Melino, G., Agostini, M., 2013. GLS2 is transcriptionally regulated by p73 and contributes to neuronal differentiation. Cell Cycle 12, 3564–3573. https://doi.org/10.4161/cc.26771

Vikhreva, P., Melino, G., Amelio, I., 2018. p73 Alternative Splicing: Exploring a Biological Role for the C-Terminal Isoforms. J Mol Biol. https://doi.org/10.1016/j.jmb.2018.04.034

Villaseñor-Altamirano, A.B., Moretto, M., Maldonado, M., Zayas-Del Moral, A., Munguía-Reyes, A., Romero, Y., García-Sotelo, Jair.S., Aguilar, L.A., Aldana-Assad, O., Engelen, K., Selman, M., Collado-Vides, J., Balderas-Martínez, Y.I., Medina-Rivera, A., 2020. PulmonDB: a curated lung disease gene expression database. Scientific Reports 2020 10:1 10, 1–9. https://doi.org/10.1038/s41598-019-56339-5

Vyas, S., Zaganjor, E., Haigis, M.C., 2016. Mitochondria and Cancer. Cell 166, 555–566. https://doi.org/10.1016/J.CELL.2016.07.002

Wai, T., Langer, T., 2016. Mitochondrial Dynamics and Metabolic Regulation. Trends Endocrinol Metab 27, 105–117. https://doi.org/10.1016/J.TEM.2015.12.001

Wang, W., Cheng, X., Lu, J., Wei, J., Fu, G., Zhu, F., Jia, C., Zhou, L., Xie, H., Zheng, S., 2010. Mitofusin-2 is a novel direct target of p53. Biochem Biophys Res Commun 400, 587–592. https://doi.org/10.1016/J.BBRC.2010.08.108

WARBURG, O., 1956. [Origin of cancer cells]. Oncologia 9, 75–83. https://doi.org/10.1159/000223920

Wenz, T., 2013. Regulation of mitochondrial biogenesis and PGC-1α under cellular stress. Mitochondrion 13, 134–142. https://doi.org/10.1016/J.MITO.2013.01.006

Wiese, M., Bannister, A.J., 2020. Two genomes, one cell: Mitochondrial-nuclear coordination via epigenetic pathways. Mol Metab 38. https://doi.org/10.1016/J.MOLMET.2020.01.006

Wildung, M., Esser, T.U., Grausam, K.B., Wiedwald, C., Volceanov-Hahn, L., Riedel, D., Beuermann, S., Li, L., Zylla, J., Guenther, A.K., Wienken, M., Ercetin, E., Han, Z., Bremmer, F., Shomroni, O., Andreas, S., Zhao, H., Lizé, M., 2019. Transcription factor TAp73 and microRNA-449 complement each other to support multiciliogenesis. Cell Death Differ. https://doi.org/10.1038/s41418-019-0332-7

Wilhelm, M.T., Rufini, A., Wetzel, M.K., Tsuchihara, K., Inoue, S., Tomasini, R., Itie-Youten, A., Wakeham, A., Arsenian-Henriksson, M., Melino, G., Kaplan, D.R., Miller, F.D., Mak, T.W., 2010. Isoform-specific p73 knockout mice reveal a novel role for delta Np73 in the DNA damage response pathway. Genes Dev 24, 549–560. https://doi.org/10.1101/GAD.1873910

Williamson, J.R., Cooper, R.H., 1980. Regulation of the citric acid cycle in mammalian systems. FEBS Lett 117 Suppl, K73–K85. https://doi.org/10.1016/0014-5793(80)80572-2

Yang, A., Kaghad, M., Wang, Y., Gillett, E., Fleming, M.D., Dötsch, V., Andrews, N.C., Caput, D., McKeon, F., 1998. p63, a p53 homolog at 3q27-29, encodes multiple products with

transactivating, death-inducing, and dominant-negative activities. Mol Cell 2, 305–316. https://doi.org/10.1016/S1097-2765(00)80275-0

Yang, A., Walker, N., Bronson, R., Kaghad, M., Oosterwegel, M., Bonnin, J., Vagner, C., Bonnet, H., Dikkes, P., Sharpe, A., McKeon, F., Caput, D., 2000. p73-deficient mice have neurological, pheromonal and inflammatory defects but lack spontaneous tumours. Nature 404, 99–103. https://doi.org/10.1038/35003607

Yetkin-Arik, B., Vogels, I.M.C., Nowak-Sliwinska, P., Weiss, A., Houtkooper, R.H., van Noorden, C.J.F., Klaassen, I., Schlingemann, R.O., 2019. The role of glycolysis and mitochondrial respiration in the formation and functioning of endothelial tip cells during angiogenesis. Sci Rep 9. https://doi.org/10.1038/S41598-019-48676-2

Youle, R.J., Strasser, A., 2008. The BCL-2 protein family: opposing activities that mediate cell death. Nat Rev Mol Cell Biol 9, 47–59. https://doi.org/10.1038/NRM2308

Zaika, A., Irwin, M., Sansome, C., Moll, U.M., 2001. Oncogenes induce and activate endogenous p73 protein. J Biol Chem 276, 11310–11316. https://doi.org/10.1074/JBC.M005737200

Zhao, L., Sanyal, S., 2022. p53 Isoforms as Cancer Biomarkers and Therapeutic Targets. Cancers (Basel) 14. https://doi.org/10.3390/cancers14133145